PULSELIKE RUPTURES ON STRONG VELOCITY-WEAKENING FRICTIONAL INTERFACES: DYNAMICS AND IMPLICATIONS

Thesis by

Ahmed Ettaf Elbanna

In Partial Fulfillment of the Requirements for the

Degree of

Doctor of Philosophy

CALIFORNIA INSTITUTE OF TECHNOLOGY

Pasadena, California

2011

(Defended 10/22/2010)

To

Noor

ACKNOWLEDGEMENTS

First and foremost I would like to express my deep gratitude to my thesis adviser Professor Thomas H. Heaton for his support and guidance during the course of my graduate study at Caltech. To me, Tom was not just a thesis adviser; he was a magnificent scientist and a very caring mentor. He willingly gave me hours of his time whenever I needed him or whenever I dropped by his office. He never got bothered by my silly questions. He always lent me an ear whenever I wanted to share any problem I had. I will ever be grateful for him and the model he set for me.

I would also like to thank Professor Nadia Lapusta for co-advising my work on the continuum fault modeling during the last two years of my thesis work. Anyone who dealt with Nadia knows what a wonderful person she is. I will always be grateful for her kindness, care, support, patience, guidance and vast knowledge. I also enjoyed very much our discussions on topics like religion and politics.

I would like to extend my gratitude to late Professor Jerry Marsden who was involved in part of this work regarding model reduction for earthquake problems. His recent death brought a great deal of sorrow to me and all his students and colleagues. I am sure we are going to miss him a lot. Professor Marsden was a gifted scientist, talented teacher and a very caring professor. I consider myself lucky to have had the opportunity to learn from him and collaborate with him for a part of my research. May he rest in peace.

My thanks also go to Professors Julia Greer and Jean-Paul (Pablo) Ampuero for serving as members in my thesis committee. Professor Greer's lectures on dislocation dynamics were

one of the best experiences I have ever had at Caltech and led to a common interest between the two of us regarding the investigation of the analogies between pulselike ruptures and crystal dislocations, which we hope will develop into a research paper soon. Julia is also a very joyful and caring person and was always available whenever I needed to discuss anything. I am also grateful to Pablo for his encouragement and the valuable advice he has provided me during the course of my research. Our discussions on chaotic dynamics, steady pulses, and continuum modeling have greatly benefited me.

Lectures and discussions with Jean-Paul Avouac, Kaushik Bhattacharya, Chiara Daraio, Julia Greer, Tom Heaton, Hiro Kanamori, Nadia Lapusta, and Michael Ortiz have taught me a lot about scientific subjects and the way to investigate them. I thank them for sharing their knowledge and insight with me.

My sincere appreciation goes to my former and current colleagues at Caltech. It has been a pleasure to discuss research with Jean Elkhoury, Yoshihiro Kaneko, Yi Liu, Hiro Noda Anna Olsen and Surendra Nadh Somala. I am especially grateful to Hiro Noda for sharing his vast knowledge of continuum modeling, pulselike ruptures and friction with me, and for giving me permission to use his dynamic rupture code. Hiro's integrity and ingenuity has been a model for many of us.

My understanding of the problem of earthquake ruptures has been enhanced through discussions with people outside Caltech, among them Jim Rice, Ralph Archuleta, Karen Dahmen, Brittany Erickson, Daniel Lavallee and Yehuda Ben-Zion. I am grateful to all of them.

My journey at Caltech could not have been possible without being surrounded by a wonderful group of friends. I would like to especially thank Aamir Ali, Mohamed Ali, Rashied Amini, Trevor Currie, Marcial Gonzalez, Vanessa Heckman, Siriki Hemanth, In Cho Ho, Gokcan Karakus, Ramses Mourhatch, Surendra Nadh, Navneet Narayan, Anna Olsen, Luigi Perotti, Akram Sadek, Phanish Suryanarayan,Tichakorn Wongpiromsarn, Gabriela Venturini and Stephen Wu for making my life at Caltech a pleasant experience. I would also like to thank my C.E. colleagues including Arnar Bjornsson, Michael Cheng, Andrea Leonard, Shiyan Song and Sweetha Veeraraghavan for many enjoyable discussions.

I would also like to thank Carolina Oseguara for being a good friend, for always asking about my family and for helping me through many of the administrative issues. Carolina is doing a great job in strengthening the faculty-student relationships and in keeping a joyful spirit in the department. I would also like to extend my appreciation to Chris Siva, the Thomas building administrator, Cheryl Geer, the option secretary, and Tess Legaspi, from the Registrar's office, for their help and support. I would like to especially thank Cheryl for taking caring of my candidacy admission and for her encouragement and support since the first day I arrived at Caltech.

I thank my parents, Dr. Ettaf Elbanna and Eng. Iman Elbanna, as well as my family in Egypt, especially my grandma Gazbia, my brother Mahmoud and my sister Mariam, for their understanding and support during my graduate study in the U.S. I have been blessed by a wonderful family who surrounded me with love and care from my first day of life and

until now. To them I say thank you, but I know that no words of appreciation could be sufficient. I would also like to thank my uncle Mohamed Elbanna for his help and support and for believing in me even through the toughest times.

Finally, I would like to express my big thanks to my wife, Sara, and my daughter, Noor, for their love, support and understanding of the difficulties of the life of a graduate student. Sara was always standing by my side at both difficult and easy times at Caltech. I cannot imagine this work to have been completed without her continuous support and love. To me, Sara appears as if she is just too good to be true. To Noor, I dedicate this work.

{And peace be upon the messengers.

And praise be for Allah the Cherisher and Sustainer of the worlds}

(As-safat: 37-181 and 37-182)

ABSTRACT

Seismic inversion and computational models have shown that earthquake ruptures may propagate in one of two basic modes; the cracklike mode and the slip pulse mode. In this work we use analytical and numerical techniques to study the dynamics and implications of pulselike ruptures propagating on strong velocity-weakening frictional interfaces using both discrete and continuum models of fracture.

Results of the study of the discrete spring block slider model suggest that strong velocity-weakening friction might yield to the propagation of unsteady slip pulses and chaotic dynamics. The prestress in most of these systems evolves into very heterogeneous spatial distributions characterized, in general, by non-Gaussian statistics and power-law spectral properties. It is also shown that the combined effect of slip pulse propagation and strong velocity-weakening friction could yield to size effects in strength with the strength decreasing as a power law with increasing rupture length.

By examining the energy budget of slip pulses in the discrete model, we show that it is possible to derive a nonlinear differential equation that could predict the final slip distribution in an event, given the prestress existing before that event and some information about friction and pulse dynamics. The equation is successful in replicating many of the macroscopic slip features, including the slip distribution and total rupture length, can also match many long-time statistics regarding the prestress evolution and the event size distribution.

Results from the continuum study suggest that the absence of steady pulses in previous studies could be attributed to the details of the nucleation procedure. We show that steady pulses could exist on strong velocity-weakening friction and uniform prestress if both the prestress and nucleation procedures are correctly tuned. We find that steady pulses are unstable to perturbations in the form of a step in the prestress and could arrest quickly in regions of low prestress. Steady pulses are also found to adapt well to local fluctuations in the prestress, leading to heterogeneous slip distributions. This result might have important implications for the problem of slip complexity in real earthquakes.

TABLE OF CONTENTS

LIST OF FIGURES

Number *Page*

LIST OF TABLES

Chapter 1: Introduction

The current understanding of crustal earthquakes suggests that they nucleate as frictional instabilities on preexisting surfaces of discontinuity, known as faults, under the action of the slowly moving tectonic plates. Once initiated, earthquakes propagate as dynamic shear ruptures along those interfaces, with rupture speeds close to the shear wave speed (subshear ruptures). In some cases they may even exceed that speed (supershear ruptures). As the earthquake propagates it leaves behind a permanent offset between the two sides of the fault along which it is rupturing. We call this offset the earthquake slip.

This work uses analytical and numerical methods, in both the discrete and continuum modeling frameworks, to study the dynamics of earthquake ruptures propagating on strong velocity-weakening frictional interfaces in the pulselike mode, and explores the possible implications for the long term evolution of fault stress and strength. In this chapter we summarize the main features of the earthquake problem relevant to this study as well as introduce the basic tools we have been using.

1.1. On the multi-scale nature of the earthquake problem, friction and prestress

Earthquakes are a perfect example of multi-scale processes in nature. To understand them fully we have to resolve mechanisms spanning spatial scales between a few millimeters, corresponding to the size of the gouge particle in the fault zone, to hundreds or thousands

of meters, corresponding to the size of the process zone close to the rupture tip and ultimately to tens or hundreds of kilometers corresponding to the overall size of the rupture, the size of the faults network, and the other processes that might be effective over that scale, such as fluid and heat transport. On the temporal scale, things do not look easier. In order to understand the evolution of a fault system under the action of a sequence of earthquakes or to understand the correlation between different earthquakes we need to be able to simulate poro-thermo-mechanical processes over tens to hundreds of years while being able to resolve the fast dynamic episodes of fractures, i.e., earthquakes, that usually span from a few seconds to less than a few minutes. Handling the spatio-temporal multi-scale nature of the rupture process is one of the current major challenges in computational mechanics and this study attempts, in part, to present a new paradigm to help solve this problem.

In addition to the challenges imposed by the multi-scale nature of the earthquake rupture process, there exist a number of fundamental questions that earthquake physicists are trying to answer. For example, how do earthquakes nucleate as frictional instabilities? [Rubin and Ampuero, 2005 and Ampuero and Rubin, 2007]; how do earthquakes propagate? [Heaton, 1990, Zheng and Rice, 1998, and Lapusta, 2000] and how do earthquakes arrest? [Husseini, 1975, and Aagaard and Heaton, 2008]. Unlike in classical engineering fracture mechanics, the inaccessibility of the rupture process in the earthquake problem (with earthquakes happening several kilometers deep in the earth) makes answering those questions a bit difficult, and we have to rely entirely on inferences from seismological observations and numerical simulations; no direct

observation is currently possible except on very limited occasions [e.g. deep gold mines in South Africa and the San Andreas Fault Observatory in Southern California].

Nonetheless the numerical simulations have their own challenges as well. As in any mechanics problem, we need to specify geometry, boundary conditions, initial conditions, and the governing stress-strain relationships. The geometry can range from simple models of straight, single, smooth faults to more complicated ones such as fractal networks of nonplanar fault surfaces. The more sophisticated the model is, the larger computational time it takes to run and the larger memory requirements it asks for. As for the governing constitutive laws for the material surrounding the fault surface, the choice can include linear elasticity, elasto-plasticity and nonlinear elasticity with damage mechanics. In this study we limit ourselves to dynamic ruptures on single fault surfaces with the governing constitutive framework being linear elasticity.

The boundary conditions represent one of the two most uncertain parts in the simulation process thanks to what one might call “the mystery of the friction law.” The other major uncertainty comes from the prestress. The debate over which type of friction law can be used to describe the dependence of the frictional strength of the fault surface on the fault slip and slip rate during rupture is not expected to come to an end soon. This unfortunate fact is due to the lack of the technology that might allow us to test frictional sliding of surfaces at slip rates and normal stresses comparable to those that exist in real earthquakes, and also due to the possibility of explaining many seismic observations with totally different friction models. Since the results of the numerical simulations are very

sensitive to the specific type of friction law implemented in the numerical model, we herein summarize the main characteristics of the different friction laws used in the literature.

The first friction law to be used in earthquake simulations was the linear slip weakening model. In this formulation the shear strength τ at a point on the frictional interface has a maximum value designated as the yield strength τ_y. If the applied shear stress exceeds the yield strength, the frictional strength will decrease linearly with the slip accumulated at that point to a new lower level determined by a critical slip value D_c, known as the slip weakening distance. For slip values greater than D_c the frictional strength remains constant at the lower value $\tau(D_c)$. Such frictional formulations have roots in nonlinear fracture mechanics and in particular the Barenblatt cohesive zone model [Broberg,1999]. Barenblatt assumes that a finite amount of work has to be done at the crack tip to break down the atomic bonds in that region and allow for the separation of the crack surface. Since the atomic bond strength is classically given as a function of atomic separation distance, it follows that a displacement-based description for the interface strength might be plausible.

The linear slip weakening model has several drawbacks. First, it was formulated for mode I fractures and its adoption to mode II and mode III frictional cracks seem not to have sound experimental support. Second, the dependence of the frictional strength on slip alone, let alone the linear dependence, is very simplistic. For example, it has been

known since the early 50s that frictional sliding between metallic surfaces shows remarkable dependence on the sliding velocity [Bowden and Tabor, 1950]. Finally the slip weakening law does not allow naturally for the healing and regaining of interface strength after the earthquake is over. This regaining of strength is essential for subsequent earthquakes to occur. Despite these drawbacks, the use of the linear slip weakening law in numerical simulations facilitated the study of several aspects of earthquake dynamics in the 70s and 80s including possible transition mechanisms to supershear propagation in inplane ruptures [e.g., Andrews, 1975] and rupture interaction with fault heterogeneities [e.g., Day,1982]. Nonetheless, it was evident that a more comprehensive law was required.

An important development in the field came with the introduction of rate and state friction based on the experimental work of Dieterich (1979) and Ruina(1983). In this framework, the frictional strength at a point is a function of the instantaneous slip rate at that point plus a number of other parameters (state variables) that account for the history of the slip rate. The state variable evolution is given as a differential equation relating the rate of change of the state variable to the instantaneous values of the state variable and slip rate. Usually the use of one state variable in numerical simulations is satisfactory. However, to fully describe the results of friction experiments, two or more state variables are usually required.

The rate and state framework overcomes many of the drawbacks of the linear slip weakening law. In particular, the dependence of the frictional strength on the slip rate

allows for the description of the frictional behavior, observed experimentally, of both velocity-weakening surfaces, where frictional strength decreases with slip rate, and velocity strengthening surfaces, where frictional strength increases with slip rate. Moreover, this slip rate dependence of the friction can allow for interfacial healing once the slip is over, and hence provides a natural mechanism for regaining interfacial strength and re-rupturing in the next fracture episode [Rice, 1982]. Other experimental observations successfully described by the rate and state laws include i) the logarithmic increase in static frictional strength with time, ii)the instantaneous increase (decrease) in the frictional strength with the abrupt increase (decrease) of the slip rate and iii) the existence of a length scale, or a slip distance, over which the evolution of the frictional strength to the steady state value dictated by the interface slip rate takes place. Unlike in the slip weakening law, this length scale is generally a function of the slip rate and is not a priori prescribed.

While it is true that the rate and state laws successfully describe many of the experimental observations of frictional sliding, particularly at low slip rates (10^{-9} – 10^{-6} m/s), and while they made the simulation of the sequence of earthquake ruptures on the same fault surface possible by providing a natural restrengthening mechanism between rupture episodes, the classical Dieterich-Ruina rate and state formulation has a major drawback when applied to dynamic slip conditions. This drawback is inherent in the logarithmic dependence of the frictional strength on the slip rate, which, given the small values of the rate and state parameters of most known materials, allows for only a small drop in the frictional strength even for orders of magnitude increase in slip rate. With the

frictional coefficient at low slip rates being between 0.6-0.9, the classical Dieterich-Ruina formulation will predict frictional coefficients of the order 0.5-0.8, respectively at seismic slip rates ($V \sim 1 m/s$). This small drop in frictional strength and the sustaining of relatively high values of the dynamic frictional coefficient is inconsistent with the absence of melting in the majority of mature faults. This inconsistency becomes to be known in the geophysics community as the heat flow paradox. The paradox arises from the existence of two conflicting situations. On the one hand many natural faults have very thin sliding zones and are subject to confining pressures of the order of 100-200 MPa. If one of those faults is to move in an earthquake episode for several meters at average slip rates of few meters per seconds and at frictional coefficients predicted by the Classical Dieterich-Ruina formulation (0.5-0.8), then the amount of heat generated will be large enough to raise the average fault temperature by thousands of degrees, sufficient to melt any type of naturally occurring rocks that might be present in the fault zone [Rice, 2006, Noda et al., 2009 and Noda and Lapusta, 2010]. Yet no significant evidence of melting or traces of pseudotachyylytes have been found in most major mature faults. This suggests that the dynamic friction during seismic slip must be much lower than the values predicted by the classical Dieterich-Ruina law and this thesis adopts the point of view that this drop in the frictional coefficient takes place dynamically as the rupture propagates. A possible mechanism is a dependence stronger than logarithmic for the frictional strength on the slip rate. This brings us to a more recent direction in friction modeling for earthquake problems, which is the use of strong velocity-weakening friction laws.

In the strong velocity-weakening formulation, the frictional coefficient decreases with increasing slip rate at a rate faster than logarithmic so that the friction coefficient at seismic slip rates is of the order of 0.1-0.2 [Tullis, 2003 and Beeler et al., 2008]. This limits the rise in temperature to just a few hundreds of degrees and rules out the possibility of melting [Rice, 2006]. A possible mechanism for the strong velocity dependence of friction is flash heating [Bowden and Tabor, 1950, Rice, 1999 and Rice, 2006] at the contact asperities. The idea is that sliding surfaces are rarely flat and when two surfaces come into contact, this takes place at a limited number of points known as asperities. Since the area of the asperities is much smaller than the gross area of the sliding surfaces, the local normal stress at the level of those asperities will be much higher than the average normal stress over the gross area. The rapid relative slip between the two surfaces leads to a local increase in temperature at the sites of the highly stressed asperities, while the overall average temperature remains low due to the inability of heat to diffuse fast enough to the surrounding material. The rise in temperature at the asperity level is high enough to cause local melting at the asperity sites, which facilitates slip at a relatively low frictional coefficient. Another possible mechanism is that the shear modulus of the asperity material is temperature dependent, decreasing as the temperature increases. Since the shear strength is directly proportional to the shear modulus, the strength of the interface will degrade as the local temperature at the asperities increase even before they melt [Brown et al., 2009]. The faster the slip rate, the higher the increase in the local temperature at the asperities level and the larger the decrease in its shear modulus and shear strength. In this study we adopt the flash heating formulation that

predicts a $1/V$ dependence of the frictional strength with slip rate V . In the continuum fault models presented in this study, we retain all the basic ingredients of the rate and state formulation, such as positive direct and finite slip weakening distance [Dieterich, 1979, Ruina, 1983, Tse and Rice, 1986], but we modify the classical framework to allow for additional weakening at seismic slip rates motivated by flash heating [e.g., Lapusta, 2001 and Noda et al., 2009]. In the discrete modeling part, however, we relax some of the rate and state constraints and use a more simplified version of the friction law [e.g., Bowden and Tabor, 1950].

So far we have discussed the challenges associated with the choice of the friction model from the physics point of view. Challenges exist too from the computational point of view. The use of more sophisticated rate and state laws with strong velocity-weakening character at seismic slip rates imposes great constraints on the grid size to be used in the numerical simulations. This is because in order to ensure convergence of the numerical solution with successive mesh refinement, we need to sufficiently resolve slip and stress gradients in the process zone near the rupture tip. For values of frictional parameters inferred from laboratory experiments, the process zone size could be as small as a few meters, which requires grid sizes in the sub-meter range. With the current computational resources we can only solve some simple 2D problems. In order to be able to solve full 3D problems the computational capabilities need to be increased by several orders of magnitude or new innovative methods for solving elastodynamics on non-uniform mesh

need to be developed. Until then the full modeling of 3D earthquake rupture problems will remain numerically impossible.

The physical and computational challenges associated with the choice of the appropriate friction law that can be used to describe fault surface constitutive law have their counterparts when it comes to the question of which prestress distribution can be used to correctly describe the stress state of real faults. Due to the repeated rupturing of fault surfaces with rupture episodes of different sizes and slip distributions, it is natural to expect that residual stresses are built up in the fault zones and the surrounding medium. The evolution of the residual stresses is, in general, a function of the fault slip history, fault friction law, and spatial distribution and temporal evolution of the fault's material properties. Given the geometric complexity of real fault systems and the nonlinear dynamic nature of strong velocity-weakening friction laws as well as the inevitable existence of spatial heterogeneities in fault material and frictional properties, it becomes nearly impossible to have a uniform state of prestress under any realistic conditions. The question then becomes: what are the statistical and spectral properties of the prestress heterogeneous distribution?

Due to the unique nature of the earthquake problem and the inaccessibility of the rupture process to direct observations, however, no clear- cut answer is readily available. We can only use intuition, available numerical procedures, and inferences based on indirect observations to arrive at an approximate answer. One method is to design thought experiments. Here is one: Consider a smooth, single fault with homogeneous frictional

and material properties that generates a power law earthquake magnitude-frequency distribution consistent with the Gutenberg-Richter law and ask the question: what possible stress state might be consistent with this event size distribution? Since the event size distribution is a power law it has no inherent length scale. With homogeneous frictional and material properties this means that the prestress distribution has to have no length scale as well. The only distributions that have no inherent length scale are the uniform distribution and the fractal distribution. A uniform prestress distribution is not feasible since in a uniform prestress state and constant fracture energy, the change in potential energy for a propagating rupture will overrun the dissipated fracture energy and hence ruptures will grow indefinitely. This is inconsistent with the power law event size distribution and the existence of events of different sizes. This leaves us with the fractal prestress distribution as the only plausible state.

However, it is highly unlikely that a single fault can host a complete Gutenberg-Richter-like event size distribution [See Page et al., 2009 for a counter hypothesis]. Consequently, mathematical fractality, or in other words the complete absence of a characteristic length scale, is not strictly required. Rather we might hypothesize that the prestress distribution is strongly heterogeneous, but not completely fractal, and with the degree of heterogeneity being consistent with the event size distribution generated by the fault. The hypothesis of strongly heterogeneous prestress is supported by a number of field observations, including the occurrence of right lateral aftershocks on the nominally left lateral San-Andreas fault, strong local variation in surface slip after some major

earthquakes with corresponding static strain of the order of 10^{-3}, and the possibly fractal spatial variation in the change in angles between focal mechanisms [Smith, 2006 and Smith and Heaton, 2010]. It is a major theme of this study to investigate the evolution of different statistical and spectral properties of the heterogeneous prestress distributions, their connection to the different event size distributions and their implications for long term fault behavior.

1.2. On pulses vs cracks:

Earthquake ruptures have been found to occur by two basic modes, the expanding cracklike mode and the self-healing mode. In the expanding cracklike mode the rupture zone on the fault keeps expanding and the slip continues to grow everywhere until information is received at respective points that the rupture has stopped. On the other hand, in the self-healing mode the rupture occurs as a pulse of slip propagating along the fault, with the slip stopping behind the pulse so that the slipping region occupies only a small width at the front of the expanding rupture zone.

In early numerical simulations for earthquake ruptures, scientists were tempted to assume uniform background stress and slip weakening friction laws in their models. As a result the only mode of rupture observed in their models was that of the expanding crack type. Although there were some attempts along the way to describe the rupture as a propagating pulse (Yoffe, 1951, Broberg, 1978 and Freund 1979), these attempts were dismissed due to their lack of a sound physical background. It was not until 1990 when

Heaton (Heaton 1990) was able to present strong evidences for the existence of self-healing mode of rupture in real earthquakes along with a plausible physical mechanism for their formation based on strong velocity-weakening friction. Heaton studied the dislocation time histories of models derived from seven earthquakes with magnitudes ranging from 5.9 to 8.1 and found that in all such models the rise time (or the duration of slip at a given point on the fault) was nearly an order of magnitude less than the overall duration of the earthquake. That is contradictory with the well-established picture of cracklike ruptures obtained from the numerical simulations previously described. Nevertheless, Heaton's arguments triggered an endless interest in the proposed rupture mode and now it is a widely accepted fact that slip pulses are an important mechanism for real earthquakes and their existence have been proven numerously through appropriately designed numerical simulations as well as some recent laboratory experiments.

An important lesson learned from the numerical simulations of dynamic shear ruptures in the last 15 years is that slip pulses do not exist arbitrarily. Certain combinations of conditions pertaining to the preexisting stress, as well as the dynamic friction law, have to exist to allow for the generation and propagation of these pulses. Various mechanisms have been proposed that allow a self-healing versus a cracklike mode of rupture. These mechanisms include stress heterogeneity, existence of barriers along the fault [Day, 1982], strong velocity-weakening friction together with low background stress [Zheng and Rice, 1998] and, finally, variation of the normal stress interacting with the rupture propagation, possibly due to the existence of a biomaterial interface [Andres and Ben-Zion, 1997]. Recently, numerous laboratory experiments have been carried out, inspired

by the pioneering work of Xia, Lykotrafitis and Rosakis (2005) and the later work of Xiao, Lapusta and Rosakis (2007), to test the significance and role of the previously mentioned mechanisms and to provide more insight towards the mechanics of the rupture process.

The self-healing rupture mode is believed to have significant implications on the dynamics and consequences of earthquake ruptures. These implications might include, but are not limited to, increasing difficulty of earthquake prediction [Heaton, 1990], spatio-temporal complexity of earthquake ruptures [Aagaard and Heaton, 2008], earthquake scaling laws, and numerical methods of earthquake simulations. Hence, a deeper understanding of the dynamics of slip pulses together with a better understanding of the friction constitutive relationships are among the most challenging tasks facing earthquake scientists in the near future. This study aims to contribute in this direction.

1.3. On discrete vs continuum fracture models

This work uses both discrete and continuum fault modeling to study the dynamics of pulselike ruptures. The motivation here is that each of these modeling approaches is believed to have advantages and limitations. Hence with the appropriate combination of both models, we may gain better understanding of the pulselike rupture processes on both the level of the detailed physics of a single rupture episode as well as on the level of the long-time statistics of the system due to the collective action of a large number of rupture episodes spanning over several orders of space and time scales.

In the continuum approach, the fault is modeled as a 1D or 2D surface embedded in 2D or 3D bulk. The governing equations of motion are usually expressed in terms of stress, which in turn can be expressed in terms of the particle displacement and particle velocity through the appropriate constitutive laws. [In the case of elastic continuum, we recover Navier's equation of motion.] The inertia of the continuum is in the bulk and none is concentrated in the fault. Accordingly the fault comes into action through the boundary conditions assigned to its surface. The boundary condition is usually defined in terms of a friction law that relates the shear stress at a particular point to the fault slip and slip rate at this point. The fundamental characteristic of the continuum is the existence of long range interactions; a finite displacement at a given point will generate stress and displacement fields that influence other points far away from the source of the disturbance. This communication between different points in the continuum takes place through the propagating wave field that carries disturbances from the point source to elsewhere. Based on the double couple model, the long range stress transfer in the continuum typically goes as $1/r^3$ where r is the radial distance between the source and the receiver. For the continuum hypothesis to be retained in the numerical simulations, the computed displacement and stress fields should show convergence with further refinement of the continuum discretization when using any of the classical numerical methods such as finite element, finite difference or boundary integral equation methods. This imposes certain constraints on the admissible set of friction boundary conditions to assure the stability of short wavelength perturbations [Rice, 1983 and Rice et al., 2001]. It

has been shown that the rate and state framework satisfies those constraints and assures the existence of a well-defined continuum limit.

On the other hand, in the discrete approach, the focus is primarily on the fault, which is discretized in 1D or 2D elements while the bulk is totally ignored or replaced by some simplistic representation. The system mass is usually concentrated in discrete sites and not distributed as in the case of the continuum models. The equations to be solved for the system are Newton's equation of motion *force = mass x acceleration* at each discrete particle site. The elastic interaction in discrete models is typically short ranged extending in most cases only to the nearest neighbors. Unlike in continuum models, the stress concentration for discrete models is independent of the rupture size. In these models, a failure of a single element independent of the surrounding ones is permitted and will define the smallest event size. This failure pattern is excluded in the continuum by the enforcement of the continuum hypothesis and the correct representation of the long range fields.

The previous discussion shows that the continuum models are usually more sophisticated and pay more attention to the correct representation of the physical and mathematical details. This is why continuum models are very useful in studying the physics of single rupture episodes, including how a rupture nucleates, propagates, interacts with systems heterogeneities, and arrests. However, continuum models have typically high computational costs. In order to retain the continuum hypothesis and have computationally stable results, the process zone near the rupture tip must be adequately resolved. The process zone size might be as small as a few meters, making the grid size

fall into the sub-meter scale. For any reasonably sized earthquake spanning a few squared kilometers, the computational requirement of the problem will simply overrun the computational power of the biggest computer on Earth. This is why continuum models still fall short of being able to analyze sequence of earthquake ruptures under realistic high speed frictional and geometric conditions.

The discrete models, on the other hand, cannot be used to describe the dynamics of individual ruptures since they lack many of the essential physical characteristics of the continuum. They, however, can provide a tool for the study of long-time system statistics in a way similar to what is done in statistical physics. This is because in many complex systems, their long-time behavior is independent of the exact details of the underlying individual events. This is where the discrete models may provide an advantage as they allow for the simulation of long sequence of events and hence the study of the long-time evolution of the system statistical and spectral properties in a reasonable computational time. Also as the physics is more simple in the discrete models, this gives an opportunity to explore surrogate strategies that can be used to simplify the computational complexities of the continuum models. Hence combining discrete and continuum modeling tools can help us understand both of the microscopic and statistical properties of ruptures as well as give insight into possible new numerical strategies.

In this work, two numerical fault models will be studied in details, one continuum and one discrete. The continuum fault model is a 2D anti-plane elastic fault embedded in a linearly elastic whole space. Rate and state friction, with additional velocity-weakening at the seismic slip rate, are used as the fault boundary conditions. The governing equations

of motion are solved using the boundary integral equation method. On the other hand, the discrete fault model we chose here is a 1D spring block slider representation of a 1D elastic fault. The fault is represented by N discrete masses that are interconnected by linear horizontal springs and being driven by a slowly moving plate, to simulate the effect of far field tectonic loading, which transfers its loading to the masses through another series of linear vertical springs [See Fig. 2.1]. The blocks slide on a frictional surface with a well-defined static friction limit and a dynamic friction law in which the friction coefficient decreases hyperbolically with the block slip rate. The governing equations of motion are solved by a 2^{nd} order explicit integration scheme. The dynamics of the discrete and continuum models is described in chapters 2 and 5, respectively.

1.4. The outline of this work

This outline of this thesis is as follows.

In Chapter 2 we describe the dynamics of the spring block model with emphasis on results pertaining to the spatio-temporal distribution of events, the statistical distribution of event sizes, the evolution of the probabilistic and spectral properties of prestress, the statistical and spectral properties of slip, and the connection between the event size distribution and the evolutionary properties of prestress and slip.

The use of strong velocity-weakening friction and the evolution of spatial heterogeneity in the prestress distribution leads to interesting size effects in the evolutionary behavior of the studied discrete system. In Chapter 3 we discuss two major examples of size-dependent effects: the first is the dependence of the prestress averaged over the rupture

size on the respective event size and the second is the dependence of the change in potential energy per unit slip per unit rupture length on the event size. We argue that our observations could be used to explain the scale dependence of strength for frictional interfaces failing under the influence of strong velocity-weakening friction.

In Chapter 4 we outline the first steps in a promising new paradigm that can be used to simulate the dynamics of pulselike ruptures and which can result in a huge computational saving. The paradigm uses the energy balance of the propagating slip pulse to formulate a nonlinear differential equation that relates the pulse slip to the presxisting stress given some information about friction and pulse energy. The results both on the level of individual events, and to some extent on the level of long-time statistics, are very promising.

We then make a switch to the continuum model in order to explore whether the conclusions based on the discrete study can be carried over to the continuum and what modifications are required, if any. In Chapter 5, we study a 2D anti-plane continuum fault and discuss the problem of pulse formation, steady propagation, and interaction with prestress heterogeneity. We examine how sensitive the pulse could be to local variations in prestress and what implications this could have on earthquake complexity. We then summarize our conclusions and present some future research directions in Chapter 6.

Chapter 2: The Spring Block Model

Systems failing at multiple length scales are abundant in nature. Examples range from strain bursts in micro-pillars due to collective dislocation movement to earthquakes on major faults in the earth's crust. We here present a parametric study for a 1D spring block slider model as an idealization of such systems. Due to its discreteness and lack of long range interaction, the spring block slider model cannot represent accurately the dynamics of a single rupture in a continuum. Nonetheless, the spring block slider can capture reasonably well the long-time statistics of complex systems with multiple repeated ruptures since the collective behavior of those systems is independent of the physics of individual events (as long as ergodicity holds, at least in an approximate sense).

Our parametric study includes investigating the effects on patterns of ruptures of changing the following parameters: 1) Loading speed of the driving plate; 2) Coil spring stiffness and the leaf spring stiffness; and 3) Amount of frictional weakening. In an earthquake setting these parameters are related to the rate of tectonic loading, the ratio of the length to the depth of the seismogenic region, and the amount of steady state velocity-weakening, respectively. We find that smaller driving speeds and higher ratios of leaf spring to coil spring stiffness favor the generation of smaller ruptures, and vice versa. The influence of frictional weakening, however, is a bit more complicated and is not monotonic. By tuning the different parameters, we can find a region in the parameter

space where events of all sizes are produced with statistics similar to the Gutenberg-Richter scaling law, with a b-value between 0.4 and 1.

We studied the long-time properties of the prestress due to the accumulation of repeated ruptures of different sizes and conclude that the prestress evolved into a heterogeneous distribution with a power law Fourier spectrum and non-Gaussian statistics. We also studied the spectral and statistical properties of the slip distribution and show that we can match the expected behavior for mature and immature faults.

2.1 On models and origins of earthquake complexity

The origin of complexity in natural systems is still an unresolved question. Since Pak et al. (1987) introduced their idea of self-organized criticality, a lot of interest arose in looking for various systems that could lie within the spectrum of self-organized phenomena. While it is possible to find many phenomena that have power law statistics, such as size distribution of landslides, magnitude-number statistics of earthquakes, and size distribution of strain bursts in micro-pillars, it is still a challenge to accurately determine the physics behind this apparent self-organization. The field of earthquake physics is no exception. There has been a lot of debate about the origin of the Gutenberg-Richter scaling and its implications for the state of stress in the earth's crust. Historically, two major schools of thoughts have emerged to explain what appears to be the scale-less character of earthquake statistics; one arguing for the dynamic origin of complexity due to nonlinear friction and the other tending to attribute it to the strong geometric and

material discontinuities that exist in natural faults. The right answer to this problem is probably a combination of both factors. It is important to mention, though, that having a better understanding for the spatio-temporal complexity of earthquakes is of great interest as it has implications on our understanding of the origin of high-frequency spectra in earthquakes as well as our assessment of the stress state on major faults. This latter issue in turn may have important consequences for our model of the strength of real faults or, more generally, the strength of systems with multi-scale fractures.

In order to address the complexity problem, we need a quantitative model for a system that can fail over multiple length scales, like the Earth's crust, simulated for long enough times so that we can carry out a systematic statistical evaluation for its asymptotic behavior. We think that the rigorous way of doing this is to have a 3D continuum model with a strong velocity dependent friction law and friction parameters that are extrapolated from actual laboratory experiments. Unfortunately such an approach is computationally prohibitive with the current computational facilities, and can only be done for simple 2D anti-plane models [Dunham et al., 2008], and for a few earthquake cycles at most. An attractive alternative is to study simple dynamical systems, which bear some relationships, at least in the statistical sense, with the more complex real systems, to try to learn the possible implications for complexity evolution that may be relevant to the continuum as well as effective methods to do large scale continuum model simulations. The hope here is that the macroscopic behavior on long-time and large spatial scales will not depend, to some extent, on the details of the microscopic physics. Although this is not rigorously proven for any real complex system, it has been empirically justified in many

cases, such as in turbulence. The dynamical system we choose to study in this work is the spring block slider model.

Although the spring block slider model was first introduced by Burridge and Knopoff (1967) as a quantitative model of earthquakes, Carlson and Langer (1989) were the first to systematically study it. They presented it as a model supporting the dynamic complexity view of earthquakes. Further studies arguing along the same line of thought included Carlson and Langer (1989), Carlson et al. (1991, 1994), Shaw et al. (1992, 1993), Pepke et al. (1994) and Erickson et al. (2007). Rice (1993) criticized such approach, arguing that the pure velocity-weakening friction used in Carlson and Langer simulations, for example, is not suitable for continuum faults models due to its ill-posed nature; short wavelength perturbations grow. He argued that systems showing self-organized criticality are inherently discrete, leading to results that are mesh size dependent, and hence could not be generalized to the continuum. In support of this argument, Rice and Ben-Zion (1996) introduced a 2D cellular fault model in a 3D continuum with long range static stress interactions included. They showed that there exists a minimum length scale that needs to be well resolved in order for their results to be mesh size independent. If the cell size they used was larger than this minimum length scale, small events complexity was produced, whereas if this length scale was well resolved, complexity disappeared and only periodic large earthquakes are produced. Although the Rice-Ben Zion model results support the argument that complexity cannot exist on a smooth fault, we think that an indirect implication of their cellular fault model is that long range fields, at least in the way they have introduced them in their cellular

model, have little to do with the evolution of complexity if local conditions are strong enough to control and arrest the rupture. These local conditions may be stress fluctuations if the rupture is pulse-like, and may not necessarily be limited to strong geometric or material discontinuities. This point is important, and we will come to it later in the discussion.

In the field of continuum fault models, Cochard and Madariage (1996) introduced a 2D anti-plane continuum fault model with a rate and slip friction law. They were able to show that the long-time behavior of such a model entails complexity if the rate dependence character of the friction law is strong enough. Myers et al. (1996) reached a similar conclusion with a crustal plane model. Nonetheless, these two models were criticized for employing an initial sudden strength drop in their friction law formulation in order to initiate rupture. Such a procedure made their model inherently discrete. Recently, Aagaard and Heaton (2008) showed that complexity, in well resolved 3D models, can be preserved, at least over few earthquakes, if strong rate strengthening friction law is employed.

Self-consistent earthquake cycle simulations in continuum fault models started to appear only a few years ago with the advance of computational facilities and modeling procedures. Shaw and Rice (2000) presented some evidence for the existence of dynamic complexity in a well resolved cycle simulation of a crustal plane model. However, their results suggest that complexity exists only for friction laws having two weakening scales, and for a narrow range of frictional parameters. Lapusta (2000), on the other hand,

presented a 2D cycle simulation for a crustal plane model with Dieterich-Ruina type friction law and showed that complexity did not exist in her simulation if small enough spatio-temporal resolution is used.

In this manuscript we are not primarily concerned with the question of the origin of complexity, but rather on its different characteristics and implications if it exists. We believe that both dynamic and geometric factors contribute to the evolution of complexity on natural faults. However, we think that the role of rate dependent friction should not be underestimated. In particular we think that pulselike ruptures, which exist naturally on faults with strong rate dependent friction (Heaton 1990, Zheng and Rice 1998), play an important role in the evolution and preservation of stress heterogeneities in the earth crust, since they appear to be very sensitive to the local fluctuation in the prestress (See Chapter 5). In our version of the spring block slider model, we found that all ruptures are pulselike and, accordingly, this study might be useful in giving some hints about what we should expect, at least in a statistical sense, if a continuum model experience repeated pulse-like ruptures of different sizes.

The questions of interest to us here are: (1) What are the different statistical asymptotic behaviors of the spring block slider model as a function of its different parameters?;(2) What distributions of prestress are consistent with the long-time behavior of our system in the different parameter regimes discussed in (1) and what does this entail for mature and immature faults?; (3) What do the statistical and spectral properties of slip and the

evolved prestress distribution imply for our understanding of the size dependent dynamics of the system?

The outline of this chapter is as follows: In section 2.2 we describe the main features of the spring block slider model. In Section 2.3 we present our numerical scheme and assess its validity for the problem. In Section 2.4 we discuss some features of the spring block model that seem to be stable and independent of the specific choice of the parameters. In Section 2.5 we present the different size distributions of events we were able to get from our simulations corresponding to different set of parameters. In Sections 2.6,2.7 and 2.8 we discuss the different statistical and fractal properties of the spring block models lying in different parameter regimes. We summarize our discussion in section 2.9.

2.2 The spring block slider model:

The setup of the spring block slider experiment is shown in Figure 2.1.

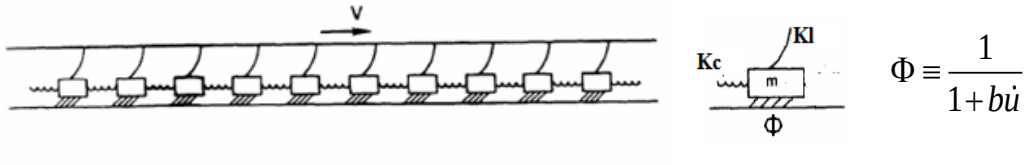

Fig. 2.1: The spring block slider model. A chain of N blocks of identical masses (m) interconnected by coil springs of stiffness (K_c) is driven by a loading plate moving at a very low velocity (v). The blocks feel the effect of the loading plate through a series of leaf springs of stiffness (k_l). Any block is stuck to the ground as long as the total elastic

force acting on it is less that the static friction threshold. Once the static friction is exceeded, a sliding block experiences a dynamic friction force ϕ that varies inversely with the block sliding velocity. The blocks are subjected to an initial stress distribution that is constant everywhere but is larger than the static friction threshold F_{st} for the middle three blocks in order to initiate rupture. As a block moves, it transfers stresses into neighboring blocks causing them to subsequently move if the static friction level is exceeded. When all the blocks that have already slipped stop, we designate this as the completion of one event.

The spring block slider model consists of a chain of blocks interconnected by one group of springs and coupled to a slowly moving driving plate through another group of springs. Frictional forces are assumed to operate between each block and hosting stratum. As long as the total elastic force on each block is less than the static friction threshold F_{st} the block is stuck in its place. Once the static friction threshold is exceeded, the motion of the i^{th} block is given by the following differential equation:

$$m_i\ddot{u}_i = k_c(u_{i+1} - 2u_i + u_{i-1}) + k_l(vt - u_i) + \sigma_{oi} - F_{st}\phi_i \qquad (2.1)$$

Where σ_{oi} is the initial traction at the position of the ith block and all other parameters are explained in Fig. 2.1. Equation (2.1) represents n-coupled ordinary differential equations where n is the number of blocks moving simultaneously. We use a second order accurate predictor-corrector scheme for solving equation (2.1). The time step is controlled by the ratio of leaf spring stiffness to coil spring stiffness as well as the rate of frictional weakening (b). The time step is chosen just small enough to balance sufficient time

resolution and reasonable computational cost. In all our simulations we assume m =1 and F_{st} = 50. We vary the other parameters according to the parametric study requirements.

It may be useful to cast equation (2.1) in a non-dimensional form as this gives further insight into the relative role of different parameters in controlling the nature of the solution. We do this by introducing the following length and time scales:

$$D = \frac{F_o}{k_l} \tag{2.2}$$

$$\tau = \omega t \tag{2.3}$$

where $\omega = \sqrt{\frac{k_l}{m}}$ is the natural frequency of the individual block when connected to the leaf spring only. Normalizing displacements by D, time by τ and introducing the stiffness ratio $r = \frac{k_c}{k_l}$, we can rewrite equation 1 in the following form:

$$\ddot{U}_i = r(U_{i+1} - 2U_i + U_{i-1}) + \gamma\tau - U_i + \frac{\sigma_{oi}}{F_{st}} - \frac{1}{1 + \frac{\dot{U}_i}{v_c}} \quad , \tag{2.4}$$

where $U = \frac{u}{D}$, $\gamma = \frac{v_p}{\omega D}$ and $v_c = \frac{1}{b\omega D}$. γ is the normalized plate loading rate whereas v_c is a characteristic velocity. It is worth to mention that a ratio like $r = \frac{k_c}{k_l}$ does appear in continuum crustal plane fault models to represent a finite seismogenic depth

[Appendix A]. The ratio ν_c on the other hand gives a measure of the strength of frictional weakening relative to the inertial and elastic properties of individual blocks. It is analogous to the T parameter [Zheng and Rice, 1998] in continuum fault studies, which gives the ratio of the slope of the steady state friction curve to the radiation damping line at a given slip rate. Hence similar parameters govern the behavior of both discrete and continuum systems.

From the mechanics point of view, the spring block model is characterized by the following three features:

1- Short range of interactions: Each block is connected only to its nearest neighbor block; there are no long range stress fields.

2- Existence of a characteristic length scale: This follows from the existence of the leaf springs with non-zero stiffness (k_l) , which introduces a natural length scale given by $D = \frac{F_{st}}{k_l}$ [See equation (2.2)]. The existence of this length scale breaks the self-similar nature of the sought solution. In the limit of infinitely rigid leaf spring, each block moves under a constant displacement boundary condition whereas in the limit of zero leaf spring stiffness, the block moves under constant force boundary conditions within an infinitely large strain energy reservoir. Hence we would expect dominance of single block events for cases with stiff leaf springs

while we expect catastrophic system-wide events for cases with very flexible leaf springs. Such a statement is made more precise in Sections 2.5, 2.6, 2.7 and 2.8.

3- Non-linear rate dependent friction: The friction law we are using is both velocity-weakening and velocity strengthening. This is achieved by assuming a constitutive law where the dynamic friction varies inversely with slip rate. Such laws lead naturally to the formation and propagation of slip pulses, where only a localized portion of the chain is slipping at any instant of time. The existence of slip pulses has strong consequences on the nature of the stress state and the energy scaling in our model as will be discussed in Section 2.5.

The spring block model with pure velocity dependent friction law was criticized for two major things: discreteness and lack of long range interaction.

1- Lack of long range interactions: Long range wave fields undoubtedly exist in continuum smooth systems. Points far away from the rupture front can still sense its effect through the wave field set up by the rupture even before the rupture front has reached these points. In the spring block models, however, each block is directly connected to its nearest neighbor only. We hypothesize here that long range wave fields may not change the nature of the complexity of the solution, but may only affect fine details of individual events, provided that ruptures propagate

in the pulse-like mode. We hypothesize that due to the local nature of the pulse like ruptures, the major factors affecting the evolution of the propagating pulse are the local fluctuations in the prestress field and not the perturbations introduced by the long range wave field. Since we are interested in the long-time statistical nature of the solution, we think that the spring block model might be sufficient for our purposes.

2- Discreteness: A linear stability analysis for the spring block slider model with pure velocity dependent friction indicates that perturbations of all wavelengths grow [Appendix A]. A similar analysis for 2D or 3D continuum systems further indicates that not only perturbations of all wavelengths grow, but also that the perturbation with the shortest wavelength grows fastest [Rice, 2001]. This signals an ill-posed problem in the mathematical sense and renders the problem discrete in the sense that individual blocks or cells can fail independently of other blocks. While we acknowledge this, we also assert that the elastic continuum hypothesis breaks at some length scale in real systems. We accordingly assume that the spacing of the blocks in our model should correspond to this minimum length scale and we are mainly interested in exploring the behavior of the system, in a statistical sense, over scale lengths larger than this minimum scale. This is why when we increase the number of blocks in our simulations; we always do it by increasing the overall system length while keeping the inter-block distance the same.

The spring block slider model, on the other hand, provides an efficient tool for studying the long-time statistics of systems failing at multiple length scales. It has a reasonable computational cost when compared to full elastodynamics continuum models of the same size. It is also shown that it can reproduce correctly many of the long-time statistics observed for different multi-scale physical systems such as earthquakes on real faults if the model parameters are correctly tuned.

Finally, we stress that our main focus here is on the statistical properties of evolving heterogeneity in systems with multi-scale failures and their implications rather than debating the source of heterogeneity in our model and whether it is completely geometric or completely dynamic. In the following section we discuss several results that support the validity of using the spring block slider system as a model for the long-time statistical behavior of systems failing at multiple length scales.

2.3 Numerical scheme

We use an explicit time integration scheme for solving equation (2.1). While this imposes strict constraints on the size of the time step to be used, it is still computationally advantageous when compared to the implicit procedure as there is no need to solve a system of non-linear algebraic equations (which appears in the implicit scheme). To solve for the displacement and slip rate we proceed as follows:

At time *t* we assume we know the block displacement u_i and slip rate $\dot{u}_i$ then the displacement at *t+Δt* can be estimated through the following second order prediction:

$$u_i(t+\Delta t) = u_i(t) + \Delta t.\dot{u}_i(t) + \frac{1}{2}(\Delta t)^2.\ddot{u}_i(t) \tag{2.5}$$

The slip rate prediction is a little more involved since the acceleration itself depends on the slip rate. We proceed in a predictor corrector fashion.

Predictor step:

$$\tilde{\dot{u}}_i(t+\Delta t) = \dot{u}_i(t) + \Delta t.\ddot{u}_i(t) \tag{2.6}$$

Corrector step:

We first calculate an estimate for the acceleration at *t+Δt* using the updated value of displacement $u_i(t+\Delta t)$ and the predicted value of the slip rate $\tilde{\dot{u}}_i(t+\Delta t)$:

$$\tilde{\ddot{u}}_i(t+\Delta t) = f(u_i(t+\Delta t), \tilde{\dot{u}}_i(t+\Delta t)) \tag{2.7}$$

A corrected value of the slip rate can now be estimated as:

$$\dot{u}_i(t+\Delta t) = \dot{u}_i(t) + \frac{1}{2}.\Delta t.[\ddot{u}_i(t) + \tilde{\ddot{u}}_i(t+\Delta t)] \tag{2.8}$$

The method is second order in slip rate and displacement. We do not rigorously estimate the time step but we check the error in energy for large events and try to limit this to less than 1% [The energy error is defined as the difference between the change in potential energy in the event and the corresponding frictional dissipation, with the result being normalized by either of them]. We apply our procedure to a test problem with 1000 blocks, systems parameters ($k_c = 2500$, $k_l = 40$ and $b = 10$) and time step $\Delta t = 10^{-5}$. The result is shown in Fig. 2.2, where the energy relative error is plotted as a function of the event index. The error is well below the 1% threshold throughout the simulation.

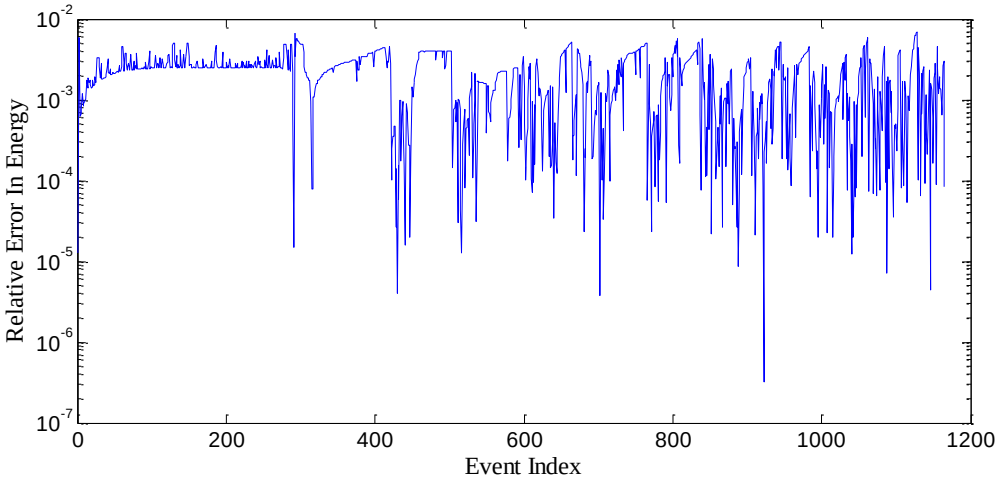

Fig. 2.2: The relative error in energy as a function of the event index. The error is calculated as the difference between the change in potential energy of the system due to an event and the frictional work dissipated in this event, with the result being normalized by the potential energy change. For the case shown, the relative energy error is well below 1%.

To test the long-time performance, we calculate the cumulative energy error for the whole sequence of events. This is done by calculating the total change in potential energy due to all events, subtracting it from the cumulative frictional dissipation, and normalizing the result by the cumulative change in potential energy. We repeat this calculation with different time steps and show the results in Fig. (2.3). The energy error is almost quadratic in the time step size.

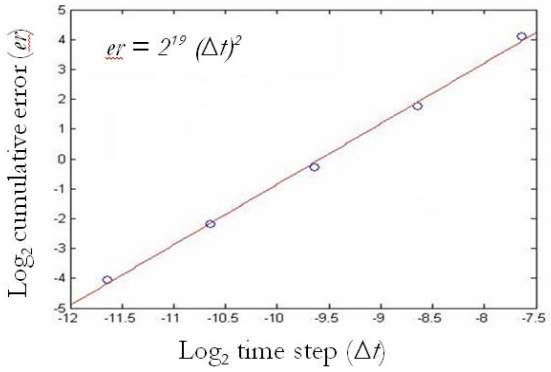

Fig. 2.3: Variation of the relative cumulative energy error with the computational time step size.

Finally, it is worth noting that there are several characteristic time scales to which we can compare the selected time step size. These include the natural periods of the coil or leaf springs and the characteristic weakening time of the friction law in use. We found that a useful guide for the choice of the time step size is to keep it below 1% of the natural period of the stiffer spring. Also, for these kinds of problems which are highly nonlinear and possibly chaotic, it is not possible to achieve convergence based on individual events or the exact sequence of events, with reducing time step.What we can hope for is that the statistics is convergent using some measures of convergence.

2.4- Slip Pulses, Event Complexity and Stability of Rupture Speed:

While the spring block model with rate weakening friction is a highly nonlinear system that is expected to depend sensitively on our choice of parameters and initial conditions, we have found some stable features for our solutions that are preserved across most of our simulations regardless of system characteristics. Before delving into the results of our parametric study, we would like to summarize these main features in the following points:

(1) *Events of different sizes are generated*. Due to the highly nonlinear, and possibly chaotic, nature of the system, it is very hard to make the system settle in an ordered state in the long run (e.g. produce periodic events). Even when we show a case for a system failing primarily in small events, and while it appears that those small events are periodic and of the same size, variability across them is found when we look close enough. [However, for that particular case, the variability is not large.] Contours for particle velocity for some of the generated events in one of our simulations are shown in Fig. (2.4).

(2) *Events propagate as slip pulses*. Figure (2.5) shows one of the generated events in greater detail reflecting the pulselike nature. The slip duration at any block that has moved in this event is much shorter than the total event time. This is the main characteristic of slip pulses. A deeper look into Fig. (2.4) reveals further that all events, spanning more than a few blocks, share this pulse-like character. There are two reasons for the generation of slip pulses in our model: i) The rate dependent friction introduces a rate dependent healing ~ as the block slip rate decreases the friction force the block

experiences increases and ultimately become high enough to stop the rupture; ii) Leaf springs of finite stiffness exist, which provides a finite reservoir of potential energy and hence any block cannot slip forever. Slip pulses have been found in continuum fault models as well [e.g. Das, 1982, Zheng and Rice, 1998], so it might be useful to learn from our simple dynamical system the implications of having repeated pulse-like ruptures and see if we can generalize any of them to the more complicated continuum case.

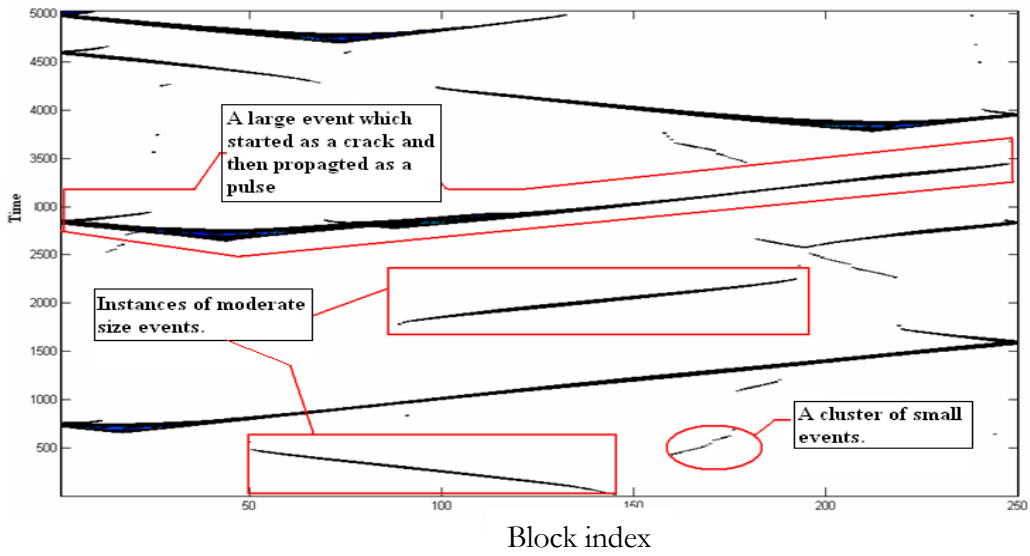

Fig. 2.4: Contours for particle velocity in a number of generated events showing a variety of event sizes as well as existence of slip pulses, since the rupture duration at any of the sliding blocks is small compared to the total rupture time in the corresponding event. White color corresponds to a stuck state.

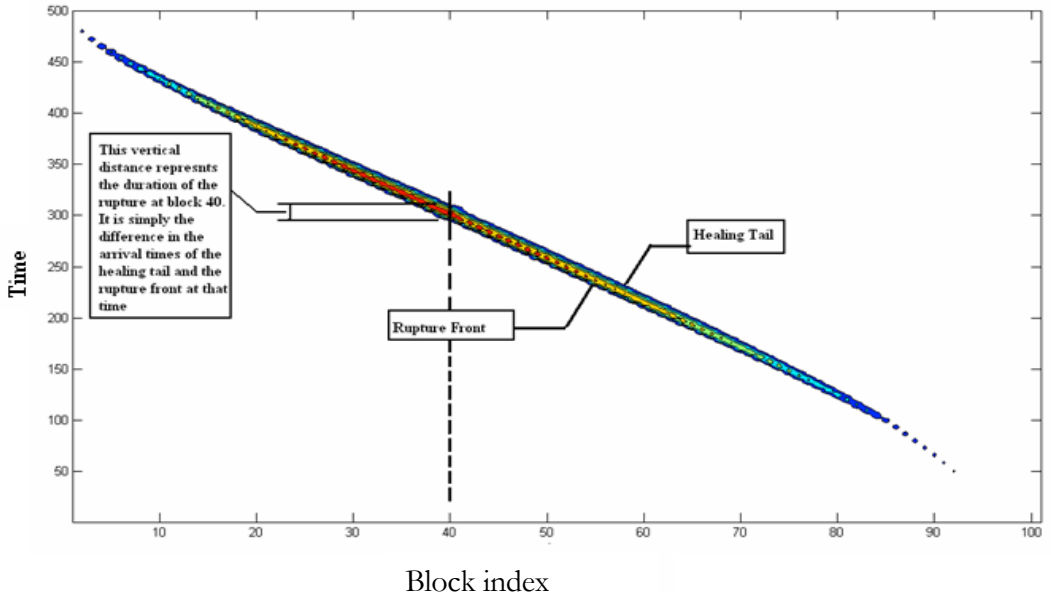

Fig. 2.5: A detailed look at the contours for particle velocity of one of the generated events (the lowermost event in the previous figure). Note that the event consists of a solitary wave of slip (the maximum duration of slip in this event is only about 5% of the total rupture time for the whole event). Colors correspond to different values of slip rate with red being the maximum and white being zero.

(3) Events have remarkably constant rupture speed. The spring block model is a dispersive frictional dynamical system. For its non-dispersive non frictional version, we can define a characteristic sound speed in the continuum limit that is related to the square root of the coil spring stiffness. When dispersion is added through the leaf springs, it can be shown that the dispersion relation takes the form [see Appendix A] $c_p = c_s\sqrt{1+k_l/(kc_s)^2}$, where c_p is the phase velocity of the perturbation with wavenumber k , suggesting that the system will propagate longer wavelengths faster than shorter ones

and both of the phase and group velocities will depend on the wavelength under consideration. The dispersion effects become stronger as the stiffness of the leaf springs increases. When friction is introduced into the system, the rupture speed, away from the discretization effects at the beginning and end of ruptures, exhibit a remarkably constant value. This can be inferred from Fig. (2.4) where events can be approximated by straight lines, in each propagation direction, in the space-time diagram, and the rupture speed is proportional to the inverse of the slope of that line. The rupture speed seems to be independent of the event sizes and, moreover, events seem to be propagating at the characteristic sound speed. The introduction of friction to the system alters the dispersion relation as we show in Appendix A and leads to both subsonic and supersonic propagation of perturbations. Also the results of this section suggest that the evolution of the prestress into a critical state due to the superposed action of repeated ruptures help fine tune the rupture speed into the value observed here. For propagation in uniform prestress fields, with all material and frictional properties held constant, ruptures will propagate faster in higher stress levels. [See Appendix A.]

In the next few sections we discuss the system behavior in different system parameters regimes and possible implications for real faults behavior.

2.5 Effect of model parameters on size distribution of events:

The non-dimensional equation (2.4) reveals that the model behavior is controlled by three main parameters: the stiffness ratio (r), the strength of the velocity-weakening (v_c) and

the normalized plate loading parameter (γ). In this section we investigate the effect of varying each of these parameters independently on the size distribution of events generated in our simulations. We use chains of 10000 blocks and simulate the system for at least 50000 events.

2.5.1 Effect of stiffness ratio (r)

The spring block slider model has two groups of springs of different stiffness; the coil springs interconnecting the blocks (k_c) and the leaf springs connecting each block to the loading plate (k_l). The short range 1D elastic interaction is effective through the coil springs, whereas the leaf springs stiffness controls the amount of available strain energy to the system. The ratio of the coil spring to leaf spring stiffness (r) controls the proportion of small to large events. We expect that in the limit as "r" goes to infinity, the chain of blocks is to behave as a rigid bar and all events become system wide events. On the other hand, as "r" goes to zero, each individual block moves independently and all events become single block events. Another way to look at these asymptotics is through assessing the available strain energy for the system. Since in order to initiate rupture the static friction threshold needs to be exceeded, the strain energy available for any block through the leaf spring is inversely proportional to the leaf spring stiffness. As "r" goes to infinity, or equivalently as the leaf spring stiffness goes to zero, the available strain energy through the leaf spring becomes very large, leading to very large events. On the other hand as the ratio "r" goes to zero, or as the leaf spring stiffness goes to infinity, the available strain energy through the leaf spring becomes infinitely small, leading to single

block events. Hence we can expect an increase in the number of large events as the stiffness ratio "*r*" is increased. This is shown in Fig. (2.6) where the maximum event size, as well as the number of large events, increases as "*r*" increases. It is interesting to note that by tuning the "*r*" ratio, with other parameters kept fixed, we can obtain a nearly power law distribution for event lengths (r = 4).

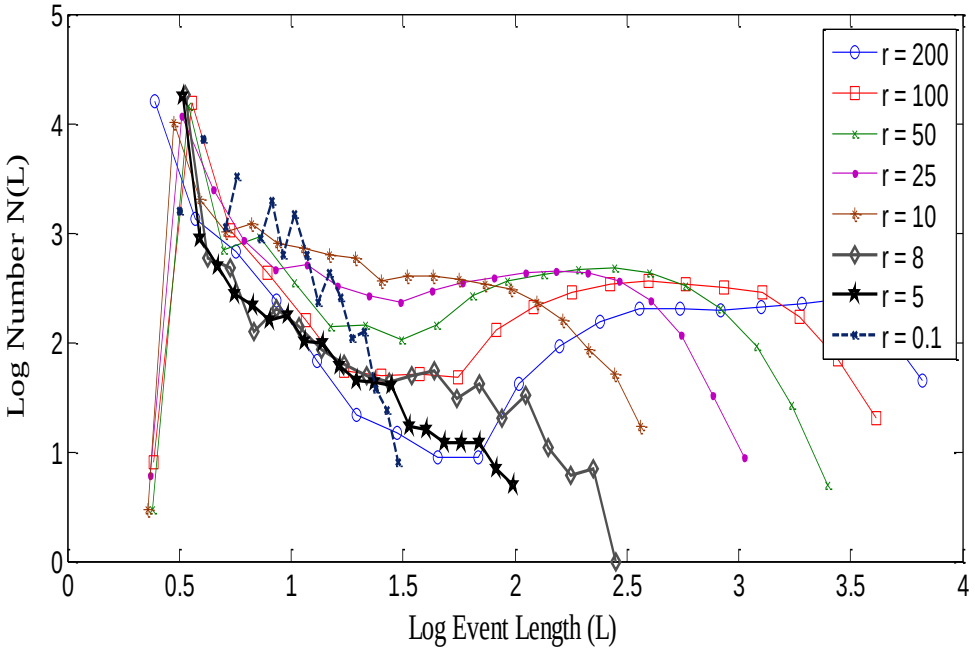

Fig. 2.6: Distribution of event lengths for different values of stiffness ratio "*r* " for ν_c = 0.01265 and $\gamma = 1.2\times10^{-7}$ The horizontal axis represents the size of the event measured by log the number of blocks which have moved in this event whereas the vertical axis represents log of the number of events having this length. As the stiffness ration is increased, the distribution changes from one which is dominated by small events (r =0.1) to one which includes an increased proportion of large events and larger maximum event sizes (r = 200). It is possible by tuning the "*r*" value, with the other model parameters kept fixed, to arrive at a distribution which is nearly power law (r ~5).

Another way to look at the effect of the increasing stiffness ratio on the distribution of event lengths is to look at the cumulative event size distribution. This is shown in Fig. (2.7) where the event length is plotted on the horizontal axis whereas, on the vertical axis, the number of events having a length greater than a given length is depicted. The trend previously shown in Fig. (2.6) is preserved here as well. One advantage of looking at the cumulative distribution is that it shows how the slopes of the linear part of the distributions compare to each other for different stiffness ratios [in an event moment distribution diagram that will correspond to the Gutenberg-Richter b-value]. It can be inferred from the figure that the linear part becomes steeper as the stiffness ratio decreases, reflecting an increased proportion of small events.

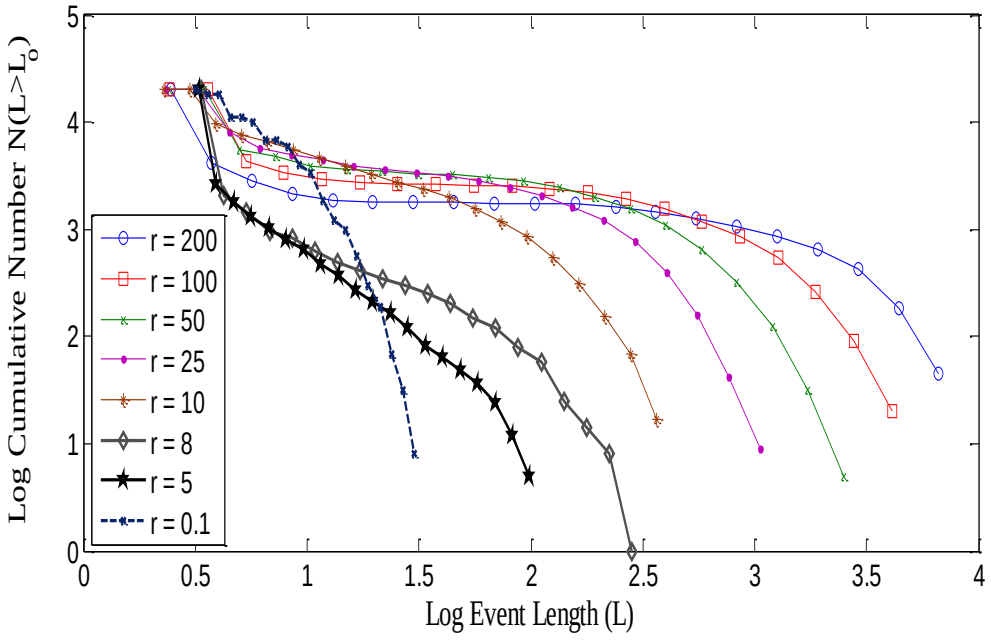

Fig. 2.7: Cumulative distribution of event lengths for different values of stiffness ratio "r" for ν_c = 0.079 and $\gamma = 1.2\times10^{-7}$ The horizontal axis represents the size of the event measured by log the number of blocks which

have moved in this event whereas the vertical axis represents log of the number of events having a length greater than a given value. The slopes of the linear part in different curves increase, in an absolute sense, as the stiffness ratio is reduced, reflecting an increase in the number of small events.

2.5.2. Effect of the velocity-weakening rate (v_c)

Another important parameter controlling the model behavior is the strength of the velocity-weakening in the friction law. This is measured in this study by the parameter $\boldsymbol{v_c}$ which gives the ratio of the rate of weakening in the dimensional form of the friction law to an intrinsic velocity of the slider that depends on the inertial and elastic properties of the system. We studied the influence of varying (v_c) on the size distribution of events but could not find a systematic trend. Figures (2.8) and (2.9) show an example of our results for two different stiffness ratio; r = 100 and r = 5 respectively. Previous studies on two-block models [Turcotte 1992, Erickson 2007] have indicated the existence of complicated Poincare maps with the system switching intermittently between periodicity and chaos as the velocity-weakening parameter (v_c) is varied. We expect that for multi-blocks systems, this switching from periodicity to chaos would translate itself into a non-systematic variation in the proportion of the small events to large events. Moreover, it should be noted that while (v_c) measures how fast the friction drops form its static value dynamically, it also measures how fast it re-strengthens as the rupture heals. The competing effects of weakening and healing also play a role in this observed complex dependence of the event size distribution on (v_c); stronger weakening should favor larger

events whereas faster healing may allow for the healing tail to catch up with the rupture front more quickly and hence leads to the arrest of rupture. The balance between those two factors will then control the ratio of small to large events in our model. It can be inferred from Fig. (2.8) that the general trend for the size distribution of the different values of v_c is essentially the same; it is that of a characteristic earthquake distribution and is analogous to the curve corresponding to r = 100 in Fig. (2.6). This suggests that the qualitative form of the event size distribution is controlled primarily by the stiffness ratio "r", for large values of "r", as the available strain energy for the system in this case is large enough to overwhelm the influence of other parameters. The weakening rate plays an increasingly important role, though, as "r" is decreased. This is shown in Fig. (2.9) where different values of v_c are used but for r = 5. This value of "r" is close to the value that corresponded to the nearly power law distribution in Fig. (2.6) . Nonetheless we observe that there are qualitative and quantitative differences in the event sizes distribution as v_c is varied. If we focus on the intermediate size range (events ranging between 10 -100 blocks), we would see that there is an excess in their number for values of v_c > 0.0316. It is also interesting to note that we can find a nearly power law distribution near v_c= 0.001265; this is different from the parameter set that yielded nearly power law size distribution in Fig. (2.6) [r = 5 and v_c = 0.01265]

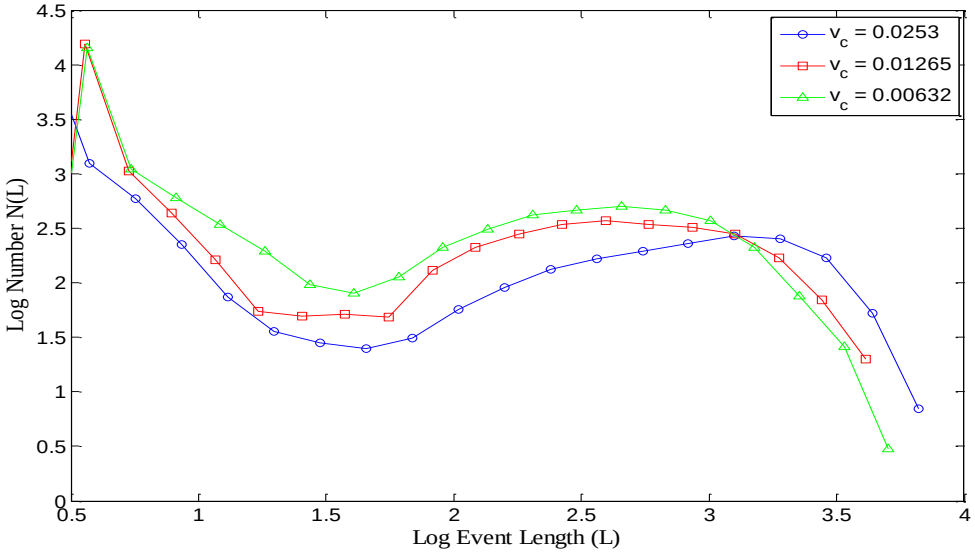

Fig. 2.8: Effect of varying the rate of weakening parameter on the event size distribution. The distributions depicted here represent a characteristic earthquake distribution, mainly controlled by the large stiffness ratio used (r=100), with second order variations due to the weakening rate.

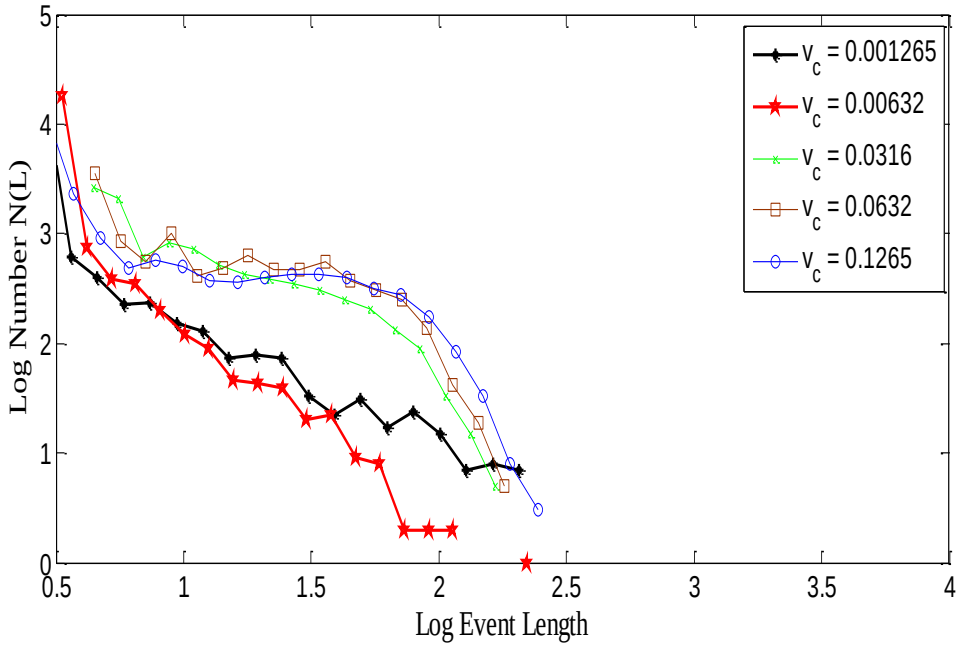

Fig.2.9: Effect of varying the rate of weakening parameter (v_c) on the event size distribution for a case with stiffness ratio r = 5. The strong influence of the frictional weakening is clear in the range of intermediate sized events (between 10-100 blocks). It is also shown that power law size distributions are attainable in the vicinity of v_c = 0.001265.

Similar to our investigation of the influence of the stiffness ratio, we can look at the cumulative event size distribution. Fig. (2.10) shows the cumulative event size distribution for r =100 and different values of v_c. As v_c decreases, the slope of the linear part increases reflecting an increase in the number of small events. However, the differences are very small.

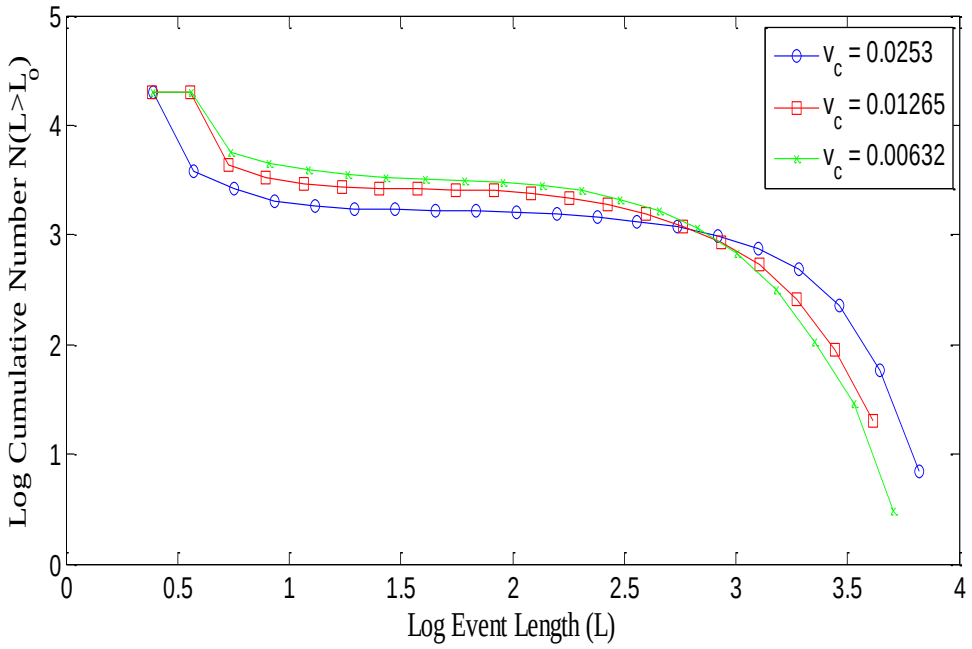

Fig. (2.10): Cumulative event size distribution for $r = 100$ and different values of v_c showing that as v_c decreases the number of small events slightly increases.

For r = 5, the cumulative event size distribution plotted in Fig. (2.11) confirms that a nearly power law distribution for event lengths is achieved at v_c = 0.001265. The dependence of the number of small events on v_c is, however, not that clear. The number of small events increases initially as v_c decreases. However, the system with v_c = 0.001265 has a smaller number of small events than the system with v_c = 0.00632. This complex dependence on v_c is, however, expected from the chaotic nature of our system.

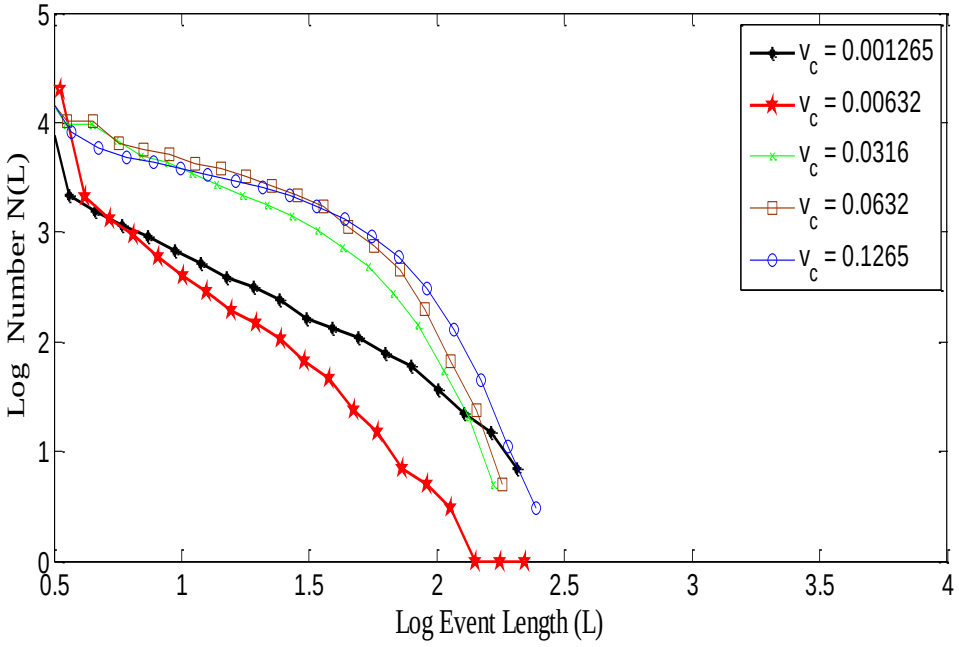

Fig. (2.11): Cumulative event size distribution for r =5 and different values of v_c showing a nearly power law event size distribution for v_c = 0.001265.

2.5.3. Effect of a normalized loading plate rate (γ)

The speed of the loading plate is the third parameter that controls the evolution of our system. Although we set the plate rate to zero in the inter-event period and started the next event in the sequence by adding the amount of stress required to just exceed the static friction threshold at the most stressed block, we let the plate rate assume a finite non- zero value during the dynamic event. In earthquake-like applications, the plate rate is typically orders of magnitude smaller than the average slip rate during the dynamic event. Nonetheless even when this is true, the variation of the loading plate rate may have a strong impact on the size distribution of events in our system. Figure (2.12) shows some results for the event size distribution when the normalized plate loading rate is increased

through five orders of magnitude. We note that the faster the loading plate speed, the larger the maximum event size and the larger the proportion of large events and vice versa. We also note that below a certain threshold, the event size distribution becomes insensitive to the plate loading rate. For the case in hand, we can see that the results for $\gamma = 1.2\times10^{-9}$ and $\gamma = 1.2\times10^{-7}$ are indistinguishable. Also, we can observe that a nearly power law event size distribution is achieved at $\gamma \approx 1.2\times10^{-7}$.[The other parameters are held at r = 8 and v_c=0.01265.] The cumulative event size distribution for various plate loading rates is shown in Fig. (2.13). Once again we can see that the slope of the linear part in those curves increases as the plate loading rate decreases, reflecting an increase in the number of small events. This shows that the faster we drive the system, the more probable it is to rupture a longer portion of the system, as in this case we can initiate ruptures at different points concurrently.

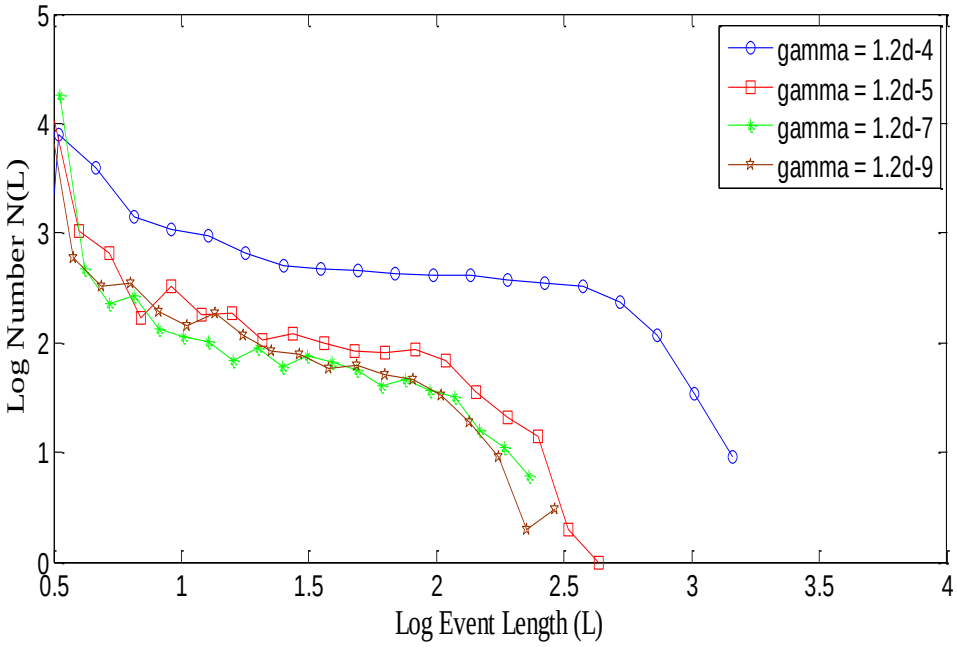

Fig. (2.12): Event size distribution for different values of loading plate normalized speed. The faster the loading plate is moving, the larger the maximum event size is and the larger the percentage of large events would be. By tuning the plate loading rate near $\gamma = 1.2 \times 10^{-7}$, and keeping the other parameters fixed [r = 8 and v_c=0.01265] , we can generate an almost power law event size distribution.

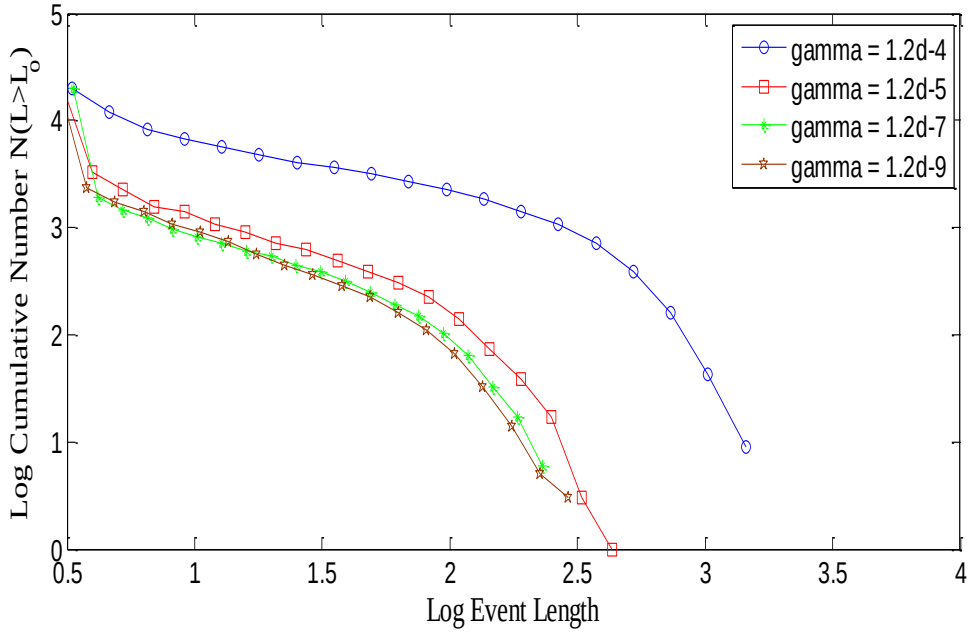

Fig. (2.13): Cumulative event size distribution for different values of loading plate normalized speed.

We conclude this section by noting that we were able to obtain power law size distributions for different combinations of model parameters (r, v_c, γ) This motivates us to hypothesize the following. If we imagine that our systems phase space is parameterized by the three parameters (r, v_c, γ) , we hypothesize that there exists a surface in this three dimensional space F(r, v_c, γ) = 0 for which combinations of parameters satisfying the surface equation would yield a nearly power law distribution.

The surface divides the phase space into two regions; one in which there is an increased proportion of large events and the other in which there is an increased proportion of small events. In the next sections we investigate the different properties of the systems that are consistent with the each of the distinct regimes of the event size distribution: the regime where large events dominate (Regime A), the nearly self-organized critical regime (Regime B) and the regime dominated by small events (Regime C).

2.6 Major characteristics of systems in regime A:

Systems operating in Regime A, according to our classification, are characterized by an increased number of large events. We pick a system with the following model parameters (r = 200, v_c = 0.01265 and $\gamma = 1.2\times10^{-7}$) as the representative candidate of this regime. In the following subsections we will discuss the major characteristics if this system, including the spatio-temporal complexity of the generated events, the spectral and statistical properties of the prestress, and the main characteristics of the slip distributions.

2.6.1 Event moment distribution and its spatio-temporal characterization

The spatio-temporal distribution of the events generated for the parameter values under consideration is shown in Fig. (2.14). It is clear that most of the events extend for more than 1000 blocks, with some even being system-wide events. Occasionally, small and intermediate size events are generated. However, an interesting observation is that the

small events are not confined only to the locations of arrest of large events but are to some extent sparsely distributed. Also small events seem to persist for some time and then disappear giving way to the propagation of larger ruptures. This kind of behavior is consistent with earthquake observations on mature faults.

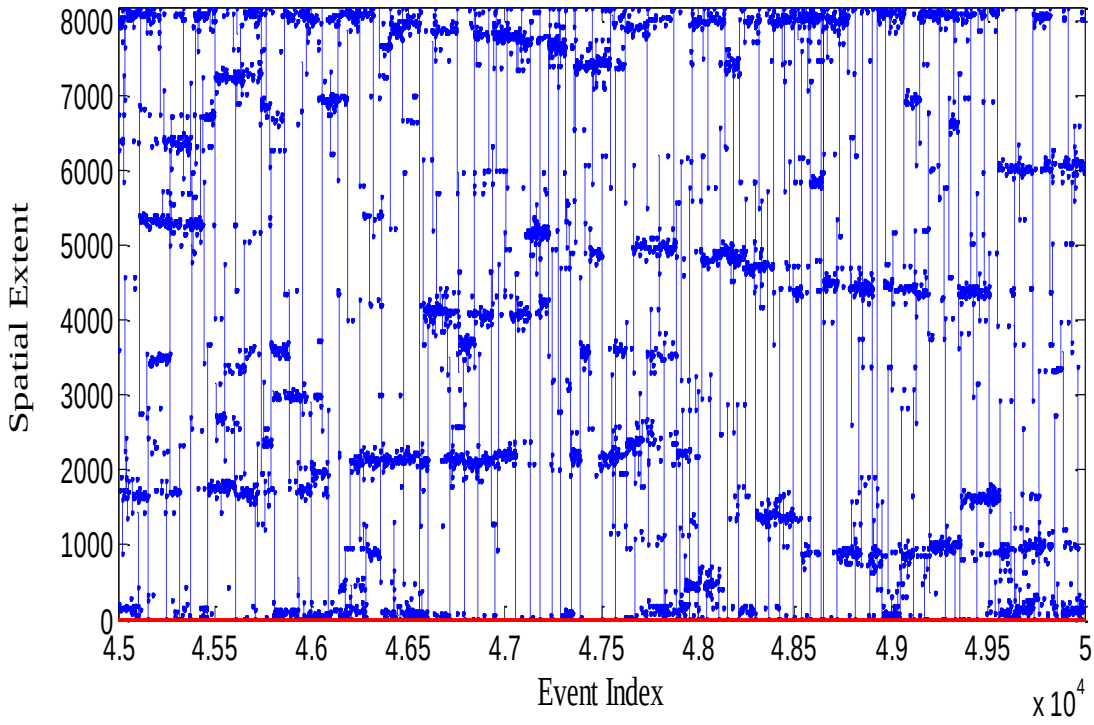

Fig. (2.14): Spatio-temporal distribution of events generated by a system with model parameters (r = 200, v_c = 0.01265 and $\gamma = 1.2 \times 10^{-7}$). The horizontal axis represents the event index while the vertical axis represents the event spatial extent. Each event is represented by a vertical line with the lower end representing the event starting location and the upper end representing the event arrest location. Most events span more than 1000 blocks but smaller

events are also generated. This is an example of a system dominated by large events and is consistent with the behavior of mature faults rupturing.

The event size distribution for this case is depicted in Fig. (2.15). The increased number of large events observed in Fig. (2.14) is reflected in the event moment statistics through the existence of a pronounced peak near event moments around M~1000. It can also be inferred from the figure that the small events have a power law distribution with a b-value close to 1.

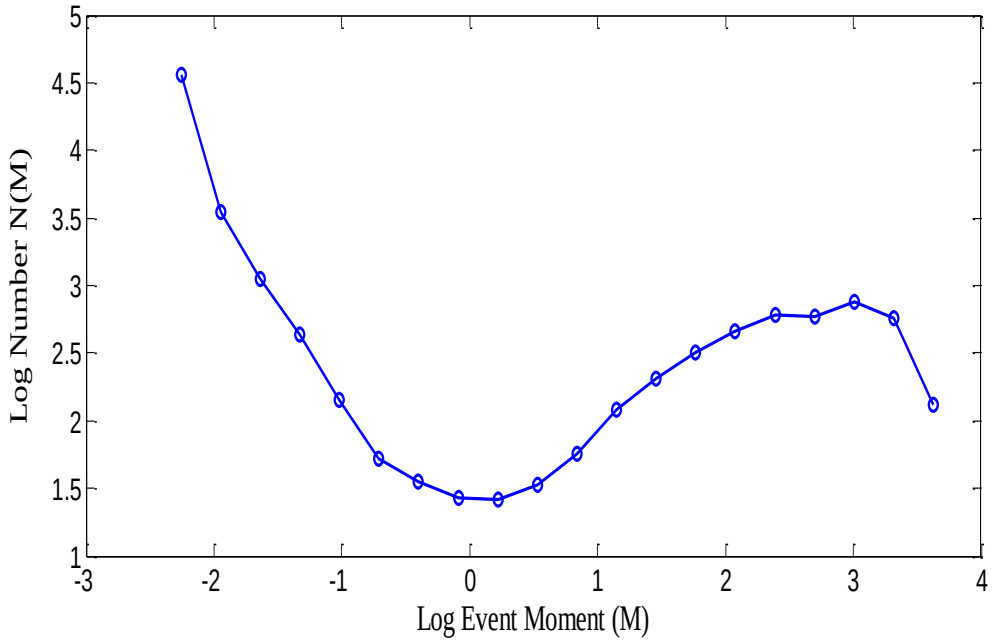

Fig. (2.15): Event moment distribution for a system dominated by large events. A pronounced peak, similar to that observed for characteristic earthquake models, exists near M~1000. The small event distribution on the other hand shows a power law behavior with b-value close to 1.

Concluding this subsection, we would like to discuss the statistics of event distribution in the time domain. Fig. (2.16) shows the distribution of the inter-event times for events spanning 1000 blocks or more.

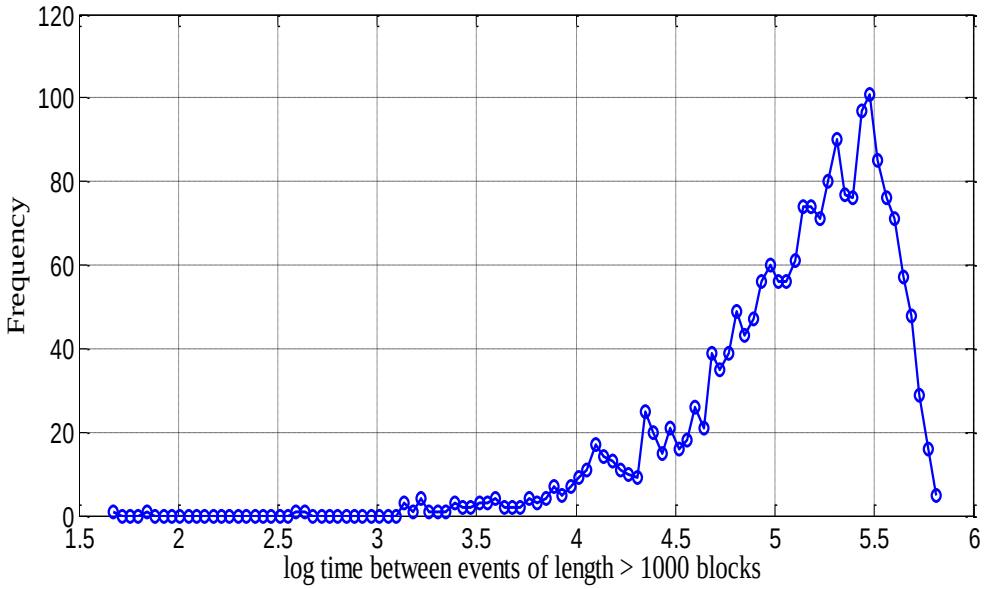

Fig. (2.16): Statistics of the inter-event time showing a peak at $dt = 10^{5.5}$

The inter-events time distribution shows a pronounced peak at $dt = 10^{5.5}$ showing a relatively characteristic long recurrence time. However, the peak is not very sharp allowing for some variability in the recurrence period; the standard deviation is of the order of $dt = 10^{4}$. The shallow tail of the distribution towards the shorter recurrence times reflects the increasingly smaller probability of having two large events separated by a very short period of time. This is analogous to the relatively long quiet times, where vigorous earthquake activity is missing, that we usually observe for mature faults such as San Andreas fault. Nonetheless we stress here that the large events we are getting in our

simulation, while showing some characteristic time behavior, are still spatio-temporally variable.

2.6.2- Statistical and spectral properties of the prestress:

In our simulations we usually start with an ordered state: homogeneous material and frictional properties and a prestress distribution that is uniform everywhere except for the intermediate ten blocks where it is increased to just above the static friction threshold in order to initiate the first rupture. Under the influence of the large number of repeated fractures that are, in general, of different sizes, as was discussed in the previous section, and of different slip distributions, the prestress distribution evolves into a heterogeneous one. The prestress distribution along the chain after 50,000 events is shown below in Fig. (2.17). We note that the overall value of the average prestress is low, of the order of 0.2 F_{st} ,and it is characterized by essentially a long wavelength variation due to the dominance of large sized events (events of length 1000 blocks or more). Nonetheless, the prestress distribution is still quite rough, with small-scale fluctuations, and spiky, possibly due to the influence of small and moderate sized events.

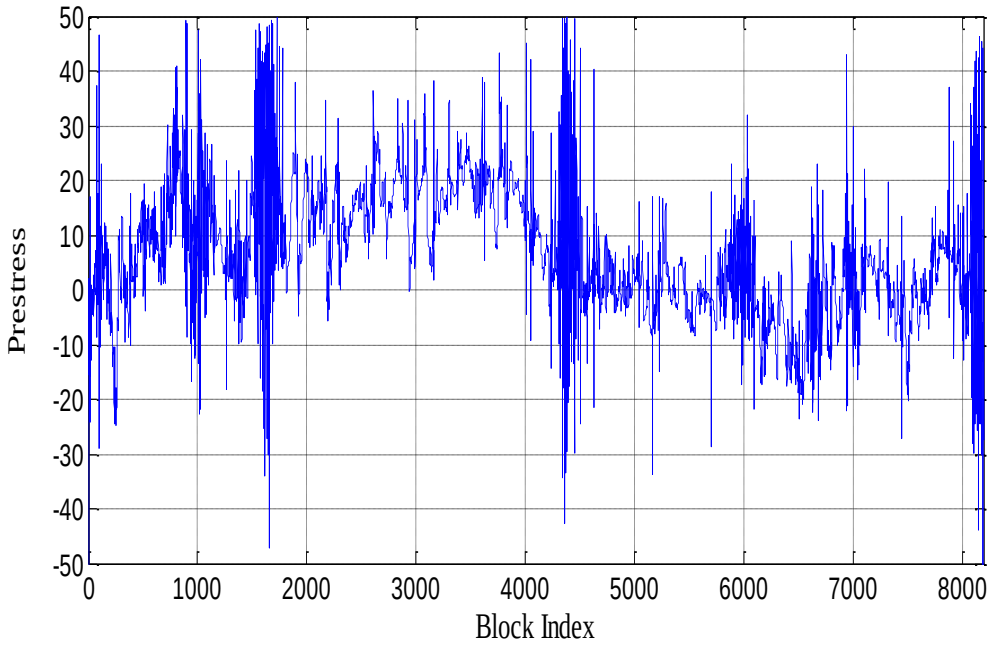

Fig. (2.17): Prestress distribution existing in the system with parameters r = 200, ν_c = 0.01265 and $\gamma = 1.2\times10^{-7}$ after 50000 events. Note that the prestress has both positive and negative values, with a quite long correlation length [the cross points with the zero axis are sparsely distributed.]

To assess the prestress distribution from a statistical point of view, we binned the stress values into a number of equally sized bins and counted the number of points occupying each bin. The result is shown in Fig. (2.18). The actual data set represented by the blue dots is best fitted with a Gaussian distribution. This is a consequence of the dominance of the large sized events, which tend to 1) smoothen the stress over long wavelengths, 2) let the system settle in a state with almost "characteristic" events, and 3) render the fluctuations by small and intermediate sized events of secondary significance. We think that this case might match the state of stress on mature major faults that have experienced kilometers of slip throughout their history and are hence expected to host relatively

smooth prestress distributions, favoring in turn the dominance of large events and characteristic earthquakes.

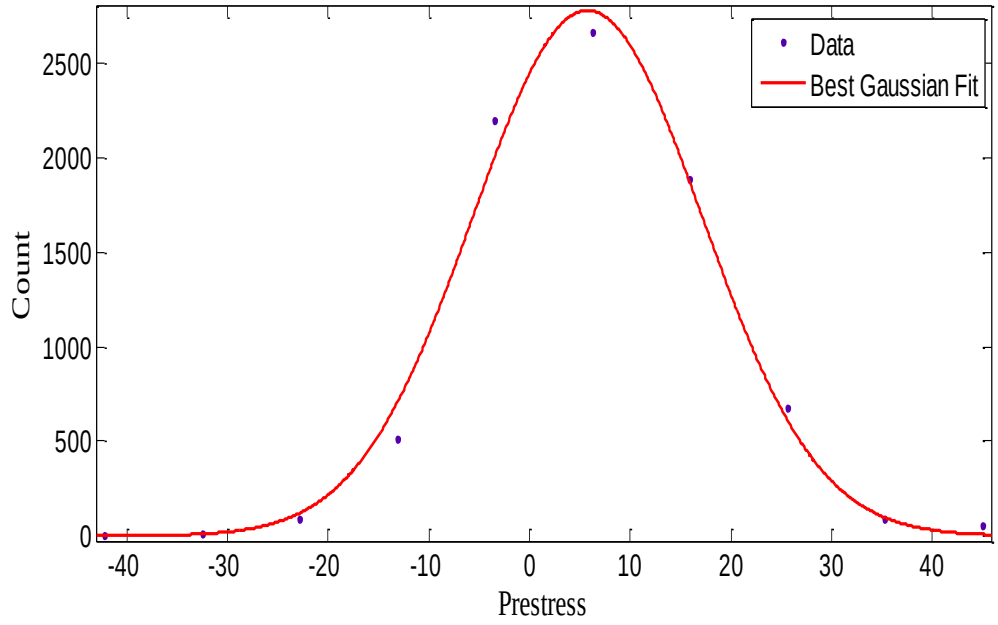

Fig. (2.18): Statistics of the prestress distribution shown in Fig.(2.17). The blue dots represent the result of binning the actual data while the red curve is its best fit. The data is well fitted with a Gaussian distribution.

Next we plot the amplitude of the Fourier transform of the evolved prestress distribution. Figure (2.19) shows that the spectrum is almost a power law except at high frequencies where a change in scaling occurs. This occurs near $f = 10^{2.5}$, and reflects the existence of a characteristic length scale introduced by the leaf springs as was discussed in Section II. The increased high frequency content is mainly attributed to the small-scale stress fluctuations and spikes left at the locations of rupture arrest which were not swept by large events. However, the overall spectrum can be fit fairly well with a straight line of

slope ~ -0.5, reflecting the relative smoothness of the prestress and the dominance of long wavelength variations.

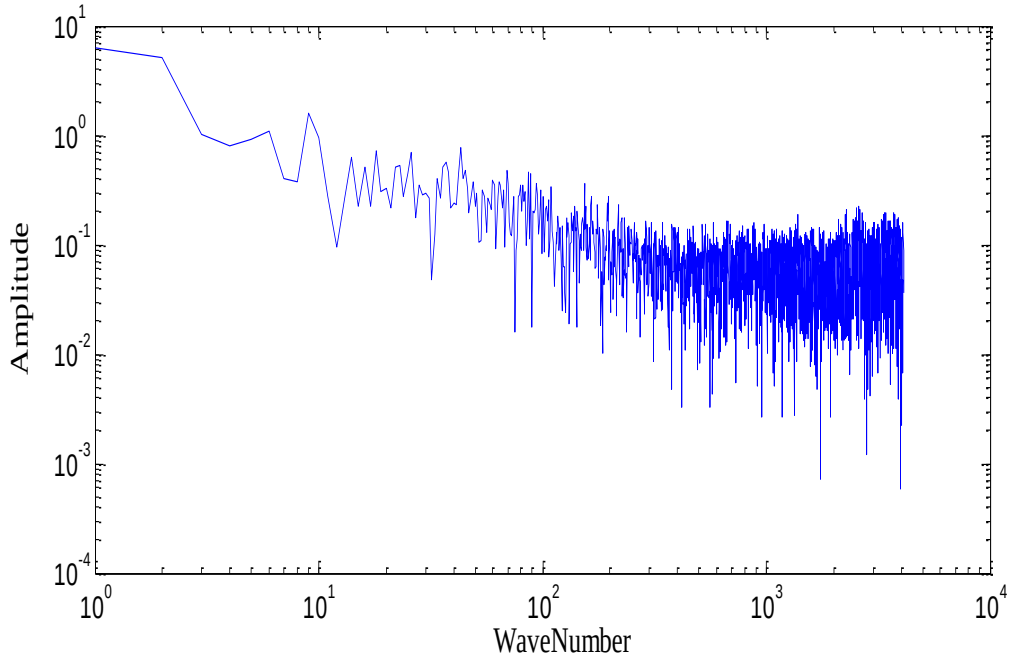

Fig. (2.19): The Fourier transform amplitude of the evolved prestress as a function of wavenumber showing a nearly power law behavior except close to high frequencies. The slope of the spectrum is nearly -0.5

2.6.3Slip Characteristics of the generated events

Looking into the slip distributions for various events generated by the spring block model, when operating in the regime dominated by large ruptures, gives further insight into the complexity of our system. While the prestress complexity cannot be directy inferred as we cannot currently make measurements of prestress variations as a function of space along real faults, slip distributions have the advantage of being possibly inferred

from seismic inversions and accordingly slip complexity from models can be checked against slip maps from inversion work.

The slip distribution in one of the events which spans more than 1000 blocks is shown in Fig. (2.20). This is a bilateral event where the rupture nucleated near block no. 1800 and propagated in both directions. There is a deficiency in the slip near the nucleation zone compared to the slip outside it; this is one feature of pulse like ruptures. The slip is also quite heterogeneous over most of the rupture length; a natural consequence of the prestress heterogeneity and the relatively narrow slip pulses propagating in the system. Figure (2.21) shows the amplitude spectrum of the slip distribution for the event depicted in Fig. (2.20). The amplitude spectrum is nearly a power law with a spectral slope in the wavenumber domain close to -2. Heterogeneous slip distributions with a k-2 spectral decay have been abundantly found in seismic inversion. A k-2 spectral decay is also consistent with Andrew's model [1981] where he suggested that such decay is required for the validity of the ω-squared model of high frequency radiation.

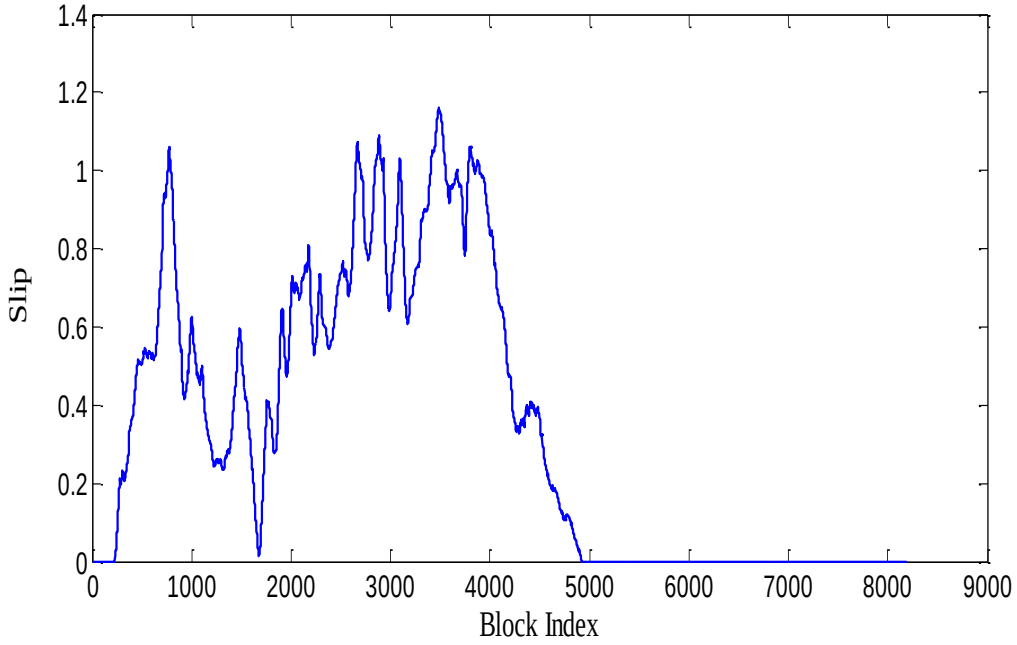

Fig. (2.20): Slip distribution for one of the events generated by the spring block model for model parameters (r = 200, v_c=0.01265 and $\gamma = 1.2\times10^{-7}$). Note the spatial heterogeneity of the slip distribution

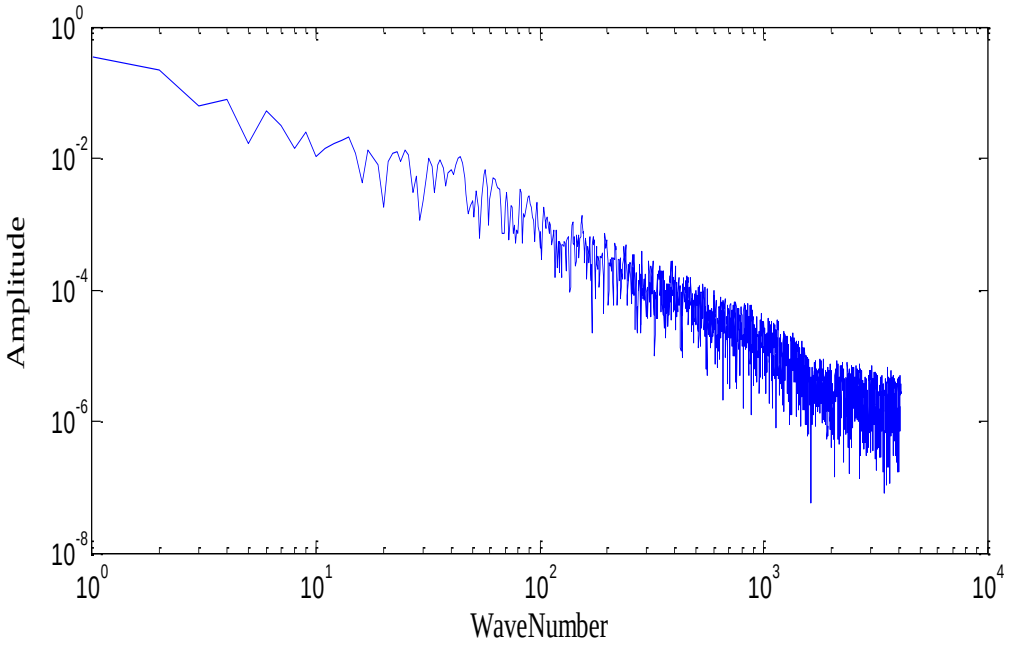

Fig. (2.21): The Fourier transform amplitude of the evolved prestress as a function of wavenumber showing a nearly power law behavior with a slope close to -2.

Finally we looked at the statistical properties of the slip. We considered a large enough sequence of events and binned the slip values obtained from them into a number of equally sized bins and count the number of points occupying each bin. The result is plotted in Fig. (2.22). The blue dots represent the actual data point from the simulations while the red curve represents the best fit for the data. The data is well fitted by a Gaussian distribution with mean ~ 0.45 and standard deviation ~ 0.35

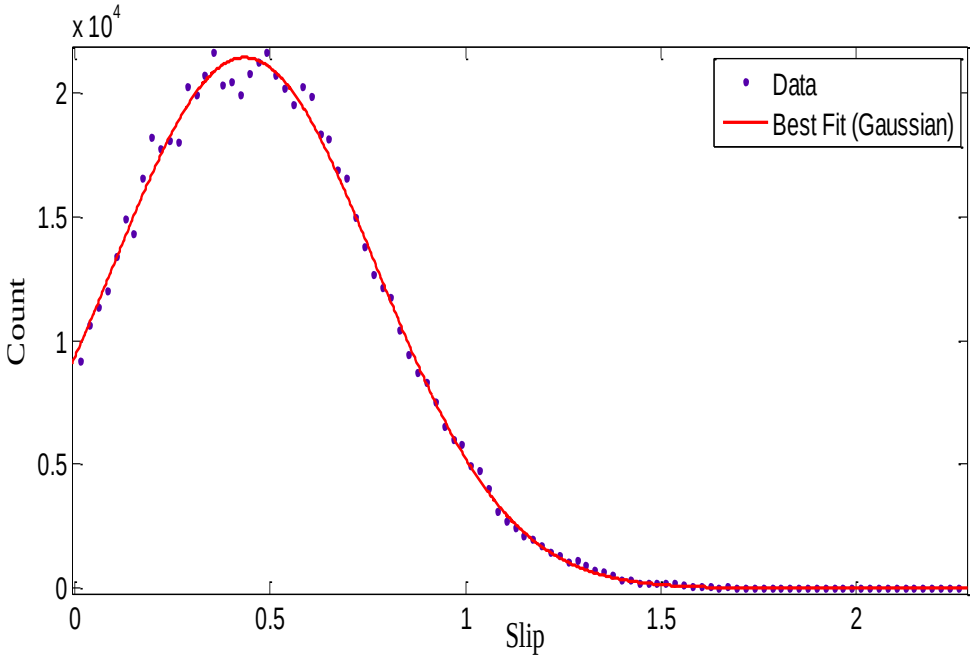

Fig. (2.22): Statistics of the slip distribution in systems dominated by large events. The slip data can be fit fairly well with a Gaussian distribution with a non-zero mean

2.7- Major characteristics of systems in regime B:

Systems operating in Regime A, according to our classification, are characterized by having event size distributions close to being power laws, with the existence of both large and small events but without the dominance of either of them.. We pick a system with the following model parameters (r = 10, v_c = 0.01265 and $\gamma = 1.2\times10^{-7}$) as the representative candidate of this regime. In the following subsections we discuss the major characteristics of this system, including the spatio-temporal complexity of the generated events, the spectral and statistical properties of the prestress and the main characteristics of the slip distributions.

2.7.1 Event moment distribution and its spatio-temporal characterization:

The spatio-temporal distribution of the events generated for the parameter values under consideration is shown in Fig. (2.23). The system is in a very disordered state with events of different sizes being generated and with an increased proportion of small and intermediate sized events when compared to systems in Regime A. Also the small events are more chaotically distributed here than for the systems dominated by large events, reflecting a possibly increasing heterogeneity in the underlying prestress distribution. Occasionally in such systems, events can go and span more than several hundreds of blocks. These large events are also chaotically distributed in space and time with no signature of apparent periodicity such as the one that could be inferred from Fig. (2.12).

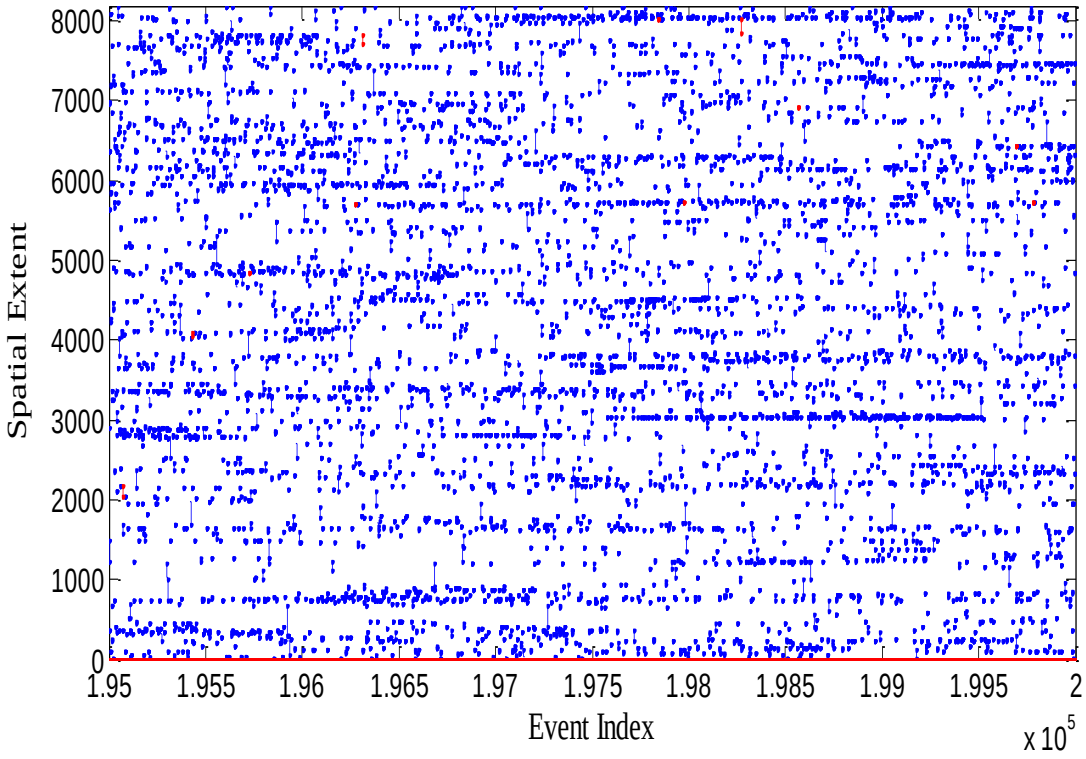

Fig. (2.23): Spatio-temporal distribution of events generated by a Regime-B system with model parameters (r = 10, ν_c = 0.01265 and $\gamma = 1.2\times10^{-7}$). The horizontal axis represents the event index while the vertical axis represents the event spatial extent. Each event is represented by a vertical line with the lower end representing the event starting location whereas the upper end represents the event arrest location. Events of different sizes are chaotically generated and distributed.

The event size distribution for this case is depicted in Fig. (2.24). The characteristic peak observed in Fig. (2.13) for systems in Regime A is absent here showing that large events no longer dominate the event size distribution. Most of the distribution in this case can be fit with a straight line of slope ~-0.4. The larger events part [events with a moment

greater than 100], however, rapidly decays with a b-value close to -2. The maximum event moment attained here is almost 300 units.

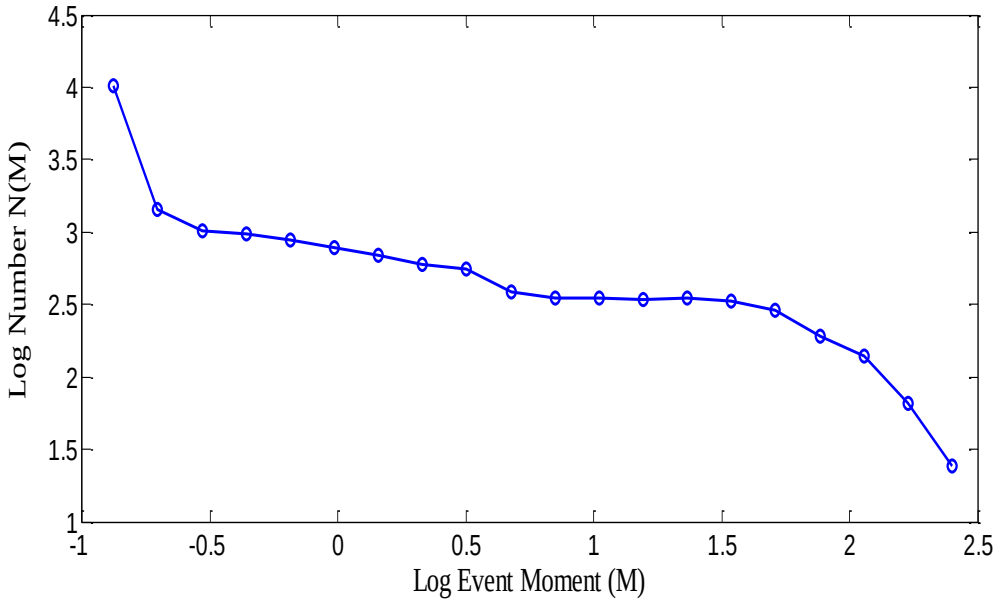

Fig. (2.24): Event Moment distribution for a system in Regime-B. Unlike systems in Regime-A, no characteristic peaks are observed and the distribution can be fit along most of it by a straight line with a slope of -0.4. Larger events tend to have a larger b-value close to 2.

Finally, the distribution of the inter-event times is shown in Fig. (2.25).

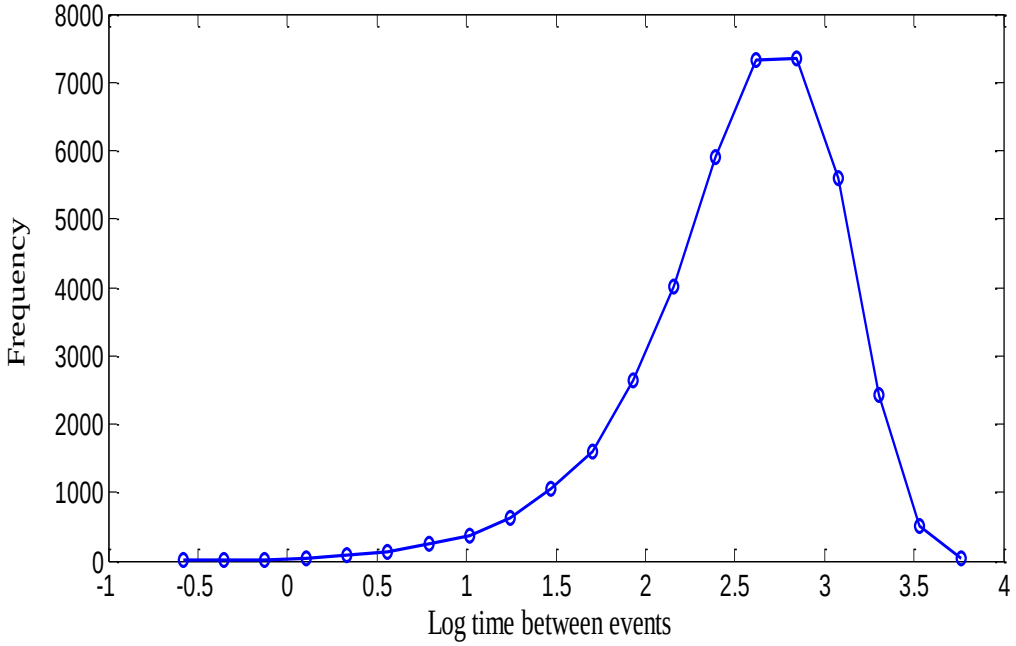

Fig. (2.25): Statistics of inter-event times for a Regime-B system showing a broad peak around $dt = 10^{2.75}$ and a heavy tail towards shorter recurrence times.

The distribution has a broad peak centered at $dt = 10^{2.75}$ and a relatively heavy tail towards shorter inter-event time values. Those characteristics reflect that there is no strong periodicity in the generated pattern of events when compare to systems in Regime A; the events here are more randomly distributed. Also the inter-event times here are on average 2 orders of magnitude less than the inter-event times recorded for large events in Regime A, reflecting that systems in this regime are more prone to frequent rupture activities. We think that Regime B systems might be a good qualitative model for immature faults where an increased number of small and intermediate sized events are generated.

2.7.2 Statistical and spectral properties of the evolving prestress:

The evolved prestress distribution after 200,000 events is shown in Fig. (2.26). When compared to the one shown in Fig. (2.16) for a system in Regime A, it is clear that the prestress distribution shown here is more heterogeneous; it has more spikes and the long wavelength variation characteristic has diminished, reflecting a shorter correlation length The overall average value of the prestress is still low but its variance is larger than the Regime A case, allowing for the arrest of an increased number of events before developing into larger ones.

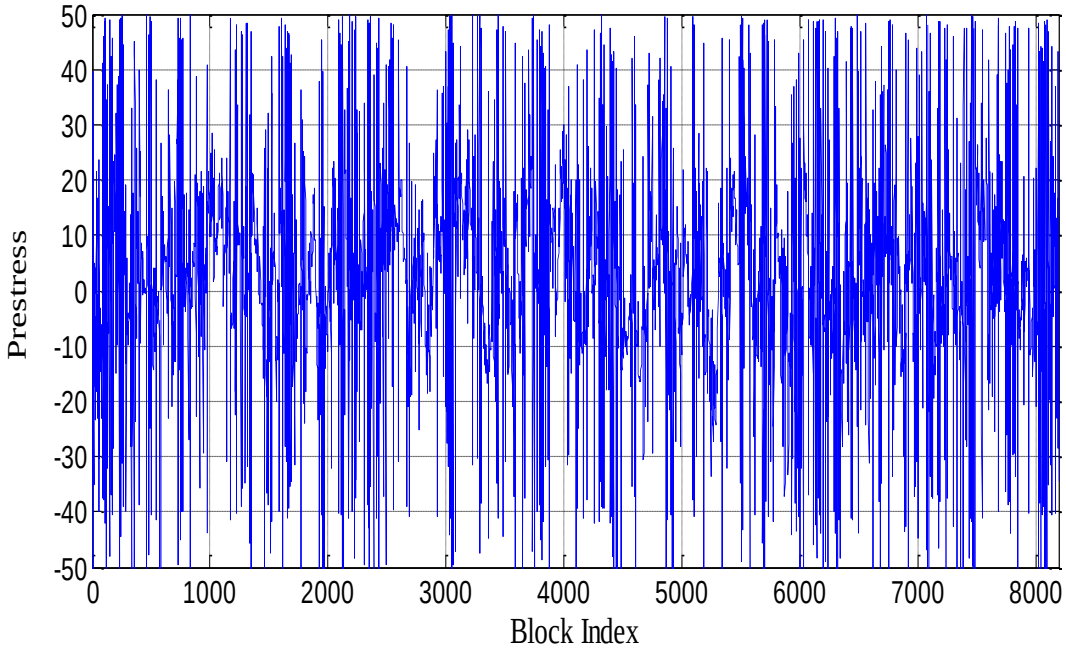

Fig. (2.26): Prestress distribution existing in the system with parameters r = 10, v_c = 0.01265 and $\gamma = 1.2\times10^{-7}$ after 200,000 events. Note that the prestress has both positive and negative values. The prestress is more

heterogeneous and spiky than the case shown if Fig [15] reflecting the presence of an increased number of small and intermediate sized events.

The statistics of the evolved prestress is shown in Fig. (2.27). As with the Regime A case, shown in Fig.(2.17) we binned the prestress into equally sized bins and counted the number of stress points occupying each bin. The result is similar to the one shown in Fig. (2.17) except for one very important difference. The data set is fit almost everywhere with a Gaussian curve except near the tails where there is a clear deviation from the Gaussian character. This signals the increased role played by the intermediate and small sized events which produce an increased number of stress spikes corresponding to their arrest locations and lead to an increased number of points near the threshold of failure. Figure (2.27) suggests that the prestress statistics in this case can be better described by a non-Gaussian distribution (e.g. Lavallee et al. 2007). Determining the exact nature of the distribution is certainly important, but what is more important is realizing that it is essentially heavy tailed and non-Gaussian.

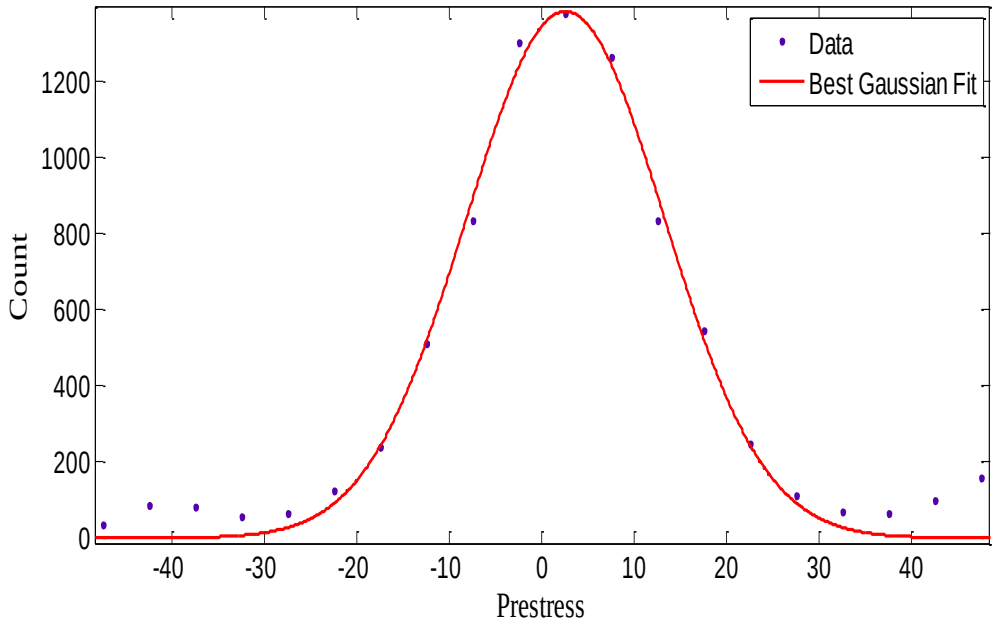

Fig. (2.27): Statistics of the prestress distribution shown in Fig. (2.26). The blue dots represent the result of binning the actual data while the red curve is its best fit Gaussian curve. There is a clear deviation from the Gaussian distribution near the distribution tail, indicating that the data are better fit by heavy tailed non-Gaussian statistics.

The amplitude of the Fourier transformed prestress is plotted in Fig. (2.28). The distribution is still nearly power law at long and intermediate wavelengths but there is a pronounced breaking in the scaling near the high frequencies. The increased high frequency content in this case, when compared to the stress spectrum in Fig. (2.18), is a direct consequence of the increased number of spikes in the real space prestress distribution due to the increased number of small and intermediate sized events.

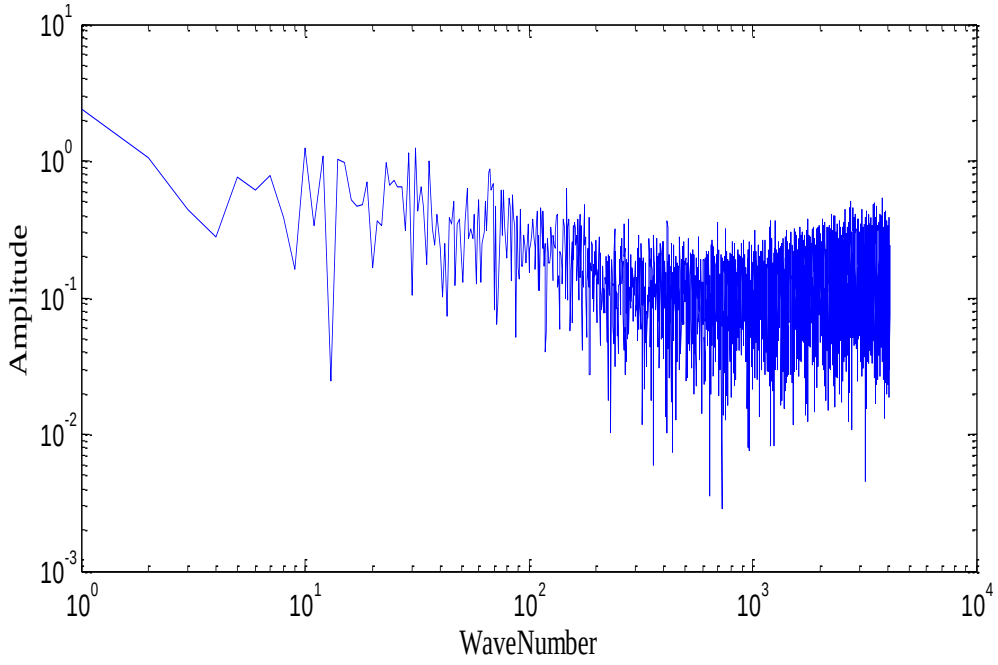

Fig. (2.28): The Fourier transform amplitude of the evolved prestress as a function of wavenumber showing a breaking in power law scaling near intermediate and high frequencies. See text for explanation.

2.7.3 Slip characteristics of the generated events

The slip distribution in one of the events which spans more than 50 blocks is shown in Fig.(2.29). This is a bilateral event where the rupture nucleated near block no. 3080 and propagated in both directions. The slip starts small in the nucleation zone and then increases outside it. As the rupture propagates it becomes influenced by the prestress distribution and starts to wiggle, showing decreasing and increasing patterns. The slip is quite heterogeneous over most of the rupture length with increased fluctuations on the

small scale. This is a natural consequence of the increased prestress heterogeneity on the small scale, and the narrow slip pulses propagating in the system.

Figure (2.30) shows the corresponding amplitude spectrum of this slip distribution. The amplitude spectrum is nearly a power law with a spectral slope in wavenumber domain close to -1. This is shallower than the slope observed for the slip spectrum in Regime A events shown in Fig. (2.21), reflecting the increased high frequency contribution.

We conclude this section by looking at the statistical properties of the spatial distribution of slip. We considered a large enough sequence of events that span longer than 50 blocks, binned the slip values obtained from them into a number of equally sized bins and then counted the number of points occupying each bin. The result is plotted in Fig. (2.31). The blue dots represent the actual data points from the simulations. A Gaussian distribution can only fit fairly well the intermediate range of values as well as the extreme tail behavior. However there is a clear non-Gaussian behavior for the slip values, ranging between .8 and 1.4 as well as values near the zero end. This suggests that a Gaussian distribution cannot satisfactorily describe the slip statistics for systems in Regime B which are characterized by non-Gaussian prestress statistics and nearly power law event size distribution.

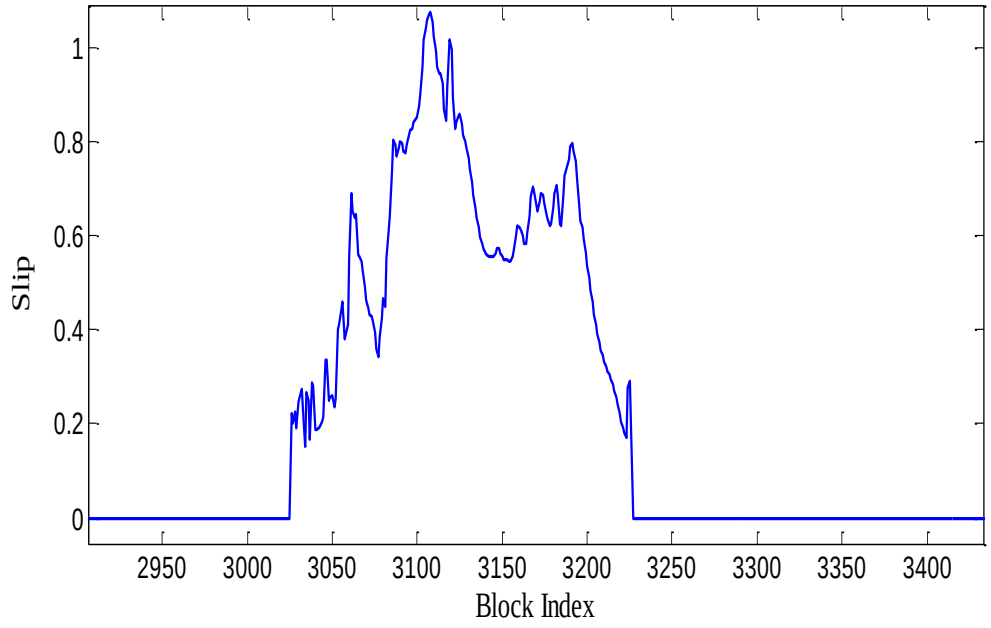

Fig.(2.29): Slip distribution for one of the events generated by the spring block model for model parameters (r =10, v_c=0.01265 and $\gamma = 1.2\times10^{-7}$). Note the increased fluctuation at the short wavelength scale.

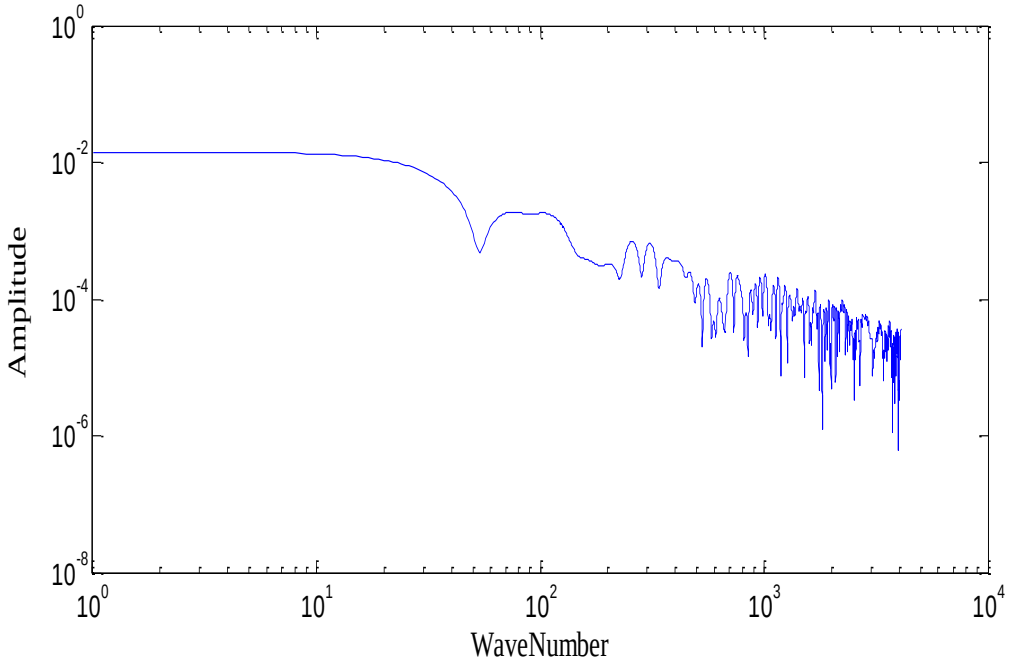

Fig.(2.30): The Fourier transform amplitude of the evolved prestress as a function of wavenumber showing a nearly power law behavior with a slope close to -1 in the high wavenumber regime.

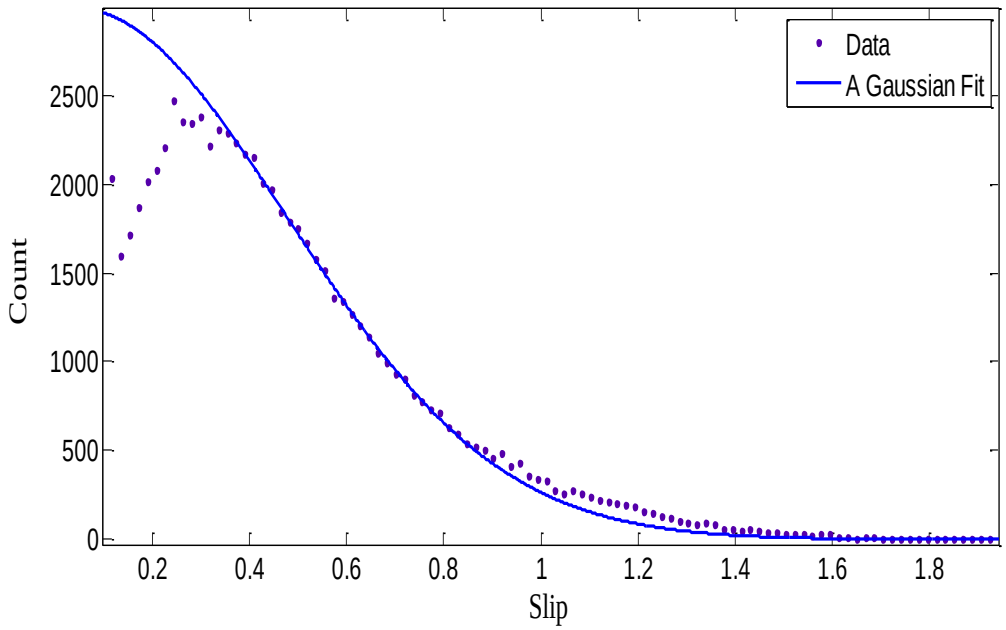

Fig.(2.31): Statistics of the slip distribution in systems dominated by large events. The slip data can be fit fairly well with a Gaussian distribution only for intermediate slip values. A more complicated non-Gaussian distribution is required to fit the whole distribution.

2.8. Major characteristics of systems in regime C

Systems operating in Regime C, according to our classification, are characterized by an increased number of small events and almost the complete absence of events spanning more than a few tens of blocks. We pick a system with the following model parameters (r = 0.1, v_c = 0.01265 and $\gamma = 1.2\times10^{-7}$) as the representative candidate of this regime.

We follow the same drill as in the previous two sections; we discuss the major characteristics of this system including its spatio-temporal complexity, the properties of the evolving prestress and the main characteristics of the associated displacement field.

2.8.1 Event moment distribution and its spatio-temporal characterization

The spatio-temporal distribution of the events generated for the parameter values under consideration is shown in Fig.(2.32). In this limit of very small stiffness ratio values, the system has limited available strain energy through the stiff leaf springs and poor communication along the blocks through the compliant coil springs. This prevents events from growing beyond a few tens of blocks and renders most of the events of length less than ten blocks. The main mode of rupture for this system turns out to be that of two small ruptures occurring simultaneously and symmetrically along the chain. Those two ruptures propagate in opposite directions until they sweep the whole chain length. At this end, the system is recharged by the loading plate and a new, similar, cycle is initiated near the chain center. This very nearly periodic behavior reflects that the system stays in a nearly ordered state and does not go chaotic as in the cases of Regimes A and B. What prevents us from labeling the system as completely periodic is the fact that when we look closely at the event size distribution, shown in Fig. (2.33), and the inter-event time statistics, shown in Fig. (2.34), we find some variability. However this variability is much less and incomparable to the variations observed in the previously studied regimes.

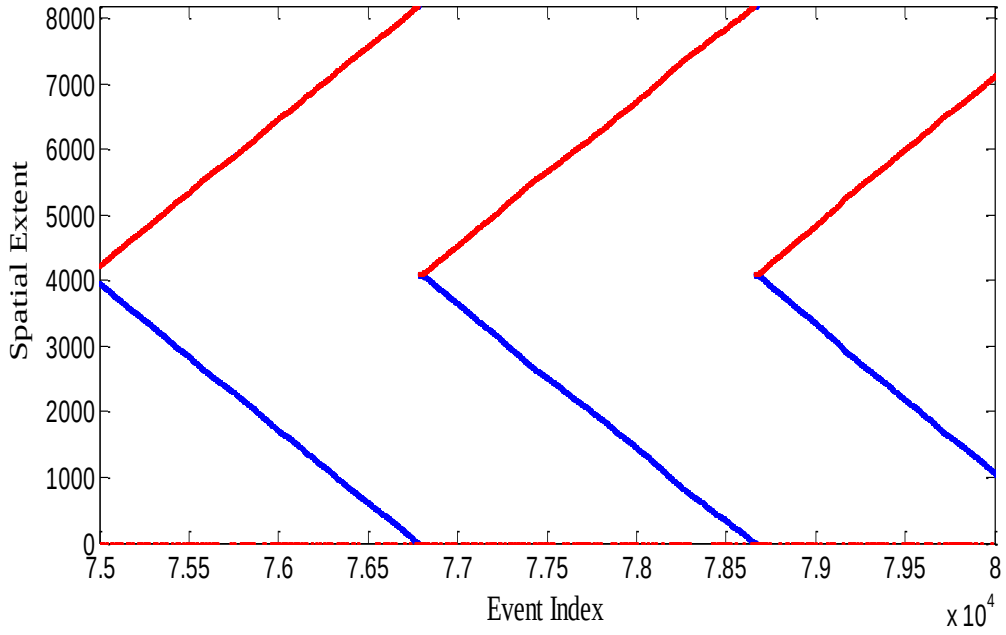

Fig.(2.32): Spatio-temporal distribution of events generated by a Regime C system with model parameters (r = 0.1, r_c = 0.01265 and $\gamma = 1.2\times10^{-7}$). The horizontal axis represents the event index while the vertical axis represents the event spatial extent. Each event is represented by a vertical line, with the lower end representing the event starting location and the upper end representing the event arrest location. Since events are very small, they appear as dots on this scale. We observe that two events are generated simultaneously and propagate in opposite directions: the blue one is propagates to the right while the red one is propagating to the left. The systems behavior is almost replicated in identical cycles. A full cycle shown above would correspond to event indices between 77000 and 78600.

The event moment distribution for this system is shown in Fig. (2.33). The event moments range spans only one order of magnitude. The distribution is almost a power law with a b-value that is close to 3.2

Finally the inter-event time distribution is shown in Fig. (2.34). The distribution shows a very sharp peak near $dt = 0.1$ which decays very quickly such that the possibility of having longer recurrence times is practically zero. This sharp localized peak reflects the nearly periodic behavior of our system. The short recurrence time also indicates that the system is continuously generating events. However, these events are small in magnitude and propagate much slower than those depicted in Regimes A and B. [As discussed in the section on rupture speed, ruptures propagate nearly at the characteristic sound speed which depends on the coil spring stiffness. For Regime C systems, the coil springs are very compliant and consequently the rupture speed is very low.] This leads us to hypothesize that this systems can be representative of creeping faults where faults displace in a caterpillar-like motion with creep-like events propagating in opposite directions.

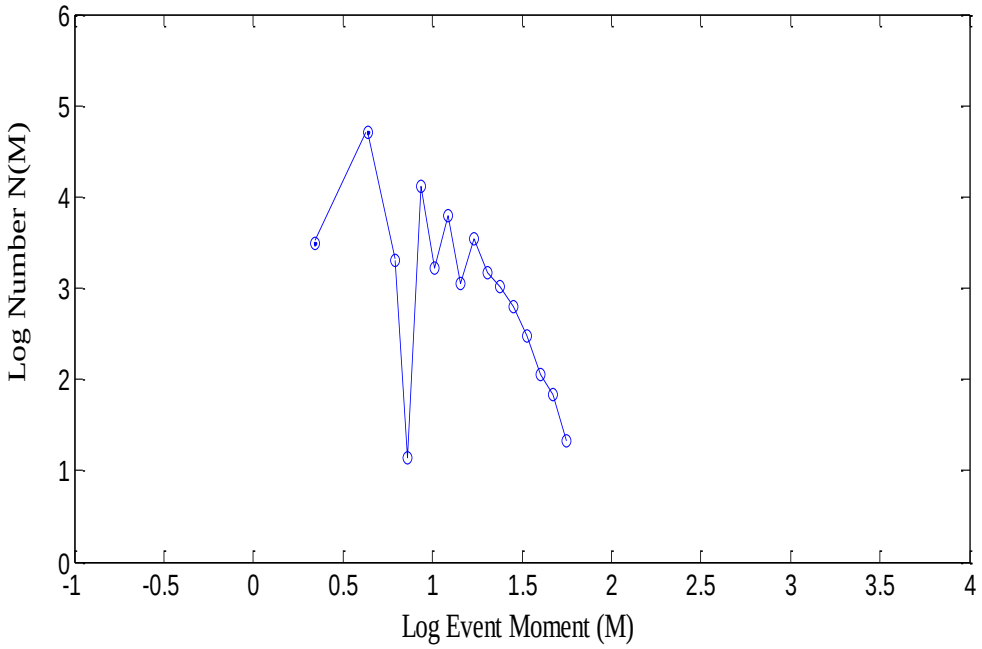

Fig. (2.33): Event moment distribution for a system in Regime C. Unlike systems in Regimes A or B, only small events are generated and the b-value for this distribution is close to 3.2.

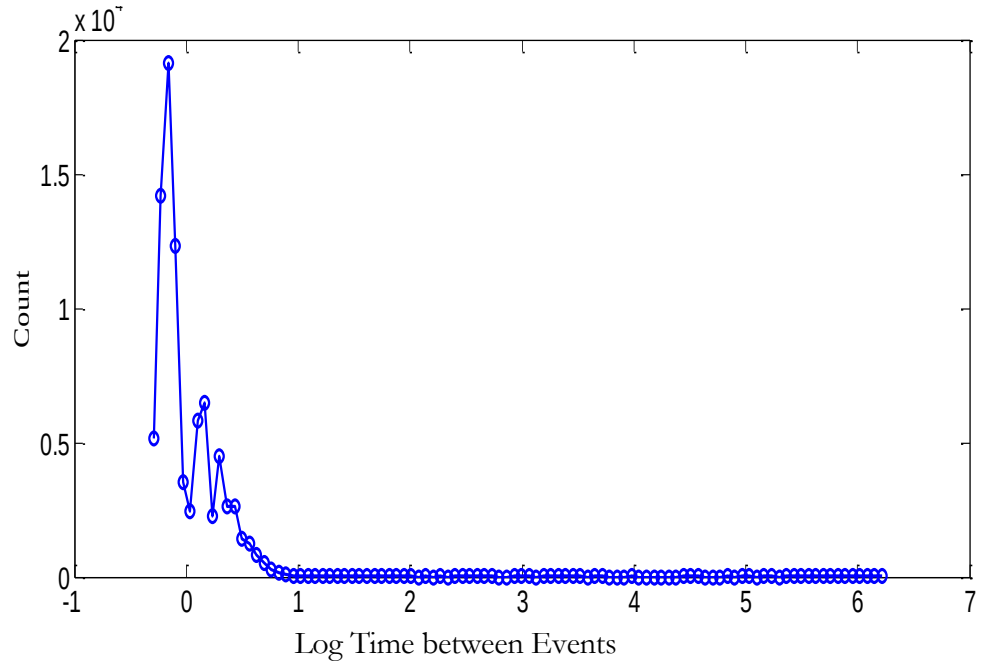

Fig. (2.34): The inter-event time distribution for the events generated in a Regime C systems sowing a very sharp peak reflecting a strong nearly periodic signature.

2.8.2- Properties of the evolving prestress:

The evolved prestress distribution after 200,000 events is shown in Fig. (2.35). The prestress is very regular and can be generated by pasting piecewise constant functions together. The snapshot of the prestress shown corresponds to a given location of the propagating events. (These locations correspond to the two positions of the steep variation in the prestress.) At another time, the propagating events will have moved to other locations and the position of the steep variations in the prestress will change accordingly. Nonetheless the prestress will conserve its general characteristic: a union of piecewise constant functions.

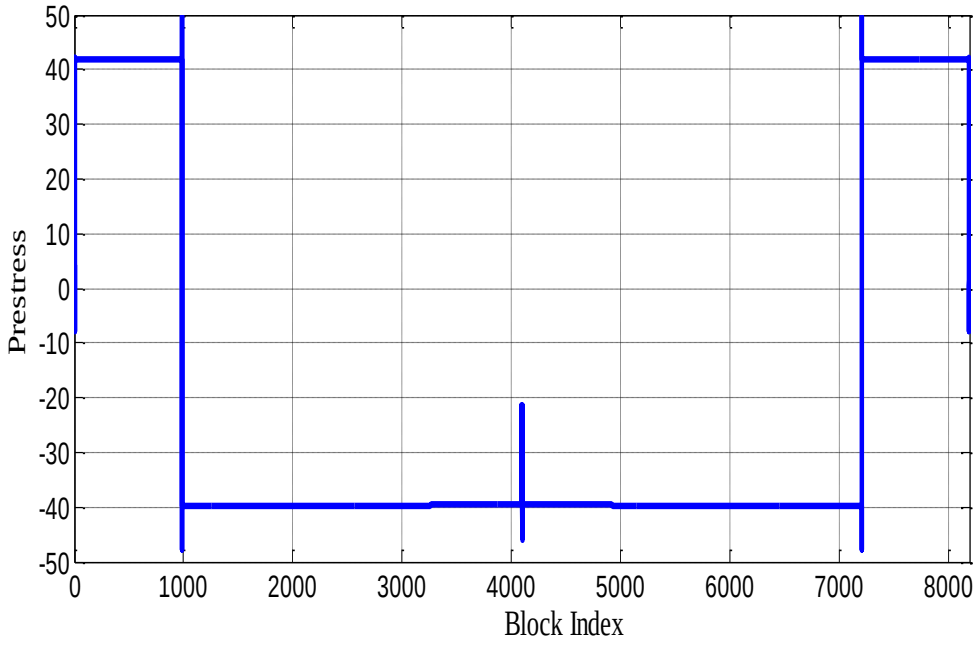

Fig.(2.35): Prestress distribution existing in the system with parameters r =0.1, v_c = 0.01265 and $\gamma = 1.2\times10^{-7}$ after 50,000 events. The prestress is basically a union of piecewise constant functions reflecting the fairly ordered state the system has settled in.

Since the prestress distribution shown in Fig. (2.35) is almost deterministic and can be approximated by a set of piecewise constant functions, characterizing either the statistical properties of the prestress or its spectral properties will be of little value. Accordingly we bypass this step for the system in hand and move on to characterize the generated displacement field.

2.8.3 Slip characteristics of the generated events:

Since most of the events generated by our model in the Regime C case span less than 10 blocks, they are not long enough to qualify for a systematic statistical study. Accordingly, in this subsection we do not look at the statistical or spectral properties of the generated slip distributions. Rather we looked at the evolution of the average displacement as a function of the event index. This is shown in Fig. (2.36) where the average displacement after each event is recorded and plotted on the vertical axis. The average displacement evolution is very well fitted by a straight line with slight variability. This indicates that the rate of displacement accumulation is nearly constant and almost independent of the event size. This linear trend in the cumulative displacement is analogous to the

displacement behavior recorded for real faults along their creeping sections.

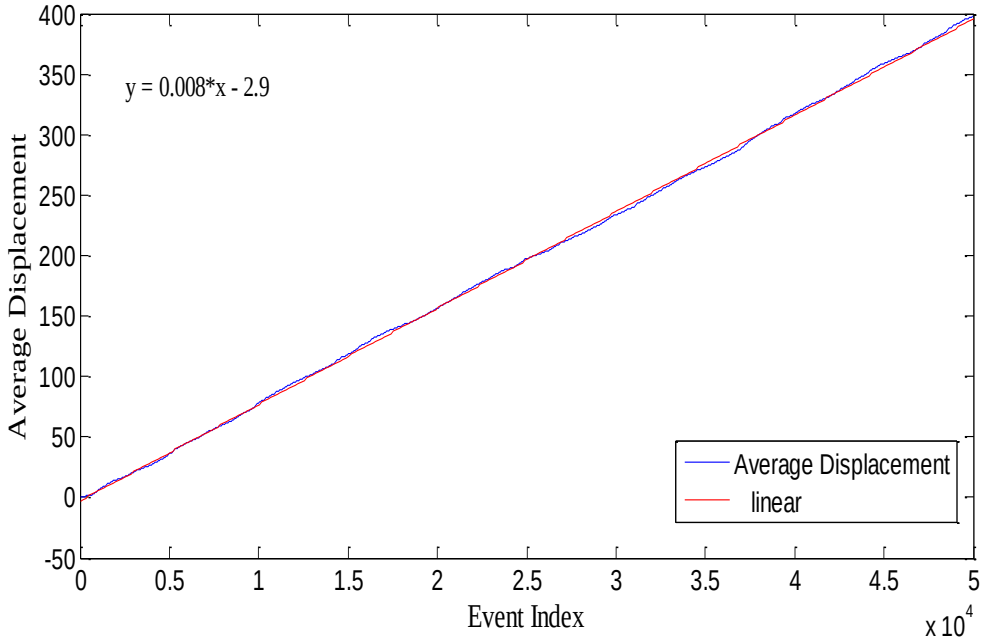

Fig. (2.36): Evolution of displacement in a Regime C system. The average displacement along the chain after each event is recorded on the vertical axis versus the event index on the horizontal axis. The average displacement is well fitted by a linear trend with some variations. This behavior is analogous to the displacement records from real creeping faults.

2.9 Discussion

Characterizing the degree of heterogeneity of the stress in the Earth's crust is very important for understanding the dynamics of earthquake ruptures. It has direct implications on our understanding for the origin of high frequency content in the seismic radiation spectrum as well as our understanding of the problem of the strength of real faults. It is also important to characterize the nature of the stress state in order to have

more realistic initial prestress conditions that can be used in sophisticated dynamic rupture simulations.

In this chapter we have tried to explore some aspects of this extremely complex problem and its implications. We used a simple dynamical system model, the spring block slider model, as a crude model for a system that fails at multiple scales and mimics some of the known long-time statistics generated by real fault systems. We tracked the long-time evolution of the prestress for systems spanning 4 spatial orders of magnitude and for time scales long enough to generate at least 50000 events. We tried to explore the implication of the evolving stress heterogeneity on our understanding of the system behavior and made some predictions about what we should expect in the more complicated continuum fault models.

Our first observation is that the prestress distribution, in most cases and no matter how smooth its initial distribution was, will evolve into a spatially heterogeneous field with some specified statistical and fractal properties that depend in some sense on the model parameters employed. Ofcourse the debate on the origin of complexity in the spring block model is very old, and whether it is really reflecting a dynamic complexity or a system with strong material or geometric discontinuities is an issue of a long standing history. While we do not delve in this chapter into the details of answering this question, acknowledging that both geometric and dynamic non-linear factors play an important role in promoting complexity in the Earth, we would like to draw the attention to a point that has not been extensively discussed before. Even in the absence of strong material and

geometric discontinuities, self-healing slip pulses can be very sensitive to local fluctuations in the prestress over length scales comparable to their width due to the nonlinear positive feedback between friction and pulse slip rates. We observe this in the spring block slider model and in 2D anti-plane continuum fault model as will be discussed in chapter 5. Moreover, slip pulses seem to die quickly when the prestress is low enough. Our observations so far suggest that it is possible to manipulate the pulse propagation through fluctuations of the prestress, leading to pulse growth if the prestress is higher than a given value characteristic of the pulse shape and friction law, and to pulse arrest if the prestress is lower than this value. This makes us hypothesize that pulse like ruptures are more vulnerable to the spatial distribution of the existing prestress, primarily its mean value and fluctuations amplitudes, than to perturbations introduced by the long range interactions set up by the wave field emitted from other points slipping on the fault. Accordingly we suggest extending the notion of relevant strong geometric and material discontinuities previously suggested by Rice and Ben-Zion (1996) to control complexity on a single fault, to include strong local variations in the prestress field if ruptures are propagating in a pulselike manner.

The second observation is related to the spring block model itself. The model proved to be very tunable and flexible enough to model different classes of real systems, at least in a statistical sense. The role of the stiffness ratio "*r*" is particularly interesting, especially because it corresponds to an obvious geometric parameter in real faults which is the depth of the seismogenic zone relative to the fault length. We have found that small values of

“r” favor small events while large values of “r” lead to the dominance of large events. The reason behind this is that since we need to overcome a fixed static friction threshold in order to initiate the block motion, the amount of strain energy available for the block is inversely proportional to the leaf spring stiffness and consequently is directly proportional to the value of “r”. Hence small “r” values correspond to smaller available strain energy per block while the opposite is true for large “r” values.

The third observation is related to the statistical nature of the prestress. Our results suggest that the prestress can have a Gaussian or non-Gaussian statistical character depending on the event size distribution in the system. System characterized by increased proportion of large events relative to what is expected from a power law event size distribution will have a Gaussian statistics for the prestress. This might be consistent with what we observe for mature major faults which rupture primarily in large characteristic events. Immature faults, however, are in a state of continuous evolution. Events of different sizes can occur along these faults. In such cases, it is doubtful that those faults have reached their equilibrium state. The stress distribution along them shows a strong non-Gaussian character.

The fourth observation pertains to the statistical and spectral properties of events slips. While we cannot directly verify how complex the prestress distribution in the crust is, since we cannot currently measure how the prestress varies as a function of space, studying the slip distributions can be very helpful in understanding conditions in the real

Earth since slip distributions can be inferred from seismic inversions. [While the inversion results are not unique since the problem is highly under constrained, heterogeneous slip is one of the robust results that should be taken as an important constraint on the physics of rupture (e.g., Mai and Beroza, 2002).] We have shown that for systems dominated by large events (Regime A), the slip distribution has a Gaussian probability density function with a non-zero mean, and a power law spectrum in the Fourier domain with amplitude spectral falloff of -2. This is consistent with the slip characteristics in large events for mature faults. On the other hand, for systems with nearly power law event size distributions (Regime B), the slip distribution has a non-Gaussian probability density function and an amplitude spectral falloff close to -1, reflecting an increased variability on the short wavelength scale.

Chapter 3

Size effects in mechanics is an issue of a long history but recently it gained increasing importance due to the wide range of scales mechanicians have to deal with, both in theory and applications, and which are spanning orders of magnitude between fractions of nanometers to thousands of kilometers. In this chapter we try to discuss some of the possible size effects that can be characteristic for dynamical systems with strong velocity-weakening friction, such as the Earth's crust, and in particular two issues; the energy-size dependence and the average prestress scaling. A question of fundamental interest to us is why do longer faults appear to be "weaker" than shorter ones and how does this relates to the underlying pulse-like dynamics?

We use the simple spring block slider model, discussed in the previous chapter, to illustrate our ideas We considered the following hypothetical question: Given two systems with identical material and frictional properties but with different total lengths, how much work is to be done in order to move each of these systems for a given amount of displacement? The answer we found suggests that longer systems, in general, will require less work per unit length per unit slip than shorter ones and will sustain lower values of average prestress. Only in the case when a system fails primarily in small sized events, does the work per unit length or the average prestress show size independence. We have also found that this size dependent behavior applies not only to the level of the systems as a whole but to the level of the individual events as well. We explain the results in the framework of strong velocity-weakening friction and the pulse-like nature of pulses

showing that the nature of our conclusions does not depend specifically on the particular setup of the spring block model but rather on general features that are applicable for both continuum and discrete systems.

3.1. A Thought Experiment:

Let's consider two versions of the spring block model which have identical blocks masses, springs stiffness and frictional properties. The only difference between the two systems is that one has fewer blocks than the other i.e. the total length of one of the systems (L) is less than the other. We then ask the following question: How much work is required to move each of these two systems for a given value of total displacement? One might be tempted to think that the value of work should be proportional to the system length. That is if one of the systems is twice longer, then to displace both systems for the same amount of displacement, the work done to move the longer system will be as twice as large as the work required to move the shorter one. The actual results however tell us something very different and it is only in very special circumstances that the intuitive linear scaling law just described would hold.

To answer the above question in a more quantitative manner let's consider two limiting cases. One case is when the coil springs are much stiffer than the leaf springs (Stiffness ratio = 200) and the other one is when the coil springs are more compliant than the leaf springs (Stiffness ratio = 0.1). We consider different system lengths. We take the shortest system to be the referential case and compare other systems to it. Table 1 summarizes the

results for systems with stiffness ratio = 200 where we calculate the work to be done in order to displace each system for a total amount of displacement of 100 units.

Table 3.1: Work (E) required to be done to move spring block systems of different lengths (L) for a total displacement of 100 units (Springs stiffness ratio = 200)

L	128	512	2048	8192
E	2.8×10^4	7.25×10^4	2.1×10^5	7.6×10^5
L/Lo	1	4	16	64
E/Eo	1	2.59	7.5	27
Reduction in Work %	0%	35%	53%	58%

It can be seen from the table that as the system length increases, the amount of work required to move the system the same amount of displacement does increase. However, it does not increase proportionally to the system length but rather nonlinearly with longer systems requiring less work than expected from the linear scaling. We calculate the reduction in work from the hypothetical linear scaling using the following relation: Reduction in Work % = $(1– E*L/E_o*L_o) *100$. The numbers are shown in the last row of Table 3.1, where for example a system which is 64 times longer than the original system, requires only 42% of the amount of work inferred from linear scaling based on the systems lengths ratio.

Nonetheless, this is not the whole story. Now consider the other limiting case: a system with compliant coil springs and stiff leaf springs (Stiffness ratio = 0.1) and repeat the

same experiment. We ask how much work is required to displace systems of different lengths from this class for the same value of displacement of 50 units. The results are summarized in Table 3.2.

Table 3.2: Work (E) required to be done to move spring block systems of different lengths (L) for a total displacement of 50 units (Springs stiffness ratio = 0.1)

L	128	512	2048	8192
E	7.0×10^3	2.8×10^4	1.12×10^5	4.48×10^5
L/Lo	1	4	16	64
E/Eo	1	4	16	64
Reduction in Work %	0%	0%	0%	0%

Unlike results shown in Table 3.1, the systems here exhibit a behavior identical to what is expected from the linear scaling; if we double the system size the amount of work required to move the new system is equal to twice the amount of work required to move the original one. This indicates that there is a different mechanism of deformation that is taking place in this version of the spring block model than in the version discussed in Table 3.1. Why do systems with large stiffness ratio show a nonlinear scaling while systems with low stiffness ratio show a closer behavior to the linear scaling hypothesis? Why do longer systems with large stiffness ratio are “weaker” than expected? What are the fundamental mechanisms of deformation in those different versions of the spring block model? It is the purpose of this chapter to try to answer some of those questions

and to shed some light on the role played by strong velocity-weakening friction in introducing size dependent dynamics and affecting the "strength" of systems with multi-scale behavior.

3.2. Why are longer systems sometimes weaker than shorter ones?

The discussion from the previous chapter regarding the spatio-temporal characteristics of the events generated for different model parameters may shed some light on the possible reasons for the size dependent dynamics observed in our thought experiment. Systems with high stiffness ratio tend to fail primarily in large events (see section 2.5) while systems with low stiffness ratio tend to fail in events spanning only a few blocks (see section 2.7). A possible explanation for this is that when the stiffness ratio is high, there is a better communication in the inter-blocks direction and less resistance to be offered by the leaf springs. Since the strain energy available to the blocks through the leaf springs is inversely proportional to the spring stiffness, reducing the stiffness tends to increase the available strain energy allowing ruptures to propagate further. When the stiffness ratio is decreases the opposite happens. But how could the nature of the event size affect the dynamics of systems with the same model parameters but different overall lengths?

To answer this question let's start with the first candidate in our thought experiment: systems with high stiffness ratio. We look first at how the average slip in an event changes with the event length. This is shown in Fig. (3.1) where the average slip is plotted as a function of the event length in a log-log plot.

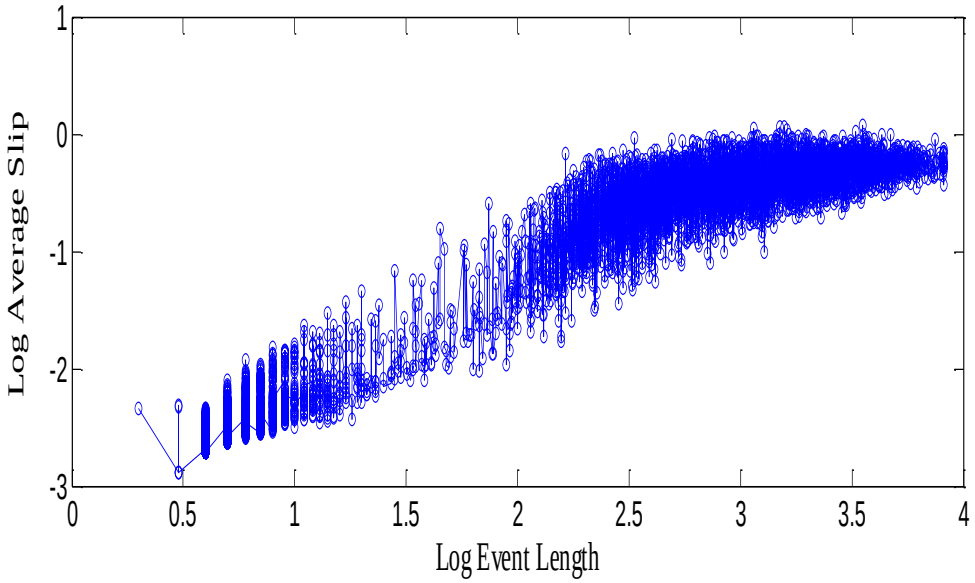

Fig. (3.1): Slip-Length scaling in a spring block slider model with a stiffness ratio = 200 in log-log coordinates. The system has 8192 blocks. The slip initially increases linearly with the event length and then gradually deviates from the linear scaling to finally saturate for large events. This behavior is typically observed for mature faults with finite seismogenic depth

We can recognize three distinct regimes in this figure. Initially the average slip increases as a power law with the event length, up to event lengths less than 250 blocks with the power law exponent close to 1. Then there is a transitional regime for events with lengths ranging between 250 and 1000 blocks where the slip continues to increase with the event length but at smaller rate. Finally for events greater than 1000 blocks, the slip length relationship nearly saturates and the slope of the curve in this regime becomes very close to zero. This kind of behavior is typically observed for mature faults with ruptures having

the opportunity to grow large enough such that they reach the boundaries of the seismogenic layer leading to the saturation of slip for very long ruptures. Hence, our first conclusion here is that *longer ruptures have on average higher slips.*

The average slip tells us something about the rupture as a whole. More information about the rupture details can be revealed if we can connect the slip to the slip pulse characteristics. Figure (3.2) shows a plot of the variation of the pulse maximum slip rate against the slip carried by the pulse at its healing end. Aside from some hysteresis *the pulse amplitude is, on average, increasing as the pulse slip increases*. Similar to the saturation observed in the slip length scaling, we do observe a similar saturation in the slip-slip rate scaling. As the slip becomes large the leaf spring becomes more stretched offering higher resistance to further sliding and leading to the slowing down of the block motion.

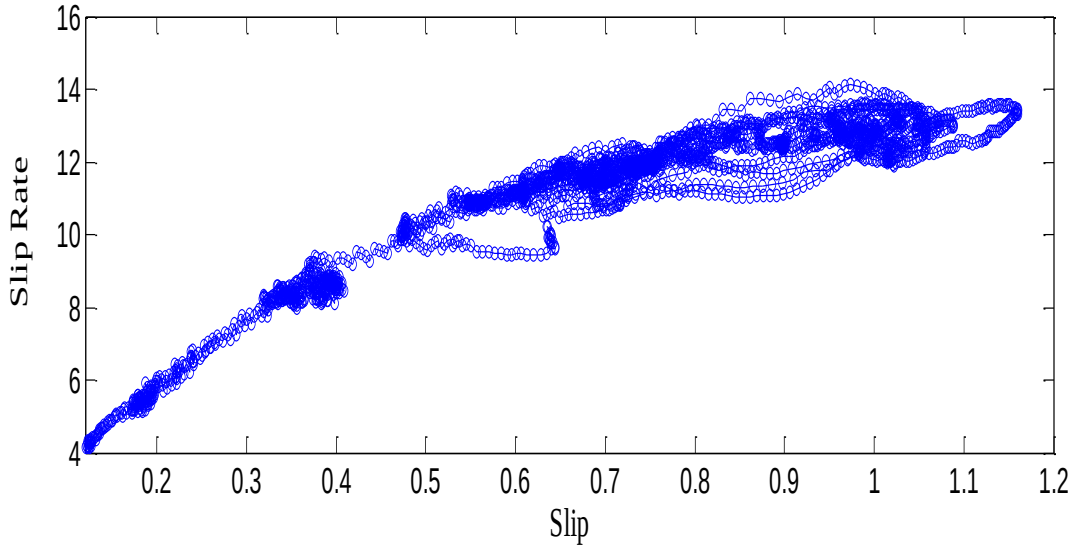

Fig. (3.2): An example of the relationship between the pulse maximum slip rate and the pulse slip accumulated at the pulse healing tail for an event generate in a spring block slider model with a stiffness ration = 200. Aside from some hysteresis the average response is such that the pulse amplitude increases nonlinearly with the pulse slip.

For higher slip rates, one expects that the dynamic friction should be lower due to its velocity-weakening character. In Fig. (3.3) we plot the variation of the average frictional force experienced by the pulse as a function of the slip carried by the pulse. The figure shows on average a decreasing trend in the sense that as *the pulse slip increases, the frictional force averaged over the pulse width decreases.*

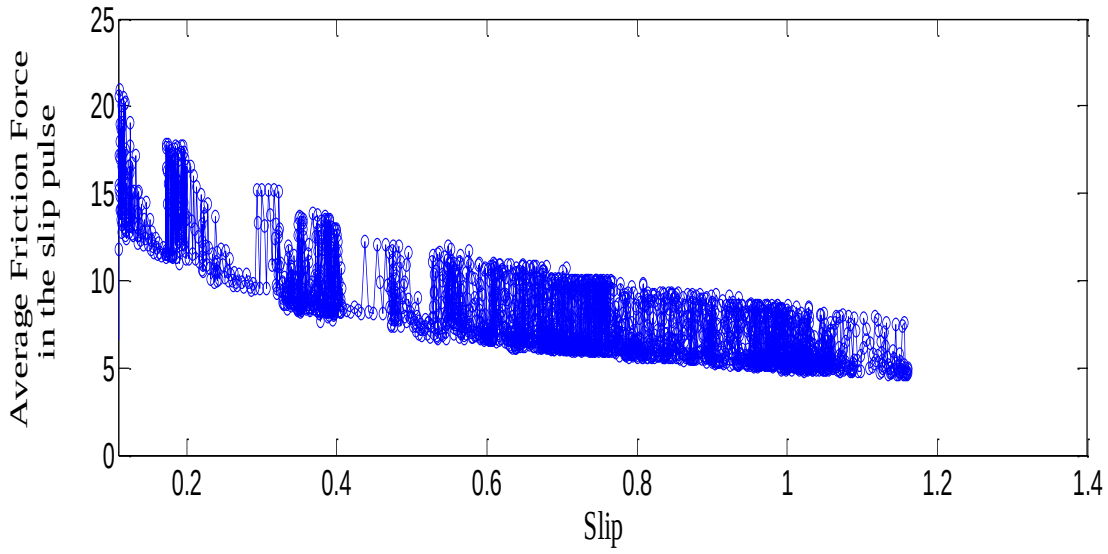

Fig. (3.3): The variation of the space-averaged frictional force within the slip pulse as a function of the pulse slip for the same event shown in Fig.(3.2). The average response indicates that the larger the slip the lower the average frictional force experienced by the slip pulse.

Now, the different pieces of the picture are coming together and we may be able to explain the results of our thought experiment for systems with high stiffness ratios. Those systems tend to rupture in large events. For the same material and frictional properties, longer systems will be able to generate longer rupture. As the rupture becomes longer, the average slip increases [Fig. (3.1)], the maximum slip rate in the pulse becomes larger [Fig. (3.2)] and the average frictional force experienced by the pulse will decrease [Fig.(3.3)]. Accordingly, if we are going to move a long system and a short system, for the same amount of displacement, it would be easier to displace the longer one; it accumulates most of that displacement value in a fewer number of longer ruptures with larger average slip, larger pulse amplitudes and lower average frictional forces. Consequently, the work done to displace a large system will be smaller than that required to move a short one (for the same value of total displacement), and this explains the general trend of the results in Table 3.1.

However, Table 3.1 tells another thing as well. As the system lengths become large enough, the difference between the amounts of work required to displace those systems declines appreciably. For example, for the systems with 8192 and 2048 blocks, the reduction in the work done to displace the longer system, relative to the shorter one, is only 10%. This might be explained by the role of slip and slip rate saturation observed in Figs. (3.1) and (3.2). As the system size exceeds 1000 blocks, the average slip and the maximum slip rate for system wide events tend to differ only by a small amount. Hence the reduction in the friction experienced by the pulse along its length will also be limited.

Accordingly, there will not be substantial difference between very large systems work wise due to the saturation phenomenon. If we imagine a hypothetical case where the leaf springs do not exist and the system has no intrinsic length scale, then we would expect that the reduction in work required for large systems to continue at the same rates observed amongst small and intermediate systems sizes (i.e. before saturation effect starts).

But before we close this section we need to explain the seemingly very different behavior for systems with low stiffness ratio as summarized in Table 3.2. For such systems, the work done per unit system length to move a system by a given displacement value is independent of the system length, despite the fact that such systems do operate under the influence of strong velocity-weakening friction too. The reason behind this is uncovered by looking at the spatio-tempral distribution of events for this class of systems shown in Fig. (2.32). When the stiffness ratio is low, the amount of strain energy available for the blocks through the leaf springs decreases preventing events from growing beyond a few blocks. In Fig. (3.4), the slip length scaling for a system with stiffness ratio = 0.1 is plotted. Unlike Fig. (3.1), we observe that the average slip is nearly independent of the events lengths. One may argue that the way events propagate in this case is in a single block manner; the block reaches its full range of motion as far as the leaf spring allows and just then the motion of the neighboring block is triggered. In other words all blocks

slip roughly for the same amount of displacement

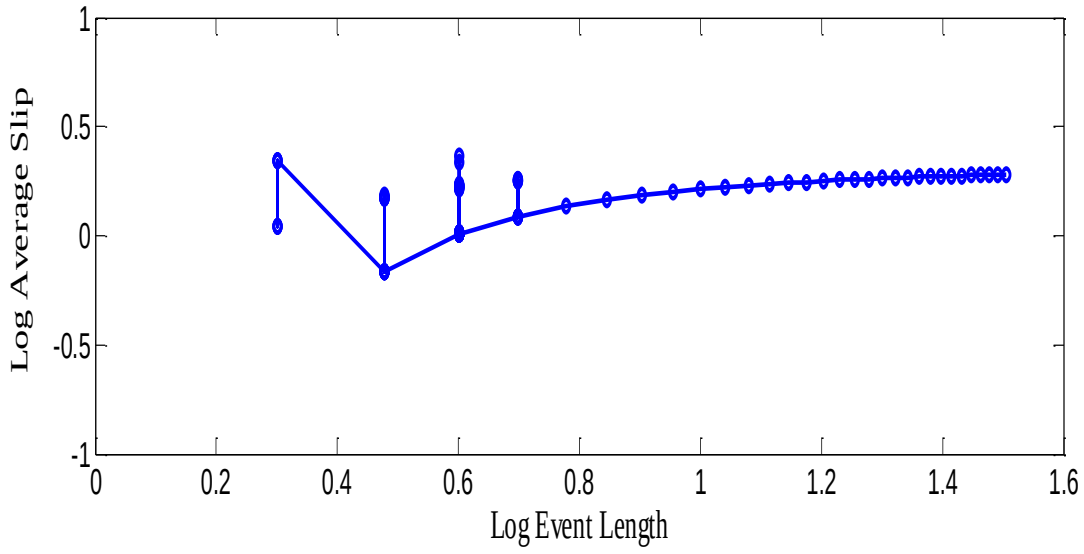

Fig. (3.4): Slip-Length scaling in a spring block slider model with a stiffness ration = 0.1 in log-log coordinates. The system has 8192 blocks. The average slip in this case is nearly independent of the rupture size.

With this is the case, one would also expect that the peak slip rates and the frictional forces attained at the different blocks are similar and almost independent of the rupture size. Hence in this case, whether we have a 100 blocks or a 1000 blocks system both will experience only small scale ruptures and the total displacement attained in either systems will be the result of accumulation of a large number of, essentially similar, small events. Since the longer system will have a larger number of those events nearly proportional to its length, the amount of work required to move it will increase proportional to its length as well but the work done by unit length will be identical for both of the short and longer systems. This explains the results in Table 3.2.

Finally, as we discussed in the previous section, one can get event size distributions that are close to being power law for intermediate values of stiffness ratios with chaotic spatio-temporal distribution as shown in Fig.(2.23). These systems should fill the gap between systems failing primarily in large events and showing significant reduction in work per unit length required to achieve a given displacement as the system size increases, and the other class of systems which fail primarily in small events and requires the same value of work per unit length independent of the system size. This is confirmed by looking at the slip length scaling, shown in Fig. (3.5) for a systems with stiffness ratio = 10. While it is not perfectly a power law, the average slip is monotonically increasing with the event size and no significant saturation is observed. With the average slip increasing, the slip pulse gets bigger and the average frictional force experienced by the pulse should get smaller. Hence we expect that the work per unit length required to move two systems in this category for a fixed amount of displacement to decrease as the system size increases. The decreasing rate however should be smaller than the one observed for systems with high stiffness ratio, at least for the same range of system sizes. The reason can be partially inferred from looking at Fig.(3.5) and comparing it to Fig.(3.1). While the average slip increases almost linearly with length in Fig. (3.1), at least initially, the best fit line for Fig. (3.5) will render a scaling exponent of ~0.5. With average slip, and consequently pulse slip rate, increasing more gently, the reduction in friction would be less significant and hence the work per unit length per unit slip will decrease as the system size increases but not as appreciable as in systems discussed in Table 3.1.

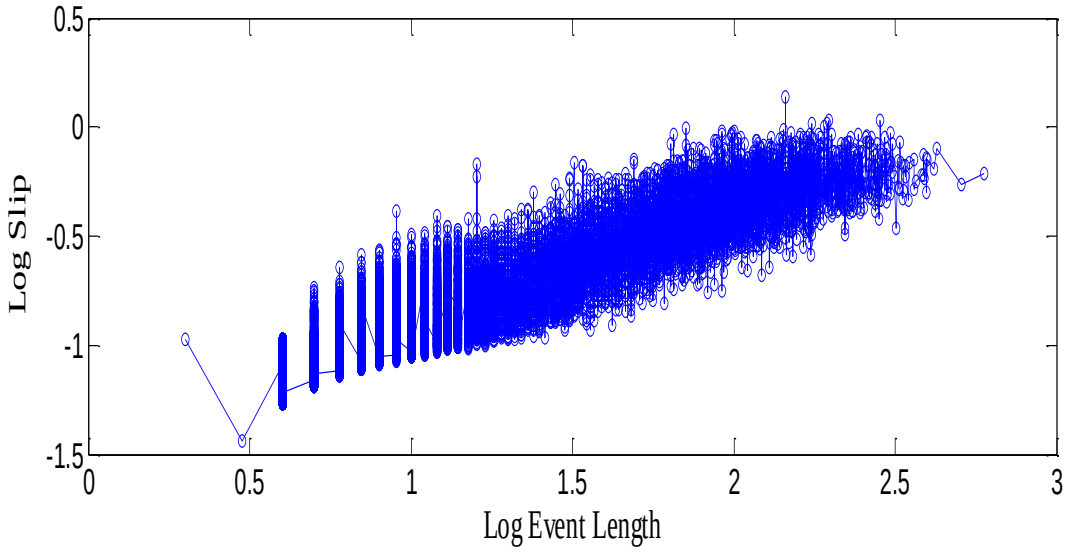

Fig. **(3.5)**: Slip-Length scaling in a spring block slider model with a stiffness ratio = 10 in log-log coordinates. The system has 8192 blocks. The slip is on average increasing as a power law in the event length with the power law exponent ~ 0.5.

In the next section we exploit the fact that the spring block slider model is capable of generating multi-scale fractures in examining how, within the same system, the energy per unit slip per unit rupture length changes as a function of the rupture size. So far, we have been considering the scaling of such a quantity for systems of different total sizes and concluded that in general it decreases as the system size increases. In the next section, we will imagine that each rupture within a given system is a sub-system and compare how easy or difficult to move such subsystems.

3.3. Energy Scaling within Systems with strong rate weakening friction

In the previous section we indirectly developed a notion of strength for systems with rate dependent friction by quantifying how much work is required to move a system of a given length, a given value of displacement. Since work per unit slip is effectively a force, we were comparing how much "energy-based" force is required to fail systems of different sizes. In this section we borrow the same idea to smaller scales within each system and investigate how energy dissipation changes between small and large ruptures.

We start our investigation with the system having a high stiffness ratio (Stiffness ratio = 200) which we have discussed its dynamics in section 2.5. For each event we calculate the total change in potential energy (or equivalently in this case the total amount of frictional work. Since there is no radiated energy, the change in potential energy due to an event should be equal to the total frictional dissipation) and normalize it by the event potency (Potency = Average slip x Event length). We plot the results in Fig. (3.6). For small event sizes (smaller than 10 blocks) the curve is almost flat. These small events usually start in the regions of high prestress and die quickly in surrounding regions of low pretress i.e. they occur in regions of high stress fluctuations. Since the events are too short, and the stresses in their regions alternate sharply, they sense similar prestress and slip conditions from the statistical point of view and the energy per unit potency shows nearly no scale dependence.

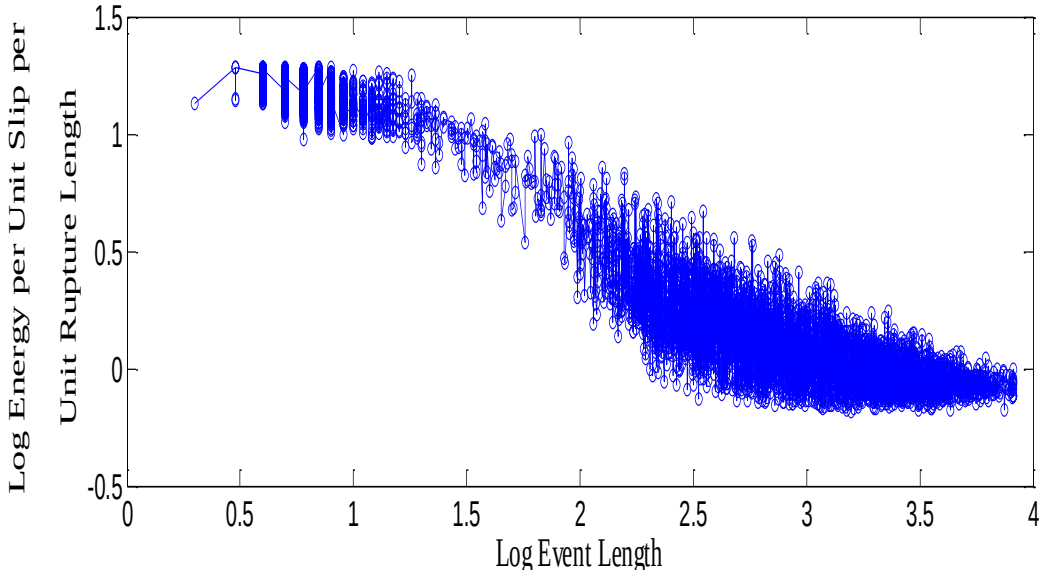

Fig. (3.6): Variation of the change in potential energy per unit slip per unit rupture length due to different events as a function of the event lengths in a spring block slider model with a stiffness ration = 200 in log-log coordinates. The graph can be divided into three distinct regimes: little or no variation in the normalized energy for ruptures spanning fewer than 10 blocks, a power law decay for intermediate sized events (between 10 and 1000 block) and an apparent saturation for very large ruptures (>1000 blocks), The overall trend can be approximated by a power law with an exponent ~ -0.47

For longer events, events spanning more than 10 blocks, the energy per unit potency decreases as the event length increases. The dependence is approximately a power law with the scaling exponent of the order of -0.47. This decrease in energy has an analogous explanation to the one we found for explaining the results of our thought experiment.

Within the same system, longer ruptures have larger average slips, bigger pulse amplitudes and hence smaller frictional dissipation which in turn allows rupture to propagate longer in lower average prestress. For very large events spanning more than 1000 blocks, however, the energy per unit potency dependence on the event size starts to level off. This is when the slip saturation [see Fig.(3.1)] due to the finite stiffness of the leaf spring comes into play. For this range of rupture lengths, the average slip and pulse amplitude changes a little bit with large increase in event size and considerably the difference in energy expended per unit slip per unit rupture length would not be significant.

In Figs (3.7) and (3.8) we repeat the same calculation but for different spring stiffness ratios. In Fig (3.7) we show the variation in the energy per unit potency for a system with stiffnes ratio = 100 whereas in Fig. (3.8) we show the energy per unit potency variation in a system with stiffness ratio = 50. The two figures share analogous features with Fig.(3.6) including the lack of size dependence for the normalized energy in the small event size regime, a nearly power law scaling for intermediate sized events and nearly saturation of scaling at larger events. However, when the best power law fit is calculated for the different plots, it is found that the scaling exponent decreases systematically as the stiffness ratio is reduced. So while it was nearly -0.47 for stiffness ratio (SR) = 200, it drops to -0.42 for SR = 100 and -0.37 for SR = 50

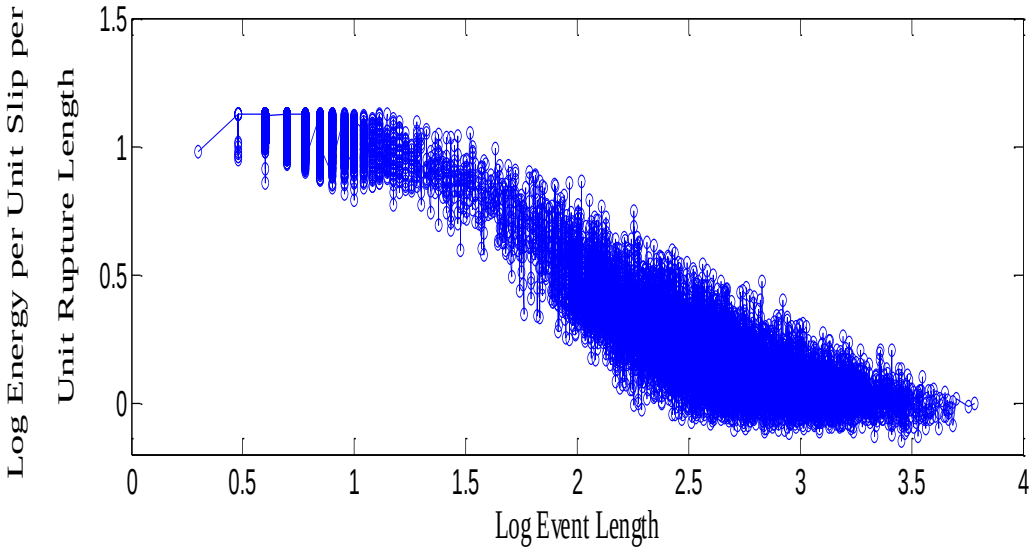

Fig. (3.7): Variation of the change in potential energy per unit slip per unit rupture length due to different events as a function of the event lengths in a spring block slider model with a stiffness ratio = 100 in log-log coordinates. The overall graph trend can be approximated by a power law with an exponent ~ -0.42

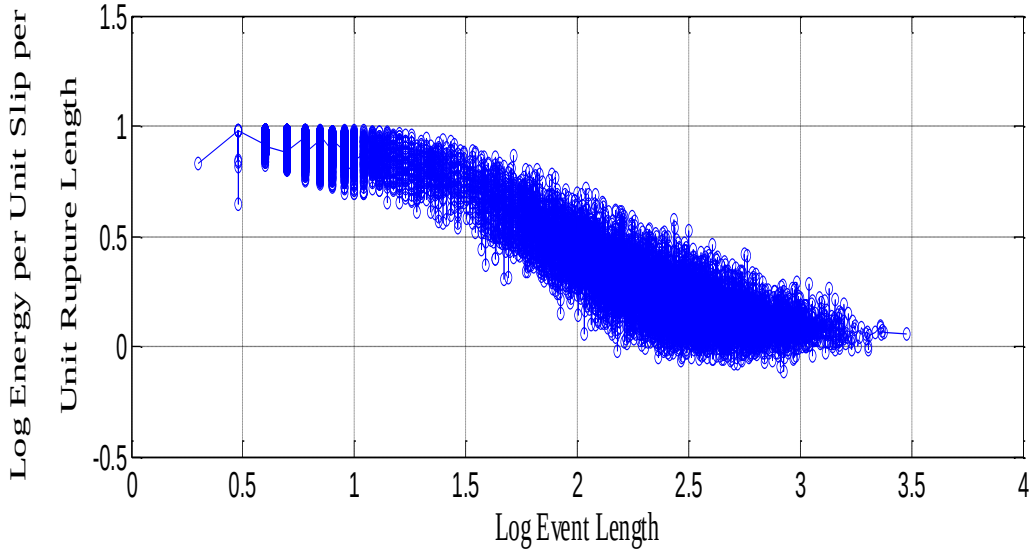

Fig. (3.8): Variation of the change in potential energy per unit slip per unit rupture length due to different events as a function of the event lengths in a spring block slider model with a stiffness ration = 50 in log-log coordinates. The overall graph trend can be approximated by a power law with an exponent ~ -0.37

The previous three systems with the assigned stiffness ratios belong to the class of systems dominated by large events. To examine the energy scaling in the regime where event size distribution approaches a power law, we consider two systems one with SR = 10 and the other with SR = 5. Fig.(3.9) shows the energy scaling results for the system with SR =10. Like the previous cases, there is a lack of size dependence in the energy per potency scaling in the small events limit. However for larger events the energy per potency decreases as the rupture length increases. We notice here that there is no significant saturation in the energy per potency scaling as was observed in the previous cases. That is a consequence of the lack of saturation for the slip length scaling in these systems (see Fig. 3.5). The best power law fit for the plot renders a scaling exponent of -0.24 consistent with the previously observed trend in which the size dependence of normalized energy is larger for systems with stiffer col springs failing in larger events.

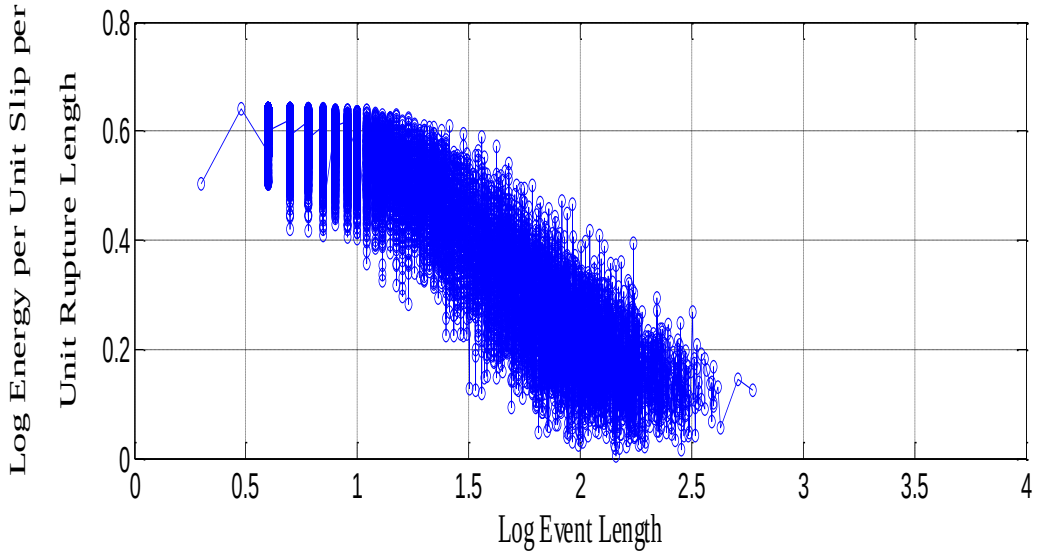

Fig. (3.9): Variation of the change in potential energy per unit slip per unit rupture length due to different events as a function of the event lengths in a spring block slider model with a stiffness ration = 10 in log-log coordinates. The graph can be divided into two distinct regimes: a regime showing nearly no dependence for the normalized energy on the rupture length (up to events slightly longer than 10 blocks) and a second regime in which the energy per unit potency (i.e. per unit length per unit slip) decreases as a power law with increasing rupture length. The overall graph trend can be approximated by a power law with an exponent ~ -0.24

For systems with SR =5, the energy per potency variation is shown in Fig.(3.10). Due to the relatively narrow range of rupture sizes, the whole diagram can be fit with a straight line with slope = -0.18

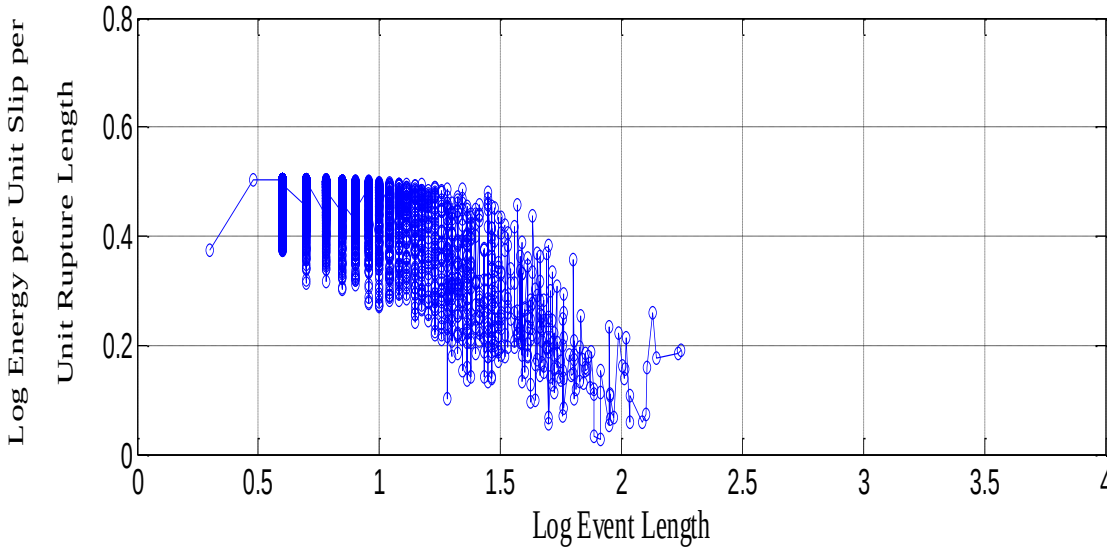

Fig. (3.10): Variation of the change in potential energy per unit slip per unit rupture length due to different events as a function of the event lengths in a spring block slider model with a stiffness ration = 5 in log-log coordinates. The overall graph trend can be approximated by a power law with an exponent ~ -0.18

Then we consider systems with low stiffness ratio e.g. SR = 0.1. Those systems fail primarily in small vents and in a quiet periodic fashion [see Fig. (2.32)]. We plot the energy per potency for an example of such systems in Fig. (3.11). As expected the energy per potency shows no size dependence. The reason is that there is no fundamental difference between the propagation of events of different sizes in this limit of stiffness ratio. Events propagate in a single block like way with slip and slip rates roughly the same along blocks moving in the same event. So while the total frictional dissipation will be proportional to the event length, its normalized version (i.e. the energy per unit slip per unit length) will be size independent.

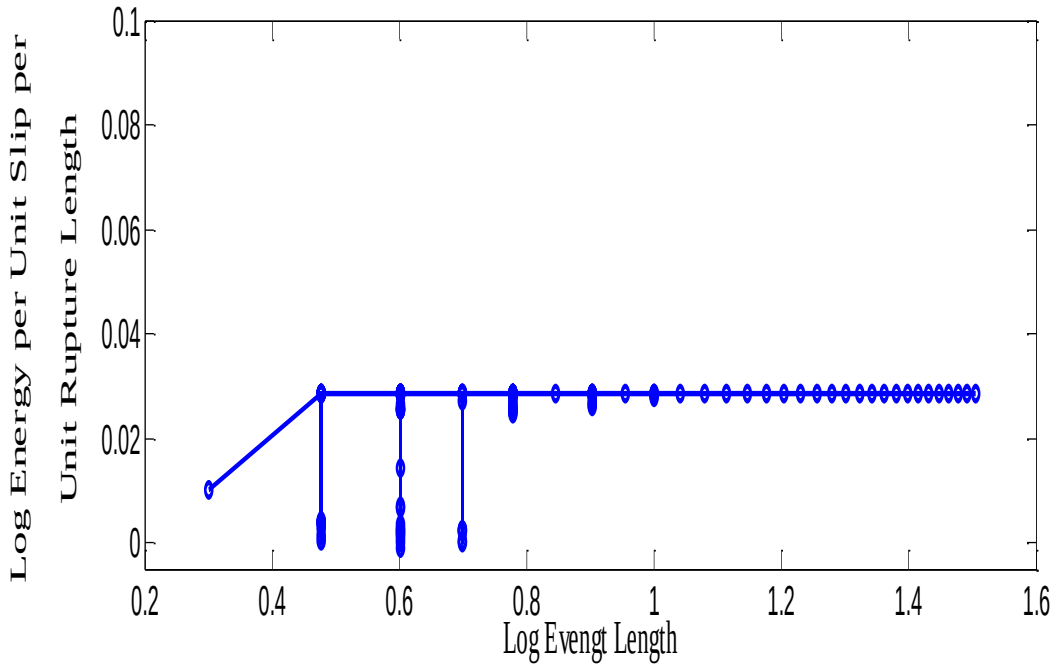

Fig. (3.11): Variation of the change in potential energy per unit slip per unit rupture length due to different events as a function of the event lengths in a spring block slider model with a stiffness ration = 0.1 in log-log coordinates. The graph shows that the energy per unit length per unit slip in this system is independent of the rupture size.

As was mentioned before, the scaling exponents for the best fit power laws that approximate the size dependence of energy per unit potency show systematic decrease with the reduction in stiffness ratio. Since the stiffness ratio is an important factor in controlling the event size distribution, this might suggest that there is a relation between the energy per potency scaling exponents and some measure of the proportions of large to small events in the event size distribution such as the Gutenberg-Richter b-value. For this purpose we plot in Fig. (3.12), the cumulative event moment distributions for systems with the values of stiffness ratios just discussed. We take the slope of the linear part in

each plot to represent the b-value of the distribution. Systems with increased proportion of large events have flatter linear portions (b-value close to 0) while systems failing primarily in small events will have nearly vertical linear parts (b-value much larger than 1).

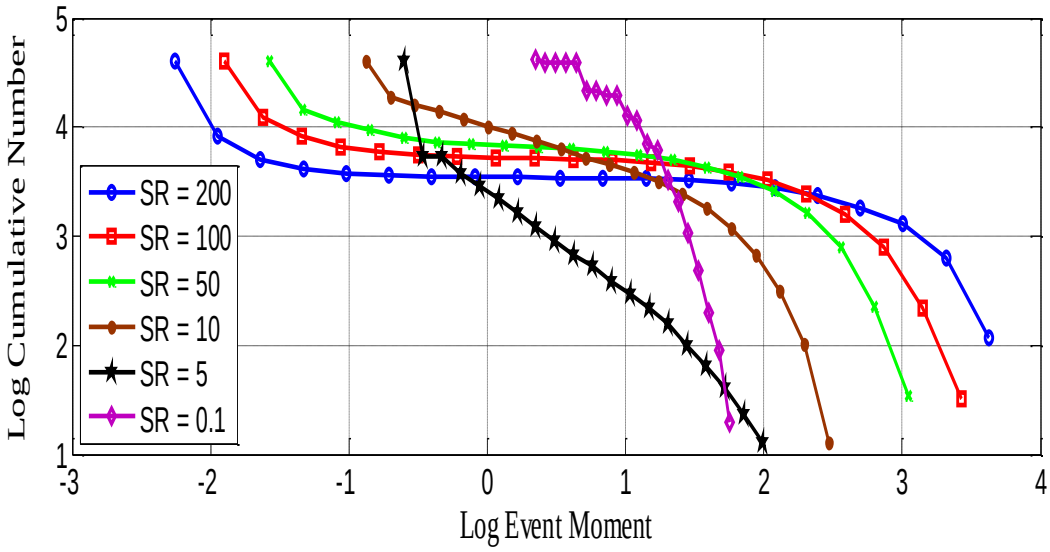

Fig. (3.12): Cumulative event moment distributions for systems with different stiffness ratios (SR). On the horizontal axis, the event moment is plotted whereas on the vertical axis we plot the number of events having a moment greater than or equal to the value on the horizontal axis. We take the b-value of the distribution to represent the slope of the linear part in the different graphs. It can be seen that there is a systematic increase in the b-value with decreasing stiffness ratio indicating the increasing proportion of small and intermediate sized events.

The b-values for the different event size distributions plotted in Fig. (3.12) are summarized in Table 3.3.

Table 3.3: b-value as inferred from cumulative event moment distributions plotted in Fig. (3.12)

SR	200	100	50	10	5	0.1
b	0.0125	0.033	0.066	~0.4	0.875	3.2

Plotting the variation of the energy per potency scaling exponent ($\varkappa$) as a function of the b-value from the cumulative event moment distribution, as shown in Fig. (3.13) suggests that for 0.0125<b<1 the functional relation between the two variables can be approximated by:

$$\varkappa = -0.069 \ln b + 0.18 \qquad 0.0125 < b < 1 \qquad (3.1)$$

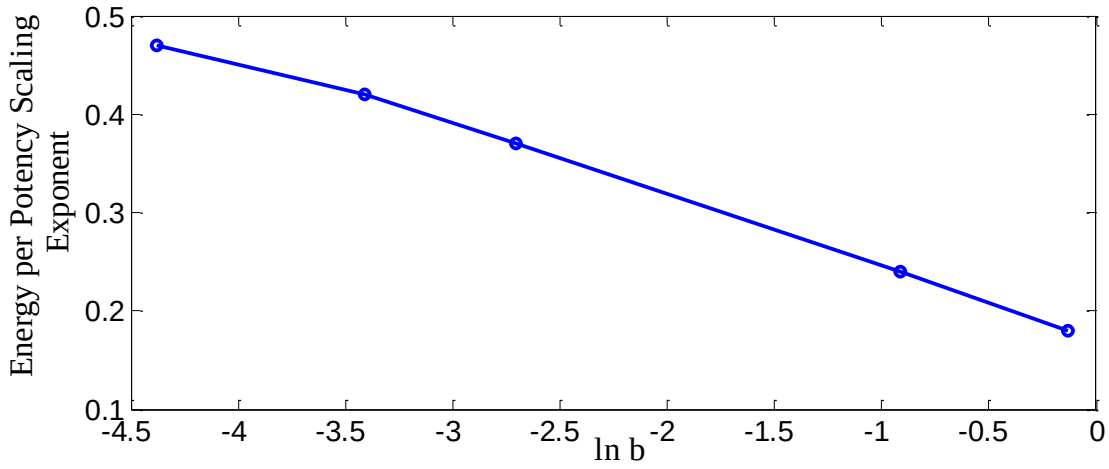

Fig. (3.13): Variation of the energy scaling exponent $\varkappa$ as a function of the b-value of the corresponding event size distribution

So far we have been concerned with the mean behavior of the dependence of the normalized energy on the event length, and we have been able to approximate it as a power law with a scaling exponent given by equation (3.1). However, in order to get a complete picture of the energy size dependence we have to quantify the scatter about the mean curve. This is beyond the scope of this chapter. Nonetheless we will briefly touch on this topic and try to explore the main statistical features of the scatter distribution. We defer a more detailed analysis of the scatter, including its event size dependence, to future work.

One way to quantify the scatter is to look at its probability density function (pdf). We will consider two cases: the first one has its energy per potency size scaling shown in Fig.(3.8) while the other one has its energy per potency scaling plotted in Fig. (3.10). To calculate the probability density function of the energy scatter for a given rupture length (L), we consider an interval of rupture lengths centered about L. Fig. (3.14) shows an example for the pdf of the scatter for L = 317 ($L=10^{2.5}$) for the energy size scaling shown in Fig. (3.6). The actual scatter data is represented by the blue dots while the best fit is represented by the red line. It can be inferred that the data in this case is fit, at least to first order, with a Gaussian function.

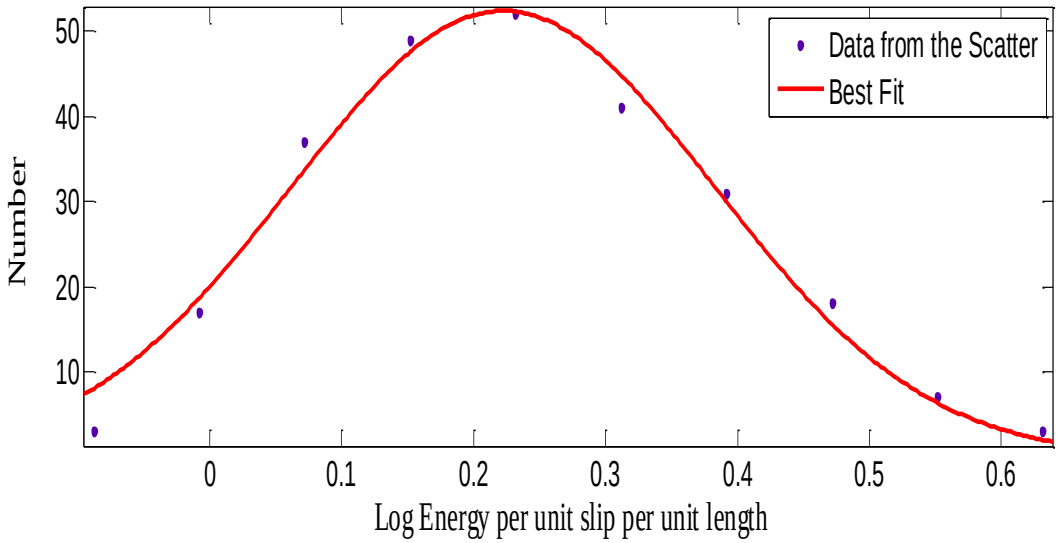

Fig. (3.14): The statistical distribution for the scatter in the energy per unit potency for rupture length L~317 extracted from Fig. (3.6). The distribution is well fitted by a Gaussian law.

In Fig. (3.15), we analyze the scatter for the energy size distribution shown in Fig. (3.8). Furthermore, we looked at two different rupture sizes (L = 31, or the blue stars in Fig.(3.16), and L=56, represented by the red filled squares in the same figure) in order to explore the dependence of the scatter distribution on the chosen event size. It can be inferred from the figure that the scatter distribution for the energy at both rupture lengths can once again be well fit with a Gaussian law. The variance of the distributions does not differ much between the two data sets. This might have been inferred from Fig. (3.8) where the scatter seems to have a nearly uniform width independent of the rupture length. This is not the case, however, in Fig. (3.6) which manifests itself in the variance of the Gaussian distribution shown in Fig. (3.13) being variable from one rupture size to another

[The variance is smaller for intermediate sized events than it is for larger events]

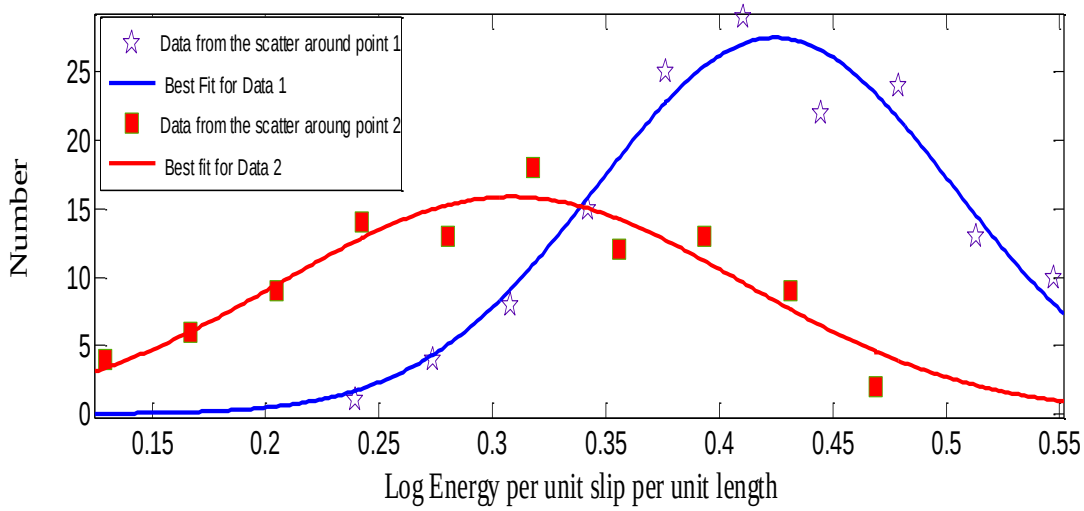

Fig. (3.15): The statistical distribution for the scatter in the energy per unit potency for ruptures of lengths L~31(the purple stars) and L ~56 (the red filled squares) extracted from Fig. (3.6). The distribution for both cases is well fitted by a Gaussian law.

In the next section we explore another aspect of size dependent mechanics introduced by the strong velocity-weakening character of the friction law: How does the prestress averaged over the rupture length change as the rupture size varies? Would longer ruptures propagate in lower average prestress than shorter one? Answering those questions can help understand the long standing problem of faults strength and the resolution of the heat flow paradox.

3.4. Average Prestress Scaling:

As we have shown in chapter 2 the spring block model is capable of generating events of different sizes and corresponding to different event size distributions, prestress may evolve differently and acquire different spectral and statistical properties. For systems dominated by large events, the prestress is relaively smooth on long wavelengths with some high frequency oscillations correponding to small and intermediate sized events. However, for systems failing in events of different sizes, the prestress is rougher and more spiky with a shorter correlation length. In this section, we are going to do the following numerical experiment: For each event, after the system has evolved into a statistically stable state, we look at the corresponding prestress distribution, calculate the integral of the prestress over the ruptured length and divide the result by the event length. This gives us a measure for the average prestress computed over the rupture length.

For a system with a prestress distribution shown in Fig. (2.17), the variation of the average prestress as a function of the rupture length is shown in Fig. (3.16). The first observation is that the average prestress initially decreases as the rupture length increases, in a nearly power law manner. This continues up to event lengths $10^{2.25}$. After that the behavior is altered and the average prestress starts to increase with increasing rupture length. For large events spanning more than 1000 blocks, the average prestress begins to saturate with the rupture length. What could possibly be the mechanism behind such non-monotonic variation?

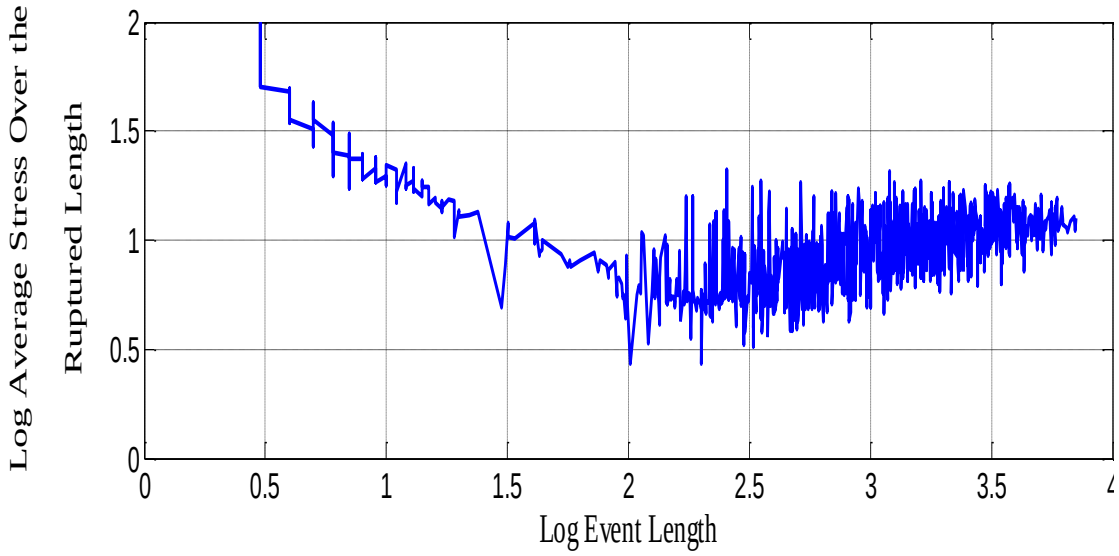

Fig. (3.16): Variation of the prestress, averaged over the rupture length, as a function of the event length for a spring block model with stiffness ratio = 200. Initially the average prestress decreases as a power law with increasing rupture length then the trend is reversed for intermediate rupture sizes. For events spanning more than 1000 blocks the average prestress shows little or no variation with the event size. [Please refer to the text for further explanation.]

To answer this question, we make use of the slip length scaling law plotted in Fig. (3.1) and our understanding for the possible influence of the leaf spring on the block dynamics. The initial decrease in the average prestress with increasing rupture length is a direct consequence of the strong velocity-weakening friction. As we previously discussed, as ruptures propagate longer they accumulate larger average slips [Fig. (3.1)] which is carried by larger slip pulses [Fig.(3.2)] leading to a reduction in pulse average frictional stresses [Fig. (3.3)]. Since pulses experience lower average friction, they can propagate longer in lower average prestress. However as we previously showed when we were

discussing the energy scaling, this line of argument only holds until the average slip starts to deviate from its linear dependence on the event length. This starts to occur near L = 250 blocks and signals that the leaf springs have started to play an increasing role in the system dynamics. If we go back to Fig. (3.16), we notice that the first point at which the average prestress – length scaling is broken is around L = 200 blocks. This makes us speculate that the breaking in scaling is closely related to effect of the leaf springs.

To test this hypothesis we plot in Fig. (3.17), the variation of the total force opposing the block sliding versus block displacement at a point within the rupture that has slipped for a distance equal to the average slip in the event. We define the total force opposing the motion as the sum of the force due to the velocity-weakening friction and the elastic restoring force due to the leaf spring. Initially the influence of the velocity-weakening friction dominates, with the resisting force decreasing as the slip increases. After that the leaf spring influence starts to kick in and take over the influence of rate weakening resulting in an increase in the total opposing force with slip since the leaf spring restoring force is linearly proportional to the spring displacement. Near the end of the block course of motion, its slip rate is appreciably reduced and the rate dependent friction would respond to that by increasing the motion resistance further until the block comes to a complete stop.

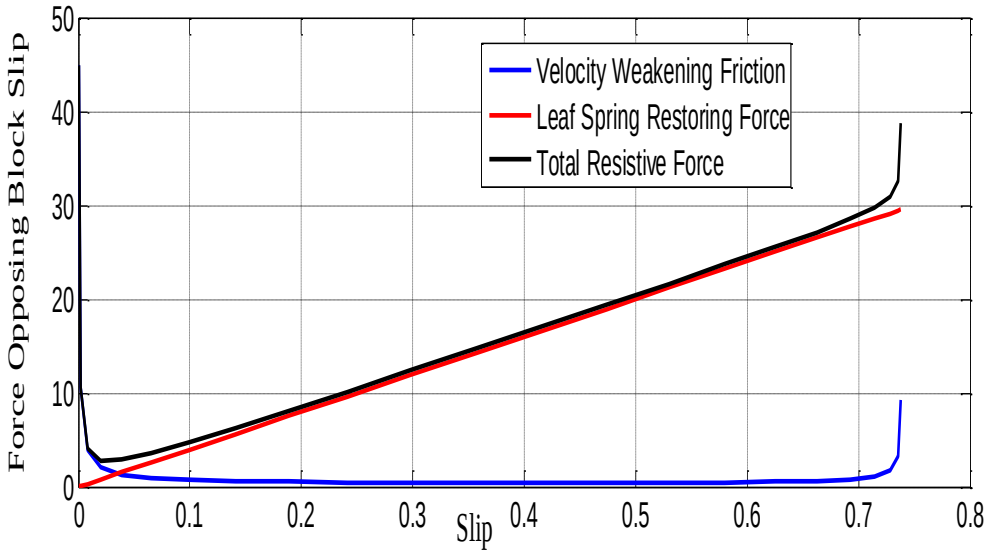

Fig. (3.17): Variation in the velocity-weakening friction force (blue), the leaf spring restoring force (red) and the sum of the two forces (black) as a function of slip at a point within the rupture that has slipped for a distance equal to the average slip in the event.[Stiffness ratio = 200]

The three stages in the variation of the total opposing force: initial drop, nearly linear increase controlled by the leaf spring and then rapid increase due to the velocity dependent healing, are better visualized in Fig. (3.18) where we plot the derivative of the resisting force with respect to slip as a function of slip. We focus more in that plot on slip values slightly greater than zero (where the rates can be highly negative) and slightly less than 0.74 (where the variation becomes highly negative). It becomes clear from the figure that the opposing force starts to be completely dominated by the leaf spring for slip values somewhere in between 0.2 and 0.3 and until slip values between 0.5 and 0.6. The evidence for this is that the rate of change of the opposing force with respect to slip in

this regime is almost equal to 40 which is the value of stiffness of the leaf springs. Now, since the block motion is controlled by the leaf springs it makes sense that if we want the block to slip more we have to apply higher stress in order to keep it moving and overcome the leaf spring stiffness. This could be a plausible reason for the increase in the average prestress with rupture length for the intermediate event sizes observed in Fig. (3.16). To further confirm this thought, we look for the range of events capable of achieving average slips greater than 0.2. The answer comes from Fig. (3.1) where it can be inferred that events of lengths greater than $10^{2.3}$ are the relevant ones consistent with the regime for which the average prestress increases with the event length. Finally the apparent saturation in the average prestress scaling for very large rupture lengths follows for a similar saturation effect in the slip length scaling seen in Fig. (3.1). For large events, there is not a significant difference between the slip values or the slip pulse sizes. Consequently, the controlling mechanisms, whether they are the friction or the leaf spring resistance, would be very similar in magnitude leading to the absence of pronounced differences in the average prestress scaling with increasing rupture length.

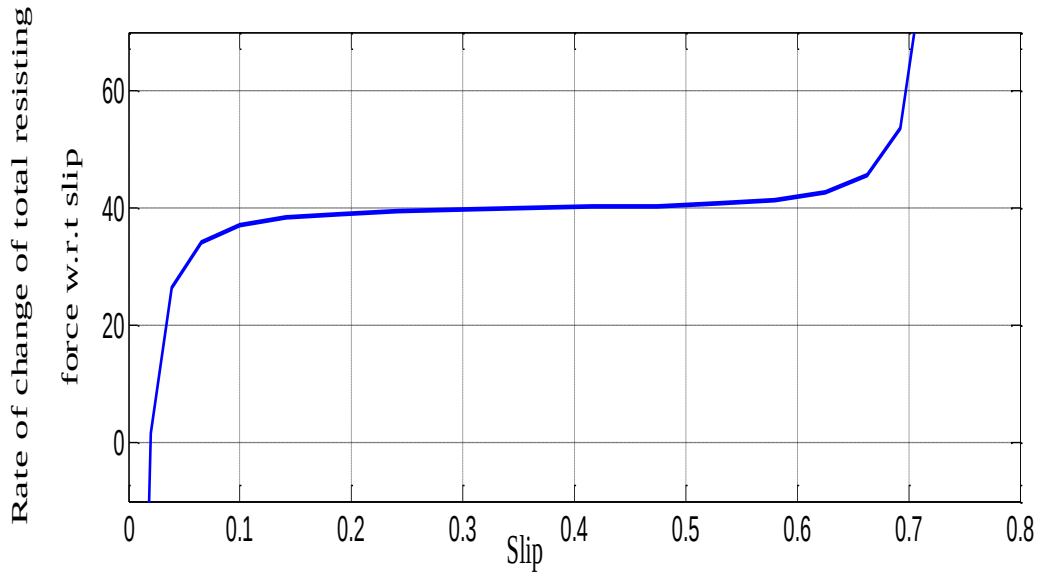

Fig. (3.18): Variation of the derivative of the total opposing force with respect to slip as a function of slip for the same point represented in Fig. (3.17)

We repeat the same procedure for a system with stiffness ratio =10. Fig. (3.19) shows the average prestress scaling in this case.

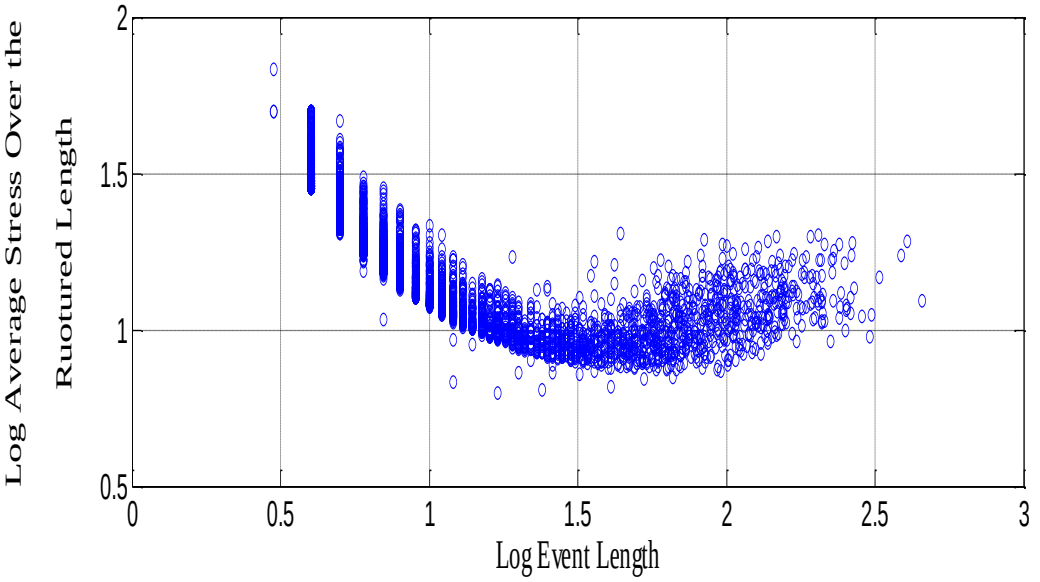

Fig. (3.19): Variation of the prestress, averaged over the rupture length, as a function of the event length for a spring block model with stiffness ratio = 10. Initially the average prestress decreases as a power law with increasing rupture length then the trend is reversed for ruptures spanning more than $10^{1.5}$ blocks. Please refer to the text for further explanation.

Similar to Fig. (3.16), initially the average prestress decreases approximately as a power law with increasing rupture length. This holds true up to rupture lengths of the order of L ~ $10^{1.5}$. After that a similar breaking in the scaling is observed where the curve trend is reversed and the average prestress increases as the rupture length increases. Our experience with the previous system (SR = 200) suggests that this breaking in scaling is attributed to the leaf spring influence. To assess this, we plot in Fig. (3.20) the total opposing force to the block motion as a function of slip at a point within the rupture that has accumulated a displacement value close to the average slip value in the event. In Fig. (3.21), we plot the derivative of this force with respect to slip as a function of slip.

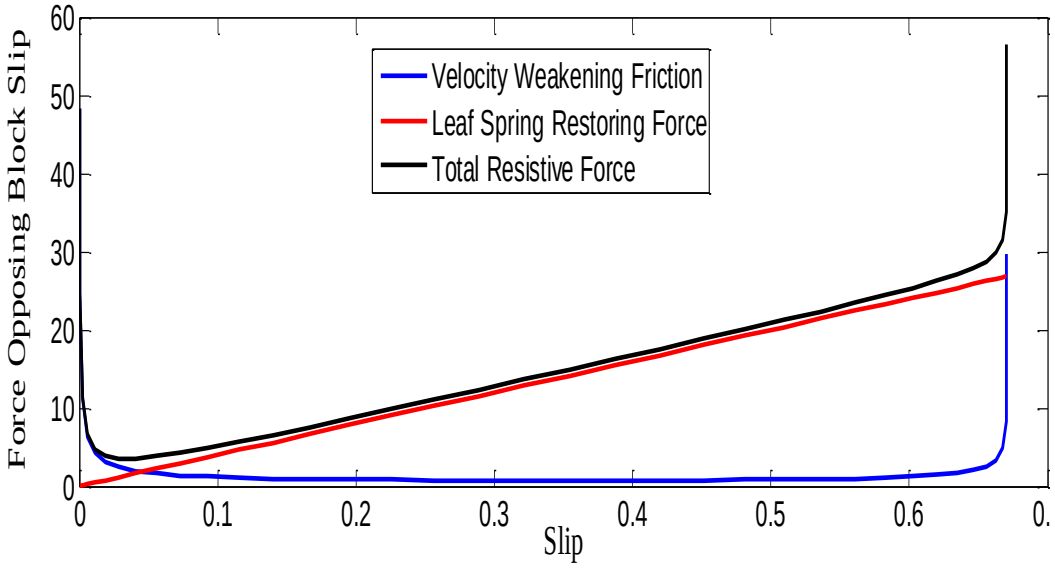

Fig. (3.20): Variation in the velocity-weakening friction force (blue), the leaf spring restoring force (red) and the sum of the two forces (black) as a function of slip at a point within the rupture that has slipped for a distance equal to the average slip in the event.[Stiffness ratio = 10]

The trend shown in Fig. (3.20) is very similar to the one shown in Fig. (3.17). The total opposing force decreases rapidly initially due to the velocity-weakening effect and then increases nearly linearly with slip due to the domination of the leaf springs effect and finally it rapidly increases again due to the velocity dependent healing. To quantify at what point the leaf spring influence dominates we plot in Fig. (3.21) the variation of the rate of change of the total force opposing the block motion with respect to slip. It can be inferred from the plot that the derivative attains a value equal to 40, which is the leaf spring stiffness, around slip values of 0.3. This value of slip is on average attained in ruptures spanning more than $10^{1.55}$ [see Fig. 10 for the average slip-length scaling in this

system]. Since this value is close to the value of the event length where the breaking in the average prestress scaling is observed, this suggests that our understanding for the role of the leaf spring in altering the scaling behavior is probably correct.

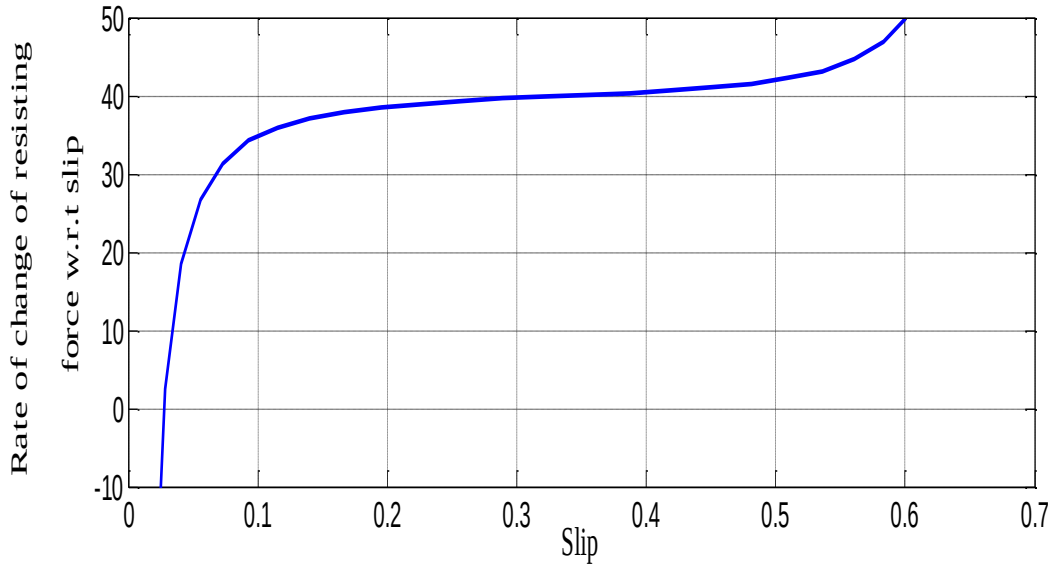

Fig. (3.21): Variation of the derivative of the total opposing force with respect to slip as a function of slip for the same point represented in Fig. (3.20)

3.5. Implications For Real Faults and Theories for Material Strength:

In this manuscript we have tried to discuss some of the possible size effects that can be characteristic for dynamical systems with strong velocity-weakening friction and in particular energy-size dependence and the average prestress scaling. We started with the following hypothetical question: Given two systems with identical material and frictional properties but with different total lengths, how much work is to be done in order to move

each of these systems for a given amount of displacement? The answer we found from modeling the spring block model was surprising and motivated us to explore more possible size effects. We stress, however, that the nature of the results we are getting does not depend specifically on the particular setup of the spring block model but rather on general features that are applicable for both continuum and discrete systems as we will shortly discuss.

We found that, for a given range of system parameters, systems with larger sizes will require less work per unit length than smaller systems in order to move for the same value of total displacement. This occurs when the stiffness of the system, represented in our model by the coil springs stiffness, is much larger than the stiffness of the loading machine, represented here by the leaf springs stiffness. Such systems generally fail in large events. With events, which are generally pulse-like in nature, propagating longer they accumulate on average larger slips which are carried by pulses with larger amplitudes leading to lower values of pulse averaged frictional stresses. With pulses experiencing lower average friction they can propagate longer doing less work. We call those systems Class-A systems.

On the other end of the spectrum, and for a totally different range of system parameters, we found that they exist systems that require the same amount of work per unit length for unit total displacement regardless of the system size. It does not matter if one of the systems is 100 times longer than the other; the total amount of work done to move the longer systems for a given amount of total displacement will be 100 times larger than that required to move the shorter one. We found that those systems are characterized by

having lower stiffness than the stiffness of the loading machine. The stiffer loading mechanism forces the system to fail in small episodes of fracture, independent of the system overall size. Consequently the only difference between a longer and a shorter system, displaced for the same amount of displacement, is that longer systems will have a larger number of fractures nearly proportional to its size, and this is the stem of the linear scaling observed for the work. We will categorize those systems as Class-C systems

In between these two regimes, there is a wide spectrum of systems which have a behavior that fits in between those two ends. Those systems have different stiffness to loading machine stiffness ratios and in general they show a decreasing value of work per unit length per unit slip with increasing system size. However, the rate of decreasing for these systems is smaller than the rate observed for Class-A systems. The reason is that they have a gentler dependence for the average slip and pulse amplitude on the rupture length than that is observed for Class- A systems. Accordingly the reduction in the pulse averaged frictional stress will not be as stronger. We will call those systems Class-B systems.

The notion of work per unit rupture length, for a given total displacement, has its roots in classical fracture mechanics. It is related to the energy release rate (G). The energy release rate has been long taken as a measure for material strength in material science and engineering application. We herein claim that the notion of work per unit slip per unit rupture length, or work per unit potency, qualifies to be a measure of strength for systems like the one we considered here and possibly for real faults as well. We will call this the energy-based measure of strength (S_E), and we can reformulate our findings so far as

follows: Systems with strong rate weakening friction, not failing in small episodes of fracture only, will have size dependent strength.

The first attempt to explain scale dependence of strength comes from linear elastic fracture mechanics (LEFM) of ideally brittle solids. It hypothesizes the existence of a sharp crack with a universal singular stress field that can be characterized by a single parameter known as the stress-intensity factor (K) and square root spatial singularity. The stress intensity factor is directly proportional to the applied remote stress field and the square root of the crack length. If the stress intensity factor reaches a critical value, which is hypothesized to be a material property, the crack loses its stability and propagates dynamically throughout the material. This means that the failure stress of a material is inversely proportional to the square root of length of the longest properly oriented crack inside it. Crack arrest is outside the scope of the classical theory of LEFM and hence the range of the materials that is covered within this theory is those ideally brittle materials which fail at the instant of the development of a crack with the critical size. If we assume that the overall size of the body and the size of the internal cracks are somewhat related; with higher probabilities of finding larger cracks in larger pieces of material, the inverse square root law for the scale dependence of strength of ideally brittle materials then follows.

However, systematic deviations from the inverse square root law have always been found. That was expected since the hypotheses of LEFM are rarely satisfied. Atomically sharp cracks are rarely found in nature and crack tips are usually blunted due to nonlinear

deformation. Moreover, the existence of singular stress fields is not possible in real materials either due to yielding at some finite stress because of nucleation and propagation of dislocation or due to the finite strength of the atomic bond. Inelastic deformations usually exist near the crack tip in most materials and off-crack plasticity and damage have to be included in any energy criterion for the onset of a critical crack and not only surface energy as usually assumed in LEFM. All these factors motivated the development of nonlinear concepts in fracture mechanics. Nonlinear deformation model of Irwin, the plastic strip model of Dugdale and the cohesive zone model of Barenblatt are just few examples of how to incorporate the nonlinear material behavior associated with cracks in the constitutive modeling of solids with defects. The J-integral of Rice (1968) was developed to give a unified description for material fracture in both elastic and inelastic setting. Since then, the interest of studying materials not abiding with the classical theory of LEFM but can be approximately modeled by one of the previously mentioned mathematical models greatly increased. It was then natural to start thinking about how to extend the theory for the scale dependence of strength to this class of materials, now known as quasi –brittle materials, as most of the materials in nature usually lies within that class. Some pioneering work in this field has been done by Zdenek Bazant and Alberto Carpentiri.

Bazant et al. (2003) proposed that the reason for scale dependence of strength in quasi-brittle material is Energetic-statistical. He introduced the notion of structures with positive geometry; these are structures which fail at the formation of a “process zone” of a certain critical size. The process zone is a region of nonlinear deformation surrounding

the crack tip where the change in strain energy is expended in forms other than surface energy such as damage, plastic deformation and cohesion overcoming. The size of the process zone is usually larger for larger cracks. Since as the size of the body increases, it becomes more probable to find larger cracks and hence larger process zones, the stress required to fail a material will decrease as the size of the piece of material increases. Due to variation in micro-structure, random fluctuations in stress and stochastic distribution of defects, the size of the process zone has a statistical component and is not solely determined by the crack geometry and energetics. Hence, while the formation of the process zone is mainly due to energetic requirements, stochastic fluctuations within the material do have an impact on determining its actual size. Accordingly the average scaling behavior has a deterministic energetic underpinning whereas the fluctuations around the mean curve is attributed to stochastic influences and hence the term energetic-statistical.

Carpentiri (1996) on the other hand proposed that the scale dependence of strength in quasi-brittle material is attributed to the geometric complexity of the micro-structure and cracks networks in these materials. He showed using an extensive database of observations that quantities like the grain size distribution have a self-affine fractal nature. He then hypothesized that any 3D solid has a lucanar like fractal distribution of defects with a structure similar to the Menger sponge. The fractal dimension of the internal structure will determine the fractal exponent in the scaling law of strength for the body. He introduced a formulation for the elasticity problem on a fractal space in order to

provide a predictability power for his hypotheses. The theory, however, is not yet fully developed.

In all of the previous theories the focus is on the applied stress that would cause the failure of the whole piece of the material. There is no consideration for rupture arrest or the multi-scale nature of the distribution of possible ruptures inside the material specimen. The latter is evident, however, in numerous acoustic emission tests. Accordingly in these theories the strength of the material piece is homogeneous and is determined by the value of the applied stress that causes a rupture spanning the whole body.

Our strength notion, however, has a multi-scale nature. We have shown that if the system fails in events of different sizes, then the scaling observed on the scale of the overall system size, has similar consequences on the scaling on the level of individual events. Longer ruptures within the same system will have lower values of S_E than shorter ones for the same reasons related to pulse dynamics and velocity-weakening friction.

However, the energy-based measure of strength is not the only possible measure for the strength in our system. One alternative comes naturally as the force to be applied per unit area of the material specimen to cause its fracture fracture. In classical strength of materials textbooks, it is understood that the force there is the sum of the externally applied force and any internal distribution of residual forces in the material that might have been set up due to previous loading histories. The residual stress field in the

specimen is a self-equilibrating field and hence cancels out in the course of averaging leaving us in the conventional case with the externally applied load only to worry about. In our systems, however, the prestress field when there is no motion balances with the frictional stresses as far as the maximum prestress has not exceeded the static friction threshold. Consequently, the average value of the prestress is generally non-zero on any finite scale and has to be considered in assessing the strength. This motivated us to introduce a stress-based measure of strength (S_σ) where for a rupture of given length, we calculate the average value of the prestress that existed over the length that has been ruptured.

This notion of (S_σ) , once again, provides a tool to assess strength in a multi-scale fashion. Our results suggest that for a range of rupture lengths S_σ decreases, nearly as a power law, with increasing rupture length. This could be understood in the lights of pulse dynamics and the role of strong velocity-weakening friction. As the rupture length increases, its average slip increases and the pulse amplitude gets bigger leading to a reduction in the average frictional force experienced by the pulse. Since the pulse experiences a lower average frictional force, it can propagate longer in lower average prestress. Nonetheless, due to the complicated interplay between the leaf spring and the velocity-weakening friction, which was explained extensively in Section V, a breaking in scaling occurs. Using lower and lower values for the leaf spring stiffness pushes the breaking point further towards larger and larger ruptures extending the region of power law scaling such that in the hypothetical limit of zero leaf spring stiffness, we expect that the average prestress will be a decreasing function of the rupture length on all scales. In

the real earth the equivalent value of the leaf spring stiffness, which is related to the inverse of the depth of the seismogenic zone, is very small and we expect its effect to not come into play except for very large earthquakes.

Another possible measure for strength in our systems is definitely the friction law itself. That is natural since the friction law gives a functional description for how the frictional strength of the interface would vary as the slip or slip rate varies. In this case, it might be argued that the strength in our model is uniform and is exactly the same at each point as we use the same frictional constitutive formulation everywhere. While this is true, we think that the friction law should not be taken as a measure of strength beyond the scale of its applicability i.e. the scale of a single block in the spring block slider model or the scale of the material specimen in laboratory experiment. In order to understand how systems fail on larger scales, we should take into account the effect of dynamic propagation and how elements communicate with each other. In such a setting it becomes useful to have some measures of strength suitable for those larger scales and this is what, hopefully, S_E and S_σ are trying to achieve. We think this is a situation similar to what we find in material science where we do have formulations for the strength of the individual atomic bonds (e.g. the bond force-displacement law), but we know that there is a dramatic difference between the behavior of the individual bonds and the whole bulk. While different mechanisms contribute to this difference, the analogy remains in the sense that we need to do some homogenization studies and scaling up in order to get notions of strength applicable to “large” structures.

So what does all of this entail for the strength of real faults? If the strength of the crust were the same for both small and large earthquakes we would face a paradox. This is because if both small and large earthquakes do the same work per unit slip per unit rupture area, a huge amount of energy would be generated as heat during the propagation of large earthquakes, which when delivered to the very thin fault slip zones, at slip rates of the order of 1 m/s and in time scales of order of few seconds, would result in a dramatic increase in the temperature of the slipping region to values that exceeds the melting temperature of all rocks known to us. However, there is little or no evidence for melting or the existence of pseudotachylytes in most fault systems. Accordingly, there must exist a mechanism for weakening of the crust on large scales so that melting becomes improbable for large earthquakes.

One possible resolution for this paradox is that faults are inherently weak on all scales. That is to say that faults, being planes of fracture inside the material, degrade the strength of the crust to values that are lower than those inferred from experiments on intact rock samples. There is no evidence, however, that this is true since experiments on rock samples at normal stresses comparable to those existent in the Earth at depths of several kilometers show practically no difference between strength values inferred for intact samples and those including pre-cut planes.

Another possibility is that the static friction of the fault plane rocks is high, but the normal stress is constantly reduced such that the frictional shear strength is always low. A possible mechanism for that is the existence of highly pressurized pore fluids which

permenantly reduce the overburden pressure and enforce the fault to slip with a reduced effective shear stress. While this seems plausible, it requires the existence of water with abundant quantities and the full saturation of pores and a mechanism to sustain these high pore pressures over long periods of time. There is little field evidence, though, that this happens within the seismogenic depth of most faults.

The third possibility, which we favor, is that faults are statically strong on small scales but dynamically weak on large scales. Several dynamic weakening mechanisms have been proposed including processes such as flash heating at microscopic asperities, dynamic pore fluid pressurization and silica gel formation. Among those mechanisms we think that strong velocity-weakening plays a dominant role in fault weakening and resolving the heat flow paradox. This becomes clear when we consider the scaling of S_E for different system classes. Mature faults which fail in large earthquakes and accumulate large amounts of slip will probably behave similarly to Class-A systems, showing strong size dependence in their energy based measure of strength. Creeping faults, on the other hand, for which their displacement is the result of accumulation of a large number of small events, will probably behave like Class-C systems with no size dependence in their strength. In between those two extremes, faults which are evolving towards maturity and which are failing in events of different sizes will generally behave analogous to Class-B systems with size dependent strength stronger than creeping faults but weaker than mature ones.

Finally we conclude this section by noting that our results suggest strong velocity-weakening friction and the ratio between the system stiffness and the loading machine stiffness to play an important role in material response. It can be argued that Class-A systems in this study are analogous to brittle materials; they fail in large episodes of fracture and show strong size dependent strength (close to the inverse square root law observed for ideally brittle material). Class-C systems are similar to creeping materials. Class-B systems could be related to quasi-brittle materials which fail in different event sizes, experience competition between healing and weakening mechanisms, and show size dependent strength that is strongly different from those of ideally brittle materials. We stress that the strong velocity-weakening character of the friction law or the influence of the stiffness ratio which have been used throughout this study to explain the results of our numerical experiments, are not restricted to the spring block slider model only. They are features which are found in real faults settings and material science experiments. Consequently we argue that our results are not restricted only to discrete systems such as the spring block model but are also relevant to the more general continuum settings

Chapter 4: The Pulse Energy Equation

In the previous chapters we discussed some of the dynamics of the spring block model, focusing on pulselike ruptures and their implications on the evolution of stress, slip and energy of the system. We have made some conclusions which we think might be relevant to the continuum. However, the simulation of a long sequence of earthquakes in a continuum model of fracture, which is necessary to study the evolution of system statistics, is still an intractable problem with the current computational methods.

In this chapter we touch on the problem of the ability to simulate a sequence of earthquake ruptures reliably and in a reasonable computational time. This is a problem that has gained an increasing momentum recently due to the increased interest in having a more accurate assessment for the physics relevant to earthquake ruptures and its seismological and engineering implications. In this chapter we introduce a new paradigm that could enable the simulation of cycles of pulselike ruptures in a short computational time. The method is developed here within the framework of the spring block model but it has the potential for generalization in a more complicated continuum modeling framework.

The basic motivation behind the approach we are adopting here is as follows. Many of the rupture variables, such as the final slip, the maximum slip rate, and the rise time, are thought to be correlated to each other. Meanwhile, the final slip is computed routinely from seismic observations and hence it provides a natural constraining variable for any computational model. What we would like to find out is whether it is possible to predict

the final slip in an event, given the prestress that existed before that event and some information about the governing friction without solving the full equations of motion. If this is possible, then a lot of computational time and resources could be saved.

In the work presented here we show that this is possible within the context of a discrete model of fracture and derive a differential equation based on the energy balance of the propagating slip pulse that yields the final slip distribution in the event, based on the pre-existing stress distribution. The equation performs significantly well on the level of individual ruptures and reduces the computational time, compared to the time taken to solve the equations of motion for the full original systems, by several orders of magnitude. The long-time solution of the equation reveals its multi-scale nature and its potential in matching many of the long-time statistics of the original system with considerable saving in computational time. Since the principles that governed the derivation of the differential equation are quite general and are not limited to the specific set up of the discrete model, we conjecture that a similar promising procedure can be developed for continuum pulse-like ruptures.

4.1. On the modeling of strong velocity-weakening slip pulses and the related computational challenges

Seismic inversions have indicated that most earthquake ruptures propagate in a pulselike mode [Heaton, 1990] in which a point on the fault slips for only a short amount of time compared to the total event duration. This is to be contrasted with the other mode of rupture, the crack-like mode, in which the rupture once started would continue to expand

coherently and would not stop until the rupture reaches the outermost boundaries of the fault where arrest waves are reflected causing the cessation of rupture at the interior points. Accordingly, in the crack-like mode, a point on the fault will continue to slip for a duration that is comparable to the overall event time [Fig.(4.1)].

A possible mechanism for the fast healing of the slip behind the rupture front in the pulse-like mode of rupture was suggested by Heaton (1990) to be strong velocity-weakening friction. This is a frictional constitutive formulation in which the frictional strength of the interface varies rapidly with variations in the slip rate [Fig.(4.2)]. This means that as the slip rate increases, the frictional strength drops significantly and vice versa. Accordingly, after an initial nucleation phase in which the rupture develops as a small coherent crack, if the slip rate behind the rupture front starts decreasing, say due to a low prestress value [See for example Zheng and Rice, 1998], the friction will start increasing and ultimately the friction will be high enough to stop the rupture. High velocity frictional experiments in the last few years [e.g. Tullis et al., 2003 and Beeler et al., 2008] have confirmed such friction-slip rate dependence.

Crack-like: A point on the fault slips for an amount of time comparable to the total event duration.

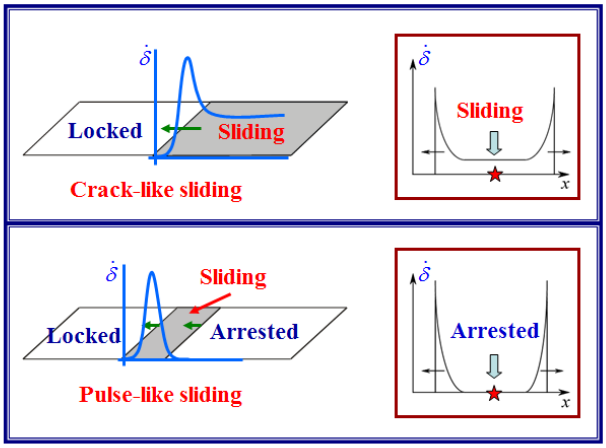

Pulse-like: A point on the fault ceases to slip shortly after the passage of the rupture front. (Heaton 1990, Zheng and Rice 1998)

Fig. (4.1): Schematic diagram showing the difference between crack-like (Top) and pulse-like (Bottom) ruptures

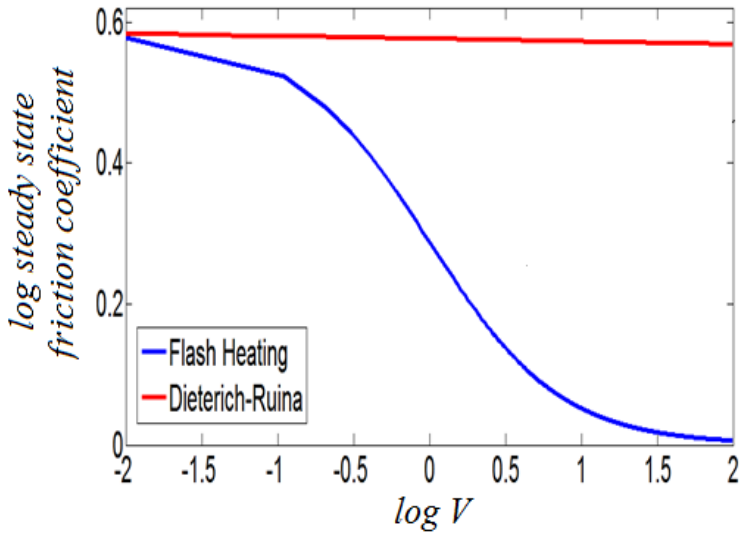

Fig.(4.2): An example of a strong velocity-weakening friction formulation (blue) based on the flash-heating formulation of Rice (1999) along with the classical Dieterich-Ruina rate and state frictional formulation (red). Note the drastic difference between the friction coefficients in the two formulations at seismic slip rates (around 1m/s). This has important implications on the dynamic rupture [Heaton 1990, Zheng and Rice, 1998].

With the advancement of computational power and the development of more efficient numerical schemes (e.g., Lapusta et. al 2000), modelers could go beyond simulation of ruptures with the classical slip weakening friction law or the Dieterich-Ruina frictional formulation and start to consider the more realistic and stronger weakening that occurs coseismically, as well as the faster rate-dependent healing that is provided by the strong-velocity friction laws. Zheng and Rice (1998) showed that low prestress is required to

favor slip pulses over cracks under rate and state friction laws with strong velocity-weakening character. Aagaard and Heaton (2009) showed that the strong velocity-weakening friction and heterogeneous prestress lead to the propagation of localized and unsteady ruptures in the form of slip pulses that are capable of sustaining prestress heterogeneity after the earthquake is over. In Chapter 5, we show that under certain conditions in nucleation and prestress, a slip pulse could propagate steadily on a frictional interface with strong velocity-weakening behavior, and that pulses are very sensitive to variations in the existing prestress, which has important implications on slip complexity and heterogeneity sustainability in the real crust.

Nonetheless, the available computational resources are still insufficient for simulating rupture scenarios in 3D settings or with frictional parameters like those inferred from laboratory experiments. While we can currently use mesh cells as small as 100 m in 3D simulations or 1m in 2D anti-plane ruptures, a model with realistic frictional parameters will require grid spacing on the sub-centimeter level. The only numerical simulation with lab-derived frictional parameters that has been done so far was by Noda, Dunham and Rice (2009). They could not go beyond a 32 m 2D anti-plane fault and the parallelized computation lasts for nearly a month (Hiroyuki Noda, personal communication). If we would like to carry over this experiment to larger faults, it is obvious that the computational capabilities need to be increased by several orders of magnitude in order for the calculations to end in a reasonable amount of time. This is infeasible, at least in the short run.

With the current limitation in the computational resources, there is an increased interest in developing physically based approximate models that can simulate reliably the main rupture variables, such as the final slip or the slip rise time, with a reasonable computational cost. In the language of dynamical systems, this usually lies within the class of problems of dimension reduction; how to take a high dimensional multi-degrees of freedom system and describe its dynamics satisfactorily with only a few degrees of freedom. In the context of pulse-like ruptures we ask the following question: is it possible to exploit the localized nature of the slip pulse in designing computational methods that can reproduce some of the macroscopic rupture variables, such as the final slip, without conducting the full dynamic simulations? An affirmative answer to this question is useful in many ways. For instance, since many of the rupture variables are thought to be correlated to each other, e.g., the final slip, the rise time, the pulse maximum slip rate,etc., knowledge of the final slip would facilitate estimating the other variables and consequently help in the fast generation of ground motion scenarios. Another useful application would be in exploring the long-time evolution of the prestress in different fault models, a problem that is computationally intractable with the current computational resources. If, however, a reliable method could simulate single-event ruptures quickly then it would be a premise for fast simulation of earthquake cycles.

It is the purpose of this chapter to explore the possibility of an affirmative answer to the question of the existence of reduced-order models for pulselike ruptures. To investigate the answer we consider a simple 1D discrete rupture model and study its evolution and the characteristics of the slip pulse generated by it. The discrete model represents the

extreme limit where all elastic interactions are short ranged and there is no radiated wave field. While this is a clear limitation for the model, it has the advantage of making us focus on pulse-related variables and gives us an intuitive picture of what is going to happen as the pulse becomes more and more sensitive to the local conditions rather than to the perturbations carried by the wave field. We will show that in the context of our discrete model, it is possible to track the evolution of energy in the system using an ordinary differential equation, which, upon its solution, yields the final slip in an event given the distribution of the existing prestress and some information about the friction. The extension to the continuum problem would require the inclusion of the far-field radiated energy. We discuss some applications of the equation and the possible extension to the continuum towards the end of the chapter.

4.2 Energy balance for propagating slip pulses in the spring block model

We start this section by a short review for the main results of the spring block model that are relevant to our attempts of developing a simplified, yet physical, description for the dynamics of pulselike ruptures. For a more extensive review we refer the reader to Chapters 2 and 3.

The main relevant results from our study of the spring block model can be summarized as follows:

1. Events propagate in a pulse-like mode with a nearly constant rupture speed [Fig.(4.3)]. Moreover, pulses seem to be approximately self-similar in shape, with

their amplitude and width changing as they propagate but their Gaussian or nearly triangular shape generally preserved [Fig.(4.4)]

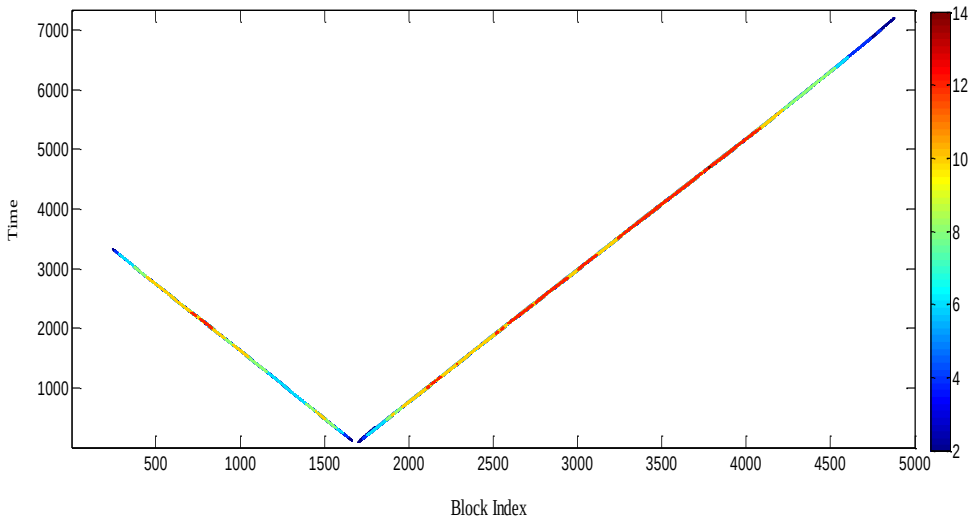

Fig.(4.3) : Contours of slip rate in one of the events generated by the spring block model, showing a nearly constant rupture speed and pulselike character.

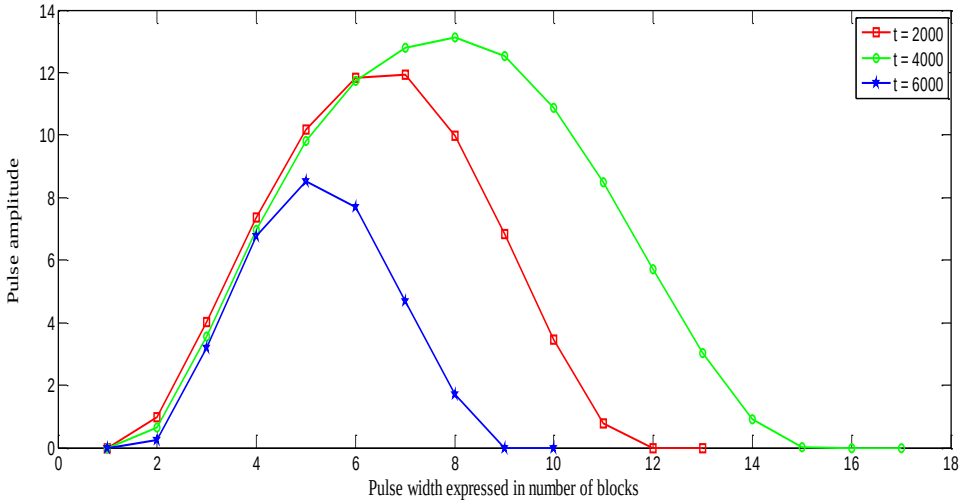

Fig.(4.4): Pulse profiles at different instants of time for the event shown in Fig.(4.3) showing growth and decay in a nearly self-similar pattern.

2. Under the influence of the positive feedback between the friction, the slip rate and repeated pulselike ruptures of different sizes, the prestress in the system evolves into a heterogeneous distribution with stable statistical and fractal properties [See Chapter 2.]

3. The slip distribution in different events is a heterogeneous function of position with a power law spectrum. The complexity of the slip distribution increases with decreasing pulse width and increasing prestress heterogeneity.

The slip pulse is the gearing mechanism for most ruptures in our model. The pulse width is found from the ensemble of simulations to be typically 1-5% of the total event length. This extreme localization of the pulse as well as its approximate self-similar nature, suggests that the systems dynamics is governed by the interplay between only a few variables characteristic of the slip pulse and the existing prestress. One can think of different variables of choice such as the pulse width and amplitude. One may also reformulate the problem in energetic terms, as energy is a macroscopic quantity of the underlying pulse variables and the prestress. We adopt this last approach in this chapter. In mechanics, it has always been the case that studying energy gives further insights into the system behavior and usually yields useful results. In what follows, we study the basic elements of the energy budget of the propagating slip pulses

We, however, stress that the setup of the spring block model, adopted throughout this work, has only short range elastic interactions and consequently the effect of the radiated wave field, characteristic of continuum media, is absent here. We will deal with the implications of this issue further near the end of this chapter. With no radiated energy, all actions taking place in the system is local. The different forms of energy that come into play as the slip pulse moves from one site to another are: the potential energy of the linear coil and leaf springs including the influence of the prestress, the frictional dissipation and the pulse kinetic energy.

As the pulse propagates, we can identify two regions in the system: the region that has slipped and is now stuck and the region that is currently slipping where the slip pulse exists. This is shown in Fig.(4.5) which illustrates a schematic snapshot of an event during a given instant of its propagation.

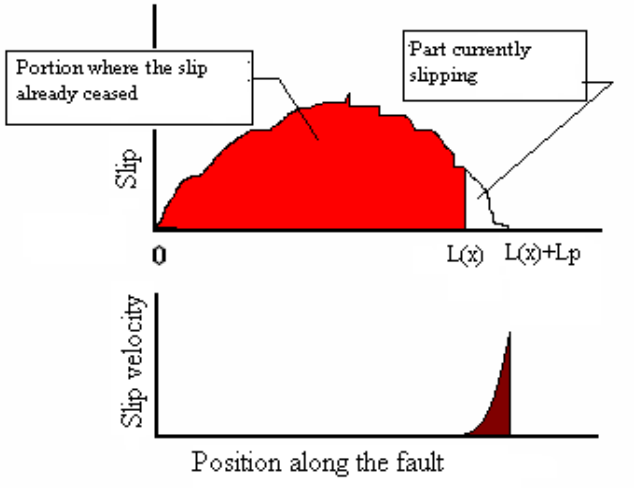

Fig (4.5): A schematic diagram showing the propagation of slip pulses in a pulse-like rupture. As the pulse propagates,

the portion of the fault behind the healing tip is no longer slip; the change in potential energy of the springs in this region can be fully expressed in terms of the final slip distribution and the prestress. The portion of the fault occupied by the pulse is currently slipping. The total pulse energy is calculated as the sum of the change in potential energy of the springs in this portion plus the sum of the kinetic energy of the blocks moving within the pulse.

As the pulse is moving from one site to another it changes the potential energy of the systems by deforming the coil and leaf springs. However, due to the frictional character of the surface on which the blocks are sliding, part of this change in potential energy get lost as frictional heat. The energy balance then dictates, since there is no radiated energy, that the other part of the change in potential energy be equal to the kinetic energy of the slip pulse. In our model the kinetic energy of the pulse is readily calculated as the sum of the kinetic energy of the blocks that are moving within the pulse. [Kinetic energy of the block is half the block mass times its velocity squared.] To summarize:

Change in potential energy of the system – Total dissipated frictional work = Kinetic energy of the pulse. (4.1)

Note that this is just a statement of the Lagrangian of the system. We can further rearrange the terms in the above equation to take advantage of the fact that the part of the system behind the healing tip of the pulse has slipped and is currently stuck. This is achieved by expressing the change in the potential energy as the sum of two parts: the change in potential energy in the stuck region and the change in potential energy within

the slipping region (i.e., the pulse). By doing this, the balance statement in (4.1) is modified to read:

Change in potential energy in the stuck portion of the system – Total dissipated frictional work = Total energy of the pulse. (4.2)

where the total pulse energy is the sum of the pulse kinetic energy previously defined and the change in potential energy of the springs, leaf and coil, in the region occupied by the pulse.

For the purpose of illustration, let's consider a test case. Fig. (4.6) shows the variation of the different energy terms expressed in the balance statement (4.2) as a function of the pulse position for a given event generated by a spring block model with system parameters (k_c = 8000, k_l=40, b=0.1 and v_c =10^{-6}). Fig. (4.6 a) shows the variation of change in potential energy of the stuck portion of the system as a function of the position of healing tail of the pulse. Fig.(4.6 b) shows the corresponding spatial variation in the cumulative frictional work from the point of initiation of rupture to the current pulse position. The spatial distribution of the total pulse energy is plotted in Fig. (4.6 c). One can readily check the validity of the equality in (4.2) by comparing the difference of the two curves in Figs. (4.6 a) and (4.6 b) with the curve in Fig.(4.6 c).

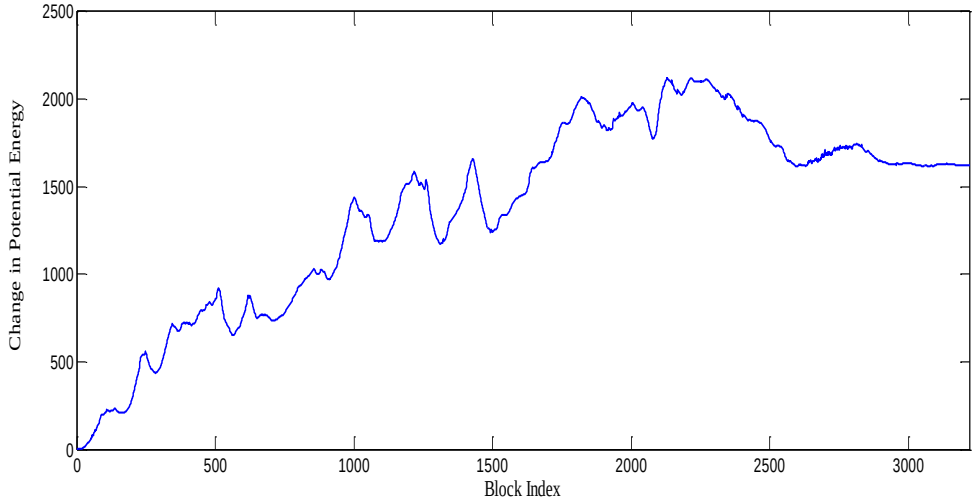

Fig. (4.6 a): Change in potential energy of the healed region as a function of the pulse healing tip position.

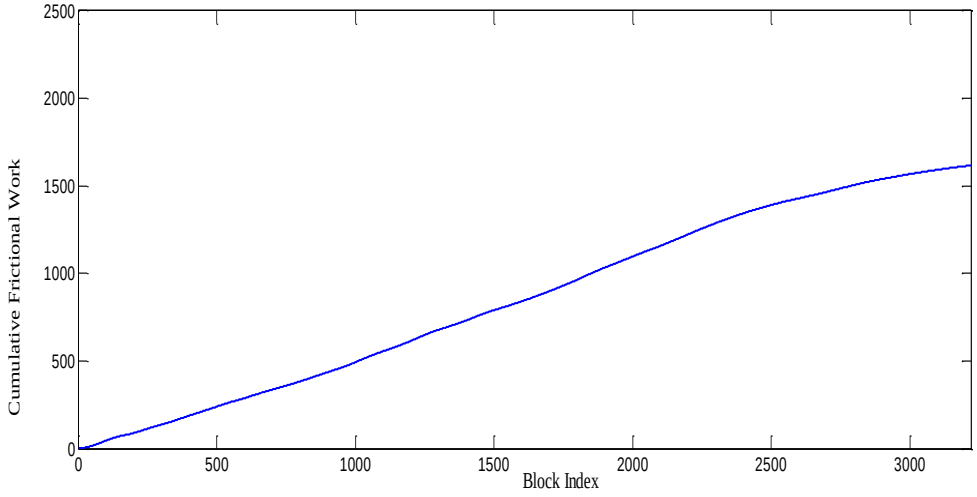

Fig. (4.6 b): Cumulative dissipated frictional work as a function of the pulse healing tip position.

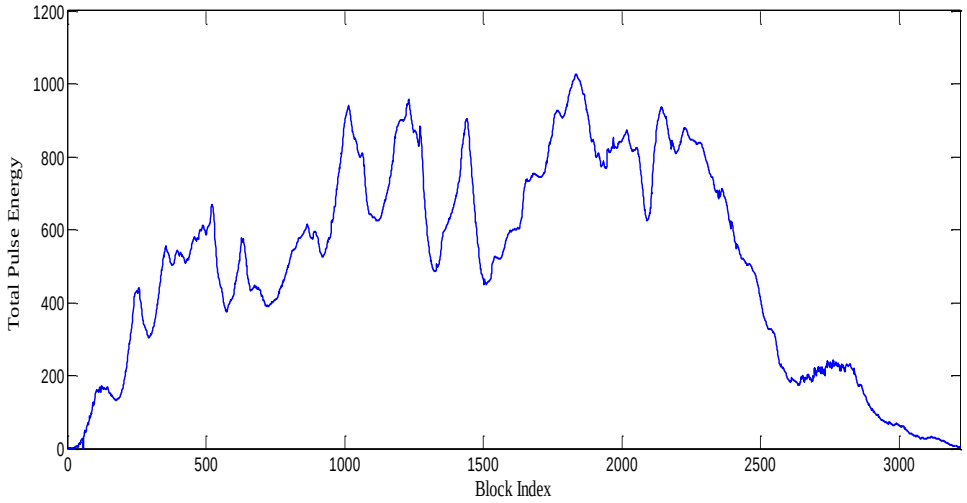

Fig. (4.6 c): Total pulse energy as a function of the pulse position. The total pulse energy is the sum of the change in potential energy of the springs in the pulse region plus the total kinetic energy of the blocks in that region. It can be checked that the vertical ordinate at any block index in this plot is the difference between the corresponding ordinate in Fig. (4.6 a) and that in Fig. (4.6 b) verifying the energy balance argument.

The formulation in (4.2) has an obvious advantage. Behind the pulse healing tip, the system has reached its final state and consequently the change in potential energy in that portion can be exactly described in terms of the final slip distribution and the prestress. All the time-dependent variables are now grouped in the pulse total energy but for this we can intuitively think that there is some correlation between the pulse energy and pulse slip; larger pulses should be more energetic and carry larger slips. Such a hypothesis can be tested from the numerical simulation results. A similar argument can be made for the

frictional dissipation. We pursue this route and formulate the statement made in Eqn. (4.2) in a differential form in the next section.

4.3. The pulse energy equation

In this section we construct the differential equation governing the energy transportation in our system via the slip pulse. Our starting point will be Eqn. (4.2) where we stated the energy balance principle for the pulse. As we just discussed in the previous section, the formulation in Eqn.(4.2) allows us to express the change in potential energy entirely in terms of the final slip and the prestress in the stuck region. This is done as follows:

Change in potential energy of the system in the healed region = change in potential energy of the leaf springs (ΔPE_{Leaf}) + Change in potential energy of the coil spring (ΔPE_{coil}).

The change in potential energy in the leaf springs per unit length is given by:

$$\Delta PE_{leaf} = -k_l u^o D - \frac{1}{2} k_l D^2 = \sigma_{ol} D - \frac{1}{2} k_l D^2 \tag{4.3}$$

where D is the final slip and σ_{ol} is the prestress in the leaf springs

The change in potential energy in the coil springs per unit length is similarly given by:

$$\Delta PE_{coil} = -k_c \frac{\partial u_o}{\partial x} \frac{\partial D}{\partial x} - \frac{1}{2} k_c (\frac{\partial D}{\partial x})^2 = \sigma_{oc} \frac{\partial D}{\partial x} - \frac{1}{2} k_c (\frac{\partial D}{\partial x})^2 \quad , \tag{4.4}$$

where σ_{oc} is the prestress in the coil springs and x is the spatial coordinate. These expressions of the change in potential energy for the leaf and coil springs are exact in the continuum limit of a 1D elastic system.

On the other hand, the total energy of the pulse can be written in principle in the following functional form:

$$E_p = G(u, \dot{u}, \frac{\partial u}{\partial t}, \frac{\partial u}{\partial x}) \tag{4.5}$$

where u and $\dot{u}$ are the current displacement and slip rates of the blocks within the pulse region. We can write down the exact form of G; it is the sum of kinetic energies of the blocks forming the slip pulse plus the sum of the change in potential energy of the leaf and coil springs within the pulse region. However, this will not be of much use as it adds more unknowns to the energy balance in Eqn. (4.2) without bringing an equivalent number of equations. Rather, we will pursue a different route. We will seek an approximation for G in terms of the final slip value at the healing tip of the pulse (D). One expects that the bigger the pulse gets the more energy it has and the more slip it carries and hence it is reasonable to assume some sort of correlation between the pulse energy and pulse slip. Accordingly, we may write:

$$E_p = E_p(D) \tag{4.6}$$

Unfortunately we cannot write down a closed form expression for E_p in terms of D as this will depend on the detailed dynamics. Nonetheless, we can derive an empirical

relation from the results of the numerical simulations of the spring block model. An example of such relation is shown in Fig. (4.7) for the same test case considered in the previous section.

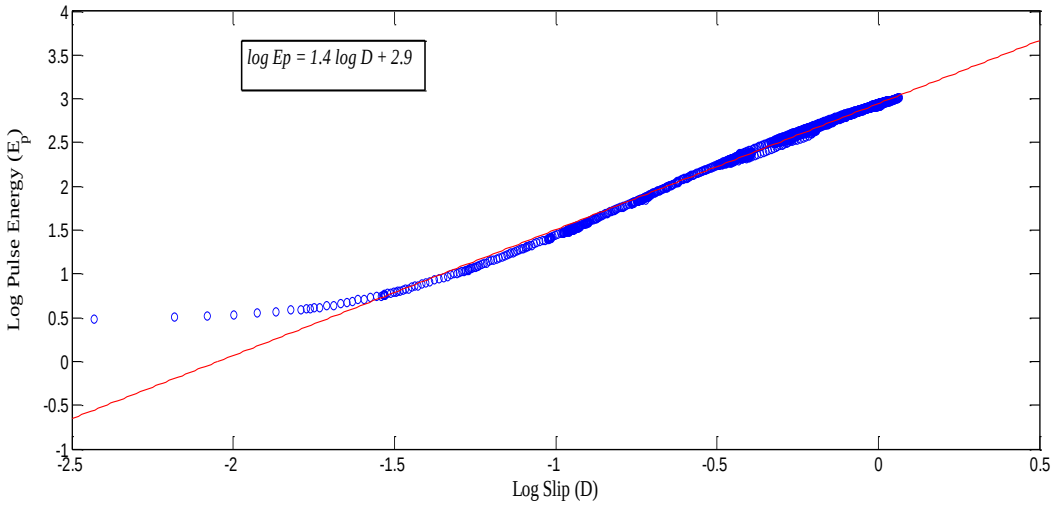

Fig.(4.7): Dependence of the total pulse energy on pulse slip. Except for very small slip, the pulse energy depends in a power law fashion on the pulse slip and the power law form is depicted in the rectangle.

Except for very small slips (D<0.03), the total pulse energy varies with the pulse slip, to a very good accuracy, as a power law given by:

$$E_p = 10^{2.9} D^{0.4} \tag{4.7}$$

Having approximated the total pulse energy, the next step is to find an analogous approximation for the frictional work term. The cumulative frictional work from the initiation of rupture and up to the pulse current position is given by:

$$W_F = \int_0^x w_f dx = \int_0^x dx \int_0^t \dot{u} f(u,\dot{u}) dt \tag{4.8}$$

where w_f is the frictional work per unit length and $f(u,\dot{u})$ is the friction functional form.

The integral $\int_0^t \dot{u} f(u,\dot{u}) dt$ can be evaluated if the time histories of u and $\dot{u}$ are given.

Since this requires a detailed dynamic modeling, evaluating the correct value of the integral will defy our model reduction purposes. Instead, similar to what we have done in the total pulse energy case, we will seek an approximation. Note that the frictional work density, or equivalently the time dependent integral, can be expressed as:

$$w_f = \bar{\tau}.D \tag{4.9}$$

where $\bar{\tau}$ is the slip averaged frictional work per unit slip ($\bar{\tau} = \frac{\int_0^t \dot{u} f(u,\dot{u}) dt}{D}$). What we will do then is to seek an appropriate approximation for $\bar{\tau}$. As a first order approximation we may assume

$$\bar{\tau} = \bar{\tau}(D) \tag{4.10}$$

We test this hypothesis for the model problem. The result is shown in Fig. (4.8). To a good approximation the relation between $\bar{\tau}$ and D is a power law with some scatter. The power law is given by:

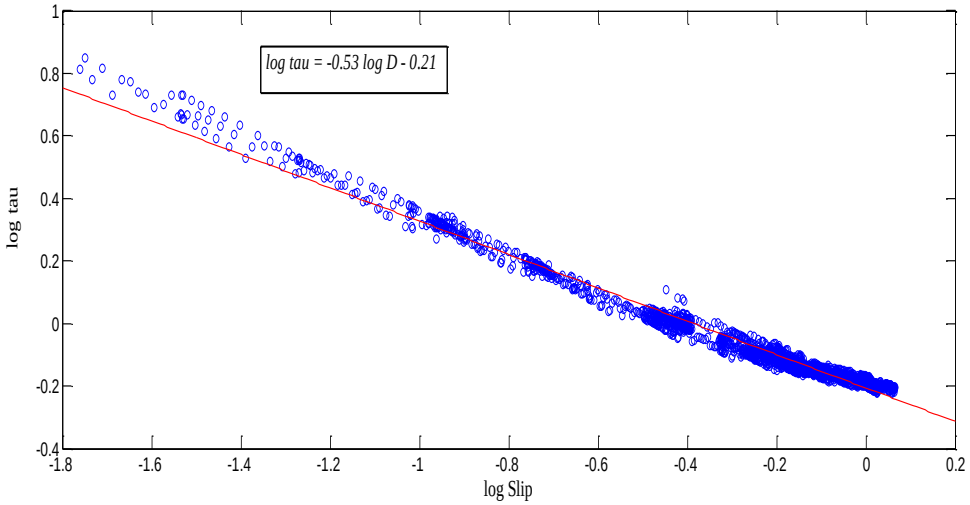

Fig. (4.8) Dependence of the slip averaged frictional force per block on the block slip

$$\bar{\tau} = 10^{-0.21} D^{-0.53} \tag{4.11}$$

Now we are in a position to formulate the sought energy balance equation in a mathematical form. Going back to equation (4.2)

$$\Delta U - W_F = E_p \tag{4.12}$$

Where ΔU the total change in potential energy in the healed region is, W_F is the cumulative frictional work in the healed region and E_p is the total pulse energy.

But:

$$\Delta U = \int_0^x \Delta u dx = \int_0^x [\Delta PE_{coil} + \Delta PE_{leaf}]dx \qquad (4.13)$$

where Δu is the change in total potential energy per unit length in the healed region , ΔPE_{coil} and ΔPE_{leaf} are as previously explained

And

$$W_F = \int_0^x w_f dx \qquad (4.14)$$

Hence one can write the balance equation in the following form:

$$\int_0^x \Delta u - w_f dx = E_p \qquad (4.15)$$

Taking derivatives of both sides, the fundamental theorem of calculus then yields:

$$\Delta u - w_f = \frac{dE_p}{dx} \qquad (4.16)$$

Substituting from (4.3),(4.4),(4.7) and (4.11) in (4.16) we arrive at the following first order second degree differential equation:

$$-\frac{1}{2}k_c(\frac{dD}{dx})^2 + \sigma_{oc}\frac{dD}{dx} - \frac{1}{2}k_l D^2 + \sigma_{ol}D - (\alpha D^\beta).D = \frac{d}{dx}(\gamma D^\xi) \qquad (4.17)$$

where we have used the power law approximations for the total pulse energy and frictional work per unit length: $E_p = \gamma D^{\xi}$ and $\bar{\tau} = \alpha D^{\beta}$. Simplifying and rearranging we get:

$$\frac{1}{2}k_c\left(\frac{dD}{dx}\right)^2 + (\gamma\xi D^{\xi-1} - \sigma_{oc})\frac{dD}{dx} + \left(\frac{1}{2}k_l D^2 - \sigma_{ol} D + \alpha D^{\beta+1}\right) = 0 \tag{4.18}$$

One can readily recognize that the third term in Eqn. (4.18) yields the condition for a pulse propagating with uniform slip. This is because in this case $\frac{dD}{dx}$ vanishes and we are left with $\frac{1}{2}k_l D^2 - \sigma_{ol} D + \alpha D^{\beta+1} = 0$, which is just a statement that the change in potential energy $\frac{1}{2}k_l D^2 - \sigma_{ol} D$ balances the frictional dissipation $\alpha D^{\beta+1}$ pointwise. This is the condition for steady propagation.

Factoring equation (4.18) gives

$$\frac{dD}{dx} = \frac{-(\gamma\xi D^{\xi-1} - \sigma_{oc}) \pm \sqrt{(\gamma\xi D^{\xi-1} - \sigma_{oc})^2 - 2k_c\left(\frac{1}{2}k_l D^2 - \sigma_{ol} D + \alpha D^{\beta+1}\right)}}{k_c} \tag{4.19}$$

To determine which sign of the radical is to be taken, we once again consider the limiting case of steady propagation. In this limit $\frac{dD}{dx}$ is zero and as we just showed, $\frac{1}{2}k_l D^2 - \sigma_{ol} D + \alpha D^{\beta+1}$ has to vanish. This is only possible if we take the positive sign. Hence,

$$\frac{dD}{dx} = \frac{-(\gamma\xi D^{\xi-1} - \sigma_{oc}) + \sqrt{(\gamma\xi D^{\xi-1} - \sigma_{oc})^2 - 2k_c(\frac{1}{2}k_l D^2 - \sigma_{ol} D + \alpha D^{\beta+1})}}{k_c} \qquad (4.20)$$

This is the final form of the pulse energy balance equation. It is important to state here that the physical derivation of this equation is exact in the continuum limit of a1D elastic system. The source of approximation comes from trying to approximate the dependence of the total pulse energy and frictional work on the pulse slip, which in our system turn out to be approximately power-law dependence as a direct consequence of the approximate self-similarity of the slip pulse. The scaling coefficients and exponents $\alpha, \beta, \gamma, \xi$ are empirically determined from the numerical simulations, and are generally functions of the system parameters [For the test model considered so far, the scaling parameters values are $10^{2.9}, 1.4, 10^{-0.21}$ and -0.53 respectively.]

To test the validity of the equation and how well it may perform, we used it to simulate some of the slip distributions generated by the spring block model. We use the same values of springs stiffness as those used in the spring block model and discretize our continuum ODE with $\Delta x = 1$ to match the model discretization. We then get a discrete map in the form:

$$D_{i+1} = D_i + g(D_i, \sigma_{oc_i}, \sigma_{ol_i}) \qquad (4.21)$$

The discrete map in Eqn. (4.21) implies that by knowing the slip and the prestress at a given point (*i*) we can use the discrete map to estimate the slip at the next point (*i+1*) and move forward until the event is over. Since the equation is first order, we need to know

the slip value at one point in order to know the values at other points. For the test purposes, we choose this point to be at the location when the nucleation phase is over and a single pulse is fully developed. The results of the equation simulation, along with the slip solution generated by the spring block model, are shown in Fig. (4.9 a). The corresponding prestress distribution is shown in Fig.(4.9 b).

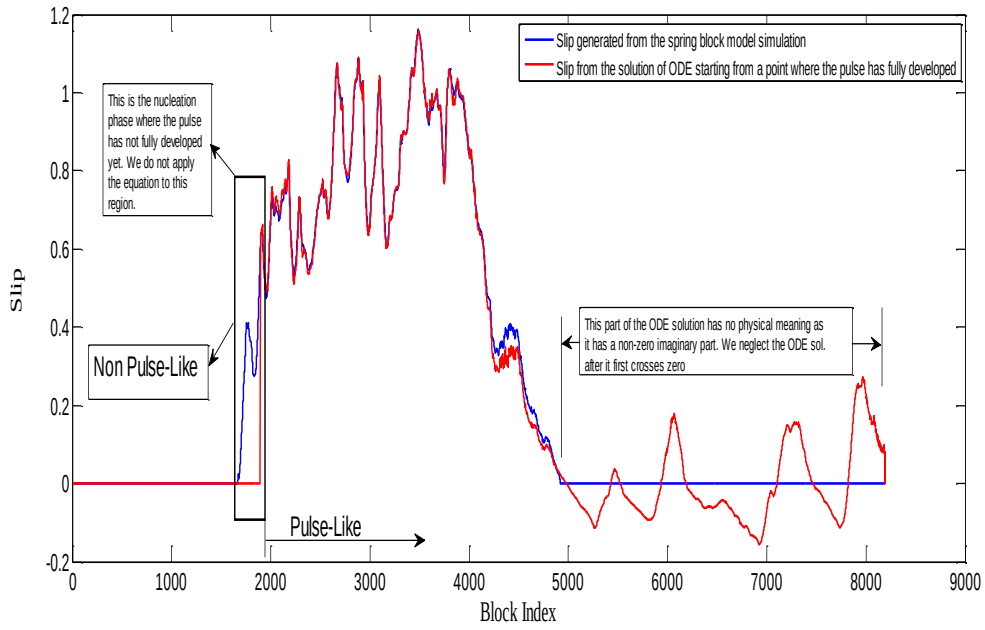

Fig. (4.9 a): The slip distribution as predicted by the pulse energy equation (red) along with the slip distribution generated by the full dynamic solution of the spring block model.

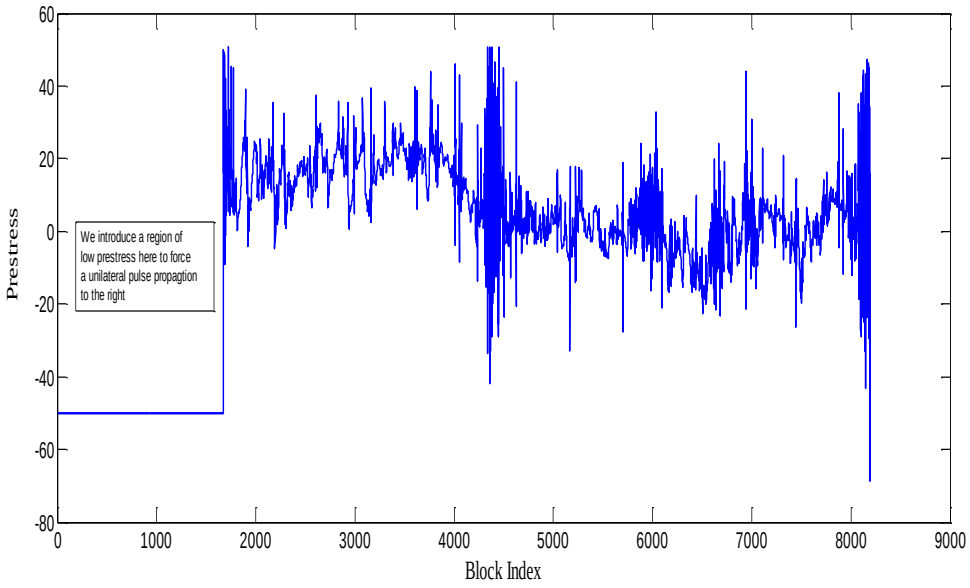

Fig. (4.9 b): Prestress distribution used to generate the slip distributions shown in Fig. (4.9 a)

The equation performs fairly well in the pulselike region matching the slip profile both qualitatively and quantitatively (to a great extent). The equation also gets the point of arrest of rupture fairly accurately. The saving in computational time is also huge; the time required to run the equation is nearly 10,000 times smaller than the time required to simulate this event using the spring block model. This gives a premise that the equation could qualify as a reduced order model for studying the long-time evolution of multi-degrees of freedom spring block models failing in pulse-like ruptures.

A question remains, however, how are we going to handle the nucleation region? This is crucial if we want to use the equation to generate a sequence of events for two reasons:

First, the equation needs to know the slip value at a given point in order for the iterative map (4.21) to get started. For the test case we were able to identify the point at which the

pulse has fully developed and apply the equation from that point on. In a sequence of events, without the full dynamic simulation results available, we do not have this possibility. How are we going to identify the initial conditions for the equation in this case?

Second, not all ruptures in a sequence of events are going to be unilateral as in the test case; some ruptures will be bilateral, propagating in both directions. Since all the interactions in this spring slider model setup are local, pulses propagating in the opposite directions do not interact with each other and hence a bilateral rupture is effectively two unilateral ruptures propagating in opposite directions. Accordingly the equation can be applied to each direction independently. However, a new problem arises; instead of needing to know the slip at only one location in order to get the equation started, we need to know the slip at two different points; one for the rupture in each direction. Once again how are we going to choose the initial conditions?

To answer the question of initial conditions, we decided that it would be best to simulate the nucleation phase accurately using the spring block model, and then once the pulse is fully developed, we can use the equation to predict the slip outside the nucleation region. In this way we would be able to get the correct initial conditions for the application of the equation, but the simulation time would probably be longer since we will spend some time solving the full dynamic equations of the spring block model. Nonetheless, since the nucleation region is generally limited in size, there would still be considerable saving in the computational time by using this hybrid approach (hybrid in the sense that the spring block is used to simulate the nucleation and the equation is used for further propagation).

This is because a major part of the simulation time for the spring block model is usually spent in simulating large- and intermediate- sized events. With the proposed hybrid model, most of those events will be quickly modeled by the pulse energy equation with no need to solve the full system of equations of motion for the blocks.

So far we have demonstrated the effectiveness of the pulse energy equation in replicating the major features of the slip solution generated by the spring block model. To further assess the quality of the match between the two models, we compare the stress change distribution resulting from the slip generated by both of the equation and the spring block slider system for the test problem. Since the stress change calculation involves derivatives of the slip, short wavelength discrepancies between the two solutions are amplified and hence can get spotted. The stress change can be readily calculated from the slip using the following formula:

$$\Delta\sigma_i = k_c(D_{i+1} - 2D_i + D_{i-1}) - k_l D_i \tag{4.22}$$

where $\Delta\sigma$ is the stress change, D is the slip and i is the spatial location index. The stress change over a part of the pulse-like rupture resulting from the slip generated by both of the equation and the spring block system is plotted in Fig. (4.10). While the equation seems to match the slip pretty well [Fig.(4.9 a)], it turns out it over-predicts the heterogeneity of the slip at small scales. This is reflected in the stress changes generated by the equation which clearly overshoots, by orders of magnitude, the stress changes predicted by the spring block model at different locations. A possible explanation for the increased heterogeneity of the slip predicted by the equation at small scales is the fact

that there is no notion for the pulse width in the equation formulation. In the simulations of the spring block model, the finite pulse width would tend to smooth the slip solution at least over distances comparable to this width and results in more moderate stress changes. In the equation, such an effect is absent, and although we are getting the energetics and the general features of slip correct from the equation, the details on the high frequency level are missing, and result in incorrect stress changes. This could be problematic in a sequence simulation and hence needs to be taken care of in order to be assured that the long-time solution of the pulse energy equation could match approximately the long-time statistics of the spring block slider.

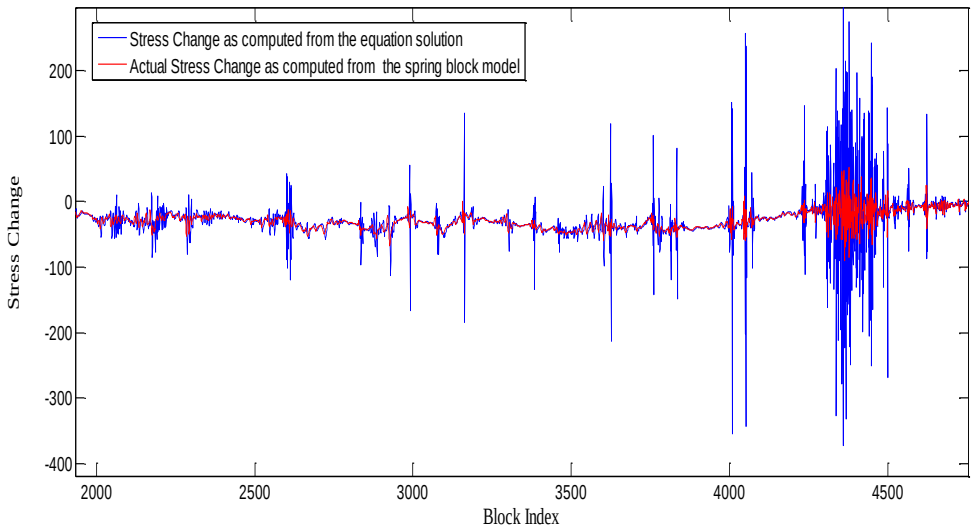

Fig. (4.10): The stress changes produced by the equation slip solution (blue) along with the actual stress changes predicted by the spring block model (red). The equation tends to overestimate the stress changes as indicated by the

high amplitude blue spikes observed at different locations. This reflects that the slip generated by the equation is actually rougher on small scales than the slip of the spring block model solution.

We test the hypothesis of the influence of the finite pulse width by filtering the slip solution generated by the equation using a moving Gaussian function, analogous to the pulse shape, of unit amplitude and a standard deviation that is a fraction of the pulse width. The pulse width is assumed to be dependent on the pulse slip, and as shown in Fig.(4.11) it can be estimated using the power law relation in Eqn.(4.23):

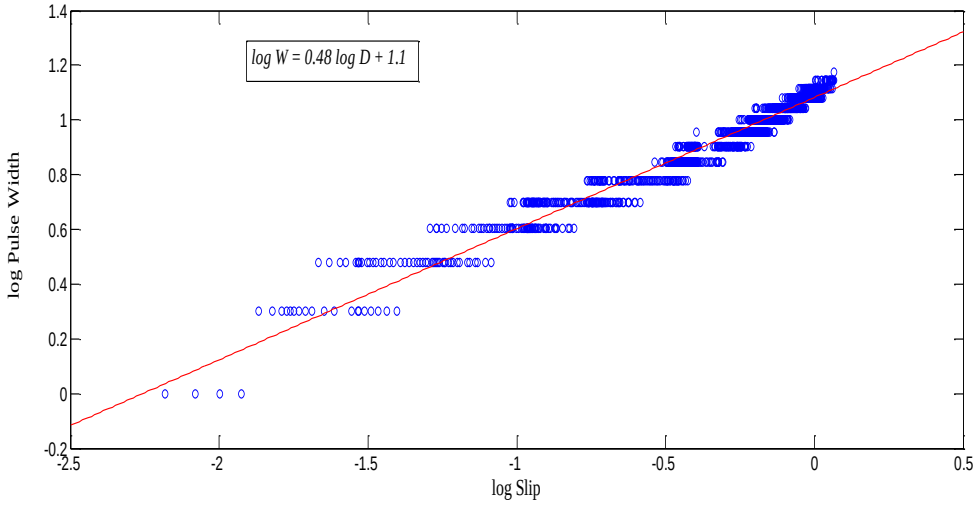

Fig. (4.11) : Scaling of the pulse width with the pulse slip. Pulses with larger slips tend to be wider. The dependence is approximately power law with some scatter.

$$W = 10^{1.1} D^{0.48} \tag{4.23}$$

The smoothed slip compared to the slip generated by the spring block slider model is shown in Fig.(4.12). Note that two solutions still match pretty well. The stress change generated by the two models is shown next in Fig.(4.13). One can notice that the overshooting in the stress changes predicted by the equation has now gone and that the slip solution generated by the equation produces stress variations comparable to those generated by the spring block model.

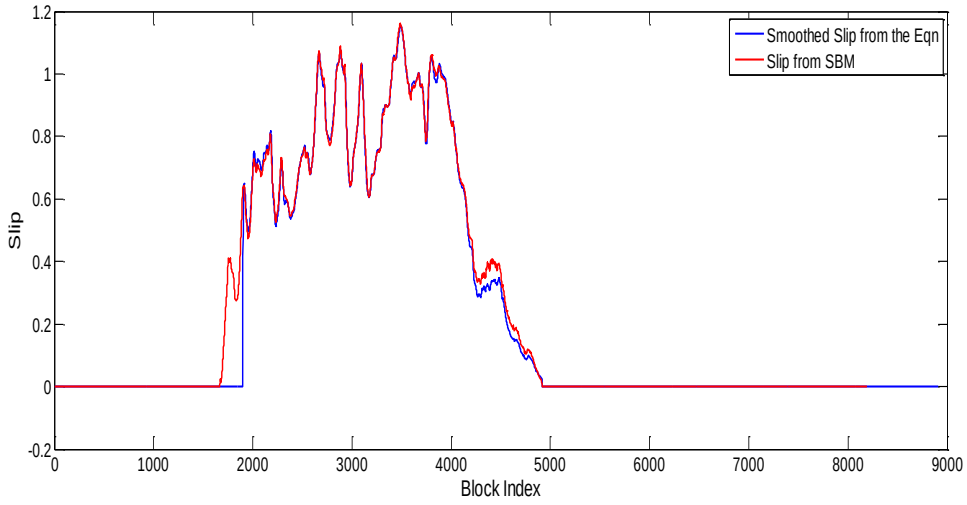

Fig.(4.12): A smoothed version of the slip generated by the equation (red) along with the slip generated by the spring block model (blue). The smoothing is carried out by convolving the equation solution with a Gaussian function of unit amplitude and standard deviation equal to a fraction of the corresponding pulse width. The smoothing process did not alter the macroscopic features of the equation solution which is still agreeing very well with the spring block model results.

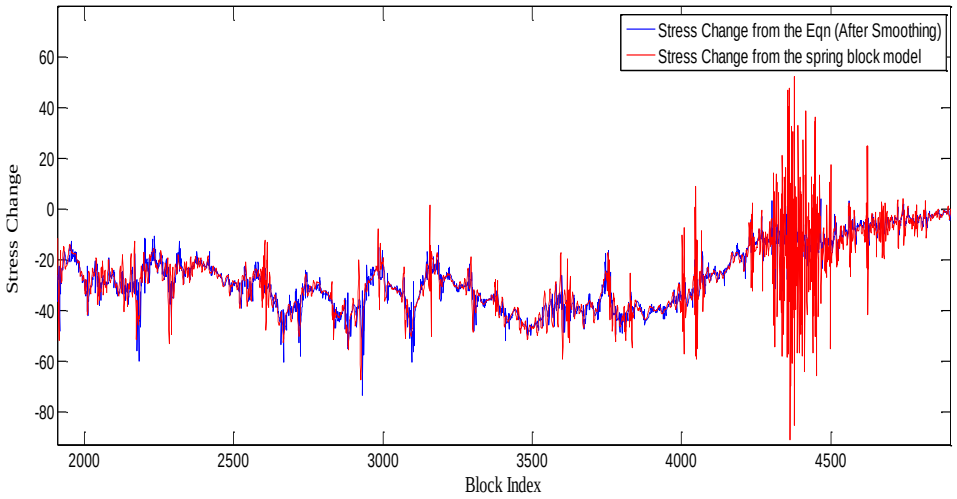

Fig.(4.13) : The stress changes produced by the equation solution after applying the smoothing operation (blue) along with the actual stress changes produced by the spring block model (red). The difference between the stress changes produced by the two models have significantly decreased, indicating that the equation solution now matches better the small scale feature of the spring block model slip solution.

To first order, the results in Fig.(4.13) confirms that considering the finite width of the pulse plays an important role in taming the stress variations and bringing the solutions predicted by the two models closer to each other. The match between the stress changes produced by the model and those introduced by the equation may be further enhanced by playing with the standard deviation of the Gaussian filtering function or by considering the pulse width explicitly as a new variable and construct its evolution equation. We plan to explore this latter option in our future studies.

4.4. Sensitivity Analysis

Since the scaling coefficients and exponents used to approximate the slip dependence of the pulse total energy and the cumulative frictional work are empirically derived from the numerical simulations, it is important to know how sensitive the equation solution is to variations in their estimates. In this section we show the results of a sensitivity analysis for the four parameters $\alpha, \beta, \gamma, \xi$. The sensitivity study is done as follows: For the test case considered, we compare the solution generated by the equation for a perturbed value of one of the parameters to the solution of the spring block model. We perturb only one parameter at a time leaving the three other parameters fixed at their values, which were estimated from the numerical simulations of the test problem. We use two measures to assess the quality of the perturbed solution: i) the ability to predict the total rupture length, this is measured by the difference between the rupture length predicted by the equation and the actual rupture length from the spring block model solution with the result being normalized by the actual rupture length, and ii) the ability to generate an analogous slip profile to that generated by the spring block model. This is measured by calculating the L_1 norm of the difference between the slip solution of the equation and the slip generated by the spring slider over the pulse-like portion of the rupture:

$$\|Error\|_1 = [\sum_{\substack{i \in \text{Pulse like} \\ \text{region}}} | D_{eqn,i} - D_{SBM,i} |] / [\sum_{\substack{i \in \text{Pulse like} \\ \text{region}}} | D_{SBM,i} | \tag{4.24}$$

The L_1 norm is technically given by the numerator. For error calculations, we divide the norm by the sum of the slip values within the pulse like region of the spring block model.

4.4.1. Sensitivity of slip solution to perturbations in the scaling parameters:

Figure (4.14) shows the influence of varying the scaling parameters for the total pulse energy and the cumulative frictional work on the relative error in the slip distribution generated by the equation. The scaling coefficient γ which controls the slip scaling of the pulse energy turns out to have the largest effect on the quality of the solution. On the other hand, the slip distribution seems to be less sensitive to variations in the parameters (α, β) governing the slip scaling of the cumulative frictional work. This reflects that the dynamics in the spring block model are strongly governed by the magnitude of energy of the slip pulse. Changing the pulse energy changes the way it interacts with stress heterogeneities and consequently changes the resulting slip distribution; for example the more energetic the pulse is, the more capable it is to penetrate through prestress fluctuations and the smoother the slip it produces for a given prestress distribution. This does not mean that friction is not important. On the contrary, it is the strong positive feedback between the friction and the slip rate that generates the localized slip pulse in the first place. But since the weakening is so strong, the friction within the pulse is generally small and the energy of the pulse, which carries within it the signature of strong rate dependent friction, turns out to have the strongest influence on the dynamics.

a

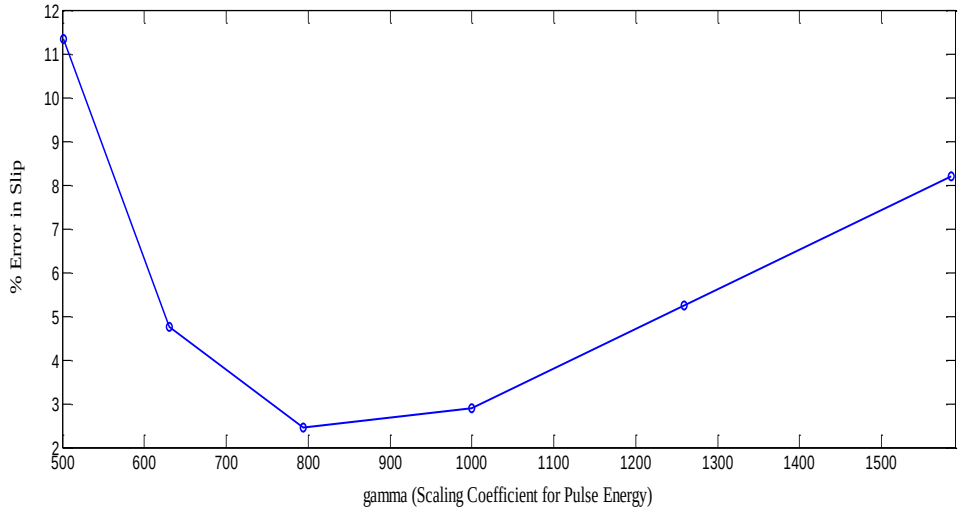
% Error in Slip
gamma (Scaling Coefficient for Pulse Energy)

b

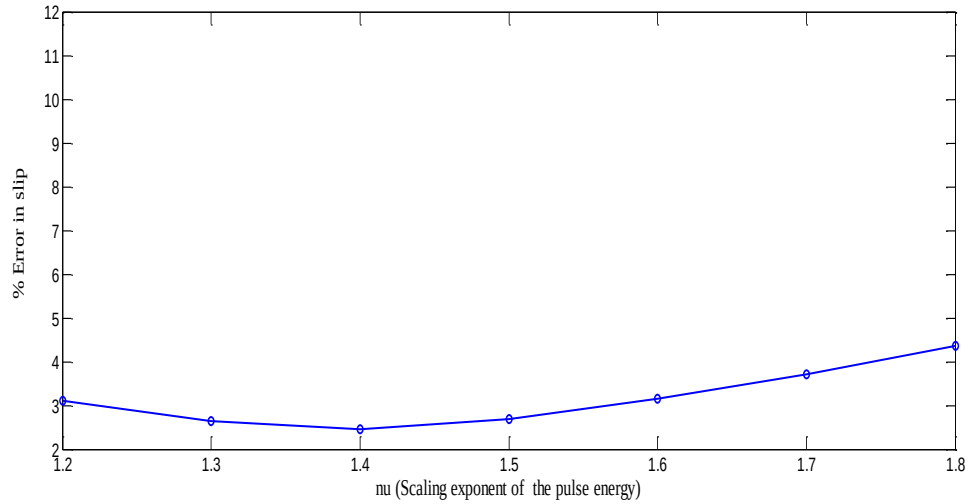
% Error in slip
nu (Scaling exponent of the pulse energy)

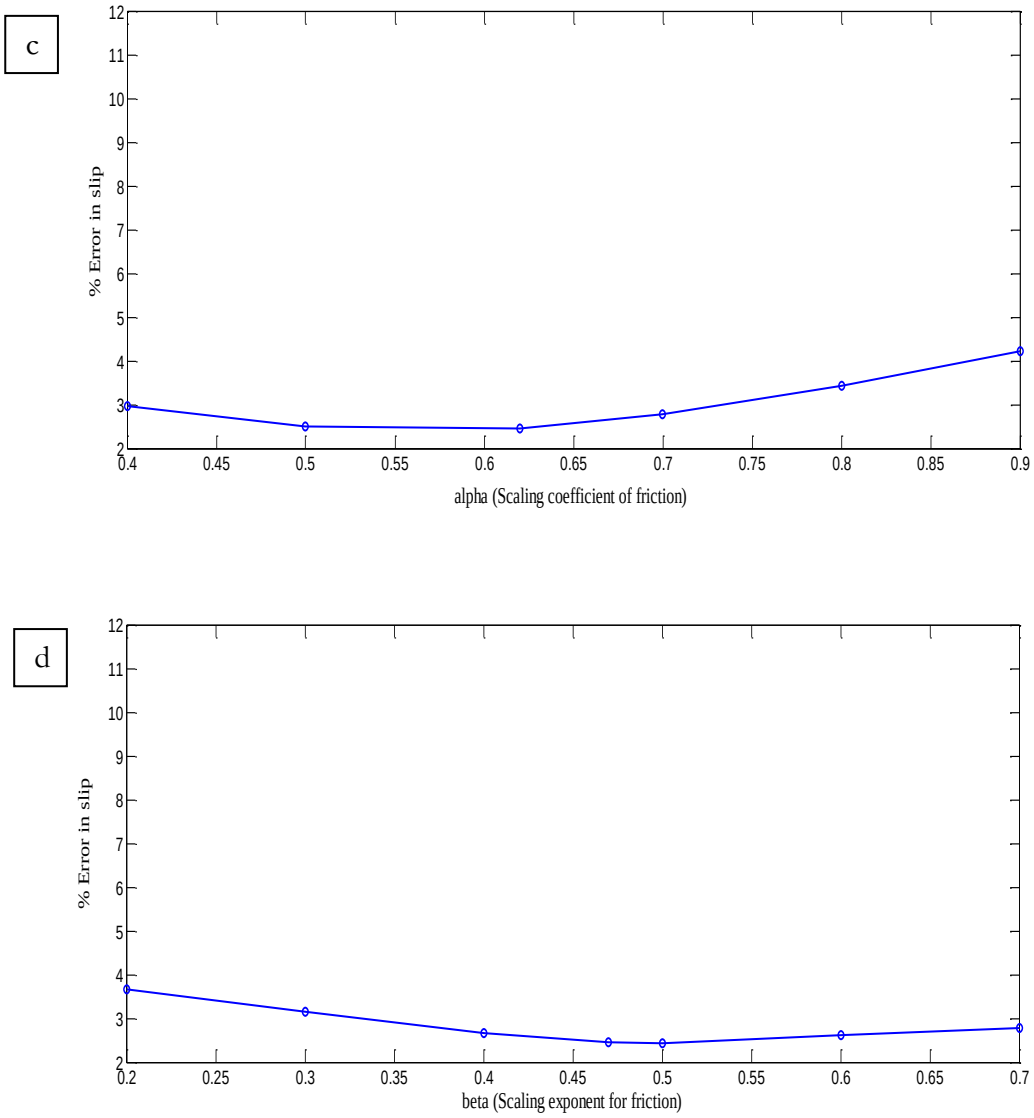

Fig. (4.14): Relative error in the slip solution, as measured by the scaled L1 norm defined in (4.24) , as a function of the different scaling parameters: (a) Effect of varying the pulse energy scaling coefficient γ while other parameters are kept constant. (b) Effect of varying the pulse energy scaling exponent ξ. (c) Effect of varying the frictional work scaling coefficient α and (d) Effect of varying the frictional work scaling exponent β.

The strongest influence on the results turns out to be due to changes in the pulse energy scaling coefficient.

4.4.2. Sensitivity of rupture length to perturbations in scaling parameters:

Figure (4.15) shows the influence of varying the scaling parameters for the total pulse energy and the cumulative frictional work on the relative error in the total rupture length predicted by the equation. Once again, varying the pulse energy scaling coefficient γ can produce significant errors in the estimation of the event total rupture length. This is because, if the pulse energy is overestimated, the pulse could propagate further in the same prestress conditions and hence the rupture length will be longer. On the other hand, if the pulse energy is underestimated, it will be easier to stop the pulse, under the same prestress conditions, and the resulting rupture length will be shorter. The other scaling parameters affect the solution as well but to a lesser extent.

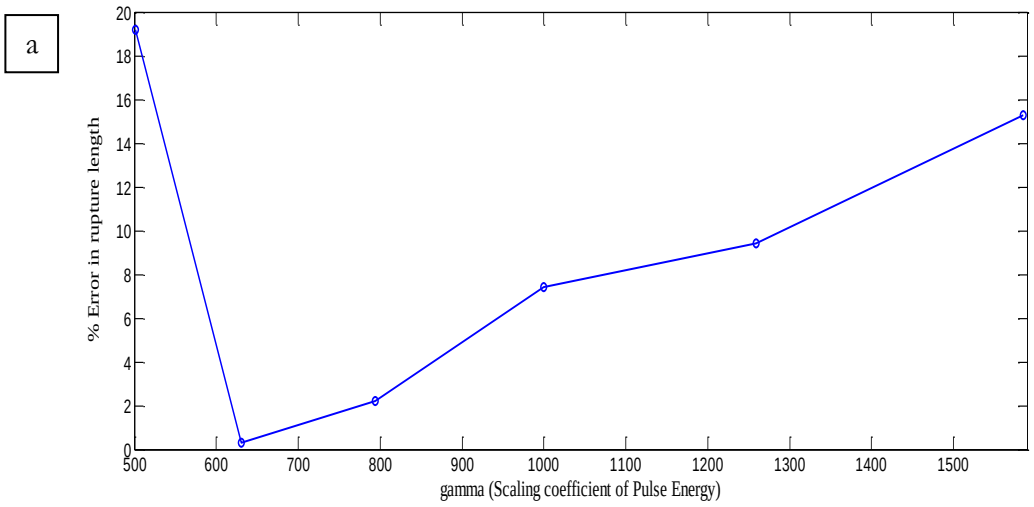

b

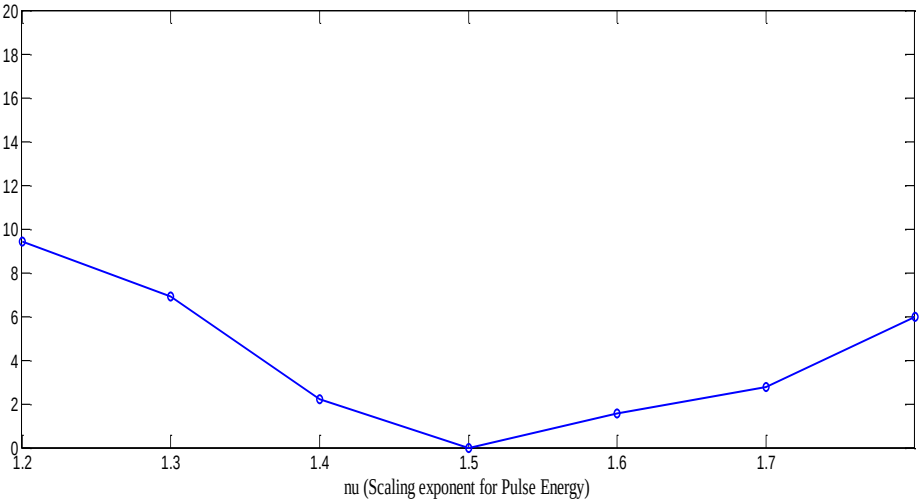
20
18
16
14
12
10
8
6
4
2
0
1.2
1.3
1.4
1.5
1.6
1.7
nu (Scaling exponent for Pulse Energy)

c

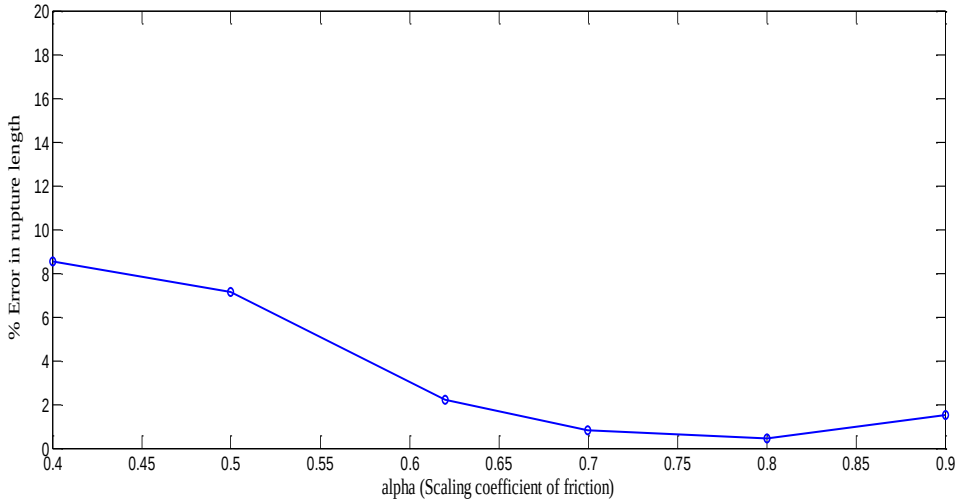
% Error in rupture length
20
18
16
14
12
10
8
6
4
2
0
0.4
0.45
0.5
0.55
0.6
0.65
0.7
0.75
0.8
0.85
0.9
alpha (Scaling coefficient of friction)

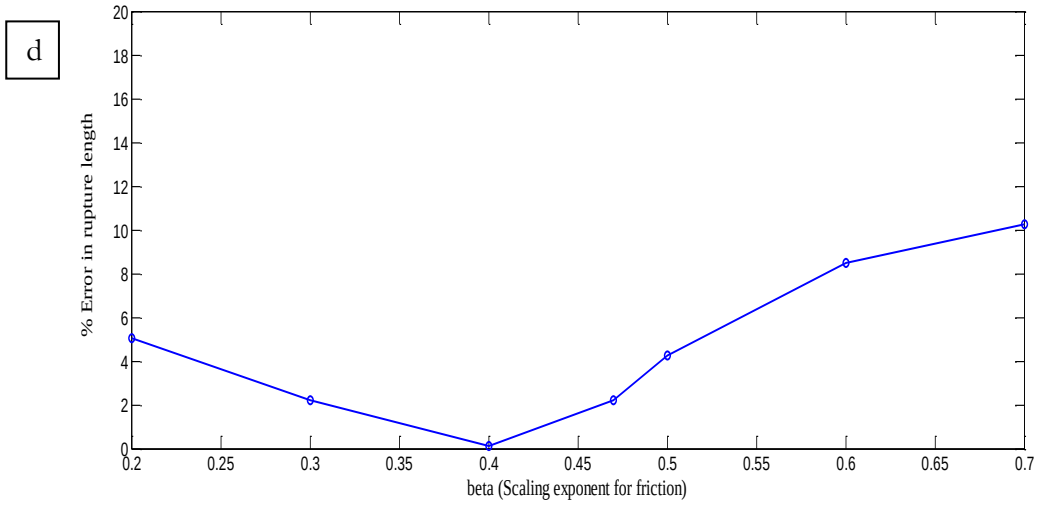

Fig. (4.15): Relative error in the estimated rupture length from the solution of the pulse energy equation as a function of the different scaling parameters: (a) Effect of varying the pulse energy scaling coefficient γ while other parameters are kept constant. (b) Effect of varying the pulse energy scaling exponent ξ. (c) Effect of varying the frictional work scaling coefficient α. (d) Effect of varying the frictional work scaling exponent β. Similar to Fig. (4.14), the strongest influence on the results turns out to be due to changes in the pulse energy scaling coefficient. However, other parameters have an influence on the rupture length that is greater than their influence on the slip solution.

4.5. Long-time simulation results for the pulse energy equation

In this section we explore some of the long-time statistics of the proposed hybrid model (spring block model for nucleation and the equation for further propagation) and its computational efficiency when compared to the full spring block slider model. A question central to this procedure is whether the scaling coefficients for the pulse energy

and frictional work differ from one event to another or not, and what are the implications of this variation, if any.

To answer this problem we have studied the energy scaling in three rupture scenarios; the test case, a case for a rupture spanning ~ 2000 blocks, and a third rupture of length ~ 400 blocks. These ruptures are meant to cover the classes of very long, long and intermediate sized event. Figure (4.16) shows the scaling of the total pulse energy whereas Fig (4.17) shows the scaling of the frictional work per unit slip at the block level.

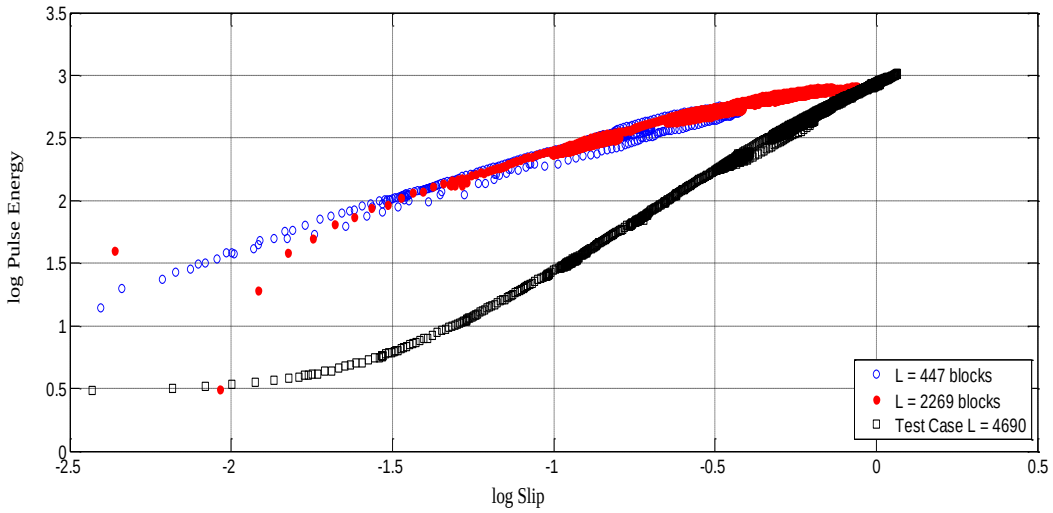

Fig. (4.16): Scaling of the total pulse energy with the pulse slip for events of different lengths. The scaling exponent ξ (the slope of the best fit straight line) shows some variation between different events groups..

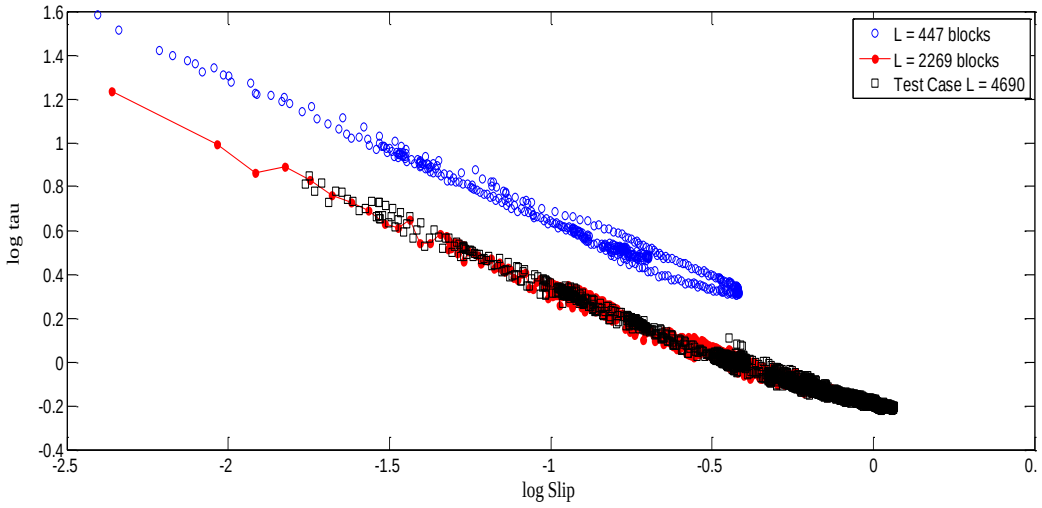

Fig. (4.17): Variation of tau τ (frictional work per unit slip at the block level) as a function of the block final slip for events of different lengths. The scaling exponent β shows a small amount of event size dependence while the scaling coefficient α shows stronger dependence.

It is evident that the scaling coefficients have some dependence on the event size. The dependence in the case of the pulse energy scaling exponent (the slope of the straight lines in Fig. (4.16)) is stronger than the dependence of the rest of the parameters. In the case of the frictional work scaling, the scaling exponent does not vary much from one event to another [Fig. (4.17)]. The amplitude of the friction, however, varies to some extent from one event to another.

While the event dependence of the scaling parameters might look as a problem, it might not be a serious one. The knowledge of the exact value of the scaling parameters on the event level is important if replicating individual events is the target. If, on the other hand,

the long-time statistics of the system are what we are looking for, it may suffice to have an approximate average value for the scaling parameters. To test this hypothesis, we run the proposed hybrid model for different combinations of fitting parameters and look for values that can yield the best approximation to the long-time statistics of the full dynamic simulation of the spring block.

For the sake of illustration, we run long-time simulations for the hybrid model with different pulse energy scaling coefficients and same frictional work scaling parameters as found for the test case. The motivation behind this is that, as we discussed in the last section, the slip profile generated by the proposed pulse energy equation seems to be less sensitive to perturbations in the frictional work scaling law than to perturbations in the pulse energy scaling coefficients. The different plots in Fig.(4.18) show the spectrum of the evolved prestress after 1000 events using the hybrid model with different total pulse energy scaling coefficients (blue) compared to the amplitude spectrum of the evolved prestress from the spring block model (red).

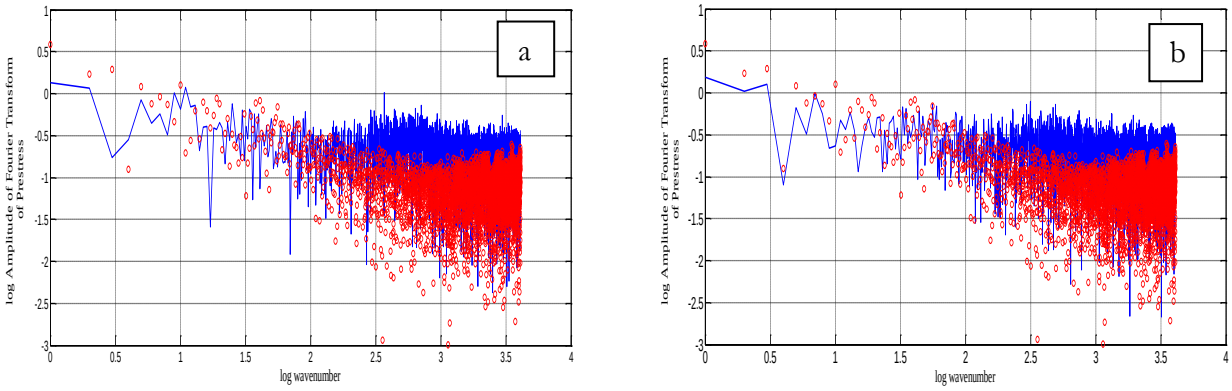

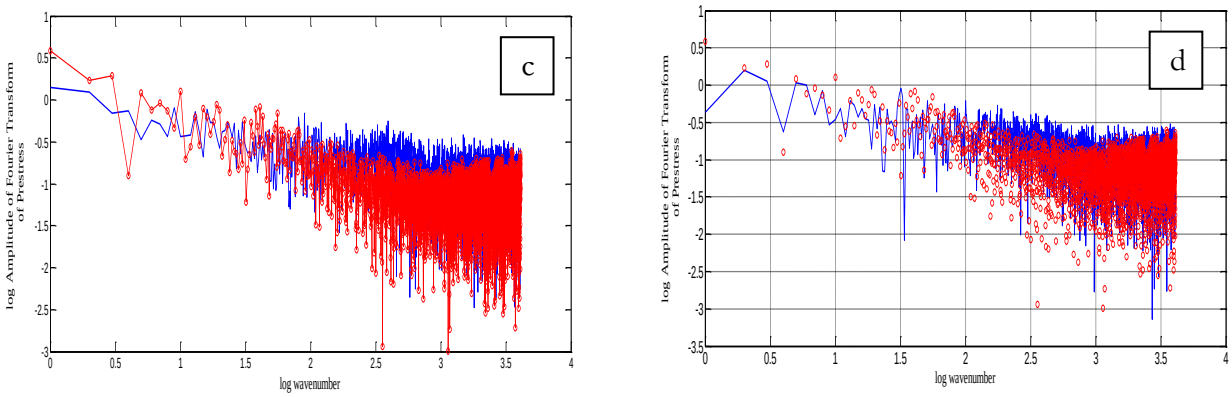

Fig. (4.18): The amplitude of the Fourier transform of the evolved prestress from the solution of the hybrid model (blue) along with the correct distribution generated from the full dynamic simulation of the spring block model (red) for different total pulse energy scaling parameters.: a) $\gamma = 10^{3}, \xi = 1.2$, b) $\gamma = 10^{2.9}, \xi = 1.4$, c) $\gamma = 10^{2.8}, \xi = 1.6$ and d) $\gamma = 10^{2.7}, \xi = 1.8$,which produces the best fit for the stress spectrum.

The above plots show the prestress amplitude spectrum for four different randomly selected combinations of the pulse energy scaling parameters (γ, ξ). We note that the smaller the value of the scaling exponent (ξ) and the smaller the value of the scaling coefficient (γ) are, the larger the discrepancy between the model prediction (blue) and the spring block slider results (red). For example, for $\xi = 1.2$ and $\gamma = 10^{3}$ [Fig. (4.18 a)] the hybrid model significantly over predicts the amplitudes of the prestress spectrum in the intermediate and large wavenumber regime ($\log f > 2.0$) compared to the true prestress spectrum from the spring block simulation. This feature fades in the other plots [Fig.

(4.18 b, c and d)] as ξ increases and γ decreases. For the case with $\xi = 1.8$ and $\gamma = 10^{2.7}$ [Fig. (4.18 d)] the spectra of the prestress generated by the two models agree fairly well.

The event size distribution for the hybrid model with the parameters $\xi = 1.8$ and $\gamma = 10^{2.7}$ is shown in Fig.(4.19) along with the event size distribution generated by the spring block model. Since events spanning a few blocks are essentially calculated by the spring block model, as they do not have the chance to grow large enough and develop slip pulses, the statistics of the event size distribution for both models in the regime of small events is very similar. On the other extreme, the hybrid model does a good job in predicting the major features of the large event statistics, including the existence of a characteristic hump and the maximum event size. The distribution of the intermediate sized events, however, shows strong discrepancy. The hybrid model overestimates the number of events in this range. Several factors might be contributing to this. For example, the choice of the scaling parameters might not have been the optimum one for generating correct statistics for the whole size distribution spectrum and we may need to search more. Also, one has to be aware that intermediate-sized events, especially in their lower range, have smaller pulses that propagate for only short distances outside the nucleation region. For small slip values, and hence small pulses, we can observe from Fig.(4.16) that there always exists a breaking in the scaling of the pulse energy. This has not been a problem for large events, but for smaller ones, this might lead to variations in the event rupture length that might be comparable to the predicted length itself, and hence change the event size distribution in this regime.

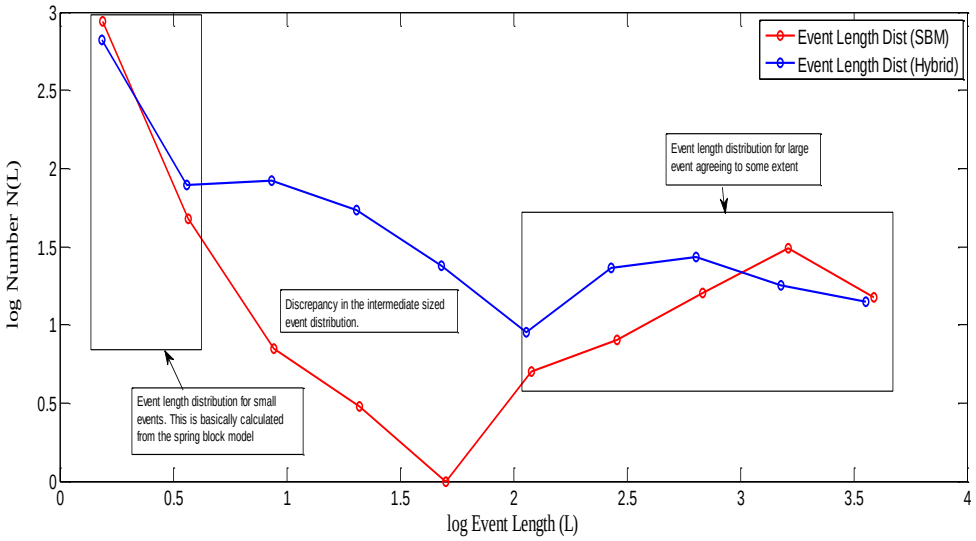

Fig. (4.19): Event length distribution generated by the two models: the hybrid model (blue) and the spring block model (red).

We show a different example for the long-time performance of the proposed hybrid model for a different combination of spring block model parameters in Appendix B.

Finally, one might conclude that the long-time simulation of the hybrid model can match some of the long-time statistics of the spring block model in a much shorter computational time, even within the first order approximation of the slip scaling of the pulse energy and the frictional work,. Both of the statistics of the evolved prestress as well as some features of the statistics of large events are reproduced to an acceptable level of accuracy.

However, there is certainly room for improvement. As part of our future work, we plan to incorporate second order corrections into the energy scaling laws we have introduced so far such as accounting for the breaking in scaling for small slips, incorporating the finite pulse width and taking into consideration the event size dependence of the values of the scaling parameters. We are also planning to develop an efficient grid search algorithm to find the optimum values of the scaling parameters for better matching of the statistics as well as to explore the dependence of this optimum value on the spring block slider model specific parameters (e.g. stiffness ratio and frictional weakening strength).

4.6. Discussion

Designing computationally efficient physically based earthquake simulators is a central problem in seismology and earthquake physics. While a detailed dynamical modeling is essential for understanding the mechanics of earthquake ruptures on the level of individual events, there are many applications in which we are interested in the statistics of the system more than in the details of single ruptures. Such applications include for example, seismic hazard analysis, the statistics of seismicity, and ground motion prediction. For such problems, we might not be interested in the detailed dynamic evolution of the rupture but a physically grounded kinematic description may be sufficient.

In this manuscript we have introduced a new paradigm for simulating earthquake slip for pulselike ruptures based on the energy budget of the propagating slip pulse. The choice of

slip as the variable to be solved has its reasons. Slip is an observable variable that is routinely inferred from seismic inversions and hence can provide a good constraint for any computational method. Also since there exist several relationships that empirically correlate the slip to the other rupture parameters, such as the maximum slip rate and rise time, by knowing the slip profile we can infer an approximation for the evolution of the slip pulse along the fault and can use it to generate ground motion quickly and reliably (assuming an appropriate pulse shape such as the Yoffee or Gaussian functions).

The method proposed here is inspired by the localization of the slip pulse. At any instant in time during a pulse-like rupture, the slip pulse only occupies a very limited portion of the fault. Moreover, many dynamic simulations, including the ones we presented here, have revealed that the pulse preserves approximately its characteristic shape during propagation; its width and amplitude may grow or shrink depending on the conditions, but the pulse has an approximately self-similar shape. These two observations, localizations and the approximate characteristic shape, suggested that only a small number of degrees of freedom may be used to describe the evolution of the pulse, and hence of the rupture. This number may be much less than the total number of degrees of freedom building up the system as a whole suggesting that a dimensional reduction or a coarse-graining procedure might be feasible.

We have found that a key to the coarse-graining for pulselike ruptures might lie in the energy balance of the pulse itself. To keep things simple and to test our hypothesis, we chose to simulate pulse-like ruptures in a discrete fracture model, the spring block model, where pulses can only sense nearest neighbor interactions. In that sense, we ruled out the

radiated energy from our model and all the dynamic changes are localized to the pulse zone. The energy balance in this case took the simple form:

change in potential energy of the system at any given instant – cumulative frictional work dissipated by the pulse up to this instant = The current kinetic energy of the pulse.

By writing down the exact change in potential energy in terms of the final slip and prestress, and by approximating the pulse energy and the frictional work as power laws in the pulse slip with power law parameters empirically derived from the numerical simulation of the spring block model, we were able to formulate the differential equation in Eqn. (4.20). While the equation is written in terms of slip, it is actually an energy balance equation with the different energy terms approximated in terms of the final slip and prestress. This is why we call this equation the pulse energy equation. The solution of the equation revealed many interesting features.

First, the equation did a very good job in replicating the basic features of the slip distribution in the pulse-like portion of the rupture, including slip amplitudes and total rupture length. Second, the equation generated stress changes that are larger than the actual stress changes produced by the full solution of the spring block model. This indicated that the micro-scale features of the slip solution generated by the equation are different from those produced by the spring block model, although the macro-scale features agree quite well. By accounting for the finite pulse width and by convolving the slip solution generated by the equation with a Gaussian function whose standard deviation is a fraction of the pulse width, we were able to make the stress changes

produced by both models become comparable to one another. Third, with the equation designed for pulse-like ruptures, it did not perform well in simulating the nucleation phase of the rupture, which is usually crack-like. To overcome this problem, we used the spring block model to accurately simulate the nucleation phase and once the rupture assumed the pulselike shape we switched to the equation for further propagation and prediction of the final slip in the rest of the rupture. By using this hybrid approach, we gained several advantages: i) we accurately computed the nucleation, ii) we obtained the initial slip value necessary for starting the equation right and iii) we could then simulate bilateral ruptures as two independent ruptures propagating away from the nucleation region in opposite directions to one another. Finally, the saving in computational time by using the energy equation, or the hybrid version, instead of solving the full dynamic spring block model was huge and of the order of 3-4 orders of magnitude.

The hybrid model also performed fairly well when used to simulate the long-time statistics, although not as well as on the level of individual events. By performing a limited search of the scaling parameters search we were able to find a combination of scaling parameters that led to long-time prestress statistics and large event size distribution, matching well with the corresponding statistics from the spring block model. The saving in computational time was almost two orders of magnitude. As part of our future work, we are planning to develop an efficient grid search algorithm to find the optimum values of the scaling parameters for better matching of the overall statistics, as well as to determine the dependence of this optimum value on the spring block slider model specific parameters (e.g., stiffness ratio and frictional weakening strength). In this

sense, once the spring block model parameters are assumed, the scaling parameters can be estimated and the hybrid model can be used with confidence.

It is interesting to note however that despite of the simplicity of the proposed equation and the rough approximation of the dependence of the pulse energy and frictional work on slip, the energy equation and the hybrid model performed well and revealed a multi-scale nature. It seems that knowing the details of the dynamic propagation, manifested for example in the exact values of the energy scaling parameters, might be important for replicating the slip features on the single rupture level. However, for the long-time statistics, one can do a good job with some average values for those parameters. This feature is common in many complex systems ranging from turbulent fluids to sand dune slide where the macroscopic long term behavior might not be sensitive to the underlying microscopic dynamics.

It is also important to note that the principles upon which the proposed pulse energy equation was derived are rather general and not limited to the details of the spring block model we have used. Those principles, such as pulse localization, energy balance and approximate characteristic shape of the pulse, are also valid in more complicated continuum simulations. There is one important difference, however. In a continuum medium, there exist long-range interactions carried by the radiated wave field. This feature is missing in the spring block model, where all interactions are short ranged and there is no radiated wave field. This undoubtedly will complicate the situation in trying to extend the proposed approach to the continuum. Nonetheless we still think that the more localized the pulse is, the more sensitive it gets to local conditions than to fluctuations

carried by the radiated wave field. That is said, we think it might be possible to extend the current approach by adding, for example, a term in the energy balance equation that accounts for the radiated energy flux.

Chapter 5: Steady Pulses in Continuum Fault Models with Strong Velocity-weakening Friction

In the previous chapter, our focus was on pulse dynamics in a discrete model of fracture; the spring block slider model. Our conclusions suggest that repeated pulselike rupturing in the presence of strong velocity-weakening friction leads to the evolution of heterogeneous prestress distribution with power law spectral properties and, in general, non-Gaussian probability density functions. We also found further implications on the energy scaling. Due to the presence of strong velocity-weakening friction and the pulselike nature of rupture, longer ruptures will dissipate less energy per unit potency than shorter ones and are characterized by lower average prestress, suggesting consisting with the observation that longer faults are "weaker" than shorter ones and providing a dynamics-based perspective for this weakness. Finally, we presented a new paradigm for the computational modeling of pulselike ruptures, based on the energy balance of the propagating slip pulse, and showed that this approach can save much computational time and produce reliable results regarding the slip distribution in individual events, as well as many long-time system statistics.

In this Chapter we extend our interest to a continuum model of fracture. It will be interesting to explore whether the conclusions we have made in the discrete framework could be generalized to the more complicated setting of the continuum or not. Our attempt here is to start this direction of study by examining the problem of slip pulse formation and propagation in a simple 2D antiplane continuum model in the presence of

strong velocity-weakening friction. A central question to us in this chapter is how sensitive the slip pulse can be to perturbations in the prestress distribution, as the answer might entail important implications for the evolution of complexity in real earthquakes. To assess this question quantitatively, we search for a steady pulse solution; a pulse that can propagate in a uniform prestress field without change of its shape. Previous studies show that the existence of the steady pulse is doubtful [Perrin et al., 1995 and Ben-Zion et al., 2003]. We, however, show here that by correctly tuning the prestress and the nucleation procedure, a steady pulse can be realized in numerical simulations. Using the steady pulse solution as a reference, we perturb the prestress conditions and examine the response of the steady pulse to perturbations of different amplitudes and wavelengths. Our results suggest that pulses adapt well to local perturbations in the prestress and this could lead to significant variability in the slip distribution, suggesting that narrow pulselike ruptures propagating in heterogeneous prestress fields are plausible mechanisms for slip complexity observed in real earthquakes.

5.1. Seismological and numerical evidence for the existence of slip pulses

Seismic inversions and computational models have shown that earthquake ruptures may occur in one of two basic modes: the expanding crack mode and the self-healing mode. In the expanding crack mode, as the rupture zone keeps expanding, the slip continues everywhere within the ruptured area. In the self-healing mode, the rupture propagates in the form of a slip pulse, with the cessation of slip directly behind the pulse, so that at any instant of the rupture, only a small portion of the fault is slipping simultaneously.

Several mechanisms can contribute to the arrest of slip behind the rupture front and hence the formation of the slip pulses. One possible mechanism is the existence of geometric confinement of the rupture domain due to the existence of unbreakable regions. Day (1982) showed such pulse-like behavior in his 3D elastodynamic simulations with constant stress drops when the rupture was confined to a long but narrow region by unbreakable boundaries. He observed that the rupture starts as classical cracklike mode near the hypocenter and propagates in all directions until arrest signals come back from the borders that effectively stop the rupture behind the crack front, leading to the formation of two slip pulses propagating in opposite directions. Johnson (1992) studied faulting in a 2D model of a brittle crustal plate that is coupled to a non-brittle substrate and found slip-pulse generation by a similar mechanism to that of Day. Johnson (1990) also studied rupture in models without the feature of confinement of slip to a narrow channel; he noticed that if the rupture initially propagates bilaterally and is then arrested by a strong barrier at one end, the healing wave, combined with the propagation of the other end, forms a pulselike rupture pattern. Perrin et al. (1995) also illustrate this barrier-based mechanism of self-healing in a case that would, otherwise, result in a cracklike rupture.

Another mechanism for the generation of slip pulses is the existence of strong heterogeneities in the stress or strength distribution along the fault. Beroza and Mikumo (1996) re-examined the 1984 Morgan Hill, California, earthquake using strong-motion data. They suggested that spatially heterogeneous fault strength, in the absence of any significant velocity-weakening at slip rates during rupture, may control the rupture

behavior and give rise to the short-duration slip pulse. By using a velocity independent failure model, they inverted for the heterogeneous distribution of a stress increase needed to initiate slip and stress drop describing strength after initiation, so that results of a spontaneous dynamic rupture analysis would give a slip history consistent with what had been obtained by an earlier kinematic inversion of the strong-motion data. Their results show the confinement of rapid slip to the vicinity of the rupture front. Apparently, the strong heterogeneities generate local arrest waves analogous to those of Day (1982) and Johnson (1990, 1992) discussed earlier. Olsen et al. (1997) also reported such behavior in a slip-weakening model of the 1992 Landers, California, earthquake, and Day et al. (1998) reported similar results for that event as well as for the 1994 Northridge and 1995 Kobe earthquakes.

A third mechanism for self-healing pulse generation relates to the possible moderate dissimilarity of material properties across a fault plane. Andrews and Ben-Zion (1997) found a dynamic slip pulse on a fault of constant Coulomb friction coefficient when the interface separates materials of different elastic properties and densities, noting that such an effect had been suggested much earlier by Weertman (1980) based on his analysis of steadily moving interfacial dislocations. The effect occurs for in-plane slip, which couples to alteration of normal stress when there is material dissimilarity. The difference in material induces different normal stress polarities, and slip effectively occurs only in a narrow region where the large dynamic normal stress variations weaken the resistance to shearing. Such effects have also been studied by Harris and Day (1997), who emphasize that it may come into play also for slippage along the border between a compliant fault

core and surrounding crustal rock. The effect is related to the discovery by Adams (1995) that steady-state sliding along the interface of two elastic half-spaces of different material properties is unstable to perturbation, in the sense that the real parts of eigenvalues, for exponential time dependence of a Fourier spatial perturbation, are positive for a very broad range of material pairs and friction coefficients. Subsequently, Adams (1998) showed that pulses of constant slip velocity can move at a generalized Rayleigh speed along such dissimilar material interfaces, with constant friction coefficients, under remotely applied shear stress levels that are arbitrarily less than the friction strength based on the remotely applied normal stress, an effect that Rice (1997) has shown to follow simply from the Weertman (1980) analysis.

However, in this study we focus primarily on velocity-weakening friction as a plausible mechanism for generating slip pulse. This was first suggested by Heaton (1990), where he conjectured that if the friction on the fault decreases with increasing slip rate, and vice versa, then the fault can lock behind the rupture front, leading to the cessation of the slip at a given point shortly after its initiation. Theoretical and numerical studies of conditions leading to self-healing pulses, in models that include the velocity-weakening of friction strength, have been given by Cochard and Madariaga (1994, 1996), Perrin et al. (1995), and Beeler and Tullis (1996). Nonetheless, not all velocity-weakening models lead to self-healing. For example, dynamic simulations of Okubo (1989), Rice and Ben-Zion (1996), Ben-Zion and Rice (1997), and Lapusta et al. (2000) based on the classical logarithmic dependence on slip velocity, as extrapolated from much lower-speed laboratory experiments, showed the cracklike mode. It may be shown that in this type of

velocity dependence, if the rupture is allowed to propagate over large enough distance, it will disintegrate into a train of slip pulses [Lapusta, 2001, Elbanna, Lapusta and Heaton, manuscript under preparation]. This is, however, outside the scope of this study.

Zheng and Rice (1998) examined the problem of rupture classification and identified conditions for which velocity-weakening friction would favor slip pulses over cracks, at least in the 2D anti-plane setting. They showed that there exists a level of prestress under which no sustained expanding cracklike rupture could exit, and hence sustained ruptures in this regime have to be of the self-healing type. They also showed that the rate of velocity-weakening plays an important rule. They introduced a parameter that gives the ratio between the rate of change of the steady state friction coefficient with respect to the velocity, to the radiation damping coefficient. Their numerical simulations suggest that if this ratio is less than 0.3, pulse-like ruptures are favored and if it is greater than 0.5 then crack-like ruptures occur.

Earlier, Perrin et al. (1995), used velocity-weakening friction formulations with enhanced weakening at seismic slip rates to investigate the problem of self-healing slip pulses. They considered the case where the slip pulse can propagate steadily without change in shape on a uniformly prestressed interface. A similar problem, but with Coulomb friction, was considered theoretically by Freund (1979). In their paper, Perrin et al. (1995) considered first the hypothetical case of a pulse propagating steadily on an infinite fault. Assuming that the pulse has been created by some process earlier, they examined under what conditions this pulse can propagate without changing its shape. They showed that,

within the scope of their simulations, there exists one pulse shape, i.e., a unique slip rate distribution, that can propagate steadily for a given prestress level, and they noted that finding this steady solution requires a large number of iterations. They also examined the asymptotic behavior of the steady pulse near its healing and rupture fronts and showed it to be a power law with an exponent that is dependent on the direct effect in the friction law. They then considered the problem of spontaneous dynamic rupture on a finite fault. The slip pulse in this case is created within the simulation by uniformly overstressing a small portion of the fault while keeping the prestress outside the nucleation zone at a lower uniform level. They could not find a steady pulse corresponding to the same values of the prestress and friction parameters they found in the idealized case of propagation over aninfinite fault. They also could not find, within the number of runs they have carried out, a steady pulse corresponding to different parameters. They conjectured that their results suggest steady pulses on velocity dependent frictional interfaces, and uniform prestress are either unsteady or there exists an attractor that has a limited basin of attraction for steady propagation. Ben-Zion et al. (2003), considering rupture propagation on a biomaterial interface and constant dynamic friction coefficient argued that slip pulses are inherently unstable and their steady propagation cannot exist.

In this study, we reexamine the problem of steady propagation of slip pulses on uniformly prestressed velocity-weakening frictional interfaces. We discuss the conditions under which steady propagation can be realized and show the crucial role played by the nucleation procedure. We also examine the stability properties of the slip pulse, its

interaction with stress heterogeneities on the fault and possible implications for dynamic complexity. The outline of this chapter is as follows. Section 5.2 describes the elastodynamic formulation of the problem and the frictional constitutive laws. Section 5.3 discusses rupture behavior on a uniformly prestressed fault with uniform overstress in the nucleation zone. Section 5.4 shows the possibility of the existence of slip pulses corresponding to non-uniform overstressing in the nucleation zone. Section 5.5 discusses the stability properties of the steady pulse to perturbations of different wavelengths and amplitudes. Section 5.6 introduces a parameter that describes some sort of average frictional dissipation within the pulse that correlates well with the pulse growth and decay and discusses its implication for the steady pulse propagation. In Section 5.7 we examine the interaction of the steady pulse with general stress heterogeneities on the fault and implications for slip complexity.

5.2. Elastodynamics and constitutive law:

We consider the elastodynamics problem within a 2-D antiplane framework, in which the fault plane coincides with the $x-z$ plane of a Cartesian coordinate system xyz and all particles move parallel to the *x* direction. The only nonzero displacement is $u_x(y,z,t)$ and we define the slip $\delta(z,t)$ on the fault plane as the slip discontinuity $\delta(z,t)=u_x(0^+,z,t)-u_x(0^-,z,t)$. The relevant shear stress on the fault plane is denoted by $\tau(z,t)=\sigma_{yx}(0,z,t)$. The shear stress on the fault plane can be expressed in terms of the slip history on the fault plane only using the following boundary integral equation [Cochard and Madariaga, 1994, Perrin et al., 1995, Lapusta et al., 2000]

$$\tau(z,t) = \tau_o(z,t) + f(z,t) - \frac{\mu}{2c} V(z,t) \qquad (5.1)$$

Where μ is the shear modulus, c is the shear wave speed, $V(z,t) = \dot{\delta}(z,t) = \frac{\partial \delta}{\partial t}$ is the slip rate, $\tau_o(z,t)$ is the loading stress (i.e., the stress that would act if the plane $y = 0$ is constrained against any slip), and $f(z,t)$ is a stress transfer function constructed as a linear functional over prior slip $\delta(z',t')$ over the causality cone (i.e., all z' and t' satisfying $c(t-t') > |z-z'|$). The last term of (1) represents the radiation damping term [Rice, 1993] and the explicit extraction of the damping term from the functional term $f(z,t)$ allows for the evaluation of $f(z,t)$ without concern for singularities.

In (1), most of the elastodynamic response is contained in the stress transfer functional $f(z,t)$. Cochard and Madariaga [1994] have expressed it as a double convolution integral in space and time. Perrin *et al.* [1995] have derived a spectral representation of $f(z,t)$ as a single convolution integral in time for each Fourier mode, when representing slip and the functional as Fourier series in space. Generalizations to general slip and/or opening states in 3-D problems are given by Geubelle and Rice [1995] and Cochard and Rice [1997]. We use the spectral representation of Perrin *et al.*[1995] and Lapusta *et al.* [2000].

We take the loading term $\tau_o(z,t)$ to be uniform at a background level $\tau_o^b(z,t)$ except for a localized region necessary to nucleate the rupture.

$$\tau_o(z,t) = \begin{cases} \tau_o^b & t < 0 \\ \tau_o^b + \tau_o^p(x) & t > 0' \end{cases} \tag{5.2}$$

where $\tau_o^p(x)$ is a stress perturbation term that acts over a localized region so as to nucleate the rupture. We show that the specific choice of $\tau_o^p(x)$ can have important consequences on the dynamics of generated slip pulse.

Constitutive laws used here are rate- and state-dependent friction laws developed to incorporate experimental observations and enhanced velocity-weakening at seismic slip rates [Rice, 2006, Beeler, 2009]. These laws include dependence of strength on slip velocity and on an evolving state variable (or variables) which characterizes asperity contacts, thus allowing for loss of strength in rapid slip and for subsequent rehealing so that repetitive failures can occur. The laws have been successfully used to explain various aspects of stable and unstable sliding between elastic solids [Ruina, 1983; Rice and Ruina, 1983; Gu et al.,1984; Tullis and Weeks, 1986] as observed in the laboratory. Also, they have been used to model earthquake phenomena, including nucleation, ductile and brittle crustal slip regions, spatio-temporal slip complexities, and earthquake aftershocks [e.g., Tse and Rice, 1986; Stuart, 1988; Okubo,1989; Horowitz and Ruina, 1989; Rice, 1993; Dieterich,1992, 1994; Perrin et al., 1995; Ben-Zion and Rice, 1995,1997; Rice and Ben-Zion, 1996; Stuart and Tullis, 1995; Tullis, 1996; Boatwright and Cocco, 1996, Lapusta et al., 2000, Lapusta and Liu, 2009].

A formulation of such laws which assumes constant normal stress and one state variable, to record dependence on slip history, is of the general form

$$\tau = \psi(V, \theta) \tag{5.3}$$

$$\frac{d\theta}{dt} = \varphi(V, \theta) \tag{5.4}$$

where θ is the state variable and τ, V and θ depend on space variables and time. In this paper we use the following form of the rate and state formulation:

$$\tau = \sigma[\, f_w + \frac{f_o + a \ln \frac{V}{V_o} + b \ln \frac{V_o \theta}{L} - f_w}{1 + \frac{L}{V_w \theta}}] \tag{5.5}$$

where σ is the constant normal stress, f_w is the residual friction coefficient, f_o is the reference friction coefficient at the reference slip rate V_o, a and b are rate and state parameters [Dieterich, 1979], L is an evolution distance for the state variable, and V_w is a characteristic velocity after which the frictional strength of the interface weakens significantly. In this study we use the following parameter values: σ =50MPa, f_w =0, f_o =0.6, V_o =1E-6 m/s, a =0.014, b =0.019, L = 8mm and V_w =1m/s. We use a regularized version of the law at V=0 [Lapusta et al. 2000]. For the state variable evolution, we use the ageing formulation:

$$\frac{d\theta}{dt} = 1 - \frac{V\theta}{L} \tag{5.6}$$

Such a formulation allows for healing of the fault at stationary contact, a feature needed to explain laboratory observations [Beeler, 1994] and was shown to be a theoretical requirement for the generation of slip pulses in the rate and state framework [Perrin et al., 1995]. However, it is worth to mention that the "slip" law [Dieterich, 1979 and Ruina, 1983] was suggested to be a better description for the friction behavior at the slip rates observed in laboratory experiments [Bayart et al. 2006] and while the slip formulation does not allow for re-strengthening at stationary contacts, recent numerical simulations [Ampuero et al., 2008 and Noda et al., 2009] have shown that slip pulses can be realized using such a law. Perhaps a combined law, of the type proposed by Kato and Tullis [2003], would be the most appropriate to use. It is possible that different state evolution laws could have important implications on the rupture evolution [Ampuero and Rubin, 2008] and it is worth exploring such implications for different formulations. We restrict ourselves, however, in this study to the ageing law formulation.

When $\frac{d\theta}{dt} = 0$, we say that the frictional coefficient has reached a steady state, i.e., there is no further evolution for the state variable. In this limit the steady state friction coefficient assumes the form:

$$f_{ss} = f_w + \frac{f_o + (a-b)\ln\frac{V}{V_o} - f_w}{1+\frac{V}{V_w}} \tag{5.7}$$

If $V << V_w$ the steady state friction coefficient reduces to the classical Dieterich-Ruina formulation appropriate for describing steady state friction behavior at low slip rates. On

the other hand if $V >> V_w$ the steady state friction coefficient approaches asymptotically the residual friction coefficient where $f_w << f_o$.

A high slip rate friction formulation like the one proposed here has its roots in both theoretical [Rice, 1995, 2006] and experimental [Beeler at al., 2009] investigations where it is motivated by certain physical processes taking place at asperity contact level such as flash heating. The rapid transition from high static friction to low dynamic friction through dependence on slip rate may be one of the possible reasons of absence of melting in many mature faults that have sustained hundreds of meters of slip. If the fault strength does not weaken during seismic slip, the temperature rise due to slipping for several meters at slip rates around 1 m/s and under normal stresses that are of the order of 100 MPa will be of the order of thousands of degrees sufficient to cause complete melting of the rocks existing in the fault zone [Rice, 2006, Noda et al., 2009 and Noda and Lapusta, 2010]. However, no significant evidence of melting has been found in many mature faults [Rice, 2006, Aagaard and Heaton,2008]. One possible resolution to this paradox is that fault frictional strength decreases during seismic slip as a function of slip rate, as suggested by (5.7), so that the dynamic friction is sufficiently low to cause temperature rise only below several hundreds of degrees.

5.3. Absence of steady pulses for nucleation zones with uniform overstressing

In this section, we explore some of the aspects of the relation between the rupture nucleation procedure and the subsequent slip pulse evolution. We consider faults that are uniformly prestressed except in a localized region where the prestress is increased uniformly to a level high enough to trigger a dynamic rupture from the onset of the numerical simulation. The transition between the peaked stress within the nucleation zone and the uniform background prestress level outside it is achieved through a hyperbolic tangent function as shown in Fig. (5.1). The use of such a smoothing function helps overcome any artifact that might be associated with the introduction of an abrupt change in the prestress between the nucleation zone and the rest of the fault while maintaining a well localized overstressed region.

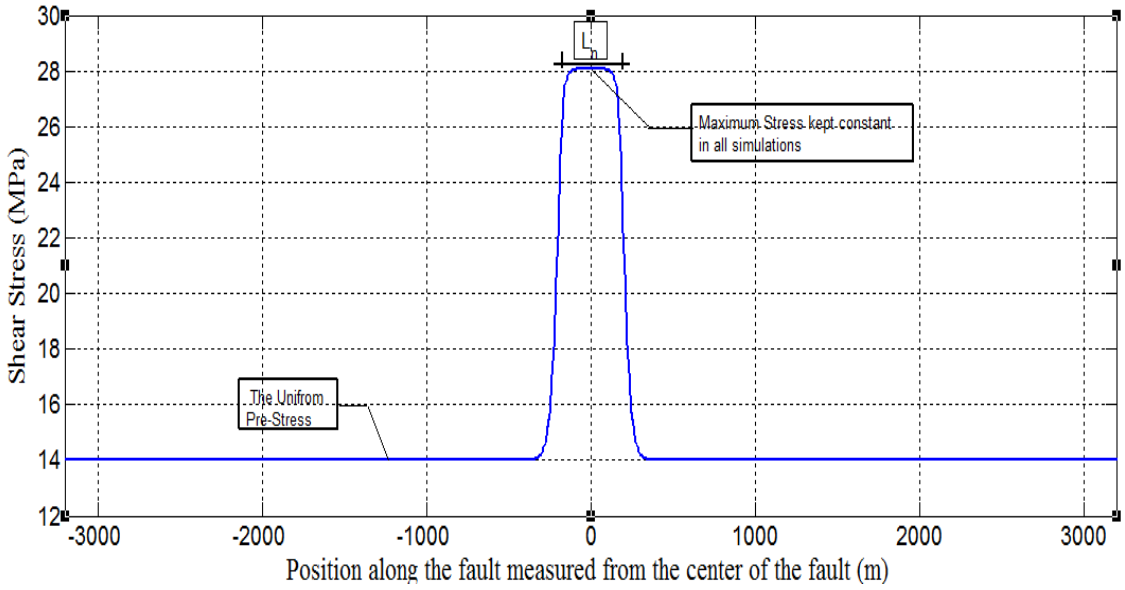

Fig.(5.1): Pre-stress distribution on the fault. The prestress is uniform outside of the overstressed patch of width L_n used to initiate rupture at the fault center. The overstressing is also uniform over most of the patch except for transitions between the two uniform stress levels described by a hyperbolic tangent function.

We first fix the nucleation zone parameters (i.e., the peak stress level and the nucleation zone width) and change the uniform value of the prestress level outside the nucleation zone. As shown in Fig. (5.2), we observe that by increasing the background shear prestress, the mode of rupture changes from a dying pulse-like rupture to a pulselike rupture with a constant slip and finally to a pulse-like rupture with a growing slip.

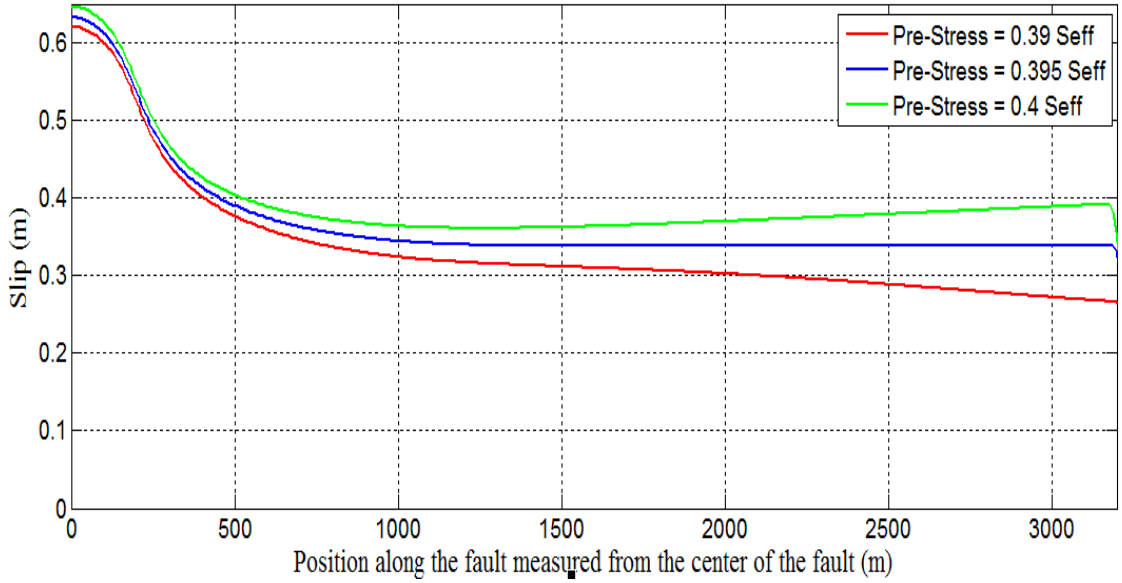

Fig. (5.2): Slip distributions accumulated by a propagating pulse-like rupture for different pre-stress levels outside the nucleation patch ("Seff" stands for the effective normal stress). Depending on the pre-stress level, slip may be increasing, decreasing, or uniform.

However, a look into the evolution of the slip pulse associated with the constant slip solution shown above reveals that the pulse is actually unsteady. Figure (5.3) shows tha

the pulse changes its shape as it propagates away from the nucleation zone for the case with uniform slip; the pulse peak slip rate increases while its width decreases in a delicate manner such that the integrated slip remains invariant with propagation.

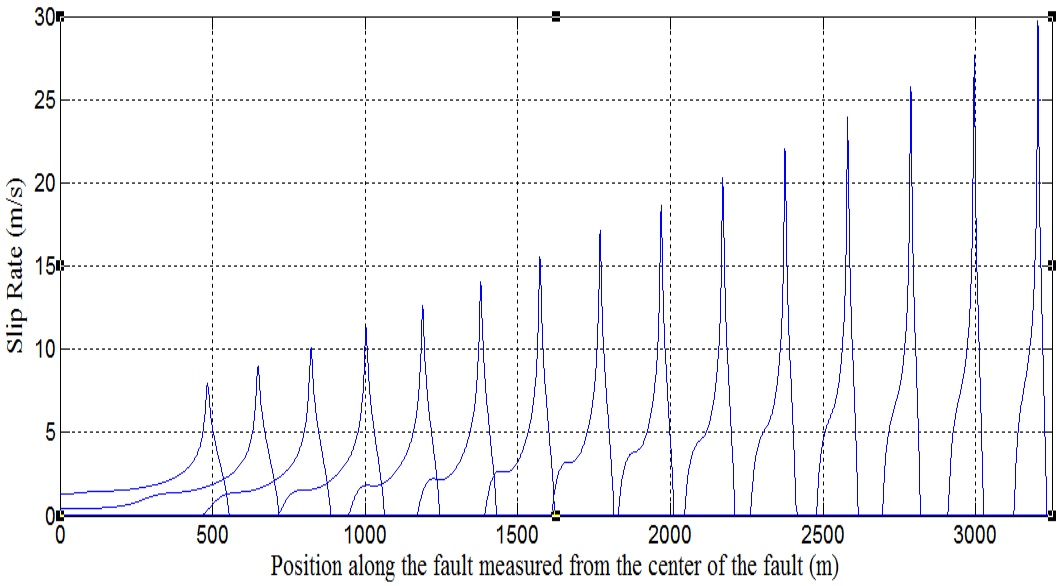

Fig. (5.3): Pulse evolution for the case with uniform slip. The maximum slip rate increases while the pulse width decreases with pulse propagation. Hence, even the case with uniform slip, for a single peak in the prestress, does not achieve steady pulse propagation.

We may alternatively try to fix the background shear prestress value outside the nucleation region but change the width of the nucleation zone for instance. As the width of the nucleation zone increases, the rupture changes from a dying pulse-like rupture to a pulse-like rupture with uniform slip and finally to a pulse-like rupture with increasing slip as a function of propagation distance [See Fig.(5.4)]. Similar to the previous case, the slip

pulse associated with the uniform slip solution is unsteady, accumulating the same amount of slip as it propagated away from the nucleation zone in shorter rise times.

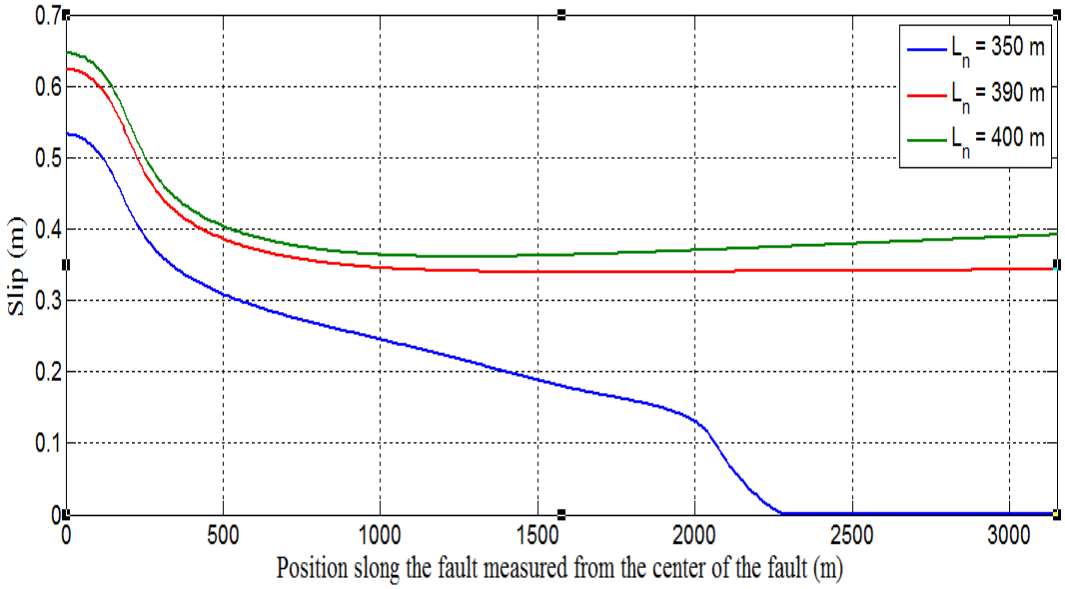

Fig. (5.4): Slip distributions for different widths of the overstressed patch L_n but a constant pre-stress level outside the nucleation zone (0.4 Seff where Seff is the effective normal stress). As the width of the nucleation zone increases, final slip distribution changes from a decreasing to an increasing function with distance. The case corresponding to L = 390m yields uniform slip.

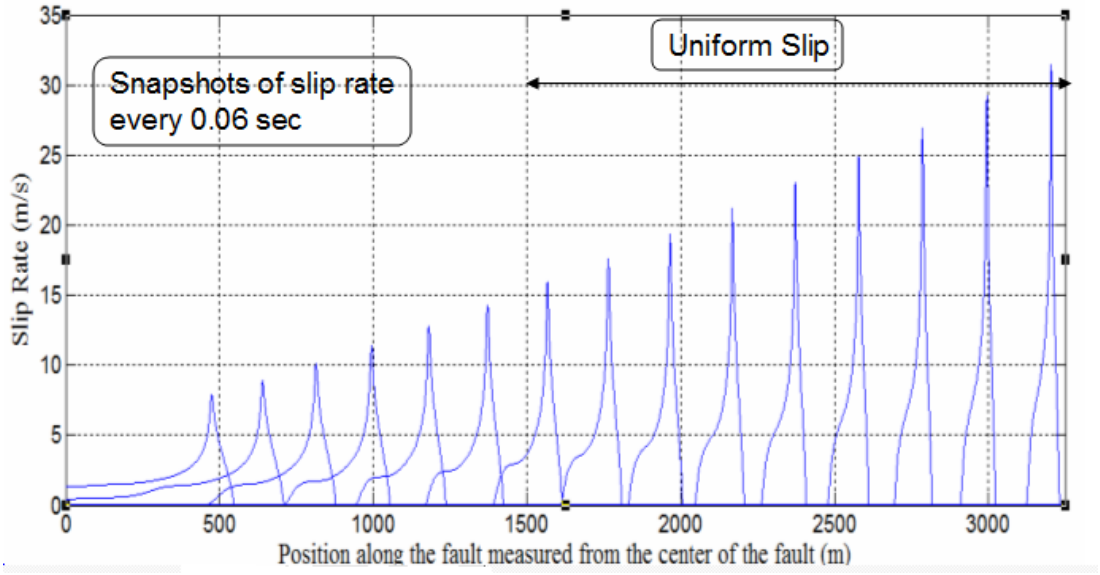

Fig. (5.5): Pulse evolution for the case with uniform slip. The maximum slip rate increases while the pulse width decreases, despite uniform final slip reflecting unsteady pulse propagation.

We also tried keep the effective width of the nucleation zone constant but change the value of the overstressing level while keeping the background shear prestress constant. Similar to the previous observations, we found that as the overstressing level increases for the same background prestress, the rupture changes its characteristic from dying to growing passing by a case of uniform slip. However, the uniform slip solution in such a case corresponds also to unsteady pulse propagation. This leads us to conclude that the steady pulse solution is absent for nucleation procedures that employ a single peak in the prestress. As previously discussed, this absence could be an inherent instability in the steady propagation of slip pulses (Perrin et al., 1995 and Ben-Zion et al., 2003). However, it is possible that the absence is just a consequence of the particular nucleation procedure we have been implementing. This latter possibility motivated us to explore the

possible consequences of trying a different procedure for the nucleating of slip pulse and this is what we are going to discuss in the next section.

5.4. Existence of steady pulses:

The classical way of investigating rupture mode classification involves, as discussed in the previous section, the use of a single peak in the prestress in an otherwise uniformly prestressed fault. The rupture would start as a small crack that will keep expanding into the uniformly prestressed fault and if an understressing condition is met, as described in Zheng and Rice [1998], the initial crack will turn into two slip pulses propagating in opposite directions. Pulses were then found to be either growing or dying. We can use a variant over this procedure and consider changing the prestress, just ahead of the formed slip pulse, to a new uniform level. Figure (5.6) shows a schematic representation for this prestress distribution.

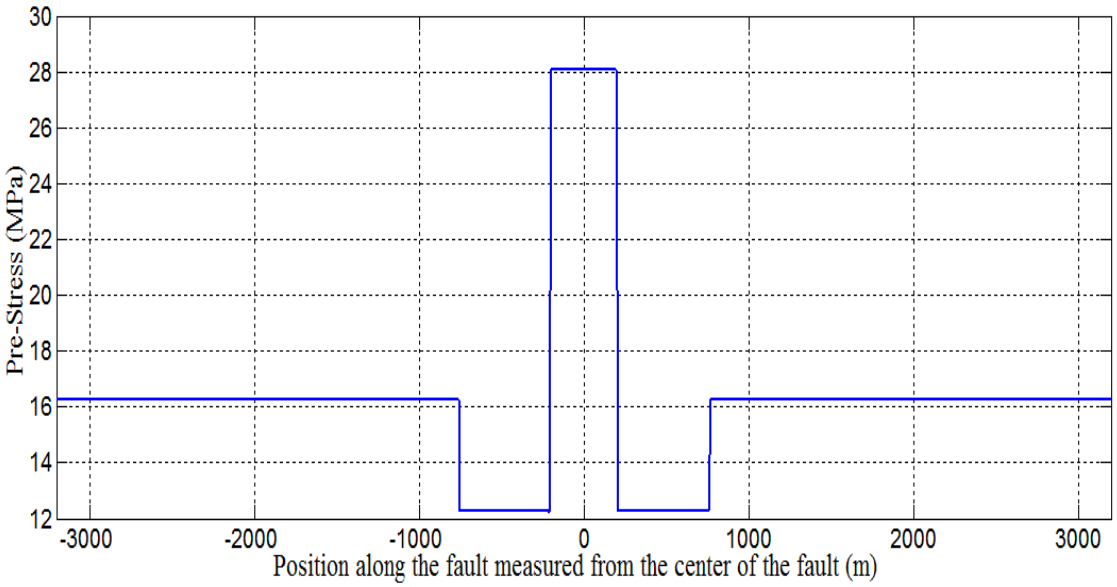

Fig.(5.6):The special nucleation procedure that yields steady pulses. The overstressing in the central region is balanced by under stressing in the surrounding zones. The positive stress drop at the center changes into a negative stress drop in the lower-stressed areas, and that creates a pulse. This initial pulse then enters the uniform prestress outside the nucleation zone.

By using this pulse nucleation approach, we force the pulse to form in the understressed region and then to interact with the uniform prestress outside the nucleation zone. In this sense, we can investigate the possible modes of rupture with a slip pulse initial condition and not an expanding crack. By varying the level of the uniform prestress outside the nucleation zone, the evolution of the slip pulse can be controlled; higher prestress levels lead to slip pulses with growing slip while lower prestress levels lead to slip pulses with decreasing slip. As in the cases studied in the previous section we also find a level of prestress for which the slip pulse can propagate with uniform slip as shown in Fig.(5.7).

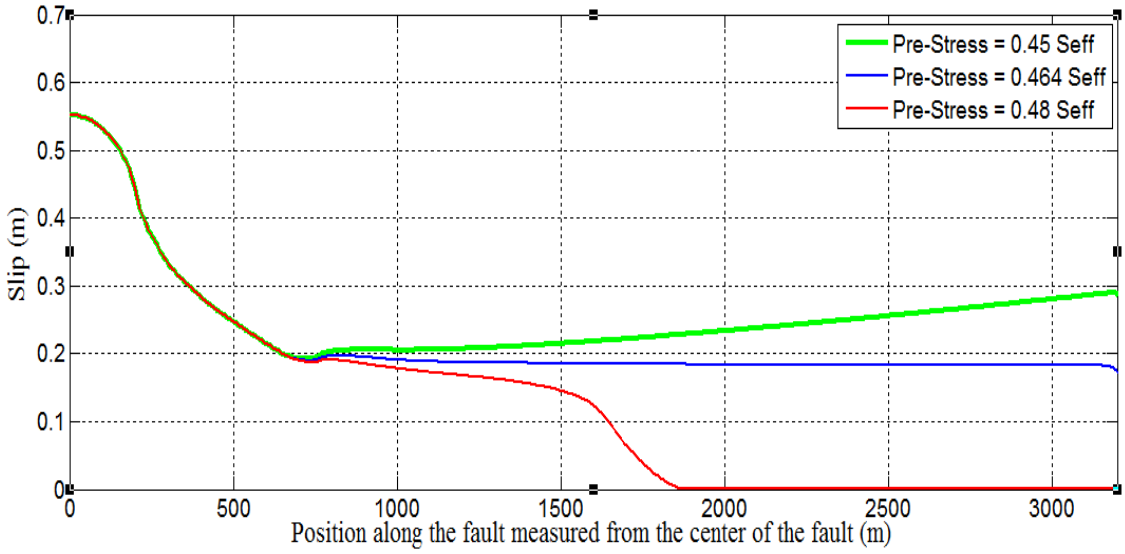

Fig. (5.7): Depending on the uniform prestress outside the nucleation patch, we can obtain increasing, decreasing, or spatially uniform slip distributions outside the nucleation zone.

However, unlike the cases studied in section III, the slip pulse corresponding to the uniform slip solution does evolve into a steady shape after an initial transient as shown in Fig.(5.8) with no apparent change in the slip pulse amplitude or width. Hence, by using the slip pulse, and not a crack, as the condition to start with for the uniform prestress field, we have succeeded in realizing the steady propagation of the slip pulse. So what is the difference between this approach and the approach we pursued in the last section?

When uniform overstressing in the nucleation region is used [Figures (5.1) to (5.3)], the crack to pulse transition occurs in the uniform stress level directly. As will be briefly discussed in Appendix D and as was shown in earlier studies [Lapusta, 2001], the fault zone behind the crack front is sliding at nearly steady state conditions. A linear perturbation analysis for this approximate steady sliding will show the existence of growing disturbances propagating with supersonic phase velocities. The healing edge of the pulse then propagates with a supersonic velocity, which leads to a decrease in the pulse width with its propagation. We hypothesize that this rules out the possibility of achieving a steady pulse shape for uniformly overstressed nucleation conditions.

With the new nucleation procedure a pulse is created first that then propagates into different prestress conditions. The linear stability analysis still approximately applies to the small region of steady sliding behind the pulse rupture front. Since the phase

velocities and the growth rates of the perturbations are functions of prestress, by propagating the pulse into a different prestress field, we can manipulate the perturbation growth rates and the phase speeds until a delicate balance is achieved that leads to the steady propagation.

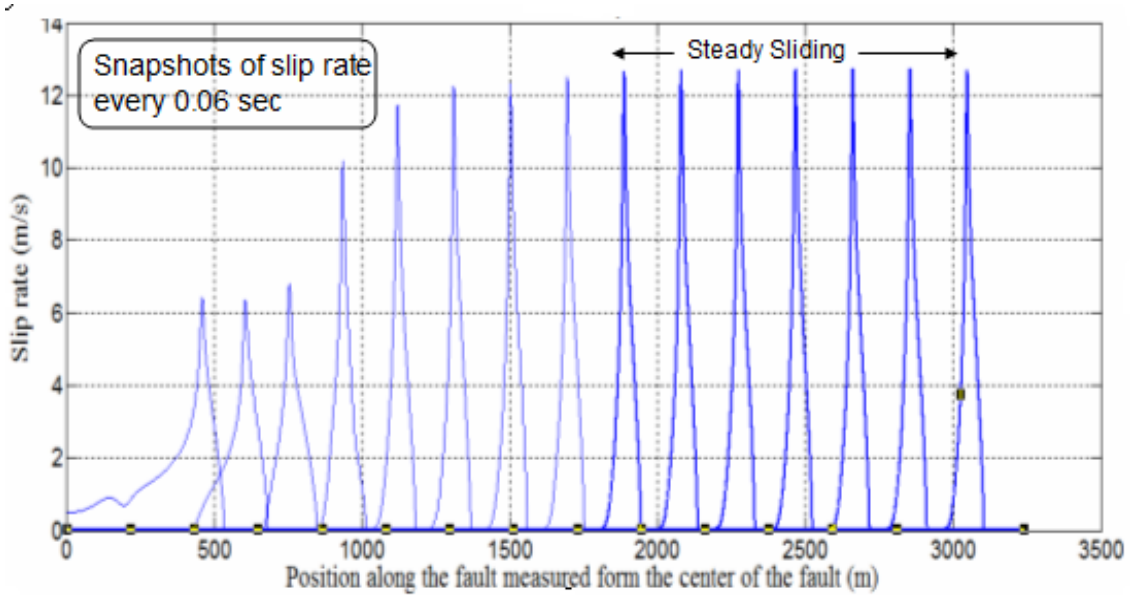

Fig. (5.8): Evolution of the pulse shape for the uniform slip solution. The pulse amplitude and width, after an initial evolution phase, settle into nearly constant values (for time $t > 0.8$ s).

It is worth stressing that the procedure we present here for the generation of steady pulses may not be unique. As we just discussed, the absence of steady pulses in the classical nucleation approach may be attributed to the properties of steady sliding behind the crack front and can be circumvented by starting with a slip pulse as an initial condition and not with a crack. Hence we hypothesize that it is possible to generate steady pulse propagation from any process that starts with a slip pulse and not a crack. Possible

processes will include, for example, manipulating the frictional strength instead of shear stress (Ben-Zion et al.,1997, Alice Gabriel, personal communication) .

Finally, by using different prestress levels in the overstressed and understressed regions of the nucleation zone, we can generate slip pulses of different initial shapes. When those pulses propagate into the uniformly prestressed region outside the nucleation zone, they will settle into steady propagation at different prestress levels and with different slip values. We have found that slip pulses with larger slip require lower prestress values to propagate. This is shown in Fig. (5.9). For a steady pulse on an infinite fault, there is no radiated energy and the frictional dissipation balances exactly the change in potential energy pointwise. In our numerical simulations, as a consequence of strong velocity-weakening friction formulation adopted here, pulses with larger slip tend to have higher slip rates and to experience lower friction. For a given prestress level, pulses with larger slip would lead to larger changes in potential energy. Hence in order for the change in potential energy to compensate for the lower frictional dissipation of pulses with larger slip, a lower prestress level has to be used. We will revisit this point in Section 5.6.

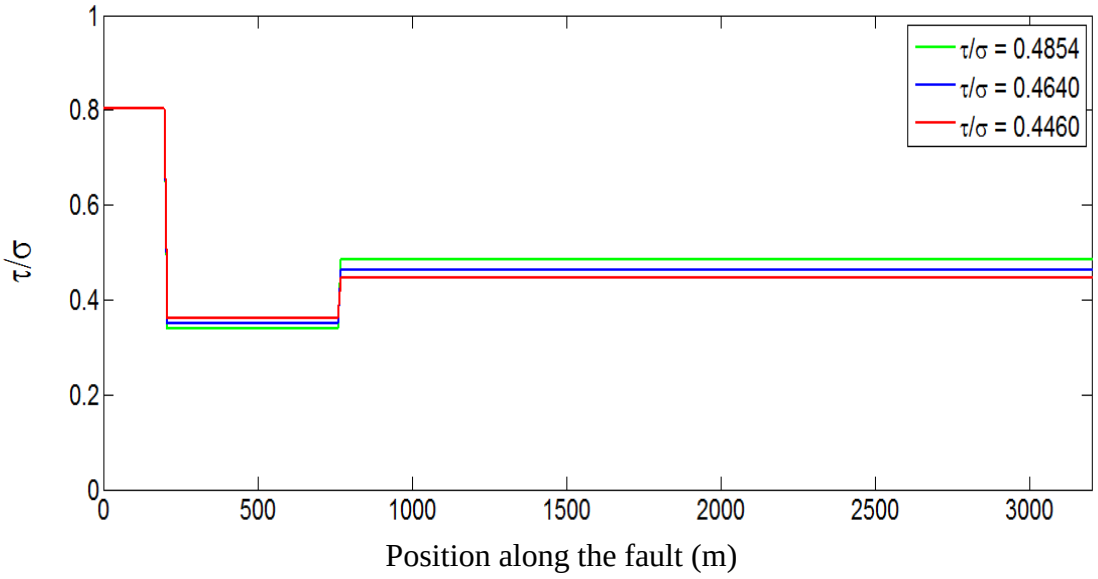

Fig. (5.9 a): Prestress distributions for different steady pulse scenarios.

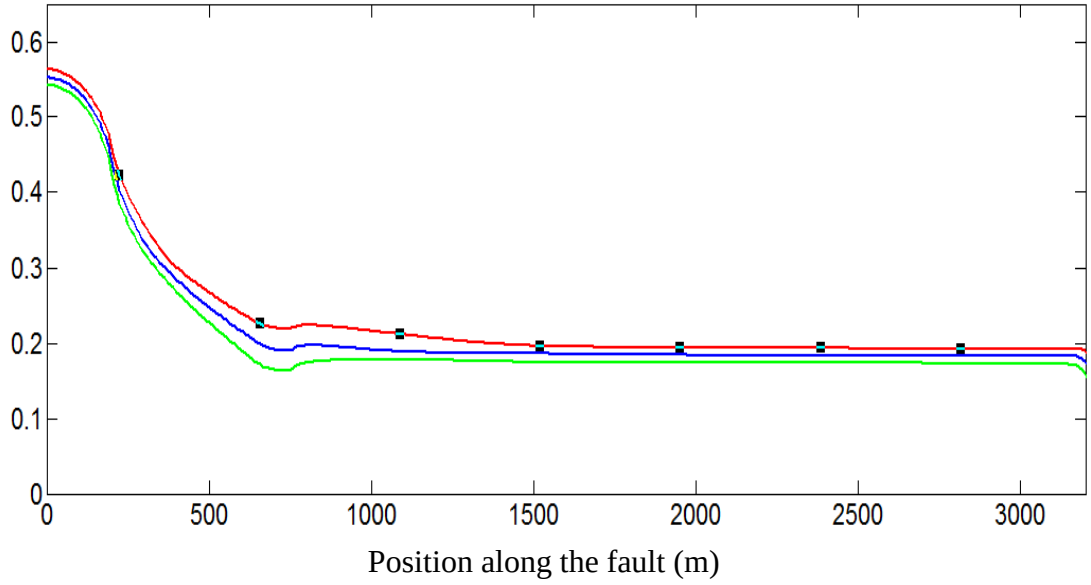

Fig. (5.9 b): Slip distributions associated with the different steady pulses. Note the matching colors in the top and bottom figures. Pulses with larger slip require lower prestress levels to propagate.

The existence of a steady pulse helps us better understand the influence of heterogeneities in the prestress or material properties on rupture propagation and the resulting slip distribution. We devote the next section to the study of steady pulse responses to perturbations of different wavelength and amplitudes.

5.5. Response to perturbations

The steady pulse solution provides a reference solution to which we can compare rupture propagation scenarios in heterogeneous condition and for which we can assess the influence of different perturbations, whether in the prestress or frictional properties, on the different rupture variables individually such as the maximum slip rate, the pulse width and the pulse slip. In this section we focus mainly on the effect of perturbations in the prestress, from the steady-state prestress level, on the pulse slip. This is achieved by creating a steady pulse that is left to propagate for some distance after which it is faced with a perturbed prestress condition. We consider both harmonic and inharmonic perturbations as well as perturbations placed symmetrically and unsymmetrically about the steady-state prestress level. By looking at the pulse response to perturbations of different amplitudes and wavelengths, we may gain insight into the problem of slip complexity (Mai et al., 2003) and the role of stress heterogeneity in the slip variability of real earthquakes [e.g. Liu et al., 2007, Aagard and Heaton, 2008 and Smith and Heaton, 2010].

5.5.1. Response to symmetric harmonic perturbations of small wavelength

The first case we are considering is response to symmetric harmonic perturbations of small wavelength and different amplitudes. The wavelength of the perturbation is measured relative to the pulse width whereas the perturbation amplitude is measured relative to the steady state prestress level. Figure (5.10) illustrates the results for two cases; the first is for a perturbation of wavelength = 3.5% of the pulse width and an amplitude of 1% of the steady state prestress level and the second is for a perturbation of the same wavelength but with much larger amplitude (20% of the steady state prestress) [See Fig.(5.10 a)]. We observe that for the smaller amplitude, the perturbed pulse slip tracks the steady state solution with no visible effect for the applied prestress perturbation. For the larger amplitude perturbation, the perturbed slip still follows the unperturbed slip solution at least for the propagation distances considered here. This suggests that the steady pulse is stable for small wavelength perturbations of small amplitude and possibly some large amplitude perturbations as well.

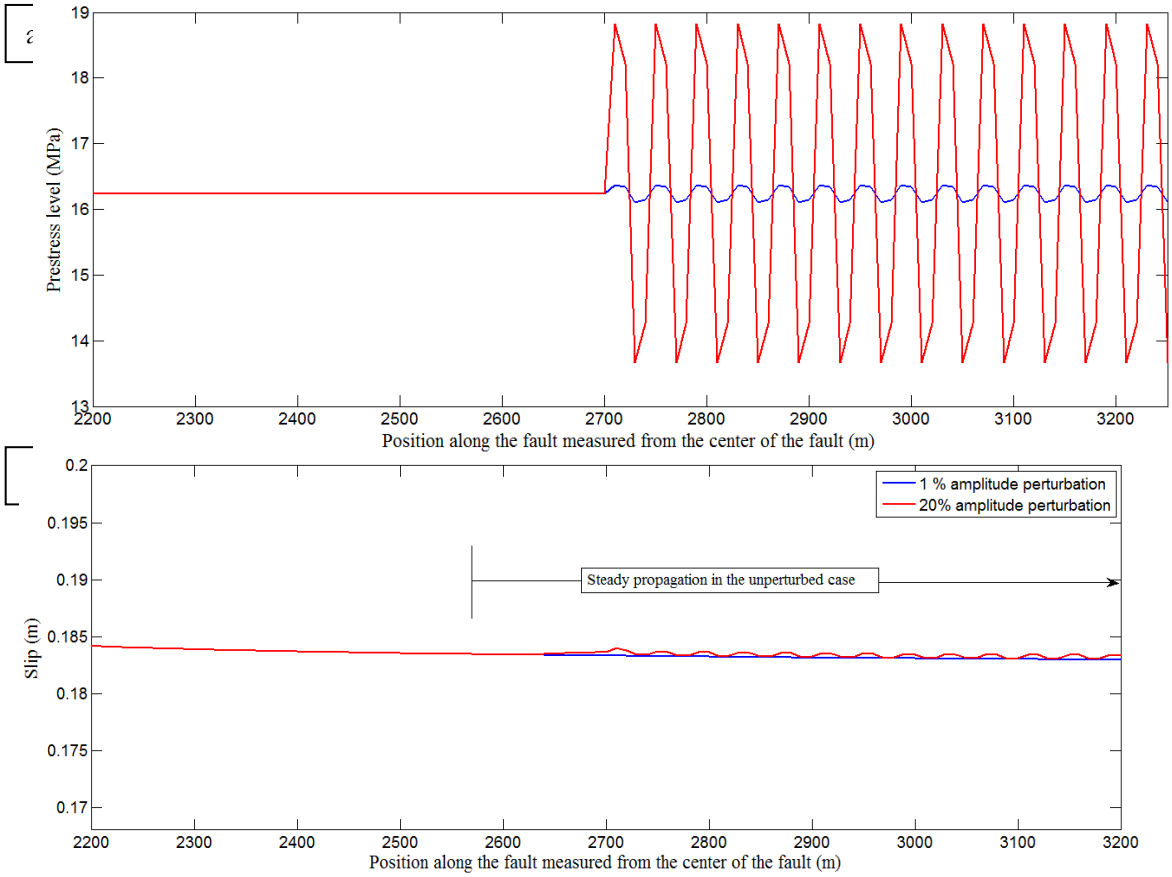

Fig. (5.10): a) Prestress perturbations of small wavelength (8 grid cells or 3.5% of the steady pulse width) and different amplitudes relative to steady state prestress level. b) Response of the pulse slip to pre-stress perturbations. We observe that the pulse is stable to perturbations of small amplitudes (e.g. 1%), with the resulting slip oscillating about the original line of uniform slip. For larger amplitudes (e.g. 20%), the average slip seems to still follow the steady-state slip level at least for the propagation distances considered here.

5.5.2. Response to symmetric perturbation of large wavelength

We next consider the response to symmetric harmonic perturbations of large wavelength and different amplitudes. Similar to the previous case, the wavelength of the perturbation

is measured relative to the pulse width whereas the perturbation amplitude is measured relative to the steady-state prestress level. Figure (5.11) illustrates the results for two cases; the first is for a perturbation of wavelength comparable to the pulse width and an amplitude of 1% of the steady state prestress level, while the second is for a perturbation of the same wavelength but with a much larger amplitude (20% of the steady state prestress). We observe that for the smaller amplitude perturbation, the perturbed pulse slip oscillates about the original line of uniform slip, whereas for the larger one, the perturbed slip clearly deviates from the uniform slip solution, signaling that the pulse deviates from the steady solution. This suggests that the steady pulse is unstable for large wavelength perturbations of large amplitude.

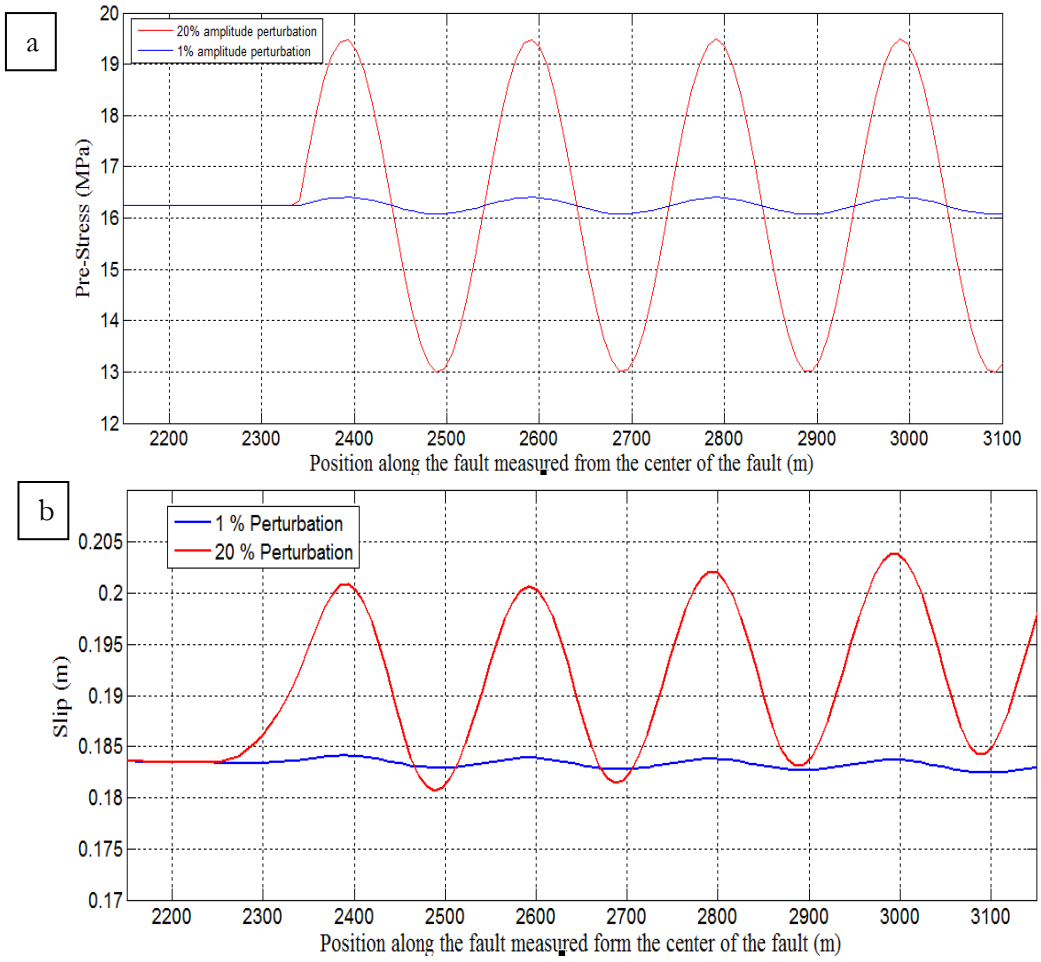

Fig. (5.11): a) Pre-stress perturbations of wavelength equal to the pulse width and with different amplitudes. b) Response of the pulse slip to the pre-stress perturbations. For perturbations of small amplitude (1%), the slip oscillates about the steady value for the unperturbed case. For perturbations of larger amplitude (20%), the average slip clearly deviates from the steady slip value, signaling that the pulse propagation deviates from the steady solution. Hence the steady pulse solution is unstable in this case.

5.5.3. Response to a step in the prestress

Symmetric harmonic perturbations are only one of many different perturbation scenarios. Another important perturbation scenario is the response of the pulse slip to a step in the prestress. Figure (5.12 a) shows one of the possible cases, where the prestress distribution is tuned to generate a steady pulse, which is allowed to propagate for some distance before a sudden change in the prestress to a new uniform higher or lower value is encountered. We keep the change in the prestress amplitude, for the example shown here, to only 1% of the steady-state prestress value. Despite this small perturbation, we observe that the pulse slip deviates clearly from the steady slip solution, indicating that the pulse either grows or dies, but does not evolve into a new steady configuration. This is shown in Fig. (5.12 b), which depicts the perturbed slip solution with propagation distance. Fig. (5.12 c) shows the evolution of the perturbed slip pulse while growing or dying. These results suggest that a steady pulse is unstable to perturbations of infinite wavelength regardless of how small the amplitude of perturbation might be.

We can attempt to explain this behavior of the steady pulse within the context of strong velocity-weakening and the relation between frictional dissipation on the fault surface and a change in the medium potential energy. Consider the case of an abrupt increase in the prestress ahead of the steady pulse. In response to this sudden increase, the pulse will initially grow. We observe in our numerical simulation that the pulse growth is primarily observed in an increase in the pulse slip rate. Due to the velocity-weakening nature of the friction law, an increase in the slip rate will lead to a reduction in the frictional force experienced by the pulse and in the case studied here will lead to a reduction in the frictional dissipation. With larger prestress and slip, the change in the medium potential energy will increase. Consequently, the difference between the change in potential energy available for rupture growth and the frictional dissipation hindering the rupture growth will increase. This positive feedback favors the continuation of the pulse growth and its deviation from the steady solution. For the case of a sudden reduction in the prestress, the opposite happens. It is not clear, however, if this will hold in all scenarios that implement dynamic weakening. For example, if the dissipation increases with the pulse slip, say for example due to pore fluid pressurization or the existence of off-fault inelasticity (damage or plasticity), then it is possible that the steady pulse will evolve to a new steady configuration. We are planning to explored this possibility in future work.

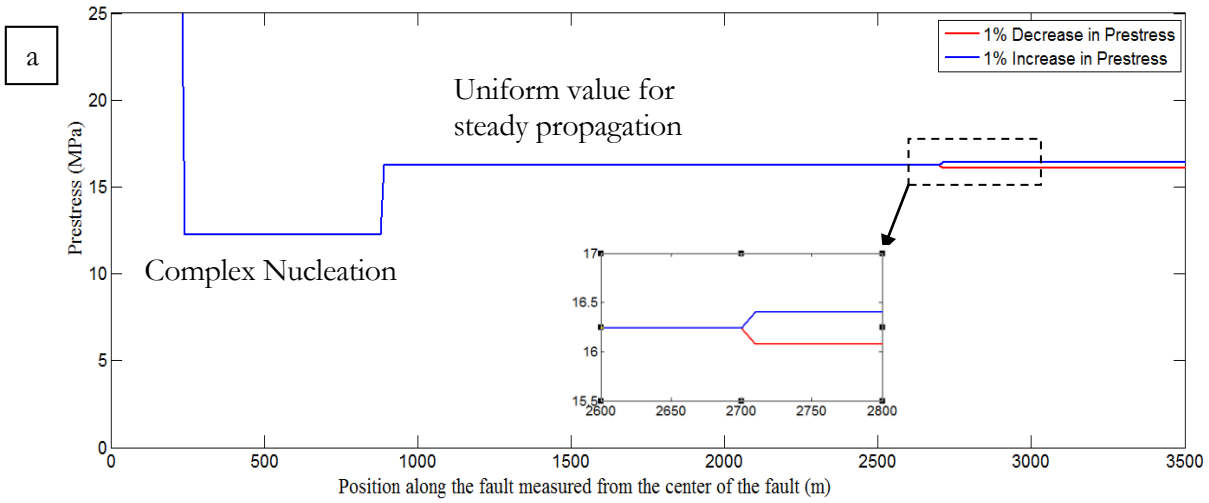
a
1% Decrease in Prestress
1% Increase in Prestress
Uniform value for
steady propagation
Complex Nucleation
Prestress (MPa)
Position along the fault measured from the center of the fault (m)

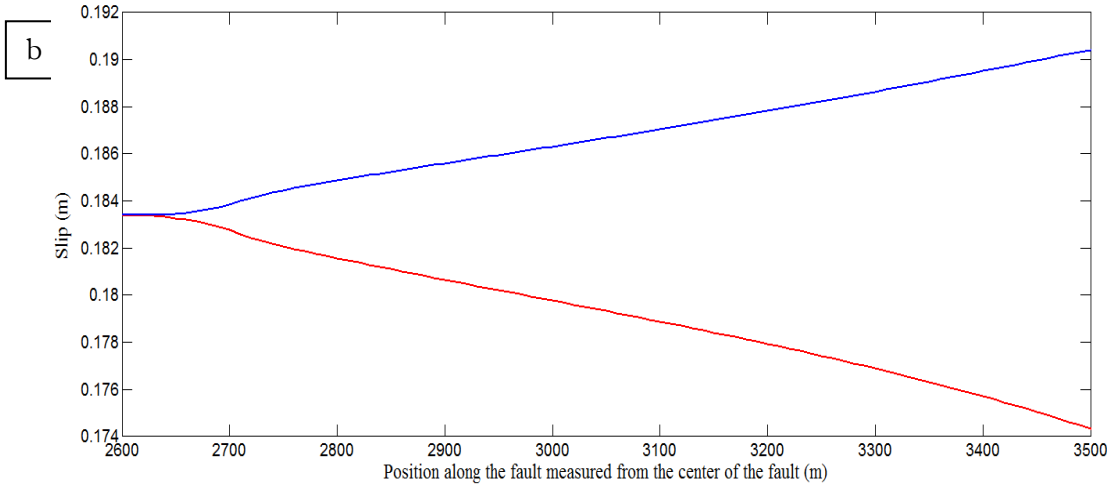
b
Slip (m)
Position along the fault measured from the center of the fault (m)

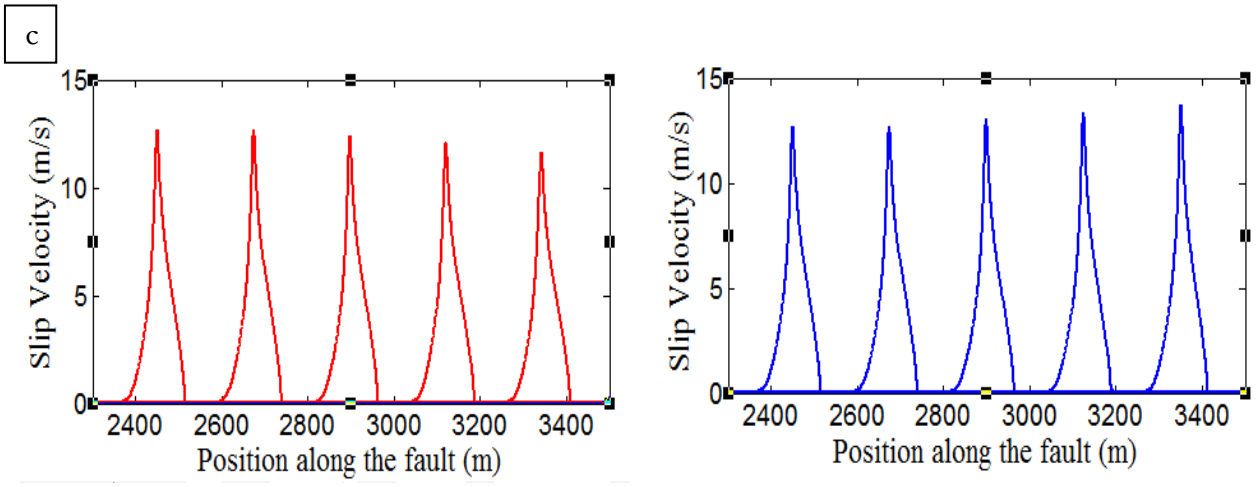
c
Slip Velocity (m/s)
Position along the fault (m)
Slip Velocity (m/s)
Position along the fault (m)

Fig. (5.12): a) Shear prestress distribution along the fault. The insert shows an enlarged view for the step in the prestress introduced in front of the steady pulse. The amplitude of the step is just 1% of the steady state pretsress. b) Perturbed pulse slip. The initial uniform slip either increases or decreases, depending on the step in the prestress, but does not attain a new uniform level. c) [Left] Evolution of the slip pulse in response to a step reduction in the prestress of magnitude of 1% of the steady state prestress. [Right] Evolution of the slip pulse in response to a step increase in the prestress of a similar magnitude.

A related problem to the response of the steady pulse to a step in the prestress is how far a pulse can propagate in a reduced prestress until it comes to a complete stop. By some measure, this could be indicative of how effective the fluctuations in the prestress might be in stopping a propagating rupture before the rupture reaches the fault boundaries and hence contributes to the ability to generate ruptures of different sizes on the same fault. We examine this problem by considering a given steady pulse and subjecting it to abrupt reductions of different magnitudes in the prestress. Figure (5.13) shows the distance required for the pulse to be arrested as a function of the amplitude of the stress reduction introduced ahead of the steady pulse.

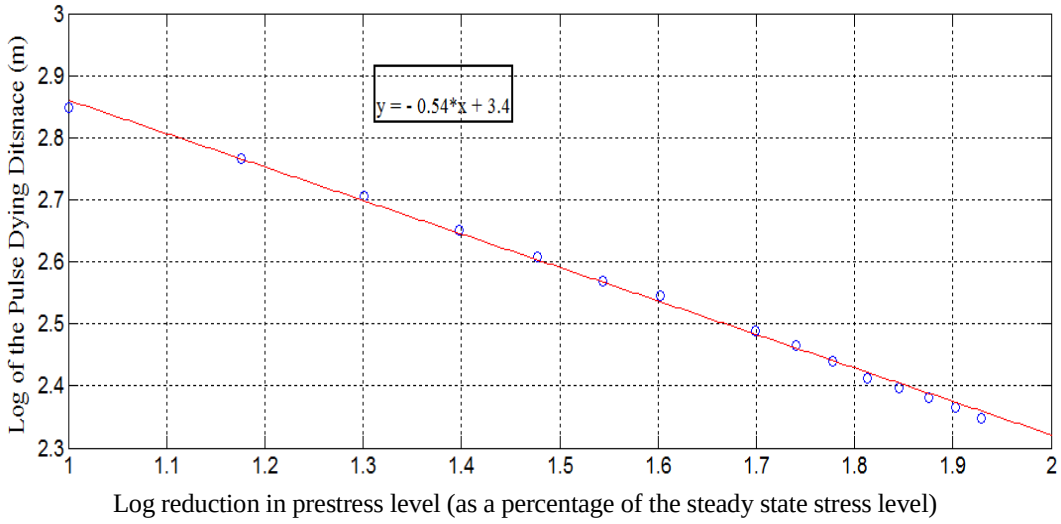

Fig.(5.13): Arrest distance for a pulse in response to an abrupt decrease in the pre-stress level. We see that the higher the amplitude of the decrease in the prestress level, the faster the pulse dies. The relation between the arrest distance and the decrease in prestress is a power law, with the arrest distance becoming infinite as the steady state stress level is approached. The ratio between the dynamic stress variation carried by the steady pulse and the imposed decrease in the pre-stress level controls the arrest distance. In this simulated case, it only takes a distance of 1.2 pulse widths for a steady pulse to be arrested in response to a pre-stress decrease to zero.

The relationship between the decrease in the prestress from the steady-state prestress level and the arrest distance is well approximated by a power law with some scatter. In the case shown here, the steady-state pulse width is approximately 170 m, which means that it only takes a distance of 1.2 pulse width for a steady pulse to be arrested in

response to a prestress decrease to zero. This suggests that strong prestress heterogeneity could be effective in the fast arrest of pulse slip.

5.5.4. Response to compound perturbations

After exploring the pulse response to harmonic and inharmonic perturbations, it is natural to consider more complex perturbation scenarios. One possible case is to consider the combination of a symmetric harmonic perturbation with a step in the prestress. This is equivalent to considering an asymmetrical harmonic perturbation about the steady-state prestress level. Figure (5.14) shows the prestress distribution when the harmonic perturbation has a wavelength of about half the pulse width and an amplitude equal to 5% of the steady state prestress level.

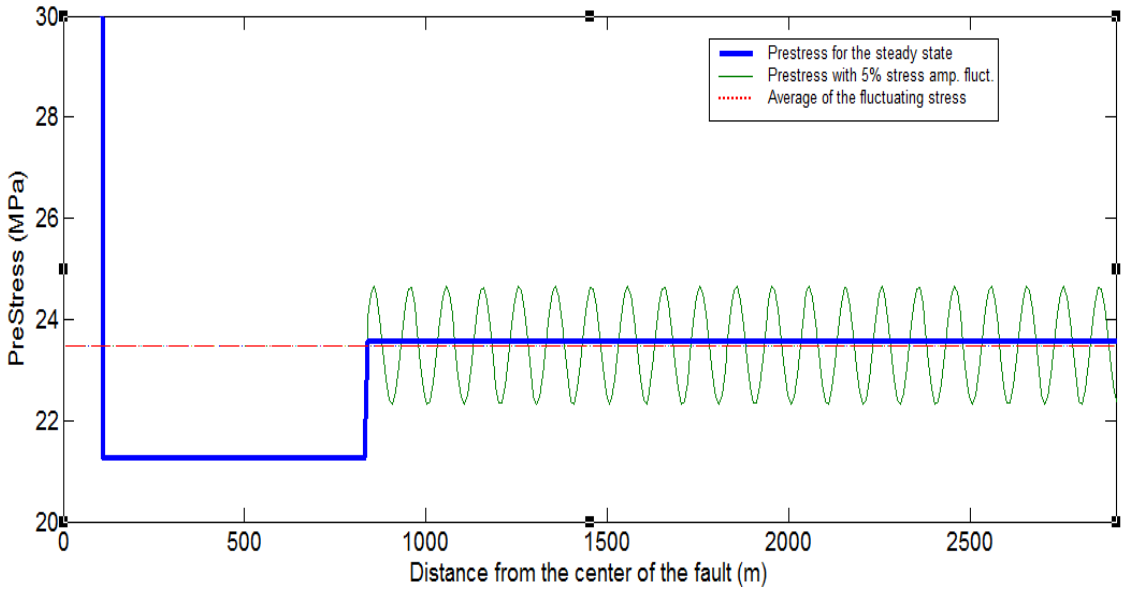

Fig.(5.14): An example of pretsress distribution with perturbations that combine both harmonic fluctuations and a step in the prestress. Note that the harmonic perturbation (light green) is symmetrical about the displaced dashed line (red) and not the reference steady state prestress level (blue).

If the harmonic perturbation, with the given wavelength and amplitude, was to be placed symmetrically about the steady-state prestress level, the resulting perturbed slip would deviate from the supposed steady slip solution. On the other hand, combining the harmonic perturbation with a step in the prestress completely alters the slip response. As shown in Fig. (5.15), the combined perturbation leads to a slip solution that is oscillating about the reference steady slip. This is further verified by looking at the evolution of the maximum slip rate of the propagating slip pulse; it shows an oscillatory behavior that closely follows the reference steady-state solution [Fig. (5.16)].

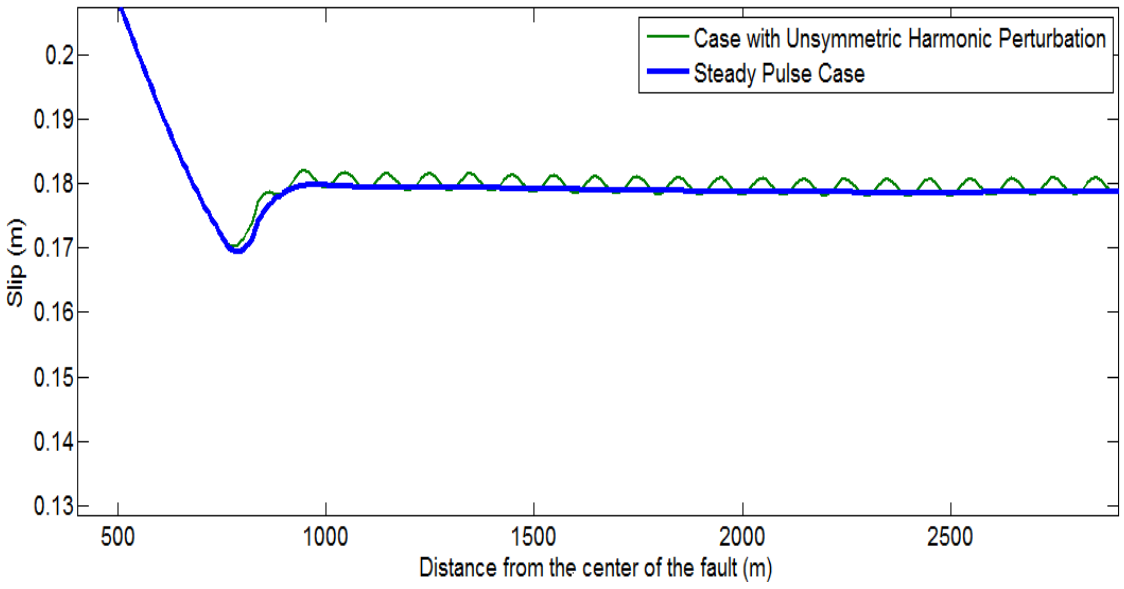

Fig. (5.15): Slip response to the combination of the perturbed prestress distribution shown in Fig. (5.14). The slip shows an oscillatory behavior following closely the steady slip solution.

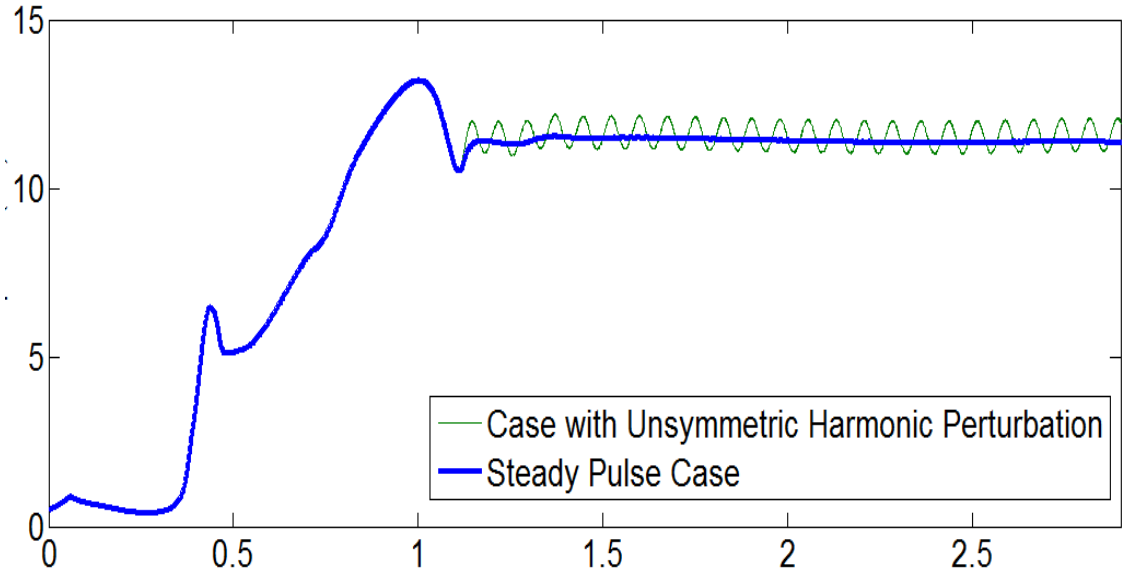

Fig.(5.16): Evolution of the maximum slip rate for the slip pulse in the case of steady propagation, and a case of the perturbed prestress distribution shown in Fig.(14). The perturbed maximum slip rate oscillates about the reference steady-state solution

These results suggest that pulse dynamics is very sensitive to the distribution of the total prestress. While for the simpler perturbation scenarios, such as the symmetric harmonic perturbations and the step in the prestress, the pulse instability is signaled by a nearly exponential deviation from the steady pulse reference solution, more complicated scenarios suggest that it is possible to keep the pulse slip bounded even for large amplitude and large wavelength perturbations. They also suggest that prestress

heterogeneities in the crust might play an important role in bounding the slip values in real earthquakes as well as causing slip spatial complexity as recorded by many slip inversions.

5.6. Energy Considerations and Pulse Propagation

The energy approach in solid mechanics is usually an attractive alternative to pursue since energy is subjected to a conservation principle from which many useful conclusions can be drawn. In Chapter 4 we showed an example of how we may benefit from energy conservation in a discrete framework of fracture to arrive at a simplified description for the pulse dynamics. In fracture mechanics, considering rupture energetics in order to formulate criteria for rupture nucleation or arrest, as well as an equation of motion for the rupture tip, was attempted early on, and has its roots in the works of Griffith [1920], Rice [1968] and Freund [1978]. In this section we examine the energy balance for a slip pulse under general propagation conditions and explore the consequences of the interplay between the different forms of energy and the pulse growth or arrest. We will also digress frequently to draw conclusions relevant to the special case of steady propagation which is the main interest to us here.

There are three major forms of energy associated with the slip pulse propagation: the potential energy, the frictional energy and the kinetic energy. The pulse propagation on the fault surface is made possible because of the available potential energy that the surrounding prestressed medium can provide to the rupture at the crack tip. Part of this change in potential energy is used to overcome the frictional dissipation on the fault

surface while the rest is radiated away from the fault and transmitted as kinetic energy in the surrounding medium through the propagating wave field. The radiated energy, as used in seismology, is just the integral of the kinetic energy flux over a contour that circumvents the fault zone and which is taken at a sufficiently large distance from the fault surface. The energy conservation dictates that after a rupture episode is over the three forms of energy have to be related through the following balance equation:

Change in potential energy = Frictional dissipation + Radiated Energy.

What is of more interest to us here is formulating an energy balance principle for the dynamic rupture during its propagation. In Appendix C, we show that for the case of 2D anti-plane rupture the energy balance can be written in the following form:

$$\int_{\Gamma}[\tau-\tau_o]\dot{u}d\Gamma=\frac{d}{dt}(T+w) \tag{5.8}$$

where τ is the current value of the shear stress, τ_o is the initial shear prestress, $\dot{u}$ is the slip rate, Γ is a contour taken over the fault surface (and since the slip rate may be taken to be zero outside the pulse Γ is effectively a contour over the currently slipping regions), T is the kinetic energy and w is the change in strain energy.

For a steadily propagating slip pulse in an infinite medium, both the kinetic and strain energy are time independent. It follows that the left hand side of Eqn. (5.8) obeys the following conservation principle:

$$\int_{\Gamma}[\tau-\tau_o]\dot{u}d\Gamma=0 \tag{5.9}$$

The significance of the above conservation law becomes clear once we realize that

$\int_{\Gamma}\tau\dot{u}d\Gamma=\int_{T_S}\tau\dot{u}cdt=c\int_{D}\tau du$ is proportional to the total frictional work dissipated at a point

(where c is the shear wave speed, T_s is the slip duration at the point and D is the total slip accumulated at this point) while $\int_{\Gamma}\tau_o\dot{u}d\Gamma=\int_{T_S}\tau_o\dot{u}cdt=c\int_{D}\tau_o du$ is proportional to the total change in potential energy density. Hence, Eqn. (5.9) simply states that for steady propagation in an infinite fault, the change in potential energy density exactly balances the frictional dissipation density leading to no net radiated energy.

We can further use the above argument and simplify Eqn. (5.9) for the case of steady propagation in a uniformly prestressed infinite medium. In this case we can write:

$$\tau_o=\frac{\int_{D}\tau du}{\int_{D}du}=\frac{\int_{D}\tau du}{D} \tag{5.10}$$

The term in the numerator is the total frictional work dissipated at a point, while the denominator represents the total slip at this point. This means that the condition for steady propagation in uniformly prestressed media is that the uniform prestress value has to be equal to the frictional heat stress, i.e., the slip-averaged frictional stress. This situation is depicted schematically in Fig. (5.17).

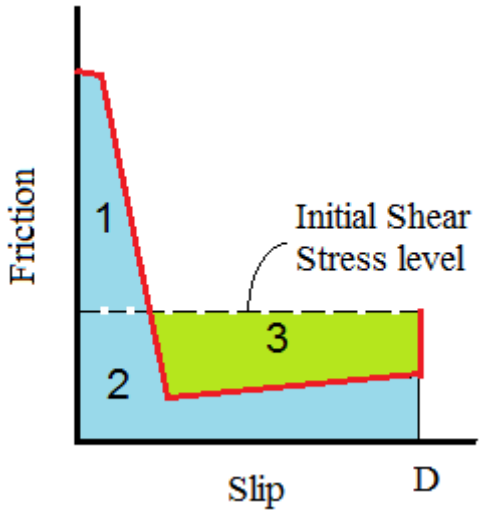

Fig. (5.17): Friction as a function of slip for a steadily propagating pulse in an infinite medium. Since there is no stress drop, the final and the initial prestress levels coincide. The condition of steady propagation is: Area 1 + Area 2 = Area 2 + Area 3. This is equivalent to the statement that for steady propagation, the initial shear prestress level is equal to the slip-averaged frictional stress.

While acknowledging that there are differences between our numerical simulations and the theoretical case of pulse propagation on an infinite fault, relations such as Eqn. (5.10) might be a useful guide to what to expect under idealized conditions. For example, Eqn. (5.10) gives the relationship between the steady pulse slip and the steady shear prestress level. One can identify three cases: i) If the total frictional work dissipated at a point increases with increasing slip at a rate smaller than linear proportionality, the larger the pulse slip and the smaller the prestress level required for its steady propagation. This is the case we have in our numerical simulations; ii) If the total frictional work at the point

is linearly proportional to the point slip then there will exist a unique steady-state prestress level regardless of the steady pulse slip; iii) Finally if the total frictional work at a point increases with the point slip at a rate larger than linear proportionality, then the larger the pulse slip the higher the prestress level required for its steady propagation. Cases i) and ii) represent steady pulses that are unstable to a step in the prestress (they will either grow or die but will not evolve into a steady pulse shape consistent with the new prestress level) and in that sense they are similar to steady pulses reported in this study. Case iii) represents a steady pulse that is stable to an abrupt change in the prestress in the sense that it evolves into a new steady shape consistent with the new prestress level. We hypothesize that such a case could be achieved by considering additional dissipation sources such as pore fluid pressurization or off-fault inelasticity.

Another useful application for Eqn. (5.10) is that it shows steady propagation to be only admissible for a certain range of prestress values. To see this, consider once again a friction-slip relation similar to the one shown in Fig. (5.17) where there exists a minimum value for the interface frictional strength (the lowest point in the curve). Let's denote this minimum value by $\tau_{\min}$. It follows that:

$$\tau_o = \frac{\int_D [\tau_{\min} + \tau^*(u)]du}{D} = \tau_{\min} + \frac{\int_D \tau^*(u)du}{D} \tag{5.11}$$

where $\tau^*(u) = \tau(u) - \tau_{\min}$. Since $\frac{\int_D \tau^*(u)du}{D} > 0$, one conclude that $\tau_o > \tau_{\min}$ in the strong sense of the inequality. Similarly one can imagine that the initial prestress cannot be very

high, otherwise the whole interface can be set up in motion almost simultaneously.

In general, however, for the case of unsteady propagation one can define a general shear stress value as:

$$\bar{\tau} = \frac{\int_{\Gamma} \tau \dot{u} d\Gamma}{\int_{\Gamma} \dot{u} d\Gamma} \tag{5.12}$$

In that sense, $\bar{\tau}$ represents a certain way of averaging the frictional shear stress over the pulse region. The numerator represents the frictional dissipation rate integrated over the pulse width while the denominator is just the potency rate. That is, $\bar{\tau}$ is the potency-averaged frictional stress within the pulse. It is easy to check that for the case of steady propagation on an infinite fault, (5.12) reduces to (5.10).

While we showed that $\bar{\tau} = \tau_o$ for steady pulse propagation in an infinite medium, it is not straightforward to derive similar strict constraints for the steady pulses realized in our numerical simulation. Several factors contribute to this, including the finiteness of the fault and the complex nucleation procedure that is required to generate the pulse in the first place. However, we think that the larger the fault becomes and the further the steady pulse propagates from the rupture hypocenter, the smaller the differences between the numerical simulation and the idealized steady pulse propagation will be. One thing, though, we can claim to be holding in our numerical simulations and that is no sustained pulse-like rupture can exist if $\bar{\tau} > \tau_o$. To see this, we refer back to (5.8) and substitute with our definition of $\bar{\tau}$. If $\bar{\tau} > \tau_o$:

$$\frac{d}{dt}(T+w) > 0$$

(5.13)

While this condition can hold temporarily, it cannot persist indefinitely; otherwise the rupture becomes a source of energy to the medium rather than an energy sink. This contradiction leads us to conclude that ruptures with $\bar{\tau} > \tau_o$ can exist in transient situations only. Figure (5.18) shows an illustrative example for a dying pulse-like rupture.

a

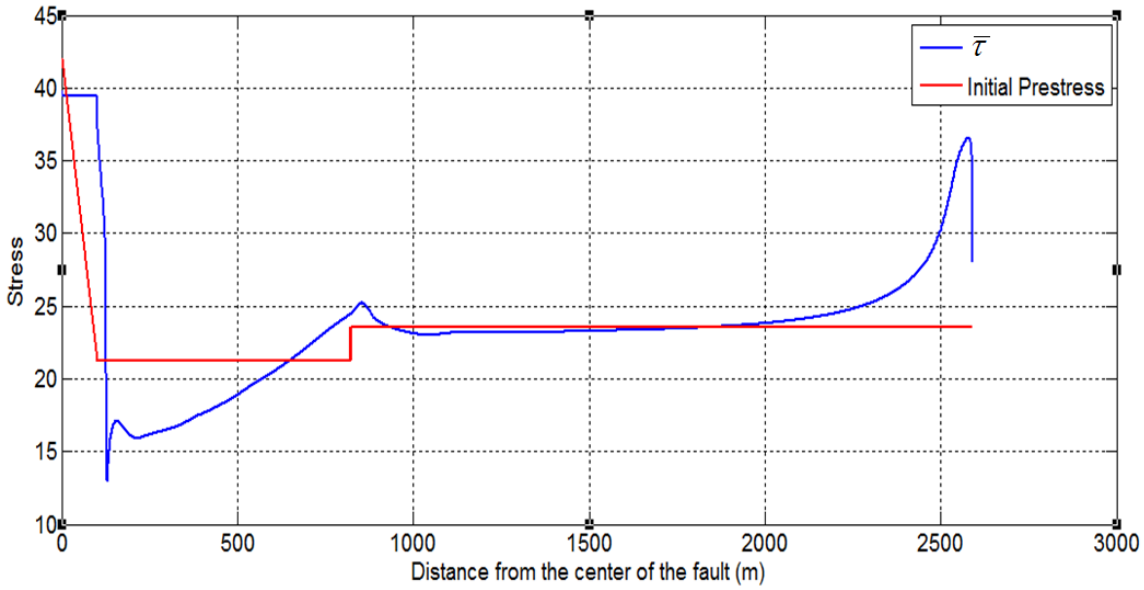

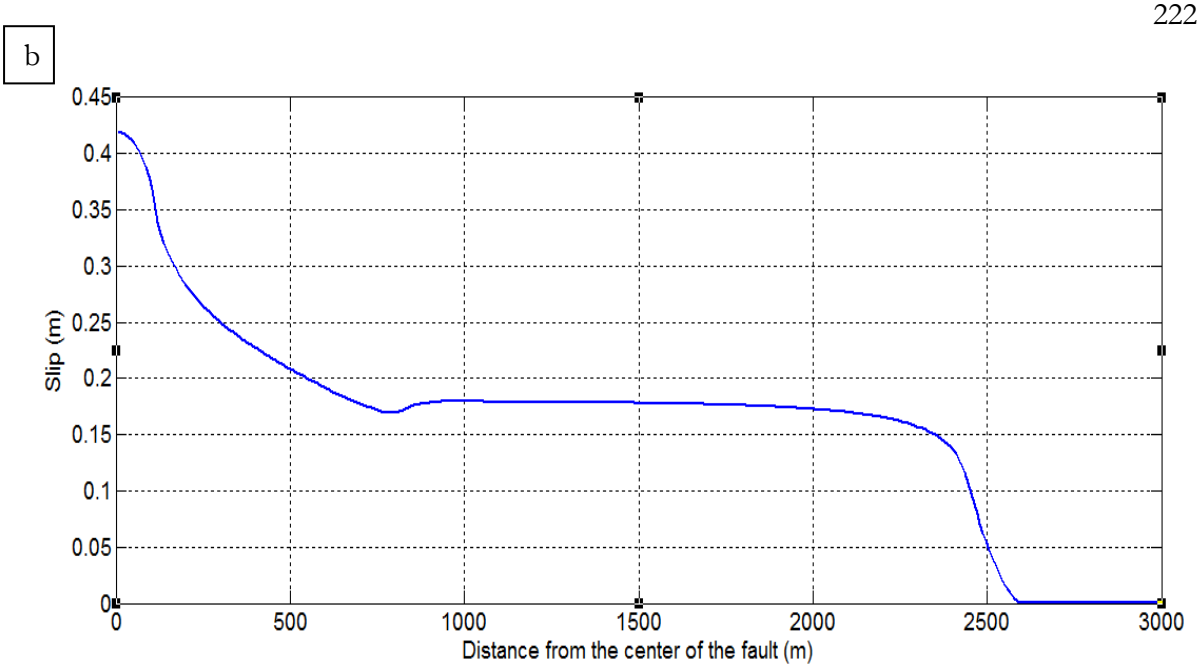

Fig. (5.18): a) Prestress distribution (red) similar to the one used for generating a steady pulse except that the uniform prestress level outside the nucleation zone is smaller than the required steady state prestress. The blue line represents the variation of $\bar{\tau}$. b)Corresponding slip distribution signaling a dying pulse. Note that as $\bar{\tau}$ becomes greater than τ_o the rate of decrease of the slip increases until the rupture is completely arrested.

On the contrary, pulse-like ruptures with growing slip show that $\bar{\tau} < \tau_o$. This is illustrated in Fig. (5.19) where a pulse is created by the same nucleation procedure used in generating steady propagation but with the uniform prestress level outside the nucleation zone slightly increased relative to the steady state prestress level. As the pulse slip grows, $\bar{\tau}$ becomes increasingly lower than τ_o and this feedback between the pulse slip and the pulse frictional stress leads to further deviation of the slip pulse from the steady pulse solution.

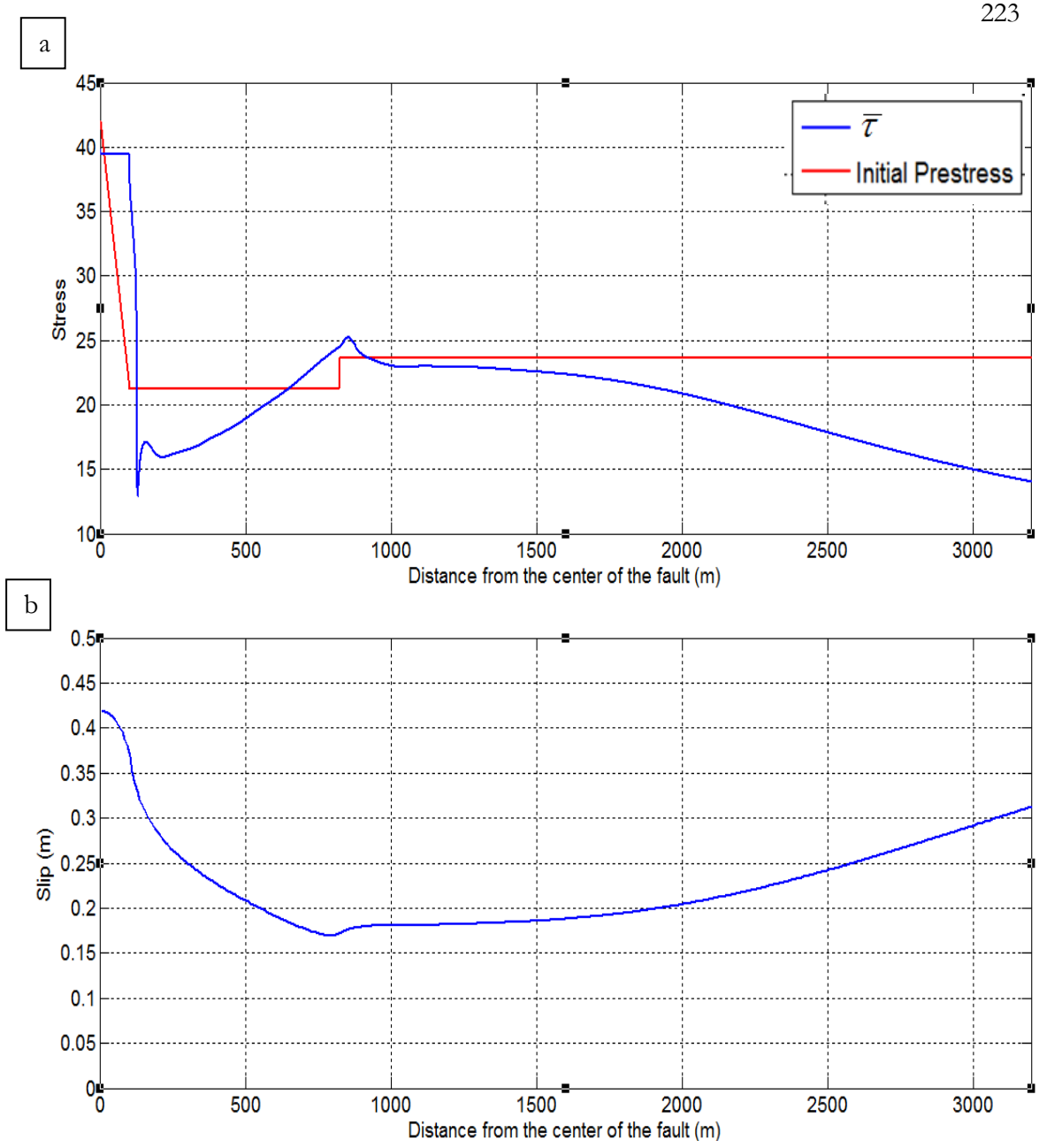

Fig. (5.19): a) Prestress distribution (red) similar to the one used for generating a steady pulse except that the uniform prestress level outside the nucleation zone is slightly larger than the required steady state prestress. The blue

line represents the variation of $\bar{\tau}$. b) Corresponding slip distribution signaling a growing pulse. Note that as $\bar{\tau}$ becomes increasingly smaller than τ_o the rate of growth of the pulse slip further increases.

In this section we have found $\bar{\tau}$ to be indicative of the pulse growth and arrest and in the idealized case of an infinite fault a zero value of $\bar{\tau}$ actually sets the condition for steady propagation. We have also shown that several interesting conclusions and constraints can be drawn based on the value of $\bar{\tau}$. We acknowledge however that due to the several complexities associated with our numerical simulations, stemming mainly from the nucleation process and the finiteness of the fault, the role of $\bar{\tau}$ is not as decisive as its role in the idealized case of propagation on infinite fault. However, we think many of our conclusions remain useful for the case of propagation in finite media, at least in an approximate sense, and have been shown to hold through our numerical simulations. In the next section, we investigate the problem of pulse propagation in general heterogeneous prestress fields and examine the correlation between $\bar{\tau}$ and the variability in pulse slip.

5.7. Pulse propagation in heterogeneous prestress fields

It is highly unlikely that prestress conditions in the earth be uniform. Routine slip inversions have systematically shown that heterogeneous slip is an essential requirement for fitting seismic observations and getting correct estimates of the radiated energy [e.g., Mai et al., 2003, Aagaard and Heaton, 2009, and Smith and Heaton, 2010]. While several mechanisms can contribute to the complexity of slip in real earthquakes, including

geometric complexity of ruptures, fault fractal surface roughness and variability of fault frictional and medium material properties, we cannot rule out the possibility that the heterogeneity of the prestress field could effectively control changes in the slip distribution on both fine and large scales. Since we do not have direct access to measuring how the prestress in the crust changes as a function of position, it becomes useful to explore under what conditions prestress heterogeneity can lead to observable slip complexity, as well as exploring the best heterogeneity model that is both physically based and satisfactory in terms of explaining the data. In this section we do not attempt to tackle all aspects of this complicated problem. However, by using a simple heterogeneous prestress distribution, we build on our findings in the previous sections and show that pulselike ruptures could be sensitive enough to fluctuations in the prestress, to the extent that is reflected in spatial variability in its associate slip. We also examine the stress after and before the event and track the evolution of the $\bar{\tau}$ parameter and its correlation with the pulse slip growth and arrest.

To pursue our problem we first generated a steady pulse using the standard procedure we introduced in Section 5.3. Then we introduced ahead of the pulse a simple scenario of prestress heterogeneities consisting of fluctuating piecewise constant stressses. An example of this prestress distribution is shown in blue in Fig. (5.20). The corresponding slip distribution is shown in Fig. (5.21). It is evident that the pulse slip correlates fairly well with the fluctuations in the prestress. After an initial transient phase, the slip settles

into a uniform value consistent with our procedure for nucleating steady pulses. As the steady pulse propagates into the fluctuating prestress steps, it grows or dies depending on the value of the new prestress. One might note that the locations at which the pulse slip starts to change its sense from decreasing to increasing, and vice versa, does not coincide exactly with the location of the stress steps, but is usually lagging behind by some small distance. This is mainly attributed to the finiteness of the pulses width; the smaller the pulse gets the shorter this transition distance will be.

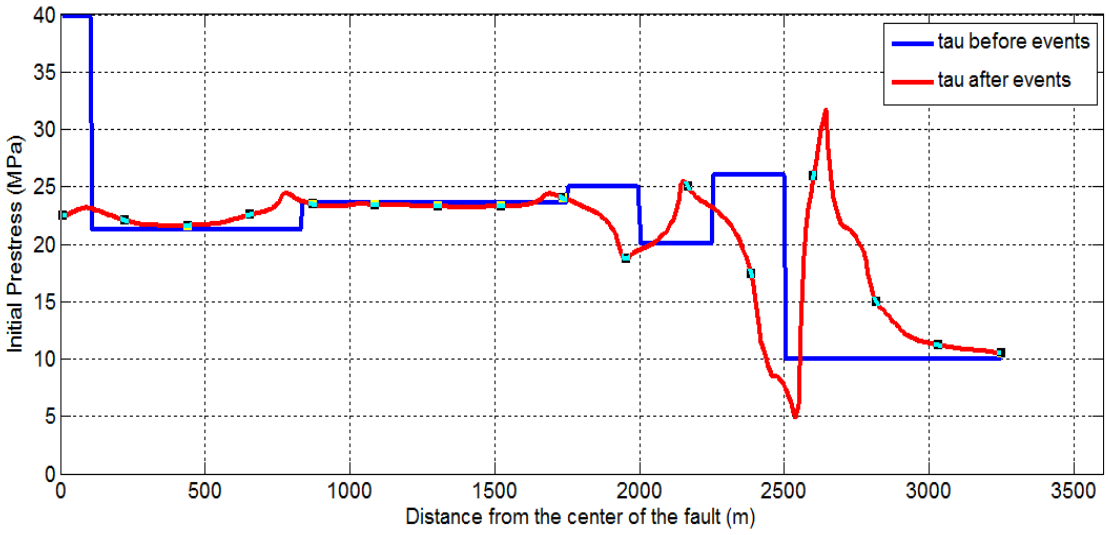

Fig. (5.20): Shear stress distributions before (blue) and after (red with squares) the pulse-like event.

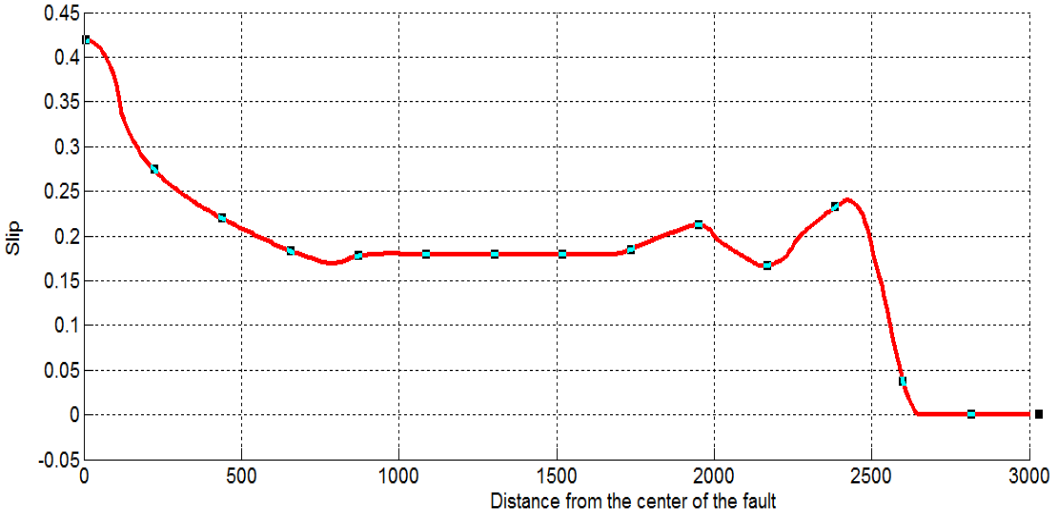

Fig. (5.21): Slip distribution corresponding to the prestress distribution shown in Fig. (5.20). Note that the slip correlates fairly well with the fluctuations in the prestress except for some memory effects due to nucleation and the finite pulse width.

A direct consequence of a heterogeneous slip distribution like the one shown in Fig.(5.21) is the generation of heterogeneous static stress drop. In Fig. (5.20) we show the distribution of the final static shear stress after the pulse-like event is over. The final shear stress distribution shows significant variability as a function of position consistent with the non-uniform prestress and slip distributions. In the zone with steady pulse propagation we have a small but nonzero stress drop due to the finiteness of the hosting fault. In regions with dying pulse slip the rupture accumulates a negative stress drop whereas in regions with growing pulse slip the rupture has a positive stress drop. The magnitude of the stress drop is a linear functional of the prestress and reflects its spatial variability.

Another interesting dynamical feature to look at is the evolution of $\bar{\tau}$, the pulse averaged shear stress, as a function of propagation distance, and how it correlates with the different phases of the pulse-like rupture. This is shown in Fig. (5.22 a) and can be readily compared to the variation in the pulse slip shown in Fig. (5.22 b) for reference purposes. Notice that $\bar{\tau}$ is almost identical to τ_o in the region of steady pulse propagation. The small difference, as we previously explained comes from the complexities associated with the nucleation process and the finiteness of the fault. In regions with growing pulse slip the condition $\bar{\tau} < \tau_o$ is predominantly

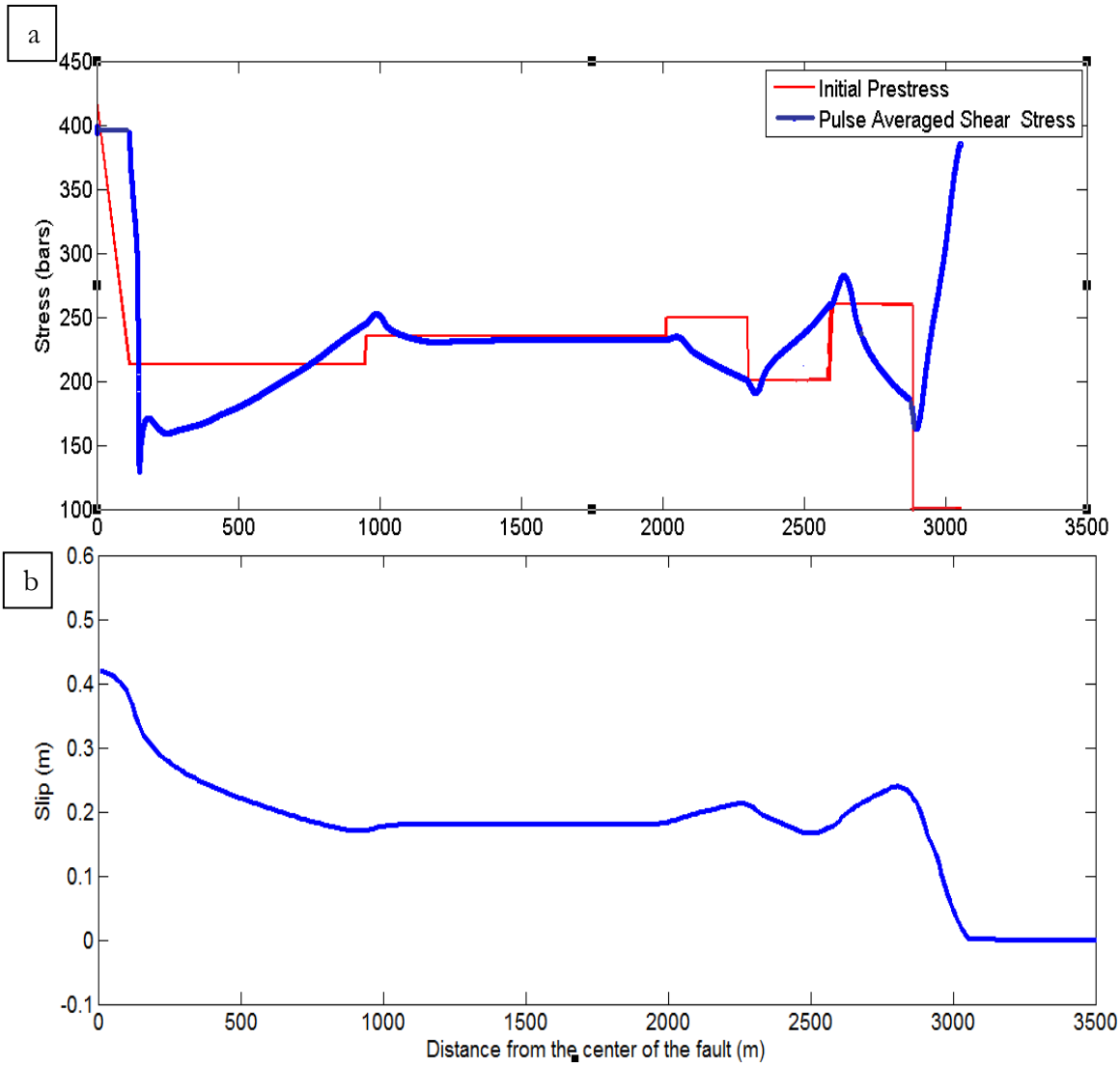

Fig. (5.22): a) Variation of the pulse averaged shear stress, $\bar{\tau}$, as a function of position along with the initial prestress distribution τ_o. b) Corresponding slip distribution. Note that $\bar{\tau}$ variations correlate pretty well with the variations in the final slip distribution.

consistent with our findings in the previous section. On the other hand, in regions with dying pulse slip the condition $\bar{\tau} > \tau_o$ is the one that is predominant. We also note that as the prestress is abruptly changed, the pulse-averaged shear stress $\bar{\tau}$ variation does not follow immediately. This is because of the finite pulse width which results in the evolution of $\bar{\tau}$ over some distance before it becomes fully adjusted to the new prestress conditions.

Based on the previous observations, one can argue that prestress heterogeneity can be an important factor in controlling slip complexity in real ruptures particularly in the case of pulse like ruptures. The spatial localization of the pulse allows it to sample more effectively shorter wavelength fluctuations in the prestress and reflect them more clearly in its associated slip. Cracks, on the other hand, due to the simultaneous movement of all the points within the ruptured zone, will tend to smooth out fluctuations over shorter wavelengths and will yield to, on average, smoother slips. An important question remains, however, whether repeated pulse-like ruptures can sustain stress heterogeneity over cycles of events. This is beyond the scope of this study. However, our results so far suggest that narrow enough pulse-like ruptures propagating in heterogeneous prestress fields result in heterogeneous after-event shear stresses. This might suggest that there is a

premise for finding a mechanism for sustaining prestress heterogeneity through repeated pulse-like ruptures.

Chapter 6: Conclusions and Future Work

In this thesis we presented analytical and numerical models to describe the dynamics of pulselike ruptures propagating on strong velocity-weakening interfaces. We also explored some of the implications of having repeated pulselike ruptures on the long-time statistical and spectral properties of fault stress, slip and strength.

We used tools from both of the continuum and discrete modeling frameworks. The continuum 2D anti-plane fault model enabled us to study slip pulse formation, propagation and interaction with prestress heterogeneities in single rupture episodes. The discrete spring block slider model was useful in exploring the long-time evolution of the statistical and spectral properties of systems with strong velocity-weakening friction under the action of repeated pulselike ruptures of different sizes. The discrete model also enabled us to examine the relationship between slip and prestress in systems with short-range interactions and gave us some clues for a promising method that can be generalized to the continuum modeling and might lead to big computational savings.

The main conclusion of this study can be summarized as follows:

Strong velocity-weakening friction leads to chaotic behavior in discrete rupture models and to the evolution of heterogeneous fault slip and prestress. The spring block slider models with strong velocity-weakening friction generate ruptures of different sizes propagating primarily in a pulse-like mode. We hypothesize that the main source of complexity in the spring block model is the local nature of the slip pulse. This conclusion might be relevant to the evolution of heterogeneity even in continuum models, as the

local nature of the slip pulse is evident as well in full elastodynamic continuum simulations, at least in the 2D anti-plane setting, as we have discussed in Chapter 5. We conjecture that slip pulses are more sensitive to local variations in the prestress than to the influence of perturbations introduced by the long-range interactions carried by the wave field set up by other points slipping on the fault. Hence even in the absence of strong geometric and material discontinuities, strong local fluctuations in the prestress field can kill the pulse and arrest the rupture. The nature of the stress heterogeneity in the spring block slider model turns out to depend on the event sizes distribution. For distributions with predominantly large events, the evolved prestress distribution has Gaussian statistics. We hypothesize that this case is relevant for major mature faults. For distributions with an increased number of small and intermediate sized events, including the case with power law event size distribution, the prestress statistics shows a strong non-Gaussian character. We think that this case may be more relevant to immature faults that have not reached their equilibrium state yet. For systems dominated by large events, the slip distribution has a Gaussian probability density function with a non-zero mean and a power law spectrum in the Fourier domain with amplitude spectrall falloff of -2, consistent with real observations for mature faults. On the other hand, for systems with nearly power law event size distributions, the slip distribution has a non-Gaussian probability density function and an amplitude spectral falloff close to -1.

Strong velocity-weakening friction and heterogeneous prestress lead to size effects in the spring block model dynamics: By using a simple spring block slider model we were

able to show the average prestress and potential energy dependence on the event size. The main parameters controlling the model response were the rate of frictional weakening and the stiffness ratio between the leaf and the coil springs. Those parameters have their counterparts in the continuum setting and hence this conclusion is not limited only to the discrete systems. For example, one may think of the leaf spring in the spring block model to be representative of a loading machine with finite stiffness, or a seismogenic layer of finite depth. We showed that in systems with strong velocity-weakening friction failing primarily in large events (Brittle), longer systems will require less work per unit length than shorter ones in order to be displaced for the same amount of total displacement. On the other hand, in systems with strong velocity-weakening friction failing primarily in small events (Creeping), the work done per unit length for the same amount of displacement is the same independent of system size.

Two measures of strength, applicable on macroscopic scales, are introduced in this study: an energy-based measure of strength given by the amount of work per unit slip per unit rupture length; and a stress-based measure of strength that can be computed as the average value of the prestress over the ruptured length. Systems with strong velocity-weakening friction failing in events of different sizes will generally show a scale dependent energy-based strength that decreases as a power law as a function of the event length. The scaling exponent was shown to vary between -0.5 (close to the ideally brittle limit when systems fail mainly in large events) and 0 (close to the creeping limit when systems fail primarily in small events). From the prestress perspective a similar conclusion can be drawn. The explanation goes as follows.Larger systems are capable of hosting longer ruptures, which in general have higher average slips and pulses with larger

amplitudes. Due to the velocity-weakening character of the friction, larger amplitude pulses will have smaller average frictional forces and consequently can propagate longer in lower average prestress while doing less work per unit length for the same amount of slip. Finally, the combined effect of strong velocity-weakening friction and the finite ratio of the system to loading machine stiffness can result in brittle, quasi-brittle and creeping system responses.

It is possible to predict the final slip distribution in a pulselike event given the prestress that existed before this event, at least in the framework of discrete rupture model. In Chapter 4, we have presented a new paradigm for simulating slip in pulse-like ruptures using an energy balance approach. The key ingredients for this paradigm are the spatial localization of the slip pulse and its preservation for a characteristic shape during propagation. The energy budget of the pulse as it propagates along the fault dictates that at any instant of time, the change in potential energy of the system minus the cumulative frictional dissipation should be balanced by the kinetic energy. Using this energy balance approach, and by approximating the kinetic energy and the frictional work by power laws in terms of the pulse slip, we were able to formulate, within a spring block model framework, a differential equation that can be used to predict the final slip in an event given the prestress that existed before it. The equation replicated the main features of slip in the pulse-like region of ruptures, including slip amplitudes and total rupture length, to a very good degree and in a much shorter computational time. The non pulselike portions of the rupture, e.g., nucleation regions, are handled through the solution of the fully dynamic spring block model. By combining the spring block model for nucleation and

the equation for further propagation (the hybrid model) we were able to match some of the long-time statistics of the solution of the spring block model, such as the prestress spectrum and large events size distribution, with a saving in computational time of almost two orders of magnitude compared to the full dynamic solution of the spring block model. A similar approach might be applied to continuum models, but in this case, long range interactions due to the radiated wave field have to be included. While the extension is not very straightforward, it might not be impossible. This is a topic we are planning to investigate further in the future.

Steady pulses may exist on uniformly prestressed strong velocity-weakening interfaces if the prestress level and the nucleation procedure are correctly tuned. Our results suggest that steady pulses with a given slip can propagate on a velocity-weakening frictional interface with uniform prestress levels if both the nucleation procedure and the pre-stress value are correctly tuned. The absence of numerically realizable steady pulses in earlier literature can probably be attributed to our observation that steady pulses need a special nucleation procedure to be generated; pulses created by uniform overstressing in the nucleation zone are found to be either growing or dying. Within the scope of the velocity-weakening law we have been using in this study, we have found that the larger the pulse slip, the lower the prestress required for its steady propagation. Moreover, if the prestress level ahead of the steady pulse is abruptly changed to a higher/lower value, the pulse grows/dies. The pulse does not assume the steady shape appropriate to that new prestress level. Regarding the stability of steady pulses, we have shown that steady pulses are stable to symmetric harmonic perturbations of small wavelength and amplitude but

unstable to large wavelength, large amplitude perturbations. Nonetheless asymmetry can modify stability; steady pulses can retain their stability in response to large wavelength, large amplitude unsymmetric harmonic perturbations.

We have found that the arrest distance for a dying pulse is controlled by the ratio of the amplitude of decrease in the steady-state stress level and the dynamic stress variation carried by the pulse. The relation between the pulse arrest distance and the drop in the prestress level is a power law, with some scatter. Moreover, we demonstrated that pulse slip seems to adapt to the local prestress value (with some memory effect) and this may have important implications for dynamic complexity and the role of repeated pulse-like ruptures in sustaining prestress heterogeneity over cycles of events. Finally, the pulse-averaged shear stress, where the average is taken with respect to the potency rate, is found indicative of the pulse growth and arrest. In the limit of steady propagation in an infinite medium, this pulse averaged shear stress is identically equal to the prestress.

While this study touches on several aspects of pulselike ruptures (in both continuum and discrete models) and their implications, we believe that there is a lot yet to be done. Possible directions for future research may include the following:

1. ***Finding the optimum value of scaling parameters to be used with the pulse energy equation for the proper approximation of the different long-time statistics of a spring block model with a given stiffness and frictional***

properties. We have found that for a given spring block system, the scaling parameters for the pulse energy and frictional work show some variation among the different events. As a result we found that the scaling parameters that might adequately fit the long-time prestress statistics might be different from the parameters that would properly fit the event size distribution. Using a properly designed grid search algorithm we can find the optimum combination of scaling parameters that can satisfactorily fit both the prestress statistics and the event size distribution.

2. ***Extending the pulse energy equation to simulate ruptures in anti-plane continuum fault models***. The extension is not straightforward as we have discussed. There are two problems standing in the way. The first problem comes from the fact that, unlike in the spring block model, the energy balance in the continuum does not have an explicit term that we might call "pulse energy." This is because, in the continuum, pulses exist on the fault surface that has zero volume, hence no energy can be formally attributed to it. In order to overcome this problem we need first to formulate a rational definition of the term "pulse energy". We are currently testing different alternatives. One is motivated by the steady propagation of slip pulses. For steady propagation there is no radiated energy and all the kinetic energy that exists in the medium is concentrated in the near field. We may accordingly adopt the near field kinetic energy as a possible measure for the pulse energy: it is concentrated near the pulse, it is directly related to the size of the slip pulse, and it vanishes

once the slip pulse size becomes zero. In case of non-uniform propagation we may retain the near field kinetic energy as a measure for the pulse energy while the far field kinetic energy is associated with the radiated energy. By adopting this classification we may write the energy balance as: *pulse energy = change in potential energy – frictional dissipation – far field kinetic energy*. However, an obvious problem with this approach is that it is not clear what determines the spatial limit that separates the near field from the far field. In an attempt to answer this question we are currently studying the spatial distribution of the kinetic energy density associated with the propagation of steady pulses. This distribution will define the extent of the near field and may be carried over to cases of unsteady propagation. This approach is currently under investigation. The other problem with the extension of the equation to the continuum model is that we have to account for the radiated wave field and the long-range interactions that were absent in the spring block model formulation considered in this study. While it is true that the radiated energy, or in general the far field kinetic energy, is a non-local quantity and cannot be expressed in a pointwise manner on the fault surface, it might be possible to find some approximation for the radiated energy flux in terms of the pointwise fault slip distribution in the limit of vanishing pulse width. Finding the correct approximation for the radiated energy will be crucial for the formulation of the energy balance equation in the continuum. This is the other major obstacle that needs to be further investigated.

3. ***Designing computational methods that can solve the elastodynamic problem on a non-uniform grid.*** As we have previously discussed, a major limitation for the current numerical techniques used in continuum fault modeling is the use of uniform grid size. In order to assure computational stability of the numerical solution, the displacement and stress gradients within the process zone near the crack tip must be adequately resolved with a sufficient number of grid elements. Since the process zone might be as small as a few meters, the grid size will typically be of a submeter scale. The uniformity of the mesh size will then yield to the use of an enormous number of grid elements with memory and computational requirements that may overrun the computational capabilities of some of the biggest computers currently available. A possible solution for this problem is the use of a non-uniform grid with finer mesh elements near the crack tip that gets bigger as we move further away from the regions of sharp stress and slip gradients. This mesh adaption may save a lot of memory and run time requirements and could make some of the currently computationally intractable problems possible. We plan to build on recent advances in computational fluid dynamics and the quasi-continuum method in solid mechanics to develop a multiscale computational fault model with dynamic mesh adaptation capabilities.

4. ***Understanding the dynamics of localization during earthquake dynamic propagation and its relation to the dynamics of fault gouge***. Many major mature faults have very thin primary slip zones. How an earthquake localizes

to such a very thin surface and avoids shuttering in the surrounding bulk is not fully understood. In order to understand this phenomenon we need a better understanding of the behavior of the gouge material existent in fault core. We plan to use recent developments in the shear transformation zone theory, originally used to describe plasticity in amorphous materials, to explore possible localization mechanisms in granular materials and their implications on the fault frictional behavior. We also plan to develop models that solve, simultaneously, microscopic models describing gouge behavior with the macroscopic elastodynamic continuum equations.

BIBLIOGRAPHY

Aagaard, B. T., T. H. Heaton, Constraining fault constitutive behavior with slip heterogeneity, J. Geophys. Res.,VOL. 113, B04301, doi:10.1029/2006JB004793, 2008.

Adams, G. G. (1995). Self-excited oscillations of two elastic half-spaces sliding with a constant coefficient of friction, J. Appl. Mech. 62, 867-872.

Adams, G. G. (1998). Steady sliding of two elastic half-spaces with friction reduction due to interface stick-slip, J. Appl. Mech. 65, 470-475.

Ampuero, J.-P., and A. M. Rubin, Earthquake nucleation on rate and state faults – Aging and slip laws, J. Geophys. Res., 113, B01302, doi:10.1029/2007JB005082, 2008.

Andrews, D. J., Rupture velocity of plane strain shear cracks, J. Geophys. Res., 81,5679-5687, 1976.

Andrews, D. J. and Y. Ben-Zion (1997). Wrinkle-like slip pulse on a fault between different materials, J. Geophys. Res. 102, 553-571.

Bak, P., Tang, C. and Wiesenfeld, K. (1987). "Self-organized criticality: an explanation of 1 / f noise", Physical Review Letters 59: 381–384. doi:10.1103/PhysRevLett.59.381242

Barenblatt, G. I. (1961/1962), Mathematical theory of equilibrium cracks in brittle fracture. J. of Applied Mechanics and Technical Physics, No. 4, pp. 3-56 (1961) (in Russian); Advances in Applied Mechanics, VII, pp. 55-129 (1962) (in English).

Bazant, Z., and Yavari, A., Is the cause of size effect on structural strength fractal or energetic-statistical?, Engineering. Fracture Mechanics,72, 1-31.,2005.

Ben-Zion, Y., and J. R. Rice, Dynamic simulations of slip on a smooth fault in an elastic solid, J. Geophys. Res., 102, 17,771–17,784, 1997.

Ben-Zion, Y. and Y. Huang, Dynamic rupture on an interface between a compliant fault zone layer and a stiffer surrounding solid , J. Geophys. Res., 107, DOI 10.1029/2001JB000254, 2002.

Beeler, N. M. and T. E. Tullis (1996). Self-healing slip pulse in dynamic rupture models due to velocity-dependent strength, Bull. Seism. Soc.Am. 86, 1130-1148.

Beeler, N.M., Tullis, T.E. and Goldsby, D.L., Constitutive relationships and physical basis of fault strength due to flash heating, J. Geophys. Res., 113, doi:10.1029/2007JB004988, 2008.

Beroza, G. C., and T. Mikumo, Short slip duration in dynamic rupture in the presence of heterogeneous fault properties, J. Geophys. Res., 101, 22,449–22,460, 1996.

Bowden, F. P., and P. H. Thomas (1954), The surface temperature of sliding solids, Proc. R. Soc. London, Ser. A, 223, 29– 40.

Broberg, K. (1978). On transient sliding motion, Geophys. J. R. Astr. Soc.,52, 397–432.

Broberg, K. B., Cracks and Fracture, Elsevier, New York, 1999.

Burridge, R. and Knopoff, L., Bull. Seis. Soc. Amer. 57, 341, 1967.

Carlson, J.M. and J.S. Langer, Mechanical model of an earthquake fault, Phys. Rev. A 40, 6470–6484 (1989).

Carlson, J.M., Langer, J.S., Shaw, B.E., Tang, C., Intrinsic properties of a Burridge-Knopoff model of an earthquake fault., Phys. Rev. A 44, 884–897 (1991).

Carpentiri, A., Size effects in the failure mechanisms of materials and structures, E & FN spon, London, 1996.

Clayton, R., and B. Engquist, Absorbing boundary conditions for acoustic and elastic wave equations, Bull. Seismol. Soc. Am., 67, 1,529–1,540, 1977.

Cochard, A. and R. Madariaga (1994). Dynamic faulting under rate-dependent friction, Pure and Appl. Geophys. 142, 419-445.

Cochard, A. and R. Madariaga (1996). Complexity of seismicity due to highly rate dependent friction, J. Geophys. Res. 101, 25321-25336.

Cochard, A. and J. R. Rice (1997b). Mode of rupture, self-healing slip pulse versus enlarging shear crack, for a velocity-weakening fault in a 3Dsolid (abstract), EOS 78, no. 46 (Fall Meeting Suppl.), F472.

Day, S. M., Three-dimensional finite difference simulation of fault dynamics: Rectangular faults with fixed rupture velocity, Bull. Seismol. Soc. Am., 72, 705–727, 1982.

Day, S. M., G. Yu, and D. J. Wald (1998). Dynamic stress changes during earthquake rupture, Bull Seism. Soc. Am. 88, 512-522.

Dieterich, J. H., Time-dependent friction and the mechanics of stick-slip, J. Geophys. Res.,116, 790–806, 1978.

Dieterich, J. H., Modeling of rock friction: 1. Experimental results and constitutive equations,J. Geophys. Res., 84, 2,161–2,168, 1979.

Dieterich, J. H., Earthquake nucleation on faults with rate- and state-dependent strength, Tectonophysics, 211, 115–134, 1992.

Dugdale, D.S., Yielding of steel sheets containing slits, J. Mech. Phys. Solids, 1960;8, 100-104.

Erickson, B., B. Birnir and D. Lavallee, A Model for Aperiodicity in Earthquakes., Nonlinear Processes inGeophysics, 2008.

Freund, L. B.,1979, The mechanics of dynamic shear crack propagation. J. Geophys. Res. 84,2199-2209.

Gu, J. C., J. R. Rice, A. L. Ruina, and S. T. Tse, Slip motion and stability of a single degree of freedom elastic system with rate and state dependent friction, J. Mech. Phys. Solids,32, 167–196, 1984.

Geubelle, P. H. and J. R. Rice (1995). A spectral method for 3D elastodynamic fracture problems, J. Mech. Phys. Solids 43, 1791-1824.

Harris, R. and S. M. Day (1997). Effect of a low velocity zone on a dynamic rupture, Bull. Seism. Soc. Am. 87, 1267-1280.

Heaton, T. H., Evidence for and implications of self-healing pulses of slip in earthquake rupture, Phys. Earth Planet. Inter., 64, 1–20, 1990.

Husseiny et al., The fracture energy of earthquakes, Geophysical Journal of the Royal Astronomical Society, Volume 43, Issue 2, pages 367–385, November 1975.

Johnson, E. (1990). On the initiation of unidirectional slip, Geophys. J. Int.101, 125-132.

Johnson, E. (1992). The influence of the lithospheric thickness on bilateral slip, Geophys. J. Int. 101, 151-160.

Kato, N. and Tullis, T.E., Numerical Simulation of Seismic Cycles with a Composite Rate- and State-Dependent Friction Law, Bulletin of the Seismological Society of America; April 2003; v. 93; no. 2; p. 841-853; DOI: 10.1785/0120020118

Lapusta, N., Elastodynamic analysis of sliding with rate and state friction, Ph.D. thesis, Harvard University, Cambridge, MA, 2001.

Lapusta, N., J. Rice, Y. Ben-Zion, and G. Zheng, Elastodynamic analysis for slow tectonic loading with spontaneous rupture episodes on faults with rate- and state-dependentfriction, J. Geophys. Res., 105(B10), 23,765–23,789, 2000.

Lapusta, N., and Y. Liu (2009), Three-dimensional boundary integral modeling of spontaneous earthquake sequences and aseismic slip, J. Geophys. Res., 114, B09303, doi:10.1029/2008JB005934.

Lavallée, D., P. Liu, and R. J. Archuleta (2006). Stochastic model of heterogeneity in earthquake slip spatial distributions, Geophys. J. Int., 165, 622-640.

Lu, X., N. Lapusta, and A. J. Rosakis, Pulse-like and crack-like ruptures in experiments mimicking crustal earthquakes, Proc. Natl. Acad. Sci. U.S.A., p.10.1073/pnas.0704268104, 2007.

Marone, C., Laboratory-derived friction laws and their application to seismic faulting, Annu. Rev. Earth Planet. Sci., 26, 643–696, 1998.

Mai, P.M., and G.C. Beroza (2002). A spatial random-field model to characterize complexity in earthquake slip, J. Geophys. Res., Vol. 107 (B11), 2308, doi:10.1029/2001JB000588.

Myers, C.E., Bruce E. Shaw, and James S. Langer, `Slip complexity in a crustal plane model of an earthquake fault', Physical Review Letters, 77, 972 , 1996.

Noda, H., E. M. Dunham and J. R. Rice, Earthquake ruptures with thermal weakening and the operation of major faults at low overall stress levels, Journal of Geophysical Research - Solid Earth, 114, B07302, doi:10.1029/2008JB006143, 27 pages, 2009.

Okubo, P. G. (1989). Dynamic rupture modeling with laboratory-derived constitutive relations, J. Geophys. Res. 94, 12321-12335.

Olsen, K. G., R. Madariaga, and R. J. Archuleta (1997). Three-dimensional dynamic simulation of the 1992 Landers earthquake, Science 278, 834-838.

Perrin, G., J. R. Rice and G. Zheng, "Self-healing Slip Pulse on a Frictional Surface", Journal of the Mechanics and Physics of Solids, 43, 1995, pp. 1461-1495.

J. R. Rice, "A Path Independent Integral and the Approximate Analysis of Strain Concentration by Notches and Cracks", Journal of Applied Mechanics, 35, 1968, pp. 379-386.

Rice, J. R., The mechanics of earthquake ruptures, in Physics of the Earth's Interior, Proc. Int. Sch. Phys. Enrico Fermi, Course 78, [edited by A. M. Dziewonski and E. Boschi, Elsevier, New York.

J. R. Rice, "Constitutive Relations for Fault Slip and Earthquake Instabilities", Pure and Applied Geophysics, 121, 1983, pp. 443-475.

Rice, J. R., Spatio-temporal complexity of slip on a fault, J. Geophys. Res., 98(B6), 9,885–9,907, 1993.

Rice, J. R., Heating and weakening of faults during earthquake slip, J. Geophys. Res., 111,doi:10.1029/2005JB004006, 2006.

Rice, J. R., and Y. Ben-Zion, Slip complexity in earthquake fault models, Proc. Natl. Acad.Sci. U.S.A., 93, 3,811–3,818, 1996.

Rice, J. R., and A. L. Ruina, Stability of steady frictional slipping, J. Appl. Mech, 50, 343–349, 1983.

Rice, J. R., N. Lapusta, and K. Ranjith, Rate and state dependent friction and the stability of sliding between elastically deformable solids, J. Mech. Phys. Solids, 49, 1,865–1,898, 2001.

Rubin, A. M., and J.-P. Ampuero, Earthquake nucleation on (aging) rate and state faults, J. Geophys. Res., 110, doi:10.1029/2005JB003686, 2005.

Ruina, A. L., Slip instability and state variable friction laws, J. Geophys. Res., 88, 10,359–10,370, 1983.

B. E. Shaw and J. R. Rice, "Existence of continuum complexity in the elastodynamics of repeated fault ruptures", Journal of Geophysical Research, 105, 2000, 23,791-23,810.

Smith, D.E., and T. Heaton, 2010, Models of stochastic, spatially varying stress in the crust compatible with focal mechanism data, and how stress inversions can be biased toward the stress rate Bull. Seismological Soc. Am., submitted

Tse, S., and J. R. Rice, Spacio-temporal complexity of slip on a fault, J. Geophys. Res., 91,9,452–9,472, 1986.

Tullis, T. E., Rock friction constitutive behavior from laboratory experiments and its implications for an earthquake prediction field monitoring program, Pure Appl. Geophys., 126, 555–588, 1988.

Tullis, T. E., Rock friction and its implications for earthquake prediction examined via models of Parkfield earthquakes, Proc. Natl. Acad. Sci. U.S.A., 93, 3,803–3,810, 1996.

Weertman, J. (1980). Unstable slippage across a fault that separates elastic media of different elastic constants, J. Geophys. Res. 85, 1455-1461.

Xia, K., Rosakis, A.J., Kanamori, H., and Rice, J.R., Laboratory earthquakes along inhomogeneous faults, directionality and supershear, Science, 308, Issue 5722, 681-684,2005.

Yoffee, E. H., 1951,The moving Griffith crack., Phil. Mag.,42; 739-750.

Zheng, G., and J. R. Rice, Conditions under which velocity-weakening friction allows a self-healing versus a cracklike mode of rupture, Bull. Seismol. Soc. Am., 88, 1,466–1,483, 1998.

Appendix A: Modal Analysis of the spring block slider model

In this Section, we show that the frictionless spring block slider model can be considered a long wavelength approximation of a 2D continuum in anti-plane elasticity. To see this we start with the 2D wave equation:

$$\frac{\partial^2 u}{\partial t^2} = c^2 \frac{\partial^2 u}{\partial x^2} + c^2 \frac{\partial^2 u}{\partial y^2} \tag{A.1}$$

where u is the displacement, c is the wave speed, x and y are spatial coordinates, and t is time.

Applying the 2D spatial Fourier transform:

$$\frac{\partial^2 \tilde{u}(k_x, k_y, t)}{\partial t^2} = -c^2[k_x^2 + k_y^2]\tilde{u}(k_x, k_y, t) \tag{A.2}$$

where k_x and k_y are the wavenumbers in the x and y directions respectively and $\tilde{u}(k_x, k_y, t)$ is the displacement function in the Fourier domain.

Now consider the limit $k_x << k_y$. This is fulfilled for length scales L in the x-direction satisfying $L >> h$ where h is the overall domain size in the y-direction. [This may correspond, for example, to a case of a long narrow plate with an infinite extension in the z-direction.]

In this limit we may set $k_y = \frac{2\pi}{h}$. Accordingly, Eqn. (A.2) can be re-written as:

$$\frac{\partial^2 \tilde{u}(k_x, t)}{\partial t^2} = -\frac{4\pi^2 c^2}{h^2}[1 + \frac{k_x^2 h^2}{4\pi^2}]\tilde{u}(k_x, t) \tag{A.3}$$

By applying the inverse Fourier transform in the x-direction to Eqn.(A.3) we recover the following relation:

$$\frac{\partial^2 u(x,t)}{\partial t^2} = -\frac{4\pi^2 c^2}{h^2} u(x,t) + c^2 \frac{\partial^2 u(x,t)}{\partial x^2} \tag{A.4}$$

This is the continuum analog of the first three terms of Eqn. (2.1) governing the dynamics of the spring block slider model. To see this, we discretize the second derivative in Eqn. (A.4) to obtain:

$$\frac{\partial^2 u(x,t)}{\partial t^2} = -\frac{4\pi^2 c^2}{h^2} u(x,t) + \frac{c^2}{(\Delta x)^2}[u(x+\Delta x,t) - 2u(x,t) + u(x-\Delta x,t)] \tag{A.5}$$

One can readily recognize the coil spring stiffness k_c as $\frac{c^2}{(\Delta x)^2}$ while the leaf spring stiffness k_l is given by $\frac{4\pi^2 c^2}{h^2}$. Hence, the leaf spring stiffness is inversely proportional to the square of the depth in the y-direction. The narrower the plate thickness, the stiffer the leaf spring and vice versa. This provides a framework for mapping the results obtained in Chapter 2 to real observations. For example, a very narrow but long seismogenic zone will fail primarily in small events but as the depth of the seismogenic zone increases, larger events can be generated.

The coil spring to the leaf spring stiffness ratio *r* can then be calculated as:

$$r = \frac{h^2}{4\pi^2 [\Delta x]^2} \tag{A.6}$$

Using the continuum limit of the spring block slider model, we investigate the response of the system to Fourier perturbations of the form $\exp(ikx + ipt)$ where $k \in R$ is the perturbation wavenumber and $p \in C$ is the perturbation growth rate. We first consider the response of a frictionless version of the system. We then add nonlinear friction to the system and analyze the response of steady sliding to perturbations of small amplitudes.

A-1: The dispersive frictionless spring block model:

The dynamics of the spring block model in this case can be described,

as was shown in Eqn. (A.4), by the following mathematical model:

$$\ddot{u} = c_s u_{xx} - k_l u \tag{A.7}$$

Where c_s is the characteristic sound wave speed in the absence of dispersion and k_l is the leaf spring stiffness.

Assuming $u = \exp(ikx + ipt)$ and substituting in Eqn. (A.7) we arrive at the following dispersion relation:

$$c_{ph}^2 = c_s^2 + \frac{k_l}{k^2} \tag{A.8}$$

Where $c_{ph} = p/k$ is the phase velocity of perturbation with wavenumber *k*.

By rearranging, Eqn. (A.8) can be rewritten as:

$$\frac{c_{ph}}{c_s} = \sqrt{1 + \frac{k_l}{(kc_s)^2}} \tag{A.9}$$

It is evident from Eqn. (A.9) that the dispersive effects become more pronounced as the stiffness of the leaf springs increases. It can also be deduced from the same relation that longer wavelengths have higher phase velocities than shorter wavelengths and that all

wavelengths have supersonic phase speeds. The group velocity on the other hand can be derived as follow. From (A.8) one can write:

$$c_g = \frac{dp}{dk} = c_s \frac{1}{\sqrt{1 + k_l / (kc_s)^2}} \tag{A.10}$$

Where c_g is the group velocity for the perturbation with wavenumber *k*. The group velocity is always subsonic for all wavenumbers (except for $k = \infty, c_g = c_s$), consistent with the causality constraint.

A.2- The full spring block system: dispersion and nonlinear velocity dependent friction:

We assume a velocity dependent friction of the form

$$f = \frac{f_o}{1 + \dot{u}/v_c} \tag{A.11}$$

Where $\dot{u}$ is the slip rate and v_c is a reference slip rate.

The governing equation for the spring block system in this case takes the form:

$$\ddot{u} = c_s^2 u_{xx} - k_l u - \frac{f_o}{1 + \dot{u}/v_c} \tag{A.12}$$

We investigate the response of steady sliding at $\dot{u} = \dot{u}_o$ for perturbations of the form $\exp(ikx + ipt)$. We consider displacement and slip rate fields of the form:

$$u = \dot{u}_o t + D\exp(ikx + ipt) \tag{A.13}$$

$$\dot{u} = \dot{u}_o + ipD\exp(ikx + ipt) \tag{A.14}$$

It follows that the acceleration field takes the form:

$$\ddot{u} = -p^2 D\exp(ikx + ipt) \tag{A.15}$$

Substituting from Eqn. (A.13), Eqn. (A.14) and Eqn. (A.15) in Eqn. (A.12) and linearizing the friction using the assumption that $D << \dot{u}_o$ we get:

$$-p^2 D\exp(ikx+ipt) = -c_s^2 k^2 D\exp(ikx+ipt) - k_l[\dot{u}_o t + D\exp(ikx+ipt)] - \frac{f_o}{1+\dot{u}_o/v_c}[1 - \frac{ipD\exp(ikx+ipt)}{v_c(1+\dot{u}_o/v_c)} + ...]$$

And by applying the equilibrium condition for steady sliding condition: $-k_l \dot{u}_o t - \frac{f_o}{1+\dot{u}_o/v_c} = 0$, Eqn. (A.16) reduces to:

$$-p^2 = -c_s^2 k^2 - k_l + \frac{ipf_o}{v_c(1+\dot{u}_o/v_c)^2} \tag{A.17}$$

Rearranging Eqn. (A.17) and letting $\Psi = \frac{f_o}{v_c(1+\dot{u}_o/v_c)^2}$ we find that *p* has to satisfy the following condition:

$$p^2 + ip\Psi - (c_s^2 k^2 + k_l) = 0 \tag{A.18}$$

This implies

$$p = \frac{i\Psi}{2}[-1 \pm \sqrt{1 - \frac{4(c_s^2 k^2 + k_l)}{\Psi^2}}] \tag{A.19}$$

Two cases follow: if $0 < \frac{4(c_s^2 k^2 + k_l)}{\Psi^2} \leq 1$, then p is an imaginary number implying that perturbations with wavenumbers satisfying this condition are unstable with zero phase velocity. If, on the other hand, $\frac{4(c_s^2 k^2 + k_l)}{\Psi^2} > 1$, then p is a complex number which can be written as:

$$p = \frac{i\Psi}{2}[-1 \pm i\sqrt{\frac{4(c_s^2 k^2 + k_l)}{\Psi^2} - 1}] = \mp\frac{\Psi}{2}\sqrt{\frac{4(c_s^2 k^2 + k_l)}{\Psi^2} - 1} - i\frac{\Psi}{2} \tag{A.20}$$

This implies that perturbations with wavenumbers satisfying $\frac{4(c_s^2 k^2 + k_l)}{\Psi^2} > 1$ are unstable with growth rate $\frac{\Psi}{2}$ and phase velocity :

$$c_{ph} = \frac{\frac{\Psi}{2}\sqrt{\frac{4(c_s^2 k^2 + k_l)}{\Psi^2} - 1}}{k} = c_s\sqrt{1 + \frac{k_l}{(kc_s)^2} - (\frac{\Psi}{2c_s k})^2} \tag{A.21}$$

This means that the phase velocity of a specific perturbation could be subsonic or supersonic depending on the value of the perturbation wavenumber, leaf spring stiffness, and the parameter Ψ .

The group velocity on the other hand is given by:

$$c_g = \frac{c_s}{\sqrt{1 + k_l / (c_s k)^2 - (\Psi / 2c_s k)^2}} \qquad \text{(A.22)}$$

It is worth to recall here that our results from chapter 1 suggests that observed rupture speeds are always subsonic with values almost equal to the characteristic sound speed of the system and hence no violation for causality is reported.

Also it is worth stressing that while our analysis suggests that perturbations of all wavelengths are unstable, the perturbation growth rates, deduced from either Eqn. (A.19) or Eqn. (A.20), are always bounded regardless of the perturbation wavenumber. The bounded growth rates make the computation with the spring block slider possible. This is to be contrasted with the results of stability analysis of pure velocity-weakening friction in the continuum (Lapusta, 2000 and Rice et al., 2001) where perturbations with larger wavenumbers have higher growth rates [In the limit, zero wavelength perturbations will have infinite growth rates!]. This latter type of short wavelength stability cannot be controlled and yields the computational problem of sliding on pure velocity-weakening frictional surfaces ill-posed.

A.3. On the effect of prestress on the rupture speed in the spring block model

The introduction of a friction law into the spring block slider system not only changes the dispersion relation of the system compared to its dispersive frictionless system, but it also

brings an additional variable, the prestress, into play. Here we briefly discuss the influence of the prestress on the rupture speed in the frictional dispersive spring block model.

Let us first consider the case with uniform prestress σ_o. Imagine that the rupture tip is at the position of the ith block. The block are interspaced equally with the distance between blocks fixed and scaled to be equal to unity. The time taken until the block indexed (*i+1*) starts to move can be calculated as follows:

The force required to move the (*i+1*) block is: $\Delta F = f_o - \sigma_o$ where f_o is the static friction force. This force is provided by the coil spring connecting the *i* and *i+1* blocks. The force in the coil spring is given by: $F_c = k_c \Delta u = k_c \bar{v} t$ where k_c is the coil spring stiffeness, Δu is the displacement of the ith block until block (*i+1*) starts to move, $\bar{v}$ is the average slip rate of the ith block during its course of motion while block (*i+1*) is stuck and t is the time taken until the block indexed (*i+1*) starts to move measured from the instant at which the rupture tip has reached the ith block. Equating ΔF with F_c we find that the time *t* satisfies the following condition: $t = \frac{f_o - \sigma_o}{k_c \bar{v}}$. The rupture speed can then be readily calculated as $c_r = \frac{k_c \bar{v}}{f_o - \sigma_o}$. This last result suggests that the rupture speed is inversely proportional to the stress deficit at a point with rupture propagating faster for prestress values closer to the static friction limit. The fact that the observed rupture speed in the numerical simulations we have carried out is nearly constant, independent of the rupture size or the distribution of

the prestress, suggests that the evolution of the prestress into a critical spatial state, with stable statistical and fractal properties, plays an important role in controlling the rupture speed and keeping it, on average, constant.

Appendix B: The Pulse Energy Equation Revisited

In Chapter 4 we showed that the proposed pulse energy equation is capable of generating many of the macroscopic features of ruptures including slip distribution and total rupture length. We also proposed a hybrid model, a spring block slider for modeling the nucleation phase, and the pulse energy equation for simulating pulselike propagation, which succeeded in matching many of the long-time statistics of the full spring block model and in a much shorter computational time.

In this section we apply the pulse energy equation and a hybrid model to a spring block slider system of different material and frictional properties from those used in the text. We consider a system with coil spring stiffness $k_c = 2500$, leaf spring stiffness $k_l = 40$ and frictional weakening parameter $b = 10$. We first try to replicate the basic features of the slip distribution in individual events and then we consider fitting the long-time statistics for an ensemble of events.

Figure B.1 shows the results of the equation solution compared to the full solution of the spring block slider model. For this case, the scaling parameters for the frictional and pulse energy are: $\alpha = 0.708$, $\beta = -0.588$, $\gamma = 501.1$ and $\xi = 1.6$

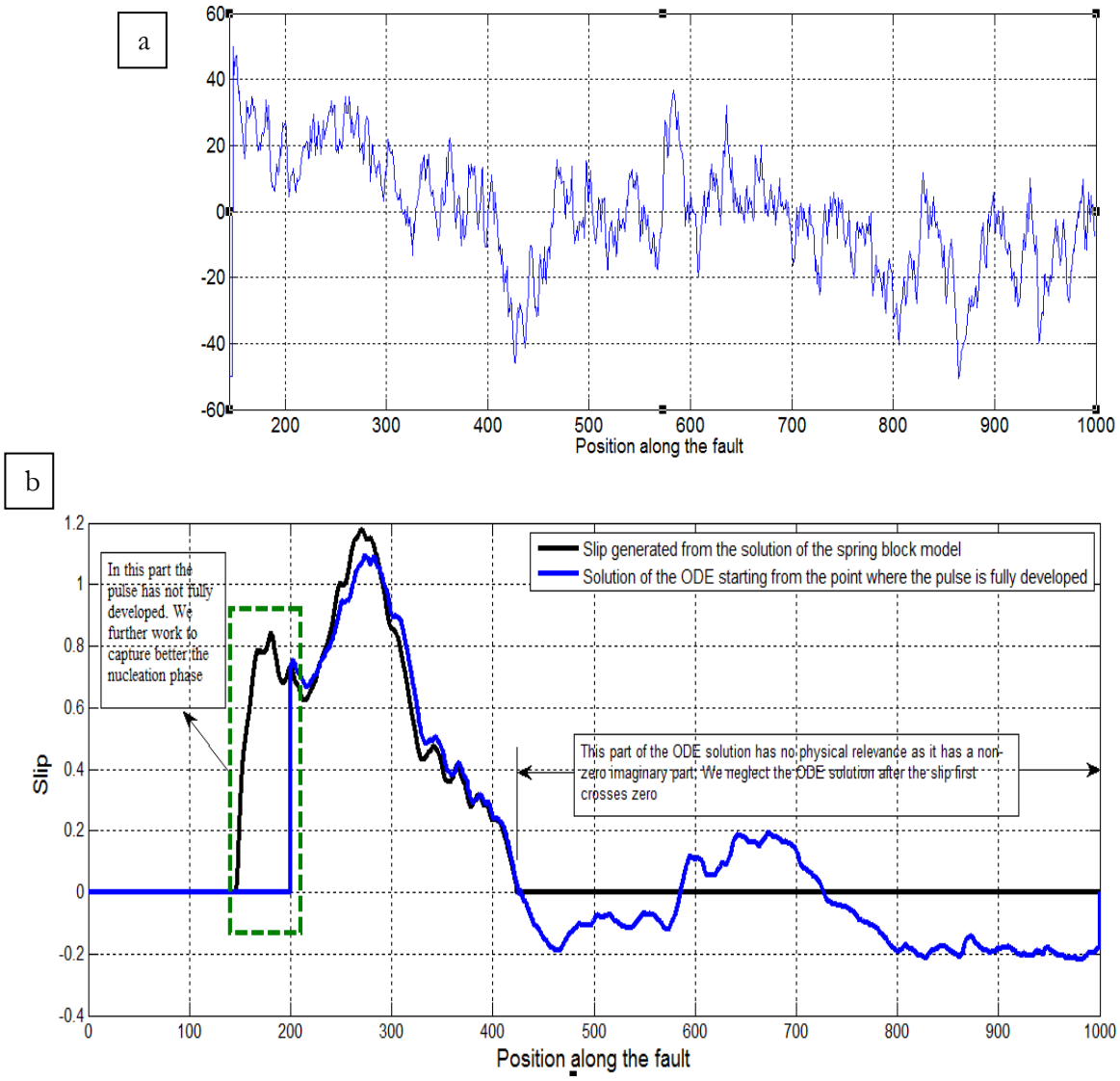

Fig. (B.1): a): Prestress distribution for the test case. b): The solution of the proposed differential equation (in blue) replicates pretty well the slip solution from the spring bock model in the pulselike region. The initial condition for the equation was taken as the slip value at the point where the nucleation phase is over and the pulse has fully developed. The nucleation phase is handled separately as discussed shortly. The saving in computational time for this particular case is 10,000 times fold.

As in Chapter 4, we here propose a hybrid model to enable us to simulate long-time sequence of events. In the hybrid model, a microscopic model (the spring block slider model) is used for rupture initiation while a macroscopic mode (the pulse energy equation) is used for pulse propagation. By this approach, we can accurately handle the nucleation phase as well as the modeling of bilateral events.

We tested the long-time performance of the proposed pulse energy equation by generating 1,000 events in the statistically stable regimes from both the hybrid model and the full spring block model. We considered several measures including: the evolved prestress spectrum [Fig. (B.2)(a)], the evolved prestress probability distribution [Fig. (B.2)(b)] and the events length distribution [Fig. (B.3)(c)]. In order to fit the different statistics we had to experiment with different combinations of scaling parameters. The values of the scaling parameters that yielded the best fit for the prestress statistics were $\alpha = 0.412,\ \beta = -1,\ \gamma = 401$ and $\xi = 2.0$, while the scaling parameters that yielded the best fit for the event length distribution were $\alpha = 0.412,\ \beta = -1,\ \gamma = 625$ and $\xi = 1.4$. The ability to fit different long-time statistics using different combinations of parameters can be understood in light of the event size dependence of the values of the scaling parameters previously discussed in Chapter 4. It is possible, however, that there exists a combination of scaling parameters that would yield good fits for the different statistics simultaneously. As part of our future work, we plan to design an efficient grid search algorithm in an attempt to find this optimum combination of parameters and its relation to

the specific values of the material and frictional properties of the spring block model. Nonetheless, we argue that our results suggest the hybrid model performs satisfactorily. There is certainly room for improvement and a premise for a better performance.

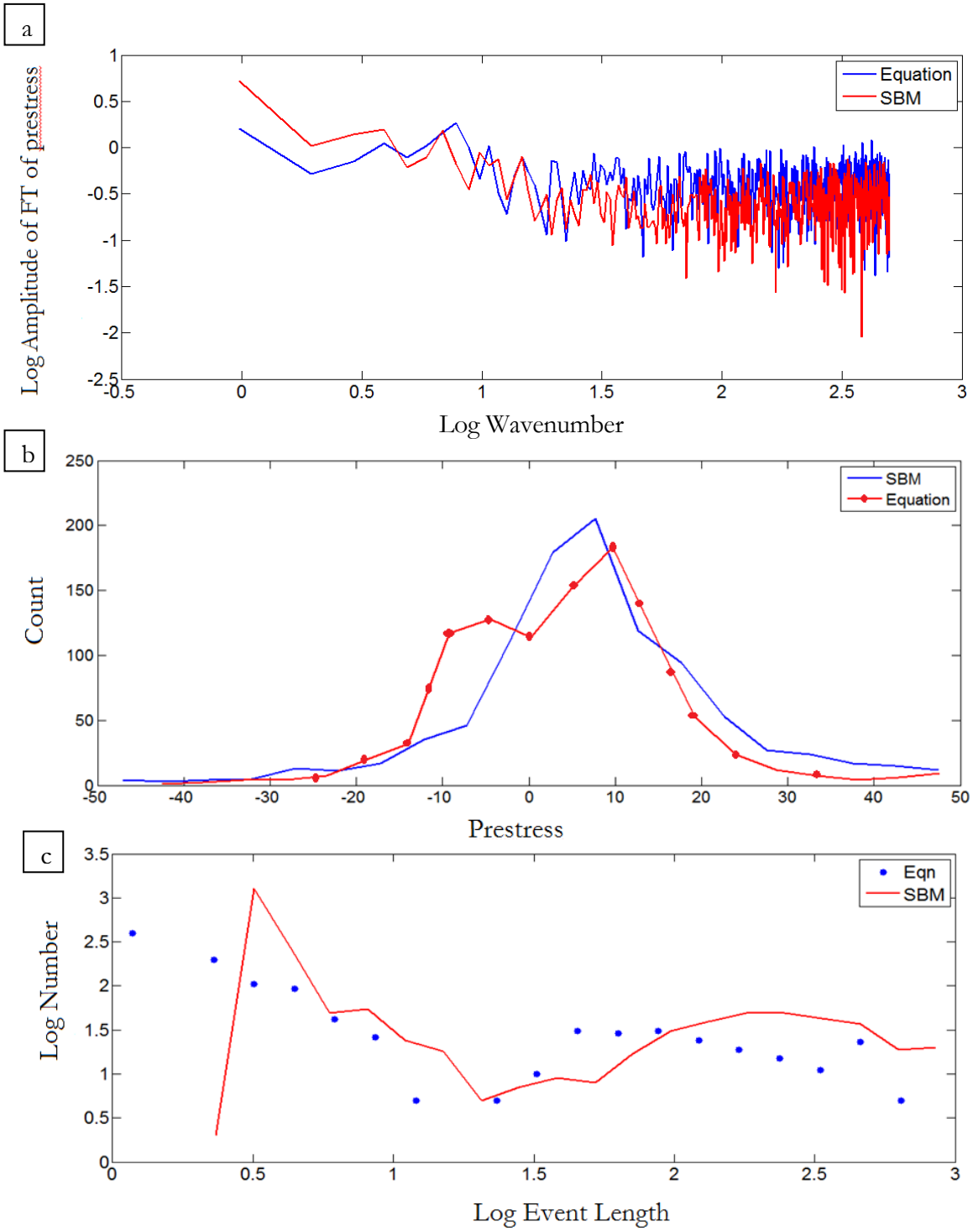

Fig.(B.2): Comparison of the long-time statistics generated by the hybrid model, the spring block model for nucleation plus the energy equation for propagation, and the statistics generated by the full spring block model (SBM). (a): Prestress spectra. (b): Prestress probability distributions. (c): Event length distribution

Appendix C: Energy budget for pulses propagating on 2D anti-plane continuum faults

We start with the equation of motion of a body in R^3

$$\rho\ddot{u} = \nabla.\sigma \tag{C.0}$$

Multiply both sides by the particle velocity and integrate over the whole volume to get:

$$\begin{aligned}\int_V \rho\ddot{u}_i\dot{u}_i dV &= \int_V \sigma_{ij,j}u_i dV \\ &= \int_V (\sigma_{ij}\dot{u}_i)_{,j} dV - \int_V \sigma_{ij}\dot{u}_{i,j} dV \\ &= \int_{C+\Gamma} \sigma_{ij}\dot{u}_i n_j dS - \int_V \sigma_{ij}\dot{u}_{i,j} dV\end{aligned} \tag{C.1}$$

Where V is the volume of the continuum body bounded in the far field by a contour C and includes a surface of discontinuity within it that is covered by the contour Γ [See the figure opposite].

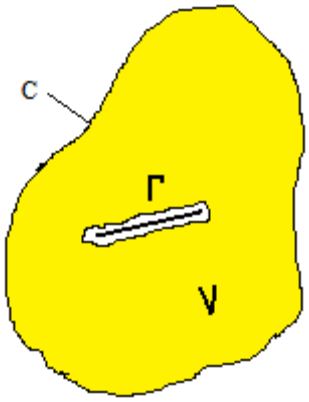

Re-arranging terms we get:

$$\int_V \rho\ddot{u}_i\dot{u}_i dV + \int_V \sigma_{ij}\dot{u}_{i,j} dV - \int_C \sigma_{ij}\dot{u}_i n_j dS = \int_\Gamma \sigma_{ij}\dot{u}_i n_j dS \tag{C.2}$$

But the total stress is the sum of the initial stress and the elastic stress change:

$$\sigma_{ij} = \sigma_{ij}^o + C_{ijkl}u_{k,l} \tag{C.3}$$

Moreover by using Reynold's transport theorem the rate of change of kinetic energy (T) can be written as:

$$\frac{dT}{dt} = \frac{d}{dt}\int_V \frac{1}{2}\rho \dot{u}_i \dot{u}_i dV = \int_V \rho \ddot{u}_i \dot{u}_i dV + \int_\Gamma \frac{1}{2}\rho \dot{u}_i \dot{u}_i v_r n_r dS \tag{C.4}$$

Where the surface integral is taken only along Γ since C is fixed in space and large enough to include the whole fault. Here *v* is the velocity by which the contour Γ is moving and n is the normal to contour surface. The normality condition cancels the contribution of the last term in (C4) for an anti-plane shear rupture. Hence we will drop this term out in subsequent discussion (If we allow for crack opening then this term will assume nonzero value)

Similarly the rate of change of strain energy (w) can be found from:

$$\begin{aligned}\int_V \sigma_{ij}\dot{u}_{i,j} dV &= \int_V \sigma^o_{ij}\dot{u}_{i,j} dV + \int_V C_{ijkl}u_{k,l}\dot{u}_{i,j} dV \\ &= \int_\Gamma \sigma^o_{ij}\dot{u}_i d\Gamma + \frac{d}{dt}\frac{1}{2}\int_V C_{ijkl}u_{k,l}u_{i,j} dV \\ &= \int_\Gamma \sigma^o_{ij}\dot{u}_i d\Gamma + \frac{dw}{dt}\end{aligned} \tag{C.5}$$

Combining all the above we arrive at the following Power Identity:

$$\frac{dT}{dt} + \frac{dw}{dt} - \int_C \sigma_{ij}\dot{u}_i n_j dS = \int_\Gamma (\sigma_{ij} - \sigma^o_{ij})\dot{u}_i n_j d\Gamma \tag{C.6}$$

We may recognize the contour integral over the far fixed contour C as the rate of change of energy radiation. If C is taken far enough then its contribution to the energy balance during rupture propagation is zero. In this case the energy balance reduces to:

$$\frac{dT}{dt} + \frac{dw}{dt} = \int_{\Gamma} (\sigma_{ij} - \sigma_{ij}^{o}) \dot{u}_i n_j d\Gamma$$

(C.7) where

$$T = \frac{1}{2} \int_{V} \rho \dot{u}_i \dot{u}_i dV \tag{C.8}$$

is the kinetic energy and

$$w = \frac{1}{2} \int_{V} C_{ijkl} u_{k,l} u_{i,j} dV \tag{C.9}$$

is the strain energy for a linearly elastic solid.

Appendix D: Analysis of stability of steady sliding on velocity-weakening frictional interfaces:

Lapusta (2000) showed that more complex rupture modes, other than the cracklike and the pulselike modes, such as multiple pulses, may result for intermediate levels of prestress and velocity-weakening. Such multiple pulses occur due to destabilization of steady sliding behind the front of the crack-like rupture that forms after the nucleation stage. The spacing of the multiple pulses can be predicted from linearized stability analysis of the steady sliding; it corresponds to the wavelength of the perturbation with the maximum growth rate. Whether the transition from the crack-like rupture to multiple pulses occurs within the rupture duration depends on the growth rates, which are higher for more pronounced velocity-weakening.

Here we explore the possibility that transition from the initial crack-like rupture to a self-healing pulse can also be understood based on such stability analysis. We conduct simulations of dynamic ruptures in a 2D antiplane fault model with rate and state friction that involves enhanced weakening at seismic slip velocities motivated by flash heating. We study spontaneous dynamic ruptures in uniformly stressed faults with a small localized region that is overstressed for nucleation purposes.

The outline of this study is as follows. In Section D.1 we describe in more details the major characteristics of the rate and state friction law used here. In Section D.2 we discuss the problem of stability of steady sliding in the presence of velocity-weakening

friction and its basic features. In Section D.3 we hypothesize a mechanism that might interpret the process of the formation of slip pulses in the light of the stability analysis.

D.1. Rate and State friction:

A formulation of the rate and state laws which assumes constant normal stress and one state variable, to record dependence on slip history, is of the general form

$$\tau = \psi(V, \theta) \tag{D.1}$$

$$\frac{d\theta}{dt} = \varphi(V, \theta) \tag{D.2}$$

where θ is the state variable and τ, V and θ depend on space variables and time.

We require that the rate and state friction law to have the following properties:
If the slip velocity V is suddenly increased or decreased, the stress τ simultaneously increases or decreases; that is, instantaneous positive viscosity is incorporated in (D.1) through the requirement:

$$\frac{\partial \psi}{\partial V} > 0 \tag{D.3}$$

This property is sometimes called “direct velocity dependence” or the “direct effect” and is well established experimentally [Dieterich, 1979; Ruina, 1983; Marone, 1998b]. For rapid enough changes in so as for the surfaces to be at the same population of asperity contacts (i.e., at a constant value of the state variable), the variation of the friction strength τ with the slip rate V is generally found to involve a positive proportionality to $\ln V$. This logarithmic form was derived from purely empirical considerations to match experimental observations done at slow slip rates. For velocity transitions at high slip

rates, the direct effect can still be observed (Prakash, personal communication). It is not settled yet whether the direct effect in this case has the classical logarithmic dependence or not. We use the logarithmic form in our simulations described later in this chapter. For the linearized stability analysis, however, the exact form of the direct effect is not important, as long as it is positive, as demonstrated by experiments and supported by physics.

If slip velocity is held constant, the state variable and hence the stress monotonically evolve toward constant values, called steady-state values and denoted $\theta_{ss} = \theta_{ss}(V)$ and $\tau_{ss} = \tau_{ss}(V)$, respectively, where θ_{ss} satisfies $\varphi(V, \theta_{ss}) = 0$ and τ_{ss} is given by $\psi(V, \theta_{ss})$. The law (D.3) is said to exhibit steady-state velocity-weakening if $\frac{d\tau_{ss}}{dV} < 0$ and steady-state velocity strengthening if $\frac{d\tau_{ss}}{dV} > 0$. We will show that all laws of the class (D.2) reduce, for near θ_{ss}, to $\frac{d\theta}{dt} \approx -\frac{V}{L}[\theta - \theta_{ss}(V)]$ where L has dimensions of slip and can be interpreted as a characteristic slip distance required for evolution to the steady state. The precise definition of L is

$$L = [-\frac{V}{\partial\varphi(V,\theta)/\partial\theta}]_{V=V_o, \theta=\theta_{ss}(V_o)} \qquad \text{(D.4)}$$

The notation $[...]_{V=V_o, \theta=\theta_{ss}(V_o)}$ means that the expression in the brackets has to be evaluated at steady state given by $V = V_o$, $\theta = \theta_{ss}(V_o)$. This definition implies that the value of L may depend on the steady state considered, but in the rate and state law as usually

formulated, L is taken to be a constant, independent of V. We note that some experiments show that L increases with V in simulated fault gouge [Mair and Marone,1999].

The state variable is usually chosen in such a way that $\theta_{ss} = \frac{L}{V}$, and is interpreted as a characteristic lifetime of the asperity population on the contact surfaces. This fits well with the convention $\frac{\partial \psi(V,\theta)}{\partial \theta} > 0$ that makes larger values of the state variable correspond to greater strength, as then the asperities with longer lifetime are stronger, as one would expect and as suggested by studies showing time-dependent regain of friction strength after a slip episode [Dieterich, 1972, 1981; Marone, 1998a].

In this study we use the following form of the rate and state formulation:

$$\tau = \sigma[\, f_w + \frac{f_o + a \ln \frac{V}{V_o} + b \ln \frac{V_o \theta}{L} - f_w}{1 + \frac{L}{V_w \theta}}] \qquad \text{(D.5)}$$

where σ is the constant normal stress, f_w is the residual friction coefficient, f_o is the reference friction coefficient at the reference slip rate V_o, a and b are rate and state parameters [Dieterich, 1979], L is the evolution distance for the state variable, and V_w is a characteristic velocity after which the frictional strength of the interface weakens significantly. In this study we use the following parameter values: σ =50MPa, f_w =0, f_o

=0.6, V_o =1E-6 m/s, a =0.014, b =0.019, L = 8mm and V_w =1m/s. At V=0 we use a regularized version of the law to handle the numerical singularity of the logarithmic term [Lapusta et al. 2000].

$$\tau = \sigma f_w + \frac{a\sigma \sinh^{-1}[\frac{V}{2V_o}\exp(\frac{f_o - f_w + b\ln\frac{V_o\theta}{L}}{a})]}{1+\frac{L}{V_w\theta}} \tag{D.6}$$

For the state variable evolution, we use the ageing formulation:

$$\frac{d\theta}{dt} = 1 - \frac{V\theta}{L} \tag{D.7}$$

Such a formulation allows for healing of the fault at stationary contact, a feature needed to explain laboratory observations [Beeler, 1994] and was shown to be a theoretical requirement for the generation of slip pulses in the rate and state framework [Perrin et al., 1995]. However, it is worth to mention that the “slip” law [Dieterich, 1979 and Ruina, 1983] was suggested to be a better description for the friction behavior at the slip rates observed in laboratory experiments [Bayart et al. 2006] and while the slip formulation does not allow for re-strengthening at stationary contacts, recent numerical simulations [Ampuero et al., 2008 and Noda et al., 2009] have shown that slip pulses can be realized using such a law. Perhaps a combined law, of the type proposed by Kato and Tullis [2003], would be the most appropriate to use. It is possible that different state evolution laws could have important implications on the rupture evolution [Ampuero and Rubin,

2008] and it is worth to explore such implications for different formulations. We restrict ourselves, however, in this study to the ageing law formulation.

When $\frac{d\theta}{dt} = 0$, we say that the frictional coefficient has reached a steady state, i.e. there is no further evolution for the state variable. In this limit the steady state friction coefficient assumes the form:

$$f_{ss} = f_w + \frac{f_o + (a-b)\ln\frac{V}{V_o} - f_w}{1+\frac{V}{V_w}} \tag{D.8}$$

If $V << V_w$ the steady state friction coefficient reduces to the classical Dieterich-Ruina formulation appropriate for describing steady state friction behavior at low slip rates. On the other hand if $V >> V_w$ the steady state friction coefficient approaches asymptotically the residual friction coefficient where $f_w << f_o$.

High slip rate friction formulation like the one proposed here has its roots in both theoretical [Rice, 1995 and Rice, 2006] and experimental [Beeler at al., 2009] investigations where it is motivated by certain physical processes taking place at the asperity contact level such as flash heating. The rapid transition from high static friction to low dynamic friction through dependence on slip rate may be one of the possible reasons of absence of melting in many mature faults that have sustained hundreds of meters of slip. If the fault strength does not weaken during seismic slip, the temperature rise due to slipping for several meters at slip rates around 1 m/s and under normal stresses

that are of the order of 100-200 MPa will be of the order of thousands of degrees, sufficient to cause complete melting of the rocks existing in the fault zone [Rice, 2006, Noda et al., 2009 and Noda and Lapusta, 2010]. However, no significant evidence of melting has been found in many mature faults [Rice, 2006, Aagaard and Heaton,2008]. One possible resolution to this paradox is that fault frictional strength decreases during seismic slip as a function of slip rate, as suggested by (D.5 and D.8), so that the dynamic friction is sufficiently low to cause temperature rise only below several hundreds of degrees.

D.2-Stability Analysis of Steady Sliding

In this section we carry out a linearized stability analysis for steady sliding on rate and state frictional surfaces with strong velocity-weakening character. For this purpose we linearize the friction law (D.1) about a state of steady sliding with constant normal stress σ, slip rate V_o, stress τ_o and state variable $\theta_o = \theta_{ss}(V_o)$. We introduce the following useful notations:

$$A = a\sigma = [V\,\partial\psi(V,\theta)/\partial V]_{V=V_o,\theta=\theta_{ss}(V_o)} \tag{D.9}$$

$$A - B = (a-b)\sigma = [V\,d\tau_{ss}/dV]_{V=V_o} \tag{D.10}$$

We then proceed as follows:

$$\begin{aligned}\tau &= \sigma f(V,\theta) = \sigma f(V,\theta_{ss}+\delta\theta) \\ &= \sigma f(V,\theta_{ss}) + \sigma \left.\frac{\partial f}{\partial \theta}\right|_{\theta=\theta_{ss}} \delta\theta \\ &= \tau_{ss} + \sigma \left.\frac{\partial f}{\partial \theta}\right|_{\theta=\theta_{ss}} \delta\theta\end{aligned} \tag{D.11}$$

Taking the time derivative of (D.1)

$$\frac{d\tau}{dt} = \sigma \frac{\partial f}{\partial V}\frac{dV}{dt} + \sigma \frac{\partial f}{\partial \theta}\frac{d\theta}{dt} \tag{D.12}$$

But the state evolution (D.2) dictates that:

$$\begin{aligned}\frac{d\theta}{dt} &= \varphi(V,\theta) = \varphi(V,\theta_{ss}+\delta\theta) \\ &= \varphi(V,\theta_{ss}) + \left.\frac{\partial \varphi}{\partial \theta}\right|_{\theta=\theta_{ss}} \delta\theta\end{aligned} \tag{D.13}$$

Substituting back in (D.12):

$$\frac{d\tau}{dt} = \sigma \frac{\partial f}{\partial V}\frac{dV}{dt} - \frac{V}{L}\sigma \frac{\partial f}{\partial \theta}\delta\theta \tag{D.14}$$

From (D.11) and (D.14):

$$\frac{d\tau}{dt} = \sigma \frac{\partial f}{\partial V}\frac{dV}{dt} - \frac{V}{L}[\tau - \tau_{ss}(V)] \tag{D.15}$$

where

$$\tau_{ss}(V) = \sigma f(V, \theta_{ss}) = \sigma f(V_o + \delta V, \theta_{ss})$$
$$= \sigma f(V_o, \theta_{ss}) + \sigma \left.\frac{df}{dV}\right|_{V_o, \theta_{ss}} \delta V \tag{D.16}$$

and $\delta V = V - V_o$

Using the definitions for *A* and *A-B* we can rewrite (D.9) and (D.10) as:

$$\frac{d\tau}{dt} = \frac{A}{V_o}\frac{dV}{dt} - \frac{V_o}{L}[\tau - \tau_o - (A-B)\frac{V - V_o}{V_o}]$$
$$\tau_{ss}(V) = \tau_o + (A-B)\frac{V - V_o}{V_o} \tag{D.17}$$

To study the stability behavior of frictional sliding, we consider the response of the sliding of two elastic half-spaces, in the anti-plane setting, to a Fourier mode perturbation, i.e., the perturbation with $\exp(ikz)$ dependence. We follow Lapusta (2000) and write the displacement field as:

$$u_x(y,z,t) = \frac{1}{2}V_o t \; sign(y) + \tilde{u}_x(y,z,t) \tag{D.18}$$

where $\tilde{u}_x(y,z,t)$ is the perturbed part and satisfies the wave equation $\tilde{u}_{tt} = c_s^2(\tilde{u}_{zz} + \tilde{u}_{yy})$. We look for a solution with z and t dependence as $\exp(ikz + pt)$ where k is real and p is in general a complex number. A possible solution can be postulated in the following form [Lapusta, 2000]:

$$\tilde{u}_x = \frac{1}{2} D \; \text{sign}(y) \; \exp[ikz - (k^2 + \frac{p^2}{c_s^2})^{1/2} \mid y \mid + pt] \tag{D.19}$$

Where the square root is cut from $i|k|c_s$ to $i\infty$ and from $-i\infty$ to $-i|k|c_s$ in the complex plane p to assure that it has a non-negative real part and that the solution remains bounded in the y-direction. The stress and slip rate perturbations on the interface y=0 then assume the forms:

$$\tau - \tau_* = -\frac{1}{2}\mu |k| \sqrt{1+(p/kc_s)^2}\, D \exp(ikz + pt) \tag{D.20}$$

$$V - V_* = pD\exp(ikz + pt) \tag{D.21}$$

where V_* is the steady sliding slip rate and τ_* is the corresponding shear stress. Substituting the shear stress and slip rate perturbations in (D.17) we find that p has to satisfy the following condition

$$\frac{1}{2}\mu |k| \sqrt{1+(p/kc_s)^2} + \frac{p(pA/V_* - (B-A)/L)}{p + V_*/L} = 0 \tag{D.22}$$

Note that $\mathrm{Re}(p)$ measures the growth rate of perturbations in time. If $\mathrm{Re}(p) > 0$ the perturbation amplitude grows exponentially in time and the steady sliding is hence unstable. However, if $\mathrm{Re}(p) < 0$ the perturbation amplitude decreases exponentially in time and the steady sliding is considered to be stable.

After some algebraic manipulations and the introduction of a few scaled quantities we can rewrite (D.22) in the following form:

$$(1-T_A^2)\bar{p}^4 + 2\bar{p}^3(1+TT_A) + \bar{p}^2(\xi^2 + 1 - T^2) + 2\xi^2\bar{p} + \xi^2 = 0 \tag{D.23}$$

where $\bar{p} = \frac{pV_*}{L}$ is the normalized growth rate, $\xi = \frac{kL}{V_* / c_s}$ is the normalized wavenumber, $T = \left. \frac{d\tau_{ss} / dV}{\mu / 2c_s} \right|_{V=V^*}$ gives a measure for the strength of the velocity-weakening of the friction law; it is the ratio between the rate of change of the steady state frictional shear stress with respect to slip rate and the radiation damping coefficient, and finally $T_A = \left. \frac{\partial \tau / \partial V}{\mu / 2c_s} \right|_{V=V^*, \theta=\theta_{ss}}$ is a measure of the strength of the direct effect of the friction law.

For the friction law used in this study the expressions of T and T_A take the form:

$$T_A = \frac{2ac_s}{\mu V_* (1 + \frac{V_*}{V_w})} \tag{D.24}$$

$$T = \frac{2c_s}{\mu} \frac{(1 + \frac{V_*}{V_w}) \frac{a-b}{V_*} + \frac{1}{V_w} (f_o + (a-b) \ln \frac{V_*}{V_o} - f_w)}{(1 + \frac{V_*}{V_w})^2} \tag{D.25}$$

For a given steady sliding velocity V_* we can calculate the values of T and T_A. We can then use equation (D.23) to solve for the perturbation parameter $\bar{p}$ as a function of the perturbation wavenumber ξ. We discuss some of the properties of the solution of equation (D.23) in the following. It was shown [Zheng and Rice,1998] that steady sliding

is stable to perturbations of infinite wavelength ($k = 0$) if the slip rate V_* is larger than a characteristic value V_{pulse}, where V_{pulse} is the slip rate defined by the tangency point of the radiation damping line with the steady state frictional coefficient curve. If $V_* < V_{pulse}$ the steady sliding is found to be unstable to perturbations of infinite wavelength. Due to the special character of $V_* = V_{pulse}$ we will study first characteristics of the solutions of equation (D.23) in the regime $V_* > V_{pulse}$ and then in the regime $V_* < V_{pulse}$.

D.2.1- Growth rates of perturbations for steady sliding with $V_* > V_{pulse}$***:***

We consider steady sliding of the frictional interface for a range of slip rates $V_* > V_{pulse}$. For the frictional and elastic parameters used in this problem, $V_{pulse} = 1.46\ m/s$. We solve for $\bar{p}$ as a function of the normalized wavelength ξ. For the growth rate of a perturbation amplitude we consider the real part of the solution $\mathrm{Re}(\bar{p})$. Figure (D.1) shows examples of the variation of the perturbations amplitude growth rates as a function of the perturbations wavenumber. Several observations follow from this curve which we will briefly discuss.

The first observation is that for every value of the unperturbed velocity V_* perturbations with wavenumber greater than a certain value have negative growth rates. This means that if steady sliding is perturbed with a perturbation of wavenumber belonging to this range, the perturbation amplitude will diminish with time and the steady sliding will be stable. This short wavelength stability is an essential requirement for the well-posedness of the elastodynamic problem with frictional boundary conditions in the continuum

setting. In particular, the short wavelength stability ensures that the solution of the problem converges as the mesh used for the solution of the initial boundary value problem is refined. In the discrete setting this requirement may be loosened as we will discuss later. Also one may note that the value of the critical wavenumber defining the stability boundary depends on the value of the unperturbed slip rate considered. However, for the cases considered here, it appears that such dependence is relatively weak.

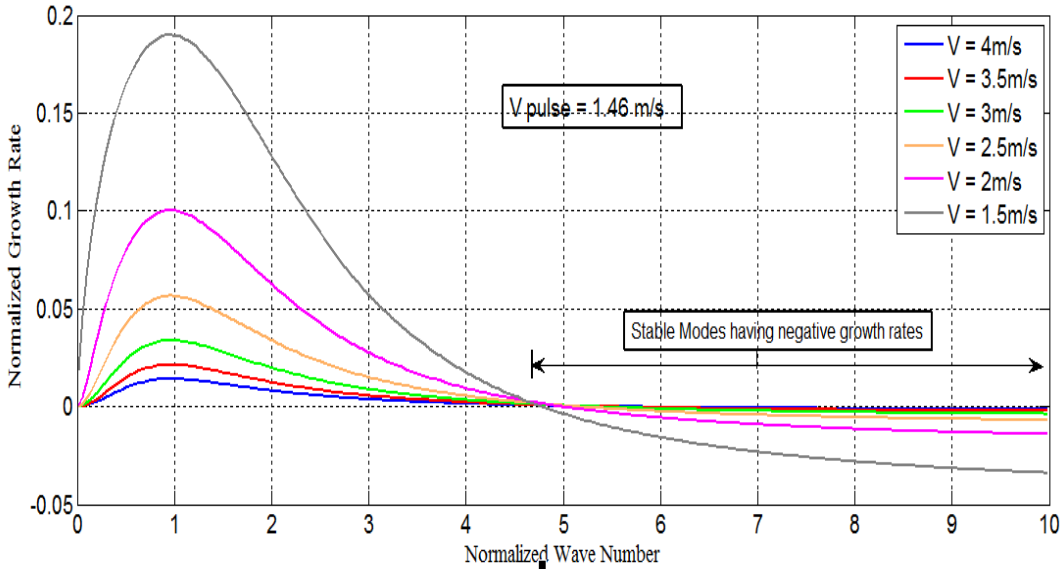

Fig. D.1: Dependence of the growth rate of perturbations on their wavenumber, for a range of unperturbed slip velocities $V_* > V_{pulse}$. Steady sliding is stable to perturbations with wavenumbers greater than a critical value, as those perturbations possess negative growth rate. For the unstable modes having positive growth rates, the growth rate increases as the unperturbed slip velocity V_* decreases. Among the unstable modes, there exists a wavenumber that has the maximum growth rate. If we have a large enough region sliding at a constant slip velocity, the sliding is expected to destabilize at this wavenumber, leading to formation of a train of pulses (Lapusta, 2000).

The second observation is that there exists a small region near $\xi = 0$ for which perturbations have negative growth rates. This reflects the stability of steady sliding, at unperturbed slip rates $V_* > V_{pulse}$, in response of perturbations with infinite and very large wavelengths. The range of wavenumbers satisfying this property decreases as the unperturbed slip rate gets closer to V_{pulse}. The analysis of Zheng and Rice [1998] shows that V_{pulse} is a bifurcation point after which steady sliding becomes unstable to perturbations of infinite wavelength. We will show this shortly.

The third observation is that for intermediate wavenumbers, each of the $\mathrm{Re}(p) - \xi$ curves show a pronounced peak indicating the existence of a wavenumber with a maximum growth rate. This was first demonstrated by Lapusta (2000). We note that the value of this wavenumber depends weakly, at least in the cases considered here, on the value of the unperturbed slip rate. We also note that as the value of the unperturbed slip rate decreases, the magnitude of the growth rate of the perturbation amplitude increases, signaling increased instability as we approach $V_* = V_{pulse}$.

D.2.2- Phase velocities of perturbations for steady sliding with $V_* > V_{pulse}$***:***

To calculate the phase velocity of a perturbation with a given wavelength, we recall from [D.19] that the solution to the perturbed elastodynamic problem just at the interface *y* = 0 assumes the form:

$\tilde{u}_x \propto \exp(ikz + pt)$

But $p = \mathrm{Re}(p) + i\,\mathrm{Im}(p)$

Accordingly $\tilde{u}_x \propto \exp[i\{kz + \mathrm{Im}(p)t\} + \mathrm{Re}(p)t) = \exp[i\{kz + \omega t\} + \mathrm{Re}(p)t)$

It then follows that: $c_{\rho h} = \omega/k = \mathrm{Im}(p)/k = \frac{\mathrm{Im}\,\bar{p}}{\xi}\frac{L^2}{V^2}c_s$ where $c_{\rho h}$ is the phase velocity and c_s is the shear wave speed.

The variation of perturbation phase velocity, normalized by the shear wave speed, as a function of perturbation wavenumber is shown in Fig. (D.2) for the same range of unperturbed slip rates considered in Fig.(D.1). We can see that for every unperturbed slip rate, there exists a range of wavenumbers that have phase velocities greater than the shear wave speed of the medium. For the cases shown here, this condition applies to wavenumbers $\xi <\sim 0.75$. Perturbations with maximum growth rate and short wavelength perturbations, however, propagate with subsonic phase speeds. For intermediate wavenumbers, one can also note the existence of a wavenumber of minimum phase velocity.

The maximum phase velocity for the supersonic perturbations increases as the unperturbed slip rate decreases. Meanwhile, the minimum phase speed decreases for the same conditions. This implies an increased contrast in the phase velocities of perturbation with different wavenumbers as the sliding slip rate approaches V_{pulse}. The contrast in phase velocities gives a measure of the strength of dispersion in the elastodynamic

solution. We explore the consequence of dispersion and existence of unstable perturbation on the pulse formation in section (D.3) .

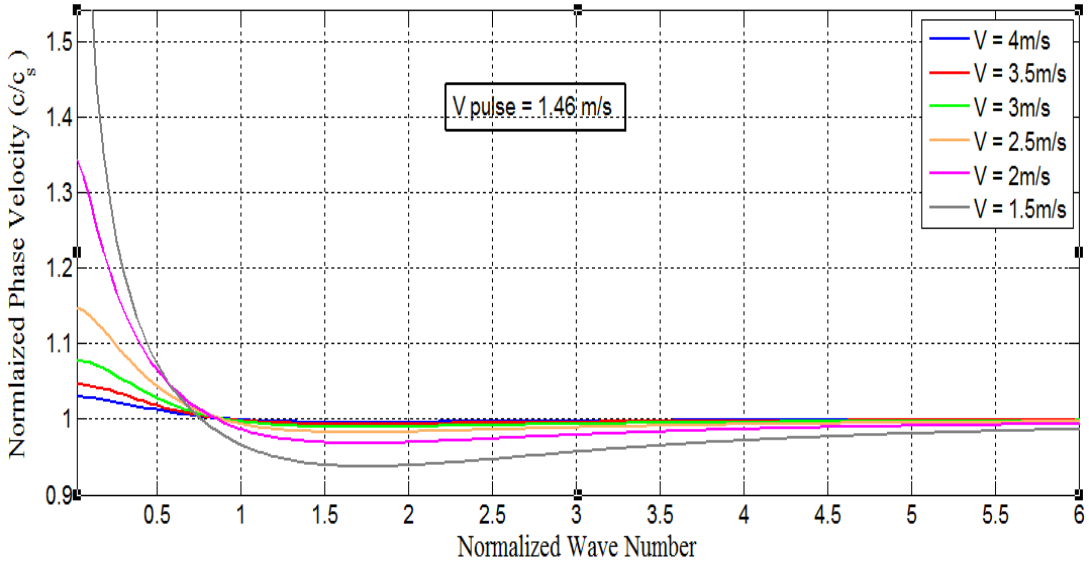

Fig. (D.2): Dependence of the phase velocities of perturbations on their wavenumber, for a range of unperturbed slip velocities V_*>Vpulse. There are modes with supersonic phase velocities. As unperturbed slip velocity decreases, not only the speed of supersonic phases increases but also the contrast in speed between the subsonic and supersonic modes becomes more pronounced. We discuss the implications of the existence of these supersonic phase velocities on the formation of slip pulses and determination of the propagation speed of their healing tails in the next section.

D.2.3. Growth rates of perturbations for steady sliding with $V_* < V_{pulse}$

We next consider steady sliding at unperturbed slip rates $V_* < V_{pulse}$. Figure (D.3) shows examples of the variation of the perturbations amplitude growth rates as a function of the perturbations wavenumber. When compared to Fig. (D.1), Fig. (D.3) shows the lack of the existence of a single wavenumber with a distinctive maximum growth rate. Rather,

several wavenumbers grow simultaneously with a growth rate comparable to the one with a maximum growth rate. (See the blue curve corresponding to $V_* = 1m/s$ as an example.) Moreover, smallest wavenumbers tend to exhibit the highest growth rates in the case shown, indicating further that steady sliding is unstable to perturbations of infinite wavelength when $V_* < V_{pulse}$. The maximum growth rates do not depend monotonically on the unperturbed slip rate as they do in Fig. (D.1) but get tangled with each other in a relatively complicated way. We may also see that the growth rates recorded here are much larger than the corresponding ones in Fig. (D.1), suggesting a stronger effect for the unstable modes as V_* drops below V_{pulse}. However, the two figures share some similarities as well. For example, Fig. (D.3) still shows the short wavelength stability phenomenon indicated by perturbations with large wavenumbers exhibiting negative growth rates. This is crucial, as previously discussed, for the physical and mathematical well-posedness of the problem.

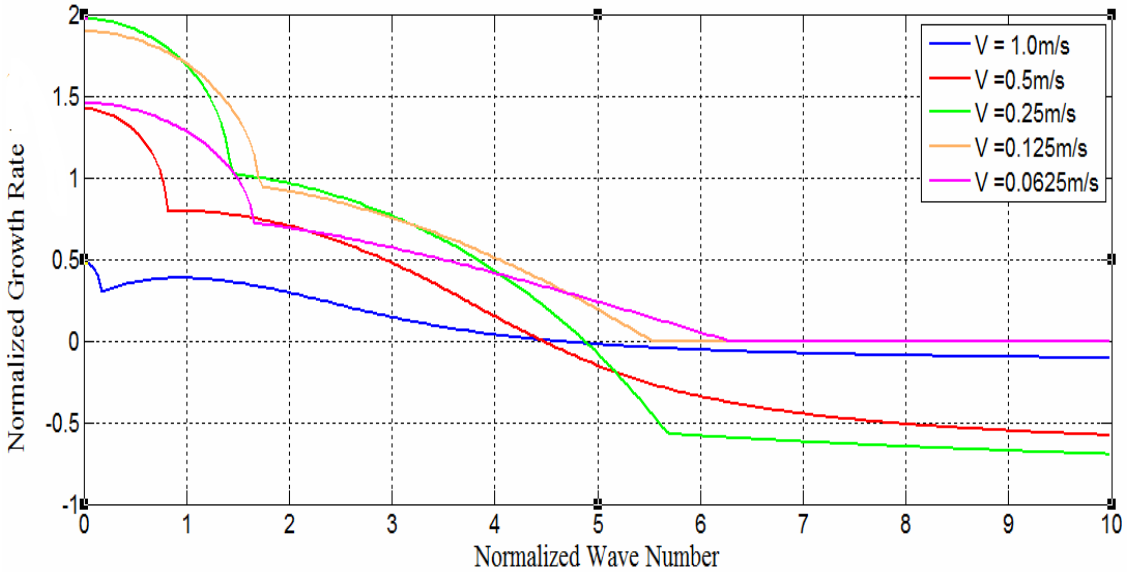

Fig. (D.3): Dependence of the growth rate of perturbations on their wavenumber, for a range of unperturbed slip velocities $V_* < V_{pulse}$. The well-posedness of the frictional sliding problem is ensured by having short wavelength stability facilitated by the negative growth rates of perturbations with large wavenumbers. Long wavenumber perturbations are unstable with several wavenumbers growing at a growth rate comparable to the one with maximum growth rate.

D.2.4. Phase velocities of perturbations for steady sliding with $V_* < V_{pulse}$

The next step is to study the distribution of phase speeds as a function of perturbation wavenumbers for different unperturbed slip rates $V_* < V_{pulse}$. This is shown in Fig. (D.4) where we observe some major qualitative and quantitative differences between the perturbation response in this case and in the case shown in Fig. (D.2). One of these differences is that all propagating wavenumbers in the current case have phase velocities smaller than the shear wave speed; there are no supersonic perturbations. Also, one may observe that for each unperturbed slip rate considered, there exist a group of wavenumbers that have zero phase velocities; they are stationary. The range of values of those wavenumbers in general increases as the unperturbed slip rate decreases. When combining Figs. (D.3) and (D.4) one may observe that all those stationary modes are unstable with positive growth rates. The existence of an unstable stationary mode may be an essential ingredient in the formation of slip pulses as we will discuss later.

For small values of the unperturbed slip rate (e.g., $V_* < 0.125 m/s$), it appears that there exists a perturbation with a maximum phase speed. While we have not considered the

implications of this phenomenon yet, it might play a role in the formation of the propagating creep fronts observed at sub-seismic slip rates.

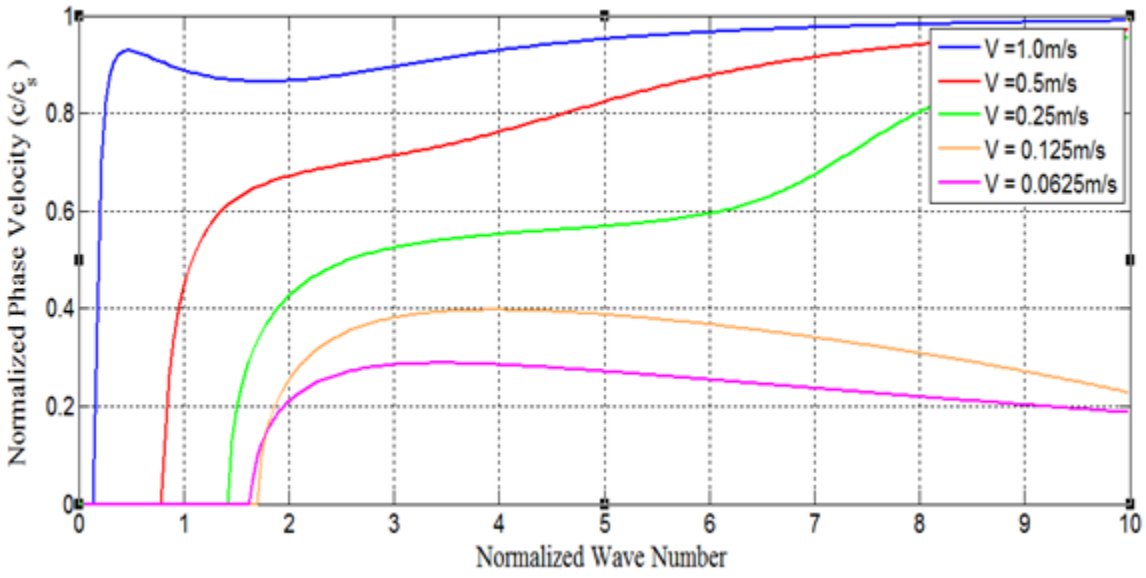

Fig. (D.4): As the unperturbed slip velocity V_* is reduced below V_{pulse} =1.46m/s large-wavelength perturbations become stationary, with zero phase velocities. The range of these stationary modes is increased as slip velocity decreases. Note that from Fig. (D.3) one can infer that the stationary modes have growth rates exceeding those possessed by the propagating modes (but this might not be true in general). If the wavelengths of the stationary modes are comparable to the size of the dynamically sliding region, they may become important in dynamic rupture, contributing to the formation of the slip pulse and the rapid arrest of the region behind the crack front, as we will discuss later.

D.3. Implications for formation of a single slip pulse

Based on the stability analysis results discussed in section (D.2) one may hypothesize that the formation of a single slip pulse is a result of a combination of factors including strong

dispersion effects, existence of unstable modes and the simultaneous arrest of a group of stationary modes. We hypothesize that for the cases leading to the formation of a single pulse, the rupture starts as an initial crack, with the region behind the crack front steadily sliding at a rate $V_* > V_{pulse}$. However V_* is usually low enough such that the contrast between the phase speeds of different perturbation, and consequently the dispersive effects, is sufficiently strong to lead to the formation of a depressed central region and observable propagating kinks as shown in Fig. (D.5). With the continuous decrease in the value of V_* the dispersive effects and the growth rates of unstable modes increase, leading to a drop in the value of V_* below V_{pulse}. In this regime of sliding velocities, we have shown that some perturbations become stationary and possess high growth rates comparable to the perturbation with the maximum growth rates. This simultaneous growth of stationary modes leads to the fast arrest of sliding behind the rupture front [See Fig. (D.5)].

A couple of questions arise. First, why is the rupture arrested and not disintegrated to a train of pulses (as in Lapusta, 2000)? The reason is that those stationary modes have wavelengths comparable to the size of the region sliding steadily behind the rupture front. This is different from the cases which lead to the formation of multiple pulses in which there is a well-defined single perturbation with a maximum growth rate and whose wavelength is only a fraction of the size of the steadily sliding region. This raises another question: why does the rupture not end up with a “hump” in its central region rather than a complete arrest? The answer might be that the harmonic perturbations we consider here do grow in both of the positive and negative directions. The growth of the negative

direction, however, dominates due to a positive feedback mechanism: as V^* decrease, the growth rate of perturbation increases and hence the instability mechanism gets reinforced.

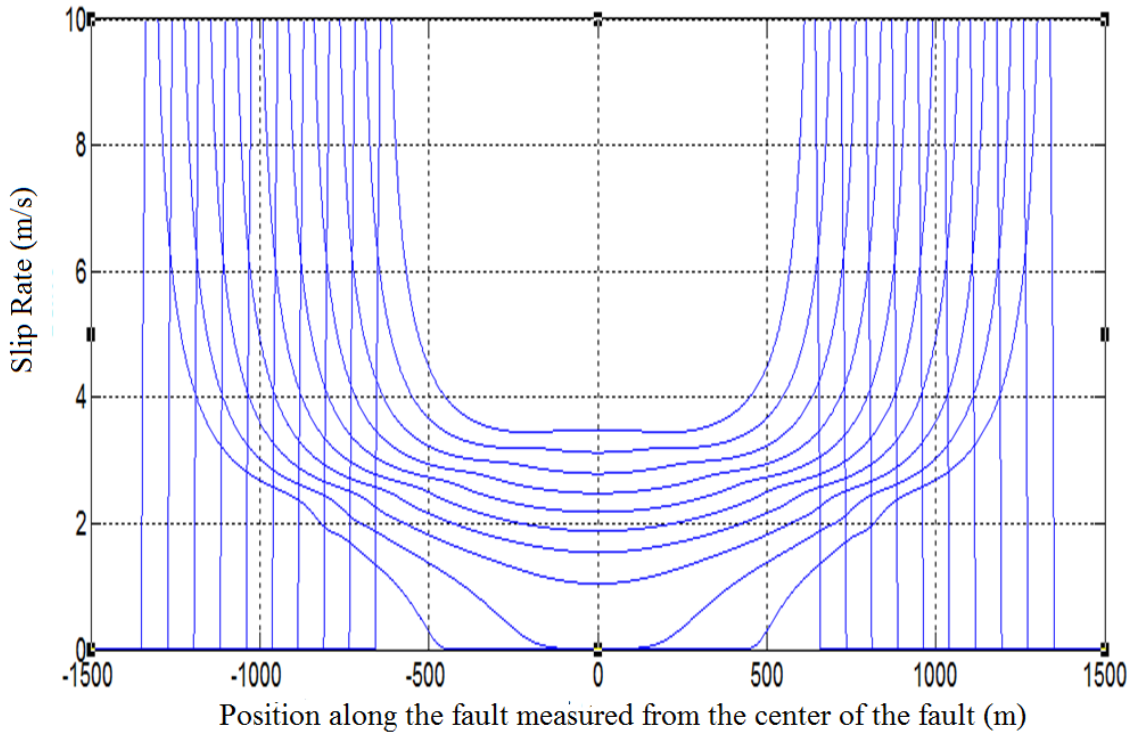

Fig. (D.5): Snapshots of the slip rate along the fault every 13 milliseconds, for a case where a slip pulse is formed. During that, slip velocity V at the center of the crack decreases to zero. We hypothesize that the pulse formation process is related to the stability properties as follows: 1. While $V > V_{pulse}$ The growth of unstable modes combined with the strong dispersion effect due to the propagation of different modes with different phase velocities [see Fig. (D.2)], spanning the supersonic to the subsonic range, lead to the decrease in V at the center of the crack and the propagation of visible instabilities. 2. When $V < V_{pulse}$ (i) A group of wavelengths grow at a rate comparable to the maximum growth rate [see Fig. (D.3)], (ii) Some modes become stationary with their phase velocities reduced to zero

[See Fig. (D.4)]. Those modes have wavelengths comparable to the size of the region sliding behind the crack front. The combined effect of (i) and (ii) lead to the fast arrest of sliding in the central region. The supersonic healing speed of the formed pulse may be attributed to the propagation of the supersonic modes previously discussed.

In future work, we will try to better quantify the preliminary observations outlined in this section and we will try to formulate a quantitative theory, based on stability analysis, which could yield a better understanding to the problem of mode of rupture selection.